Environment Canada Environnement Canada

Canada

PHYSICAL PROCESSES IN WESTERN LAKE ONTARIO AFFECTING SUSTAINABLE WATER USE

K.C. Miners, F. Chiocchio, Y.R. Rao, B. Pal and C.R. Murthy

NWRI Contribution No. 02-176

Physical Processes in Western Lake Ontario Affecting Sustainable Water Use

K.C. Miners[1], F. Chiocchio[1], Y.R. Rao[1], B. Pal[2], and C.R. Murthy[1]

[1]National Water Research Institute
Canada Centre for Inland Waters
Aquatic Ecosystem Management Research Branch
867 Lakeshore Rd, P.O. Box 5050
Burlington, Ontario L7R 4A6

[2]Canadian Institute for Climate Studies
130 Saunders Annex
University of Victoria
P.O. Box 1700 Sta CSC
Victoria, BC V8W 2Y2

NWRI Contribution # 02-176

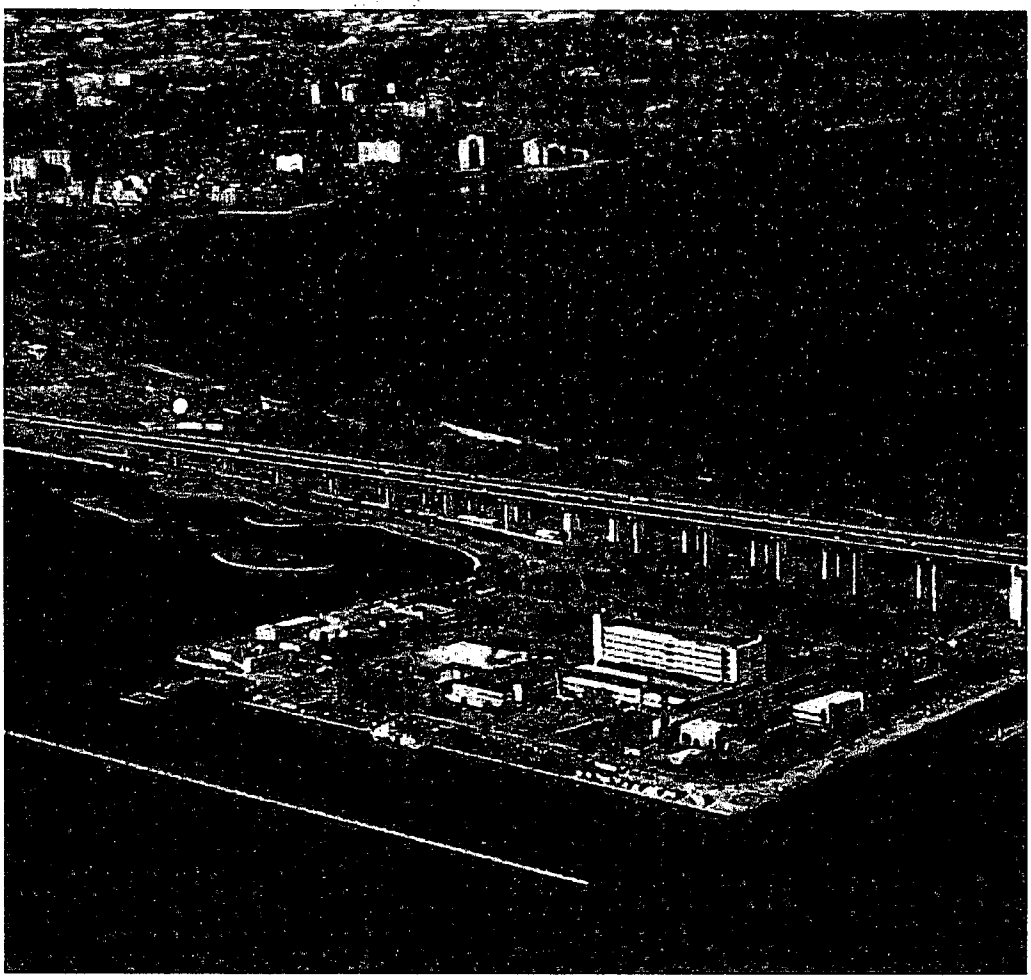

Oblique Aerial Photo Showing Part of Study Area

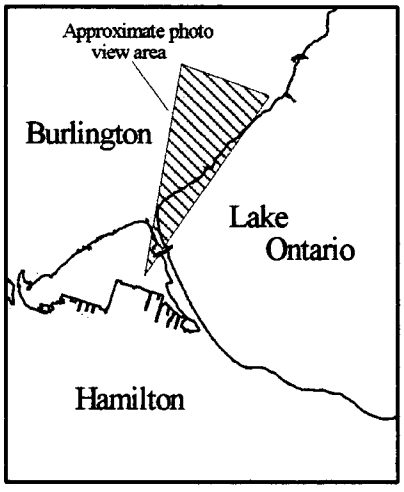

Management Perspective

The western Lake Ontario shore is rapidly becoming one continuous urban community that heavily depends on the lake for drinking water and discharge of wastewater. Characterizing the properties of the nearshore receiving waters to which wastewater is discharged is the first step to assess the nature of the pollutants and for developing sustainable strategies for the protection, restoration and conservation of the western Lake Ontario coastal ecosystem. Meteorologically forced episodic events are largely responsible for dispersing and exchanging wastewater discharged into the nearshore areas. Upwelling and downwelling of coastal waters generate intense mixing of nearshore water masses with the offshore of the lake during the summer months when the lake is thermally stratified. Over the last ten years there has been a question of whether municipal treated sewage presently discharged to Hamilton Harbour could be discharged into Lake Ontario as is the practice in other municipalities. Alternate strategies of lake discharge may alleviate the need for unusually stringent treatment needed to meet water quality goals of the Hamilton Harbour Remedial Action Plan (HHRAP). The latest update of the HHRAP recommended a study of the possibility of offshore discharges.

This report systematically parametrizes the nearshore physical processes for developing coastal outfall transport models for sewage waters originating from the City of Burlington in the Regional Municipality of Halton, and the City of Hamilton. Near-field dilution obtained from a mixing zone model shows that for treated effluents with existing discharge conditions at a proposed outfall site at Burlington, the dilution ratios are in the range of 13:1 to 28:1 for weak to moderate currents during summer stratification. Winter dilution ratios increased significantly in the absence of stratification. The near-field dilution ratio decreased considerably when the treatment capacity was increased to the value representing the combined outfall of Burlington and Hamilton however the concentrations are below the prescribed exceedance limits of water quality. Far-field studies showed no contamination near Hamilton and Burlington water intakes and beaches. The results are based on sound physical limnological principles and are therefore general to apply to manage wastewater effluents in other coastal areas of the Great Lakes.

Processus Physiques En Jeu Dans L'ouest Du Lac Ontario Et Affectant L'utilisation Durable De L'eau

K. C. Miners[1], F. Chiocchio[1], Y. R. Rao[1], B. Pal[2] et C. R. Murthy[1]

Sommaire à L'Intention de la Direction

La rive ouest du lac Ontario se transforme rapidement en une communauté urbaine continue qui dépend fortement du lac pour ses approvisionnements en eau de boisson et pour le rejet de ses eaux usées. La caractérisation des propriétés des eaux réceptrices de la zone riveraine dans laquelle les eaux usées sont rejetées est la première étape de l'évaluation de la nature des polluants et du développement de stratégies de développement durable pour la protection, la remise en état et la conservation de l'écosystème riverain de l'ouest du lac Ontario. Des événements épisodiques forcés par les conditions météorologiques sont largement responsables de la dispersion et de l'échange des eaux usées déversées dans les secteurs riverains. Pendant l'été, au cours de la période de stratification thermique du lac, les remontées et les plongées des eaux riveraines créent une zone de mélange intense des masses d'eaux du rivage avec les eaux du large. Au cours des 10 dernières années, on s'est demandé si les eaux usées municipales traitées qui sont actuellement rejetées dans le port de Hamilton ne pourraient être déversées dans le lac Ontario, comme c'est le cas de celles d'autres municipalités. De nouvelles stratégies de rejet des eaux dans le lac pourraient permettre d'alléger les traitements très rigoureux nécessaires pour satisfaire aux exigences de qualité de l'eau, en application du Plan d'action pour l'assainissement du port d'Hamilton (PAPH). La dernière version du PAPH recommandait une étude sur la possibilité de rejeter les eaux résiduaires loin des rives.

Ce rapport dresse une liste systématique des processus physiques riverains pour le développement de modèles de transport à exutoires côtiers pour les eaux usées de Burlington (municipalité régionale de Halton) et de Hamilton. D'après des études de dilution semblables, effectuées dans la zone rapprochée et préparées selon un modèle de zone de mélange, on a montré que, avec des effluents traités et les conditions actuelles de rejet au site d'exutoire proposé pour Burlington, les rapports de dilution seraient de l'ordre de 13:1 à 28:1 avec les courants faibles à modérés observés pendant la stratification d'été. Mais, en hiver, en l'absence de stratification, les rapports de dilution augmentent significativement. Le rapport de dilution a beaucoup diminué lorsqu'on a accru la capacité de traitement à une valeur représentant celle de l'exutoire combiné de Burlington et Hamilton, mais les concentrations dépassaient les limites prescrites pour la qualité de l'eau. Des études des eaux du large ont montré qu'il n'y avait pas de contamination près des entrées d'eau et des plages de Hamilton et de Burlington. Ces résultats sont basés sur des principes de limnologie physique bien fondés, et sont donc assez généraux pour servir à la gestion des effluents d'eaux usées dans d'autres régions côtières des Grands Lacs.

Abstract

The western Lake Ontario shore is rapidly becoming one continuous urban community that heavily depends on the lake for drinking water and discharge of wastewater. Population and development estimates predict that by the year 2011 the Region of Halton will require enhanced capacity of wastewater treatment facilities. In order to maintain the permissible effluent limits, an outfall has been proposed to be installed in the lake. Substantial advances have been made in regulating the outfall locations and permissible effluent quality, however, the ever increasing total volumes of wastewater heighten the need to understand coastal physical processes in more detail due to the complexities introduced by basin shape and bathymetry at the western end of the lake. Historical data show high variability of flow with frequent occurrences of stagnation of currents. In consideration of these water quality concerns and with a long-term interest in sustainable use of nearshore waters, the National Water Research Institute (NWRI) undertook a comprehensive study of physical characteristics of the coastal areas of the western Lake Ontario.

The kinetic energy of coastal currents shows a maximum at 10-12 days periodicity, which is due to large-scale meteorological forcing of the lake during summer stratification. A secondary peak was also observed at a period of 16-18 hours due to near inertial oscillations. Superimposed on this large-scale circulation, coastal currents exhibit episodic events of shorter duration (typically 2-3 days) such as upwelling/downwelling, strong alongshore coastal jets and weaker stagnation currents interspersed with reversals. Coastal circulation features introduce a wide range of nearshore/offshore exchange processes. For example, alongshore exchange coefficients are typically higher than cross-shore turbulent exchange coefficients by a factor of 2-3. Upwelling events are characterized with weak static stability whereas downwelling events are characterized with strong currents and weak turbulence. During winter homogeneous conditions the coastal currents are mainly characterized by a 4-day period oscillation associated with large-scale wind forcing. However coastal circulation exhibits strong alongshore currents interspersed with current reversals. Parameterization of such complex coastal processes appropriate for coastal transport modeling is a challenging task. In this report we have attempted to provide a hierarchy of schemes for parametrizing the coastal physical processes.

Coastal transport modeling is an important adjunct to the experimental work in western Lake Ontario. The wealth of carefully scrutinized current data is used to synthesize transport and dispersion scenarios for actual and hypothetical effluent rates discharging at different locations under different conditions in coastal transport models. By using the U.S.EPA-RSB near-field dispersion model, we have obtained the near-field dilution rates under the present discharge conditions as well as for expected future discharge scenarios. The model results show that for the present discharge conditions the near-field dilutions are in the range of 13:1 to 28:1 in the summer, and 21:1 to 96:1 in the winter period for weak and moderate currents. Far-field studies, employing a Gaussian plume model and a two-dimensional numerical model, showed no contamination near the existing Hamilton and Burlington water intakes. The model results also showed no significant contamination with increased treatment capacity for a typical summer current distribution. There could be some problems if untreated effluent were to be discharged during strong shore parallel current episodes where pollutants are advected rapidly to water intake locations. However, both municipalities could retain their present capability to allow discharge of untreated waste into the harbour if necessary to protect lake water sources if periods of plant upset occur.

Résumé

Le rivage ouest du lac Ontario se transforme rapidement en une communauté urbaine continue qui dépend fortement du lac pour ses approvisionnements en eau de boisson et pour le rejet de ses eaux usées. Selon les prévisions relatives à l'accroissement de la population et au développement, en 2011, la région de Halton aura besoin d'installations de traitement des eaux usées améliorées et à capacité accrue. Afin de maintenir les limites autorisées pour les effluents, on a proposé l'installation d'un exutoire dans le lac. Même si on a réalisé des progrès substantiels pour optimiser la réglementation des emplacements des exutoires et de la qualité des effluents, l'augmentation constante des volumes totaux d'eaux usées impose de mieux comprendre les processus physiques riverains à cause de facteurs complexes dus à la forme du bassin et à la bathymétrie de l'extrémité ouest du lac. Les données historiques indiquent une variabilité élevée de l'écoulement, avec des cas assez fréquents de stagnation des courants. Compte tenu de ces préoccupations relatives à la qualité des eaux, l'Institut national de recherche sur les eaux (INRE), qui s'intéresse depuis longtemps à l'utilisation durable des eaux du rivage, a entrepris une étude générale sur les caractéristiques physiques des secteurs riverains de l'ouest du lac Ontario.

L'énergie cinétique des courants côtiers présente un maximum avec une périodicité de 10 à 12 jours, qui est due à un forçage météorologique à grande échelle sur le lac pendant la stratification d'été. On a aussi observé un pic secondaire d'une périodicité de 16 à 18 heures, due à des oscillations quasi inertielles. Superposés à cette circulation à grande échelle, les courants côtiers comportent des événements épisodiques de courte durée (habituellement de 2 à 3 jours) comme les remontées et les plongées, de forts courants côtiers le long des rivages et des courants de stagnation plus faibles, entremêlés à des zones d'inversion de courant. Les caractéristiques de la circulation côtière sont à l'origine d'un grand nombre de processus d'échange entre les eaux du rivage et celles du large. Par exemple, les coefficients d'échange le long du rivage sont habituellement supérieurs d'un facteur de 2-3 aux coefficients d'échange turbulent perpendiculaire au rivage. Les événements de remontée sont caractérisés par une faible stabilité statique, et les événements de plongée, par des courants forts et de faibles turbulences. Pendant les conditions homogènes d'hiver, les courants côtiers sont surtout caractérisés par une période d'oscillation de 4 jours associée à un forçage éolien à grande échelle. Toutefois, le profil de la circulation côtière présente de forts courants le long du rivage, entremêlés à des zones d'inversion de courant. La paramétrisation de ces processus côtiers complexes, qui est utile pour la modélisation du transport côtier, est une tâche ardue. Dans ce rapport, nous tentons de présenter un ensemble hiérarchisé de schémas pour la paramétrisation de ces processus physiques côtiers.

La modélisation du transport riverain facilite grandement les travaux expérimentaux dans l'ouest du lac Ontario. Les données sur les courants, très riches et de grande qualité, servent à l'établissement de scénarios de transport et de dispersion pour étudier, à l'aide de modèles du transport riverain, les débits d'effluents réels et hypothétiques à différents emplacements et dans diverses conditions. En utilisant le modèle RSB de dispersion dans la zone rapprochée (EPA), avec divers scénarios de rejet, nous avons obtenu des débits de dilution dans la zone rapprochée pour les conditions actuelles de rejet, ainsi que pour les conditions futures prévues. Les résultats des essais de modélisation indiquent que pour les conditions actuelles de rejet, la gamme de dilutions dans la zone rapprochée est comprise entre 13:1 et 28:1 en été, et entre 21:1 et 96:1 en hiver pour les courants faibles et modérés. Les études sur la zone éloignée, qui utilisent un modèle

de panache gaussien et un modèle numérique à deux dimensions, n'indiquaient pas de signes de contamination près des entrées d'eau actuelles de Hamilton et de Burlington. Les résultats de la modélisation ont aussi indiqué que, avec une répartition des courants typique de l'été, il n'y avait pas de contamination significative pour une capacité de traitement accrue. Il pourrait cependant y avoir des problèmes si des effluents non traités étaient rejetés pendant les épisodes de forts courants parallèles au rivage, car alors les polluants seraient transportés rapidement par advection vers les sites des entrées d'eau. Toutefois, les deux villes pourraient conserver leurs installations actuelles afin de pouvoir rejeter des eaux résiduaires non traitées dans le port, en cas de besoin, afin de protéger les réserves d'eau du lac lors des périodes de panne des installations d'épuration des eaux.

Executive Summary

The western Lake Ontario shore is rapidly becoming a continuous urban community. Population and development estimates formulated in the mid 1990's for the Region of Halton predicted that, by the year 2011, the capacity of the Skyway Wastewater Treatment Plant (WWTP), which serves part of south Halton, would have to be increased by 50% from the current capacity of 93,000 m^3/day to 140,000 m^3/day.

A list of 40 alternatives for providing wastewater services to South Halton was prepared by a special study group with input from Halton's Technical Agencies Committee and a Stakeholders Group. By 1996 this list had been reduced to 5 alternatives that were felt to best meet the selection criteria. Two of the alternatives involved retaining the Skyway WWTP at existing capacity, and directing flow in excess of its rated capacity to the Woodward Avenue WWTP in the Region of Hamilton Wentworth; a plant which also discharges into Hamilton Harbour. Further assessment of these alternatives failed to resolve the question of whether or not the Woodward Avenue facility would have the capacity to handle the increased load within the required time-frame. In addition, the cost of implementation, and strong indications that the scheme would fail to meet the Remedial Action Plan (RAP) loading targets, all led to the ultimate rejection of these alternatives.

The preferred alternative of the original short list called for expansion of the Skyway and Mid Halton treatment plants, with Skyway continuing to discharge into Hamilton Harbour, while maintaining "Best Available Technology Economically Achievable" (BATEA) effluent limits. The other two remaining alternatives were also based on these expansions; however, one scheme would add tertiary treatment at Skyway to meet RAP loading targets, and the other would relocate the plant discharge from the harbour into Lake Ontario. The improvement to wastewater quality that one could reasonably expect from upgrading to tertiary treatment - a very costly option - might still fail to prevent an unacceptable increase in nutrient loading to the harbour at the projected wastewater volume. After several meetings with input from a number of agencies and the public, the alternative involving relocation of the wastewater outfall in Lake Ontario was deemed most desirable. Subsequently, the operators of the plant discovered how to optimise treatment efficiency so that initial RAP targets were met. Due to population growth, the question of whether to treat to a higher level or discharge in the lake is expected re-emerge in five-to-ten years.

The rationale for supporting discharge into the lake is based on the intuitive notion that the comparatively huge volume of the lake and its anticipated efficient mixing would effectively disperse the effluent. In fact, mixing zone studies were conducted prior to the expansion of the Oakville Southwest-Mid Halton WWTP for its combined outfall, that showed chemical and bacteriological parameters lower than Provincial Water Quality Objectives at a distance of about 900m from the source for an average flow rate of 195,460 m^3/day (Anderson, 1985). Not only is this flow rate substantially greater than the projected discharge for Skyway (by almost 40%), but the updated Skyway plant would maintain year-round non-toxic effluent quality through nitrification, and non-toxic disinfection, which would likely reduce the size of the effective mixing zone even more.

Placement of an outfall from Skyway WWTP in Lake Ontario would be subject to physical constraints imposed by coastal morphological features. Based on previously established

guidelines, a minimum 3 km distance from a potable water intake, and a minimum 900m from the shore would be required. This would substantially restrict the area where the proposed outfall could be located, since the present water intake for Burlington is situated about 4 km from the Skyway plant, part of which would be taken up by the required offshore allowance for the outfall. The Burlington Ship Canal, which provides access between Lake Ontario and Hamilton Harbour, is situated about a kilometre south of the Skyway WWTP. The shipping lanes leading from the open lake to the canal form a southern boundary restricting the placement of the outfall.

Despite the favourable inferences from the planning studies done for the Mid Halton outfall there are sufficient differences between the Mid Halton site and the proposed Skyway outfall site to warrant a very careful look at the specific characteristics of the Skyway site. The striking differences, imposed by topographic and bathymetric characteristics at the two sites contribute to different coastal climatology of currents and thermal structures. The Mid Halton outfall is situated on a stretch of shoreline that is, at least in the gross sense, relatively straight; and, therefore, subject to substantial shore-parallel currents typical of such coastlines. The shore at the extreme western end of Lake Ontario where the proposed Skyway outfall would be situated, curves rather abruptly from a roughly northeast-southwest orientation through about 120° to roughly north-northwest - south-southeast direction, forming an open embayment. The lake bottom at both locations is similar and the gradient from shore to 10-m depth is almost identical; however, the slope increases beyond 10-m at the Mid Halton site, and decreases for similar depths at the Skyway location. The horizontal distance between the 10-m and 20-m contours at Mid Halton is about 750-m. At the Skyway location the distance between the 10-m and 20-m contour is over twice this amount, and south of the Skyway location the 20-m depth contour swings offshore even more; increasing the offshore distance from about 2.6 km to a distance of over 4.6 km, further impounding the proposed outfall area; thereby diminishing currents which are the mechanism whereby outfall pollutants would be dispersed.

The shoreline in the area of the proposed Skyway outfall is predominantly parkland. The only significant sandy beach on the western end of the lake extends about 9 km south-southeast from a point a kilometre or so north of Skyway WWTP. In addition, Burlington and Hamilton municipal drinking water intakes both lie within a few kilometres of the site. As mentioned above the curvature of the shoreline and gradual offshore slope of the lake bottom in the area impede any strong currents which would be effective in efficiently dispersing outfall contaminants. Moreover, the sheltering effect of the north-south shore virtually eliminates generation of locally wind-induced currents for winds from any direction in an arc extending counter-clockwise from about 40° to about 180°. This includes the prevailing westerly winds usually associated with fair weather. The area is exposed to easterly winds, usually associated with storms, and often quite strong, which have the potential to generate strong alongshore currents at depth, but also drive surface waters onshore. Easterly winds travelling over a fetch of about 200 km generate large waves capable of causing substantial resuspension of sediments which include sand near shore, changing to silt-sand, then silt-clay with increasing distance offshore (Rukavina, 1969). Under the influence of weak currents during periods of calm weather lasting several days, contaminants which adsorb onto fine sediments, or settling organic material, could accumulate only to be reintroduced into the water column at higher concentration during wind events.

In consideration of these water quality concerns and with a long-term interest in sustainable use of nearshore waters, the National Water Research Institute (NWRI) undertook a comprehensive study of the physical characteristics of the area near the proposed outfall in the hope of providing scientific data and results needed by the municipal engineers concerned with its location and design. The first phase of the study was to search NWRI data archives for historical data from previous studies in the area that may have been conducted. The second phase was to plan and conduct our own measurements in the area in order to describe the physical processes important to outfall placement in the best way possible, and at the same time compliment any information from the historical work to the best advantage.

The search of historical data turned up a number of studies conducted in western Lake Ontario west of 79° 40' west longitude, and dating back to 1969. Some of the studies used moored electronic current meters (Eulerian measurements) and a few used position tracking of drogued drifting buoys (Lagrangian measurements) to measure the currents. Only experiments yielding credible data of substantial duration for locations near the proposed outfall were considered for additional analysis. Notable among the records reviewed were the current data files for an experiment conducted in 1982-83 by the Ontario Ministry of the Environment (MOE) wherein currents were measured at a single depth at each of four locations around the western end of Lake Ontario, including one site very close to the proposed outfall location. The results of extensive analysis of data from this study, including chemical and biological data, were presented in "Impact of Hamilton Harbour on western Lake Ontario" (Poulton et al, 1986). In addition to the wealth of data available from the Ontario Ministry of the Environment studies, NWRI data at two locations from 1990 and 1992 were also chosen for detailed analysis.

Some of our statistics and methods of presenting them (e.g., wind and current rose-plots) are similar or identical to those in the MOE report; however, they are products of our own analysis and were included for ease of comparison across our larger database. We included additional calculations not typical of previous NWRI climatological reports, such as a persistence factor which was included in the MOE report for 1982-83 data and was considered to be a potentially useful parameter for the other data as well. We also included calculations aimed at identifying and quantifying periods of very low currents, often referred to as stagnation currents. In order to quantify what might be considered stagnant currents we have chosen a duration of twelve hours or longer to be a significant period for currents to remain stagnant. Poulton et al, in their report on 1982 Lake Ontario data, chose 5 cm/s as the threshold speed below which currents were considered stagnant. Four to 5 cm/s is also typical of the minimum detection threshold of the savonius rotor type current speed sensor on the AAnderaa current meters used to record these data. Data after 1990 were collected with current meters utilizing acoustic phase-shift sensors to determine current velocity. Since there are no moving parts, the lower speed measurement threshold is only about 1 cm/s. The threshold of stagnation currents for these data was chosen to be 3 cm/s, to be on the conservative side. Based on these selection criteria, the frequency of stagnation events was determined for increasing duration in 12-hour increments. For the 1982-83 data, the closest station to the proposed Skyway WWTP outfall site, had the highest occurrence of significant stagnation periods, at 77% of the time. This station also recorded a single instance of stagnation lasting fourteen days, while at the other three stations, the longest stagnation period was nine days. Since these measurements spanned the typically higher energy winter period, where many later measurements did not, it was somewhat surprising that stagnation appeared to be so

prevalent; however, improved instrument sensitivity, and lower measurable velocity threshold for later experiments no doubt contributed significantly to much of the discrepancy with later work.

While lacking the spatial extent of the MOE experiments the measurements from 1990 and 1992 each dealt with two levels in the water column, thereby providing insight into the effects of stratification on mixing processes. Episodes of upwelling and downwelling could be readily identified in these data records. Prevailing winds from the west and north-west, even at modest velocity were found to be capable of generating upwelling of cold subsurface waters along the western and north-western shore of western Lake Ontario. Downwelling of warmer surface waters was associated with winds from the east. Such winds are often associated with storm systems and tend to be somewhat more energetic than fair-weather winds.

A stable stratified system may allow contaminants released near the bottom to reach higher than normal concentrations in a low energy regime isolated by a thermocline from wind-induced mixing in the surface layers. Upwelling and downwelling are important perturbations to the stable system because they can cause a contaminated water mass to disperse harmlessly into the surface waters or, less favourably, to spread into nearshore areas before adequate mixing has occurred. Thus, it was important to quantify these effects in order to determine their importance.

Lagrangian experiments employing satellite-tracked drifting buoys were conducted on several occasions in 1989 from a release point just off the Burlington Ship Canal. Data from these experiments were used to calculate mean and root-mean-square velocities for individual trajectories, plus ensemble-averaged longitudinal and transverse velocities from which turbulent dispersion coefficients were computed.

Following a review of the analysis of historical data, measurements of physical parameters were conducted in western Lake Ontario between May 23, 1996 and October 21, 1997. Recording instruments measuring current, water temperature, and several meteorological parameters were deployed in the western end of Lake Ontario. Single sensor current meters were deployed at stations around the shore, usually at two levels per station to capture variations in vertical current and temperature distribution. Acoustic Doppler Current Profilers (ADCP) capable of sensing currents at numerous levels in the water column were also deployed at one or two locations during portions of the experiment. During the summer of 1997 instrumentation was increased including the addition of two fixed temperature profile (FTP) stations which consisted of a number temperature logging recorders mounted at depth intervals along a taut-wire mooring. A heavily instrumented offshore reference station was established 10 km east of the Burlington Ship Canal to record current, temperature, and meteorological parameters. Also, three intensive two-week study periods were included, during which launch based vertical temperature profiling and longitudinal current profiling measurements were made along three shore-perpendicular transects which converged at the offshore reference station. Satellite-tracked drifters were deployed, usually two per day, from a location about a kilometre offshore at the extreme western end of the lake.

The 1996-97 data provided the basis for detailed coastal transport calculations the results of which are summarized very briefly below. Coastal processes differ substantially between summer and winter primarily resulting from the presence of thermally generated vertical density gradients (stratification) in summer as opposed to near isothermal conditions in winter.

In summer, alongshore currents are stronger than offshore currents with a primary energy peak at a period of 10-12 days corresponding to the large-scale response to meteorological forcing. Another major peak is located near the inertial period (about 17 hours). Winds toward the north-east induce alongshore currents causing offshore drift in the surface levels indicating upwelling of bottom waters. Westward (onshore) winds induce typically stronger currents and often generate downwelling of surface waters. The root-mean-square (RMS) values of fluctuating currents show variable conditions in the surface levels and nearly homogenous conditions in the middle and bottom depths. Upwelling episodes show less turbulent activity due to the reduction of near-inertial oscillations. During the downwelling events turbulence intensity increases in the bottom layers accompanied by a downward shift of the thermocline.

During summer the mean flow kinetic energy is significantly higher than turbulent kinetic energy, and average alongshore exchange coefficients are higher than cross-shore values during the summer season, but upwelling events reduce both alongshore and cross-shore turbulent exchange coefficients. Upwelling events show decreased static stability and increased vertical current shear resulting in higher vertical exchange coefficients. A decrease in vertical exchange coefficients is typically associated with downwelling events.

Winter currents are mainly characterized by a 4-day period oscillation associated with large-scale wind forcing. In western Lake Ontario the mean currents are mainly toward the west; however, there are typically frequent episodes of alongshore and cross-shore current reversals. Fluctuating currents are less significant than in summer and are nearly isotropic in the bottom layers. Alongshore exchange coefficients are slightly higher than cross-shore values near the surface, but become closer to equal with increased depth.

Analysis of Lagrangian drifter trajectories from the 1997 studies yielded 35 drifter days of observations at typically 6-m depth. The analysis was performed in the same manner as for the 1989 data previously outlined, and yielded comparable values for zonal (along the mean current direction) and meridional (perpendicular to the mean direction) mean velocities (5 cm/s and 1 cm/s, respectively). Zonal and meridional root-mean-square velocity values were 7 cm/s and 6 cm/s, respectively for the same observations. Actual values appeared to be strongly dependent on the duration of the observations.

Coastal transport modeling is an important adjunct to the experimental work. For western Lake Ontario we used the wealth of carefully scrutinized current data to synthesize transport and dispersion scenarios for actual and hypothetical effluent rates discharging at different locations under different conditions. Coastal transport models were developed to calculate effluent concentrations and dilution ratios for E. coli. Locations north and south of the Hamilton Harbour ship canal were modeled. Potential may exist for other locations south and east of the canal in the City of Hamilton. The modeling assumed an effluent of well treated sewage with effective disinfection.

- Near-field dilutions obtained from a mixing zone model show that for treated effluents with existing discharge conditions (2 m^3/s) at the proposed outfall site at Burlington, the dilution ratios are in the range of 13:1 to 28:1 for weak to moderate currents during summer

stratification. Winter dilution ratios increased to 21:1 for weak currents and to 96:1 for moderate currents.

- By shifting the proposed Burlington outfall location to 2 km from the shore initial dilution increased marginally.

- With the proposed Burlington outfall location and discharge conditions no far-field contamination is observed near the beaches or at drinking water intakes of Hamilton and Burlington for typical summer and winter current regimes.

- With increased treatment capacity to 6.94 m^3/s (representing the combined flow from Burlington and Hamilton outfalls) the near-field dilution ratios decreased considerably. However the concentrations are below the prescribed exceedance limits of water quality.

- The far-field models have not shown any significant contamination near the beaches or water intakes even with increased treatment capacity of 6.94 m^3/s (representing the combined flow from Burlington and Hamilton outfalls) for a typical summer current distribution.

Table of Contents

1. Introduction

The Laurentian Great Lakes - Superior, Michigan, Huron, Erie, and Ontario - and their interconnecting channels form the largest fresh water system in the world. This great watershed drains to the Atlantic Ocean through the St. Lawrence River, by which the tiny sailing ships of the early European explorers first reached Lake Ontario in the 1600's. Although this was the onset of modern development in the watershed, the area's vast resources had already long been enjoyed by the Iroquois and Algonquin Indians; by the Woodland Indians before them; and by primitive Plano tribes before them, as far back as 7000BC.

White settlements sprang up all around Lake Ontario, usually at the mouths of rivers which served as a haven for larger vessels from lake storms, and provided the simplest passage inland for the canoes and small craft of traders and early settlers. A number of factors have favoured growth around the western end of Lake Ontario in particular. Strategic access to the developing upper lakes regions; proximity to large areas of fertile farmland; a climate moderated by a combination of its southern latitude and proximity to both Lake Erie and Lake Ontario; and the presence of two large, deep, naturally protected embayments, one on the north-western shore, and one at the extreme western end of the lake which respectively became Toronto and Hamilton harbours, are some of the important natural factors. The area attracted many British Empire Loyalists, especially from New York, and Pennsylvania when what was to become the United States moved toward independence. Many of these settlers were ambitious and skilled farmers, business people, and manufacturers who contributed greatly to the area's development. With U.S. independence, a political border was established, splitting Lake Ontario in two from the Niagara River to the St. Lawrence River, and separating the State of New York from Upper Canada which later became the Province of Ontario.

In the mid 19th century, ports all along the north shore of Lake Ontario were bustling with ships carrying timber and other resources back to England and Europe. Ports east of York - now Toronto - suffered a decline when the area forests were depleted, but in the area around western Lake Ontario - the area now often referred to as the Golden Horseshoe - the foundations were established for what has become the largest metropolitan centre in Canada, and the hub of Canadian business and manufacturing.

Originally, only Lake Ontario could be accessed from the Atlantic by ship because of the hundred-metre difference in elevation between Lake Ontario and Erie which manifests itself in the form of impassable rapids and the spectacular Niagara Falls in the Niagara River. The first Welland Canal opened in 1833 allowing ships to traverse to and from Lake Erie through a series of 40 locks over its 44 km length across the Niagara Peninsula west of the Niagara River. The present canal accomplishes the task with just 8 locks, 3 of which are twinned to permit two way traffic.

The Welland Canal contributed greatly to the development of the steel industry in Hamilton, even though the first foundries were built to supply steel for the first railways, because both iron ore and coal have to be brought in from distant mining areas. Hamilton mills still account for over half of Canada's steel production, supplying an ever growing manufacturing community in

the Golden Horseshoe area, along with export markets around the globe. Since the opening of the St. Lawrence Seaway in 1959, deep draught ocean-going freighters can sail to any major port on the Great Lakes thanks mainly to new channels and locks at locations along the St. Lawrence River previously too shallow or treacherous for large vessels to pass. This has only served to expand development on western Lake Ontario by providing economical transportation to the ports of the world.

Communities on the shores of Lake Ontario have long relied on the lake as a potable water source; a vast recreational playground; and a convenient place to dispose of waste of all kinds. Although it is the smallest of the Great Lakes in extent, with a surface area of 18,960 sq km, it is large enough that little serious concern was given to the long-term effects of waste disposal on the lake until the past fifty years or so. With a mean depth of 90-m and a volume about three and a half times that of the second largest of the lakes - Lake Erie - Lake Ontario endured at least the visible effects of indiscriminate disposal practices surprisingly well. Being the lowest in the chain of lakes, water use practices which influence the persistent water quality in any of the lakes ultimately affects water quality in Lake Ontario, since water from throughout the system eventually ends up a part of the approximately 6500 m^3/s discharge of the Niagara River into Lake Ontario, accounting for about 84% of Lake Ontario's 7700 m^3/s discharge into the St. Lawrence River. Residence time for the lake works out to about six years.

Today the Lake Ontario basin is home to approximately 7.5 million residents, of which over 5.4 million reside in Ontario. The Golden Horseshoe area now forms an almost unbroken urban landscape from Clarington, east of Toronto, to St. Catharines near the Niagara River, and is home to over 4 million residents. These communities turn to Lake Ontario almost exclusively for both water supply and wastewater disposal. Intakes and discharges alike are typically installed in a narrow band of the lake extending, at most, a couple of kilometres offshore. Improvements in water purification, and sewage treatment technology have, to some degree, offset the deleterious effects of increased development; however, current treatment technology seems to be nearing its practical design limit, while the demand for clean water, and the need for suitable waste disposal facilities continue to rise at an ever increasing rate.

In the past, because the volumes of waste effluent were low enough, and separation between wastewater outfalls and water intakes was sufficiently large, even high waste concentrations were usually diluted to acceptable levels through mixing before reaching any water intake. Also, natural purification processes, such as biological degradation of harmful components, adsorption and settling of persistent toxins into sediments, etc., could assimilate the volumes that were introduced. While some local degradation often occurred, mid-lake water quality remained high, enabling nearshore-offshore exchange processes to restore nearshore water quality. With the recent enormous growth in population, the volume of wastewater has also risen to the extent that even mid-lake water quality has declined, thereby diminishing the cleansing effect on the increasingly stressed nearshore zone.

One factor that has helped to minimize the degradation of the extreme western Lake Ontario waters has been that the wastewater treatment plants of Burlington and Hamilton discharge into Hamilton Harbour. This, of course, has been greatly detrimental to water quality in the harbour.

The Hamilton Harbour Remedial Action Plan (RAP), formulated through a tremendous amount of effort by a wide variety of government, private sector, and community participants, provides the framework for numerous initiatives aimed at restoring, and maintaining the harbour environment. RAP guidelines call for further reductions in contaminant loading over time, while continued development in Hamilton Wentworth and Halton Regions calls for substantial expansion of wastewater treatment facilities to meet the additional demand. For facilities discharging into Hamilton Harbour it will likely be very difficult to meet RAP loading targets and still keep up with future demands using foreseeable improvements in treatment technology.

The South Halton Wastewater Master Plan is the basis whereby the wastewater treatment facilities for the main urban areas of Burlington, Bronte, and Oakville are kept up to date in terms of both capacity and treatment technology. It is the source for much of the information presented here, that is specific to Halton wastewater treatment and facilities. This plan, like the RAP, evolves out of a process which involves a wide variety of experts and members of the community, including several groups and individuals involved in RAP. Current plans are formulated to meet projected needs to 2011 as determined from studies conducted in the mid 1990's. Projections to 2011 based on development estimates from the study indicate a required increase in the mean flow capacity at the Skyway Wastewater Treatment Plant (WWTP), which handles the wastewater from Burlington, Aldershot, and part of Bronte west of Bronte Creek, from the present 93,000 m^3/day to 140,000 m^3/day .

A list of 40 alternatives for providing wastewater services to South Halton was prepared by a special study group with input from Halton's Technical Agencies Committee and a Stakeholders Group. By early 1996 this list had been reduced to 5 alternatives that were felt to best meet the selection criteria. Two of the alternatives involved retaining the Skyway treatment plant at existing capacity, and directing flow in excess of its rated capacity to the Woodward Avenue WWTP in the Region of Hamilton Wentworth; a plant which also discharges into Hamilton Harbour. Further assessment of these alternatives failed to resolve the question of whether or not the Woodward Avenue facility would have the capacity to handle the increased load within the required time-frame. In addition, the cost of implementation, and strong indications that the scheme would fail to meet RAP loading targets, all led to the ultimate rejection of these alternatives.

The preferred alternative of the original short list called for expansion of the Skyway and Mid Halton treatment plants, with Skyway continuing to discharge into Hamilton Harbour, while maintaining "Best Available Technology Economically Achievable" (BATEA) effluent limits. The other two remaining alternatives were also based on these expansions; however, one scheme would add tertiary treatment at Skyway to meet RAP loading targets, and the other would relocate the plant discharge from the harbour into Lake Ontario. The improvement to discharge quality that one could reasonably expect from upgrading to tertiary treatment - a very costly option - might still fail to prevent an unacceptable increase in nutrient loading to the harbour at the projected effluent volume. After meetings providing input from a number of agencies and the public, the alternative involving relocation of the outfall was deemed most desirable.

The rationale for supporting discharge into the lake, over and above the desire to get it out of the harbour, has a basis in the intuitive notion that the comparatively huge volume of the lake and its anticipated higher energy dynamics would much more effectively disperse the effluent. In fact, mixing zone studies were conducted prior to the expansion of the Oakville Southwest-Mid Halton WWTP for its combined outfall, that showed chemical and bacteriological parameters lower than Provincial Water Quality Objectives at a distance of about 900-m from the source for an average flow rate of 195,460 m^3/day (Anderson, 1985). Not only is this flow rate substantially greater than the projected discharge for Skyway (by almost 40%), but the updated Skyway plant would maintain year-round non-toxic effluent quality through nitrification, and non-toxic disinfection, which would likely reduce the size of the effective mixing zone even more.

Placement of an outfall from Skyway WWTP in Lake Ontario is subject to physical constraints imposed by other area features (Figure 1.1). A minimum 3 km distance from a potable water intake, and minimum 900-m from shore would apply. This would substantially restrict the area where the outfall could be located, since the water intake for Burlington is situated about 4 km from the Skyway plant. The Burlington Ship Canal, which provides access between Lake Ontario and Hamilton Harbour, is situated about a kilometre south of the Skyway WWTP. The shipping lanes leading from the open lake to the canal are deemed to form a southern boundary to the practical placement zone for the outfall.

Despite the favourable inferences from the planning studies done for the Mid Halton outfall there are sufficient differences between the Mid Halton site and the proposed Skyway outfall site to warrant a very careful look at the specific characteristics of the Skyway site. The most striking differences, and ones that could cause vastly different dynamics at the two locations, are differences in topography and bathymetry. Mid Halton outfall is situated on a stretch of shoreline that is, at least in the gross sense, relatively straight; and, therefore, subject to substantial shore-parallel currents typical of such coastlines. The shore at the extreme western end of Lake Ontario where the proposed Skyway outfall would be situated, curves rather abruptly from a roughly northeast-southwest orientation through about 120° to roughly north-northwest - east-southeast direction, forming an open embayment. The bottom at both locations is relatively featureless and the gradient from shore to 10-m depth is almost identical; however, the slope increases beyond 10-m at the Mid Halton site, and decreases for similar depths at the Skyway location. The horizontal distance between the 10-m and 20-m contours at Mid Halton is less than half that at the Skyway location. South of the Skyway location the 20-m depth contour swings offshore even more; increasing the offshore distance from about 2.6 km to a distance of over 4.6 km, further impounding the proposed outfall area.

The shoreline in the area of the proposed Skyway outfall is predominantly parkland. The only significant sandy beach on the western end of the lake extends about 9 km south-southeast from a point a kilometre or so north of Skyway WWTP. In addition, Burlington and Hamilton municipal water intakes both lie within a few kilometres of the site. As mentioned above the curvature of the shoreline and gradual offshore slope of the lake bottom in the area impede any strong currents which would be effective in efficiently dispersing outfall contaminants. Moreover, the sheltering effect of the north-south shore virtually eliminates generation of locally wind-induced currents for winds from any direction in an arc extending counter-clockwise from about 40° to about 180°.

This includes the prevailing westerly winds usually associated with fair weather. The area is exposed to easterly winds, usually associated with storms, and often quite strong, which have the potential to generate strong alongshore currents at depth, but also drive surface waters onshore. Easterly winds travelling over a fetch of about 200 km generate large waves capable of causing substantial resuspension of sediments - which include sand near shore, changing to silt-sand, then silt-clay with increasing distance offshore (Rukavina, 1969). Under the influence of weak currents during periods of calm lasting several days, contaminants which adsorb onto fine sediments, or settling organic material, could accumulate only to be reintroduced into the water column at higher concentration during wind events.

In consideration of these concerns and others raised in conjunction with a long-term interest in sustainable use of nearshore waters, we at NWRI decided to undertake a detailed study of the physical characteristics of the area near the proposed outfall in the hope of providing knowledge helpful to those charged with the task of deciding if the outfall would be moved; and if so, to those concerned with its location and design. The first phase of the study was to search NWRI data archives for existing relevant data from any previous studies that may have been conducted. The second phase was to plan and conduct our own measurements in the area to describe the physical processes important to outfall placement in the best way possible, and at the same time compliment any information from the historical work to the best advantage.

A search of NWRI data archives produced a number of current records acquired during the last three decades or so. A few of the records were of sufficient length and were obtained at locations close enough to the proposed outfall site to warrant detailed examination. They are discussed in detail under Historical Data below.

The core physical measurement phase of the study covered the period from May 1996 to October 1997, and provided time-series data from various deployments of moored current meters, moored Acoustic Doppler Current Profilers (ADCP), moored recording temperature sensors; and buoy or tower mounted meteorological instruments. These measurements were augmented in the spring-summer-fall periods by periods of current measurements using drogued launch-tracked (1996) and satellite-tracked (1997) drifting buoys released in the area of the proposed outfall; by horizontal transects of current measurements using a vessel-mounted ADCP; and by vertical temperature profiles taken from launches.

As mentioned earlier, understanding the physical processes in the coastal area near the proposed Skyway WWTP outfall is the main concern of the work described in this report; however, a topic of broader interest, and one which will be increasingly important with further urban development in the future, is the water movements in the entire western ten or so kilometres of the lake, where the restricting topography of the tip of the lake basin and its orientation to lee of the prevailing wind may create less favourable transport and dispersion conditions than one could expect to find in the nearshore zone of the rest of the lake. In order to understand what occurs at the outfall site, information from a much wider area is required. While the measurements made during these experiments do focus on the proposed outfall site, the data describe, in some detail, the circulation in the whole western end of Lake Ontario out to about ten kilometres east of the Burlington Ship Canal.

The complex exchange between Hamilton Harbour and Lake Ontario through the Burlington Ship Canal can, under certain conditions, spread harbour water into the area of the proposed outfall, with whatever water quality implications there might be at the time. This exchange process has been the subject of numerous studies in the past (Dick and Marsalek, 1973; Ontario Ministry of Environment, 1974; Poulton et al, 1986; Wu et al, 1996) and was the subject of measurements for a modeling study which were made concurrent with the experimental work described here (He and Hamblin, 2000); and, therefore, is not discussed in detail here. Our objective here is to illustrate the main current characteristics which ultimately determine the transport and diffusion of contaminants; and the temperature characteristics which, as in the case of well developed thermal stratification, profoundly affect the circulation regime itself. Where possible, local wind data are presented along with current and temperature data to provide an estimate of the wind's influence on specific dynamic events in the lake.

2. Historical Data

2.1 Introduction

All of the data archived in the main current meter database at NWRI, from stations in the main body of Lake Ontario west of 79° 40' W longitude, were reviewed. Numerous satellite-tracked drifting buoy trajectories resulting from deployments near the proposed outfall site were also considered. Details of the available data, and those files ultimately analysed, are summarized in Table 2.1, and discussed in more detail below. Figure 2.1 is a map of the area showing key features including instrument locations, and the drifter deployment site.

One of the best current data sets considered, in terms of spatial and temporal coverage, was collected at four sites by the Ontario Ministry of the Environment in 1982-83, and subsequently archived at the Canada Centre for Inland Waters (CCIW). A comprehensive report, "Impact of Hamilton Harbour on Western Lake Ontario" (Poulton et al, 1986), includes results from the analysis of data from these four current meter stations. Readers are strongly encouraged to consult that report for a detailed analysis of a broad range of physical, biological, and chemical parameters. Some of the statistics and methods of presenting them (e.g., wind and current rose-plots) presented here are similar or identical to those in the MOE report. They are products of our own statistical analysis and have been included for ease of comparison across the larger database we are dealing with. We have included additional calculations such as a persistence factor which was included in the MOE report for 1982-83 data and was considered to be a potentially useful parameter for the other data as well. Those comparing 1982-83 results in the two reports are cautioned to carefully observe value ranges and data periods when dealing with what may otherwise appear to be identical presentations.

2.2 Database

All time-series current data from NWRI archives for Lake Ontario stations west of 79° 40' W longitude were reviewed. The qualifying data included files collected from 1969 to 1992, and are summarized in Table 2.1. Data collected prior to 1982 were not analysed because of short duration and/or suspicious quality. After careful screening, the MOE data from 1982-83, and NWRI data from 2 depths at a single location from each of 1990 and 1992 were chosen for detailed analysis.

The four 1982-83 moorings provide quite good horizontal resolution of the western tip of the lake, but the single instrument at each site provides no direct insight into vertical structure. Also, the instrument depths varied, with two instruments at 3-m, and one at each of 4 and 6-m. This could make spatial comparison of data difficult; however, some differences that we show among the stations would likely be enhanced if all were at the same depth. The records span almost a full year from May 10, 1982 until mid to late April 1983, except for station 176. The single moorings in each of 1990 and 1992 both had instruments at 5 and 10-m depth, providing some information about the vertical current and temperature structure. These locations correspond

reasonably well with 1982 moorings; so, while we cannot draw specific comparisons between measurements widely separated in time, we feel that these data show a number of additional features sufficiently well to warrant their inclusion in this analysis. The proximity of stations 174 and 13 to the proposed Skyway outfall site makes further analysis of these past data records quite relevant.

Current meter data include time-series current speed and direction data plus water temperature at instrument depth. Where possible, nearby concurrent meteorological data are also included in the analysis. Time-series meteorological records include wind speed and direction, air temperature, surface water temperature, and relative humidity. For this analysis, only wind stress computed from wind velocity data is presented.

A variety of sample periods typically ranging from ten minutes to an hour are represented in NWRI archived current and meteorological data. The analyses presented here were performed on hourly time-series with samples centred on the hour, as generated from original data.

In addition to data from moored current meters and meteorological stations, results of the analysis of trajectories of satellite-tracked drifting buoy released about a kilometre east of the proposed outfall site in 1989 are also included in this discussion. The drifting buoys were equipped with "roller-blind" type drogues suspended at about 3.5-m depth. Twelve releases from May to October 1989 were analysed. They are summarized in Table 2.1. Unfortunately, none of these experiments included concurrent deployments of both current meters and drifting buoys. Drifting buoy data consisted of asynchronous series of time and position with sample intervals ranging from a few minutes to several hours. A computer program employing a polynomial function which preserves original values (Akima, 1972) was used to generate the hourly time-series which formed the basis for further analysis.

2.3 Analysis

Rose histograms, vector 'stick-plots', temperature plots, some progressive vector diagrams, and the calculations associated with these and some of the statistical summaries were produced by custom Unix-based programs. Maps, speed and stagnation period histograms, some progressive vector diagrams, and variance ellipse diagrams, along with many of the related calculations, were generated by a variety of PC graphic and spreadsheet software.

Where time-series output, illustrations, and values are based on other than hourly samples, it is so stated. In some cases the data have been averaged to a longer sample period; in others, only values at some fixed interval are displayed to improve clarity. Both wind and current vectors are always shown as direction to.

Three types of analysis are presented here: 1) graphic and statistical summaries, which cover whole record periods, and are presented in similar format for all data records used; and 2) specialized analysis directed toward a specific phenomenon or event, or employing specialized or enhanced techniques to achieve a specific result based on the time-series current and temperature

data, and 3) specialized analysis of Lagrangian drifter data. In general, Tables 2.1 and 2.2, Figures 2.1 through 2.8, and related text fall into category 1. Figures 2.9 through 2.18 and their related text better fit category 2), and are the results of an effort to look at the data more intensely, from a new perspective, or at a different scale. Table 2.3, Figures 2.19 through 2.21, and related text fall into category 3).

2.4 Descriptive Summaries

Table 2.1 summarizes all of the data showing the station number used in this report (corresponds to NWRI mooring number), sensor depth, water depth, and a time bar indicating the period over which data was collected. Instrument stations, drifter release locations, and a few local features are shown on the map of the western end of Lake Ontario in Figure 2.1. Some of the statistical methods used to summarize the data are consistent with previous NWRI limnological summaries (Jordan and Bull, 1977). While specific format and scale vary widely, rose-plots, vector 'stick-plots', progressive vector diagrams, and time-series temperature plots like those presented here have become standard tools for looking at features of large time-series data records.

Table 2.2 summarizes several statistical parameters based on whole data records. Where gaps existed in the data, parameters have been determined only from values present, with no interpolation. Users are cautioned to verify that data records are from the same period and are of equal length, before making absolute comparisons in statistics. The persistence factor (resultant vector speed/mean scalar speed for same period) shown in Table 2.2 was given in the MOE report for 1982-83 data, and has been included here for all stations.

The rose histogram plots tabulate hourly wind and current data for 1982-83 (Figure 2.2), and for 1990 and 1992 (Figure 2.3), into speed and direction ranges. Vector directions are sorted into eight 45-degree sectors (directions are "towards" for both wind and current in all types of vector plots). Speed ranges are defined as 0 to 3, 3 to 7, and greater than 7 cm/s for current. For wind the numeric range limits are the same but units are metres per second. Different speed ranges are indicated in the drawings by the indicator's line width as shown in the key. The percentage of the total data record comprised of values of a given speed and direction is shown by the radial length of each segment of indicator line with respect to the radial percentage scale. The rose-plots are drawn on a station map with shaded pointers showing the station represented.

Figures 2.4 and 2.5 show progressive vector diagrams for 1982-83, and for 1990 and 1992, respectively. These types of diagrams are created by drawing the hourly vectors with the start of each hour's vector joined to the end of the previous hour's vector. Vectors point in the correct direction and are scaled proportional to the displacement that would be achieved by maintaining the represented speed for an hour. The completed plot is a scaled representation of the actual displacement a free moving particle would undergo if subjected to the velocity regime defined by the current record. Each page shows an appropriate displacement scale and a key map indicating the stations represented. Naturally, such a representation created from a velocity record measured at a fixed point will bear little relation to actual displacements of particles subjected to the physical restraints and spatial variability of the real lake basin, but it does serve to illustrate

characteristics of the velocity at the point of measurement, such as directional persistence, rotations, periodic meandering, etc. Note that locations of the progressive vector diagrams segments on the page, including the relative location of subsequent segments of the same record after a gap in the data, are not to true scale.

Figures 2.6, 2.7, and 2.8 show time-series wind stress (unfiltered), filtered current vector 'stick plots', and temperature vs. time plots for entire data periods in 1982-83, 1990, and 1992, respectively. For current stick-plots a low-pass digital filter with 18 - 24 hour cut-off was applied to the data to eliminate oscillatory motions at frequencies higher than the inertial frequency (about 17 hours for Lake Ontario). Elimination of the high frequency oscillations associated with turbulence, gives a clearer picture of longer period motions typically associated with larger scale forcing agents like basin-wide circulation phenomena, and significant meteorological events. The stick-plots in these figures show every second hourly vector in each of the series to retain some semblance of graphic quality at the greatly compressed time-scale used.

2.5 Specialized Analysis

Current speed distribution is plotted separately for each sensor depth at each station in Figures 2.9 (1982-83 data) and 2.10 (1990 and1992 data). For long records covering a full range of seasonal and meteorological conditions, such plots provide a fair indication of the current speeds one might expect to find at a particular location, at least for comparable conditions. The number of instances of hourly current speeds in 1 cm/s ranges from 0 to 20 cm/s were plotted. Although lower speed values have been reported separately, readers are cautioned to avoid drawing any firm conclusions about the relative distribution of values which may fall below the sensing threshold of speed sensors used to collect the data. The threshold for 1982-83 data is likely about 5 cm/s; and for 1990 and 1992 it would be down around 1 cm/s. This topic is dealt with in more detail below, in the discussion on stagnation speeds. The cumulative percent of readings is included on each of the speed distribution plots. This curve provides another quick indicator of the relative importance of stronger currents at a site. As an example, if one compares the graphs for stations 174 and 176 in Figure 2.9, the velocity distributions show a very high instance very low current speeds at station 174, with very few instances of speeds above 10 cm/s, while at station 176 the spike at low speeds is absent and an almost even distribution exists for speeds up to about 13 cm/s. The percent cumulative occurrence curves for these two stations indicate that readings below about 6 cm/s account for ninety-five percent of all values at station 174, while at station 176 speeds of 6 cm/s and below account for less than forty-five percent of all readings. Stations 175 and 177 produce profiles which show distributions somewhere between these two extreme examples. Similar profiles for 1990 and 1992 data indicate broad peaks at low values with relatively few higher speeds, probably owing to the fact that the records covered periods during which thermal stratification tended to isolate lower depths from the winds influence. Most of the late-fall, winter, spring isothermal period which is also a period of relatively strong wind events and better air-water energy coupling was missed in the 1990 and 1992 experiments. Somewhere in the hierarchy of factors influencing measurements taken in the different years, lies the effect of improved instrument sensitivity in the 1990 and 1992 records.

Extended periods of consistently low currents, referred to as stagnation currents, can lead to serious accumulation of contaminants around outfalls. When the volume of water passing the outlet drops, not only is simple dilution reduced, but vertical and lateral diffusion are greatly diminished and any thermal stratification present may inhibit the dispersion processes. The actual current speed and contaminant loading rate determine local concentrations, and the duration of the stagnation period determines the spatial extent of the contaminant 'patch'. The ultimate severity of the event obviously depends on these factors plus the proximity of the outfall to shore and sensitive water users (recreation areas, water intakes, wildlife, etc.). We have attempted to arrive at some reasonable estimate of the frequency and duration of current stagnation in the western end of Lake Ontario from the current data analysed. The results are shown in Figures 2.11 and 2.12 for 1982-83, and 1990 and 1992 data, respectively. In order to quantify what might be considered stagnant currents we somewhat arbitrarily chose a duration of twelve hours or longer to be a significant period for currents to remain stagnant. Poulton et al, in their report on 1982 Lake Ontario data, chose 5 cm/s as the threshold speed below which currents were considered stagnant. Four to 5 cm/s is also typical of the minimum detection threshold of the savonius rotor type current speed sensor on the AAnderaa current meters used to record these data. A further complicating factor enters into interpretation of data from instruments using this type of sensor. Since the savonius rotor is not sensitive to the direction of the flow, readings 15% to 25% above true speed may be obtained in instruments mounted close to the surface, due to the 'pumping' action of wave induced oscillatory motion. This speed enhancement effect is not likely to come into play at speeds down around instrument threshold, since winds strong enough to generate waves large enough to influence instruments several metres below the surface would, in all probability generate (non wave-related) currents well above threshold. The 1990 and 1992 data were collected with Neil Brown current meters utilizing acoustic phase-shift sensors to determine current velocity. Since there are no moving parts, the lower speed measurement threshold is only about 1 cm/s. The threshold of stagnation currents for these data was chosen to be 3 cm/s, to be on the conservative side. Based on these selection criteria, the frequency of stagnation events was determined for increasing duration in twelve-hour increments. The fraction of the total duration of the data record spent in stagnation, according to the above definitions, was also determined, and is presented for each station as a percentage on the line headed '% Time in Stagnation' in Table 2.2. Station 174 has the highest occurrence of significant stagnation periods, at 77% of the time. It is also closest to the proposed Skyway WWTP outfall site. Station 13 (1990) was less than a kilometre from 174, but recorded significant stagnation periods only 38% of the total time. All else being equal one would expect the opposite difference, since station 174 was mounted closer to the surface than station 13, and was operated throughout the high energy winter period, where station 13 was not. Differences in instrument sensitivity, and the lower threshold used for station 13 calculations, may account for much of the discrepancy. It is also interesting that station 174 recorded incidents of stagnation lasting fourteen days, while at the other three stations in the 1982-83 experiment, the longest stagnation period was nine days (station 177).

While mean currents largely determine simple dilution rates and transport characteristics, variations in currents due to turbulence and other high frequency perturbations can be very important in dispersing contaminants through mixing and diffusion. The variance in a data record is a measure of these variations. Vector data can be manipulated to find the direction along which

the sum of the squares of orthogonal components resolve to an x-axis lying in that direction is a maximum. Such an axis is sometimes called a 'principal axis'. Ellipses with major and minor axes respectively proportional to variance of the flow along and perpendicular to a principal axis were drawn for all current stations to provide an estimate of dispersion at each site. These are shown in Figures 2.13 and 2.14 for 1982-83, and 1990 and 1992 data, respectively. Owing to the gaps in 1982-83 data, the segments were processed independently and the results superimposed. The mean vectors for each segment are also plotted at each station, and, while scales differ, are intended to illustrate that the variance is much greater than the mean current; and hence, is much more important in determining the dispersion.

Figures 2.15, 2.16, and 2.17 are plots of current and temperature data for periods four to nine days in length, and chosen to illustrate, in some detail, one or more features characteristic of thermally stratified conditions. Each consists of a progressive vector diagram of currents, vector stick-plots of the same current data, and a corresponding plot of temperature vs. time for the same instruments. The episodes are all from 1990 and 1992 where stations had instruments at two depths, and contain examples of upwelling/downwelling, shear currents, and currents induced by internal waves. Each episode is described in some detail below. Although detailed local wind measurements were not available for the two periods in July 1990, daily velocity values from wind summaries for Toronto's Pearson Airport were used to approximate the wind field affecting the lake at that time. Comparisons with locally measured winds at times when they were available suggest that this was not an unreasonable approximation for our purposes here.

Upwelling and downwelling occur close to coastlines as part of a complex response to energy imparted to the water surface by wind drag, and are easiest to observe in temperature data, under thermally stratified conditions. This upward movement of cooler bottom water or downward flow of warmer surface water can be an important factor in the replenishment of nearshore waters, especially where contaminants are discharged below the thermocline where weak currents may fail to provide adequate dispersion in the receiving waters. Upwelling and downwelling events are more readily interpreted in data from stations with sensors at multiple depths.

Figure 2.15 illustrates conditions at station 13 over an eight-day period, July 7 to 14, 1990, which included an episode of upwelling followed by downwelling. Temperatures indicate stratified conditions, and a look back to Figure 2.7 which covers a much longer period, shows that this episode occurs on the underlying gradual summer warm-up cycle in the lake. On July 7 and 8, moderate winds with a significant component from the east appear to have forced warmer surface water into the western end of the lake, gradually elevating temperatures at both 5 and 10-m depths by about 4°C. The progressive vector diagram in Figure 2.15 indicates currents at both levels at station 13 were light and toward the south. On July 9 somewhat stronger winds, predominantly from the west, swept surface waters eastward, drawing colder bottom water into the west end of the lake at lower levels, and upward in the water column near the western shore. Currents on July 9 were very light and toward the west at 5-m depth, and toward the west south-west at 10-m. On July 10 moderate northerly winds produced little change in the thermal structure, and currents virtually died out. Beginning on July 11, light winds with a component from the east returned; southerly currents resumed; water temperatures rose about 10°C in a couple of days; and stratification between the two sensor levels vanished as downwelling

intensified, and thus, thickened the warmer surface layer. Note that currents at the two levels differed little from each other throughout this period.

Figure 2.16 is a similar plot covering the eight-day period July 22 to 29, 1990 at station 13, and illustrates some substantially different features from the earlier period. At the beginning of the period there was about a three- to four-degree gradient between 5-m and 10-m depths. Winds were light and blowing offshore. About mid-day on July 22 temperatures at both depths began to rise quite rapidly until the temperature at both depths reached about 19°C early on July 23. The surface temperature is unknown, but it seems reasonable to assume that it was not likely much higher than 19° C; therefore, we see what appears to be an episode of downwelling - an intrusion of surface water into lower depths - but without any obvious forcing mechanism, such as wind, to overcome the relatively stable stratified conditions and enable the comparatively light surface waters to descend. Somewhat higher currents than would seem likely with the existing light offshore winds at the time, suggest that the warm water was swept into the area from further up the shore to the north-east, perhaps by forces generated by internal wave action. After a few hours the 10-m temperature fell off rapidly, while the 5-m temperature remained steady, resulting in an even stronger stratification than before the episode. This situation persisted throughout the rest of the period, with the occurrence of some cyclical temperature variations of 1° to 2°C which appear synchronised at both levels, lending more support to the presence of internal waves. The currents at both levels were well coupled prior to and during the downwelling event; however, as the progressive vector diagram clearly shows, there was a marked shear between currents at the two levels after the redevelopment of stratified conditions. Continuing light offshore winds resulted in weak erratic currents at 5-m with a mean component heading roughly north-west, almost into the wind. At 10-m they maintained their almost southerly flow throughout the period then weakened and turn westward, almost onshore, on July 29. This less than spectacular period serves well to illustrate how complex the water movements can be even under light, relatively steady forcing conditions. A downwelling event such as the one described provides a mechanism whereby effluent from a source at or near the bottom can mix vertically through the entire water column during a time when stratification might reasonably be expected to trap it below the thermocline.

A third episode illustrated in Figure 2.17 presents data from station 29 during the period August 4 to 7, 1992, and includes wind data from station 9 located on the east end of the pier along the Burlington Canal. This example demonstrates similar features to those in Figure 2.16 - light predominantly offshore winds, a thermally stratified water column, and strong current shear between the 5- and 10-m levels. Station 29 was situated further offshore and in a much more open location than station 13 (see Figure 2.1); and therefore, may show some characteristics typical of open lake stations. Inertial oscillations, with a period of about 17 hours at the latitude of Lake Ontario, develop in diminishing current fields after the driving force(s) - usually wind - relax, where depth and distance from shore are sufficient to minimize frictional damping. While some of the oscillations in this example have periods in the inertial range, they could also be a result of internal wave activity, generated by the response of a stratified water body to wind forcing. These wave-related current oscillations often exhibit periods close to the inertial period (Mortimer, 1975). The brief episode presented here distinctly shows oscillations in both the temperature and current records from the 10-m depth. At 5-m, similar oscillations are visible in

the current data, but are not so obvious in the temperature record. The marked cycling of the temperature at 10-m may have been a result of vertical thermocline oscillations set up by the internal waves, causing the thermocline, with its sharp temperature gradient, to sweep up and down past the thermistor mounted on the moored current meter. Note the lack of coupling between the two current records - at times travelling in the same direction at other times in the complete opposite direction - indicating, as does the temperature record, that the water masses at the two depths were moving almost independently of one another. The progressive vector diagram shows that the mean flow over the period was indeed in opposite directions. Oscillatory motions and shear currents like those in this example, and turbulence associated with them, are very important factors in the dispersion of contaminants introduced into the nearshore zone, especially in the absence of a well defined shore-parallel current regime.

Currents along straight coastlines of large water bodies are predominantly shore-parallel, relatively strong, and typically persist for several days between direction reversals (Murthy and Blanton, 1975). Naturally, with such well defined structure, the velocities are often similar at any given time at widely separated locations along the shore, and the similarities are readily visible in parallel time-series vector "stick-plots'. By contrast, similar plots of velocity vectors from stations along curved shorelines, such as the shore at the western end of Lake Ontario often appear erratic, even if there is a shore-parallel flow, simply because shore-parallel is at different directions at each location. Since large-scale features such as shore-parallel currents are important in dissipating contaminants, it is advantageous to be able to recognize if and when they develop in an area. Also, if such gross features are more easily identifiable, other features may also become easier to recognize. Figure 2.18 is the result of an attempt to make shore-parallel currents more readily detectable in the records from 1982-83 stations 174, 175, 176 and 177. A large-scale counter-clockwise rotation is known to develop on occasion (Murthy and Miners, 1989) in Lake Ontario west of the Niagara River. Such a large-scale feature could have significant impact on the transport and dispersion of contaminants, and could be a significant part of the circulation climatology in an area. The four stations placed around the western shore in 1982-83 presented the opportunity to observe such shore-parallel flow if, indeed, it passes that close to the extreme western shore, and if it could be detected in the data. Normally, we plot easterly vectors up the page when dealing with Lake Ontario to clearly illustrate the dominant east-west component which aligns with both the lake axis and the prevailing winds; however, in Figure 2.18, in order to better visualize the data in terms of shore-parallel and shore-perpendicular components, we essentially 'unfolded' the end of Lake Ontario by resolving each station's velocity components to new axes which align with the local shoreline instead of aligning with compass direction. Unlike the normal plot of this type where any direction on the plot is a constant geographic direction, the up-page direction here corresponds to shore-parallel currents to the right looking offshore; in other words, a counter-clockwise rotation around the west end of Lake Ontario. The plots are arranged down the page in the order in which one would encounter the current meter stations travelling in a counter-clockwise direction around the western shore. Vectors are daily averaged velocities. The compass diagram beside each set of vectors indicates the geographic orientation for that stations vectors. There are several significant features illustrated in this plot. As we might expect, the shore-parallel component dominates, especially in a strong current field, a fact dictated by topographic constraints. Also, stronger currents are generally associated with the counter-clockwise circulation due to the interaction of

prevailing winds and basin geometry. When we look at concurrent vectors at stations 177 and 176, the north-eastern and south-eastern extremes respectively, we find numerous instances of currents flowing, still shore-parallel, but away from the west end of the lake at both locations. This scenario prevails a good part of the time from September through November 1982. Obviously, water must come into the end of the lake to replenish this apparent outflow along both shores. Such a sustaining current is not evident in Figure 2.18, but if we look closely at data from stations 13 and 29, Figures 2.7 and 2.8, respectively, we find cases where currents at one or both depths travel at a considerable angle to the shore, suggesting an inflow (in the scenario described here) or outflow at depth, which could very well be a balancing flow for nearby currents of an opposite sense. The other important feature of Figure 2.18 is the weak current regime at station 174, and its apparent lack of coupling with the other stations. As indicated above, even conditions of opposing flows at the other three stations can be reasonably explained as an area-wide phenomenon, but station 174, with notable exceptions during strong wind/current episodes, exhibits weak, erratic currents, suggesting that the area is generally outside of major circulation systems sweeping across the western end of the lake. This is in agreement with the stagnation calculations described earlier, and strengthens the importance of caution in the design and placement of contaminant outfalls in the area.

2.6 Dispersion Characteristics

Satellite-tracked drifting buoys were deployed in western Lake Ontario, in the vicinity of the Burlington Ship Canal, from May through October 1989. The duration of experiments ranged from 7 to 14 days. The drifter trajectories from all of the experiments are superimposed in Figure 2.19. The mean, and root-mean-square (RMS) velocities of individual drifter trajectories, and the ensemble averaged zonal (east-west) and meridional (north-south) velocities for the combined data set were computed. Zonal and meridional mean velocities were 6.0 cm/s and -0.4 cm/s, respectively. Corresponding RMS velocities were 9.2 cm/s and 7.0 cm/s, indicative of large-scale turbulent fluctuations; and therefore, enhanced mixing. Table 2.3 summarizes the mean and RMS velocities for all experiments.

To quantify the dispersion characteristics, we have applied Taylor's theory of single-particle motion. The database was enhanced by using a method first described by de Verdier (1983). Assuming that drifter velocities become decorrelated within one integral time-scale, any two locations of the same drifter separated by more than one integral time-scale may be considered independent and restarted as a new track. For a decorrelation time-scale of 50 hours, which is roughly twice that of typical integral time-scale in the lake, the time-series of hourly positions of the individual drifters were split up into a number of non-overlapping 50-hour time series. End segments shorter than 50 hours were not used. This yielded 57 pseudo drifter trajectories. The ensemble mean zonal and meridional velocities of the pseudo drifters are, 6.7 cm/s, and 0.1 cm/s, respectively. Corresponding RMS velocities are 12.7 cm/s, and 8.8 cm/s. The apparent differences in the values for unmodified and modified series are due to loss of data in the end segments that were shorter than 50 hours long and were not used in the single-particle analysis.

To derive the single-particle statistics, we first remove the background circulation. The dispersion is estimated from the cumulative effect of the motion due to turbulence. Figure 2.20 shows the 'smoke-stack' dispersion plot of the pseudo-drifters all emanating from the same location. Except for a few trajectories which show saturation effect just after deployment, the dispersion grows with time. The dispersion along the zonal direction is stronger than that along the meridional direction.

We also calculated autocorrelation functions from the pseudo-drifter trajectories. Both zonal and meridional autocorrelation functions fall off slowly with increasing time-lag (Figure 2.21). The zonal integral time-scale is 12.3 hours, which is about twice the size of the meridional integral time-scale of 6.7 hours. Corresponding zonal and meridional eddy diffusivities are 7.1 X 10^6 cm^2/s and 1.9 X 10^6 cm^2/s, respectively, and saturate after about 25 hours. These values are indicative of good mixing of water masses; however, it is important to note that these figures are based on drifter experiments lasting several days. This introduces a strong bias toward those periods when well established currents sweep through the area, which, as we have seen from current meter data are not necessarily typical of the area. Data from numerous drifter deployments were not considered because drifters were grounded after a few hours by weak onshore currents.

2.7 Conclusions

A variety of statistical and graphic analysis techniques applied to historical data records taken in the western end of Lake Ontario have provided a fairly good picture of the physical limnological characteristics of the region. Without resorting to highly sophisticated analysis and modeling procedures it was confirmed that the area is not a particularly energetic part of the lake as one would guess from basin topography and typical area meteorology; but that the extreme north-west 'corner' of the area is substantially less energetic than the remaining part. That area, which encompasses the proposed Skyway WWTP outfall, based on minimum physical placement practices, appears to escape all but the most vigorous circulation 'systems' that develop in that region of the lake by virtue of its sheltered location.

Theoretical diffusivity estimates based on drifting buoy trajectories indicate adequate mixing, but are biased by the fact that calculations were, naturally, based on successful missions, while many missions were excluded because weak local currents grounded drifters in shallow water after a few hours. These findings alone, indicate the need for cautious and thorough study before constructing any kind of outfall (or intake) in the extreme western end of the lake.

3. Experimental Plan

3.1 Time-series Measurements

Between May 23, 1996 and October 21,1997 recording instruments measuring current, water temperature, and several meteorological parameters were deployed in and on the western end of Lake Ontario. While data records for any one location or depth do not span this entire period, there are no gaps greater than a few days - typically during an instrument refurbishment - without data from more than one current meter and from at least one local meteorological system. Some current data were lost to instrument failure. Station locations are shown in Figure 1.1. Instrument location, depth - where applicable - and data return are summarized in Table 3.1.

Eulerian (Fixed-point) Current Measurements

Every effort was made - given the limited number of current meters available - to obtain current measurements over a sufficiently broad area, including coastal and offshore stations and multiple depths where possible, to enable a reasonable reconstruction of the overall current regime in the western-most 10 km or so of Lake Ontario. Most current meter moorings were outfitted with Neil Brown Vector Averaging Current Meters (VACM) each capable of measuring and recording current at a single depth. These instruments also record temperature from a single case-mounted thermistor, with each current reading. Each mooring had a current meter one metre off the bottom and another, usually around the minimum practical sampling depth of eight to ten metres, taking into consideration wave action and potential for damage by passing ship traffic. At the proposed outfall site, two moorings (stations 1 and 2), each equipped with current meters at two depths, were deployed within a couple of hundred metres of one another to improve chances of getting useful data, even in the event of instrument loss or failure. Station 4 was also equipped with two current meters but both instruments were located within a few metres of the bottom, since the bottom topography at this location forms a shallow trench which, we speculated, might play a significant role in the counter-circulation set up to offset onshore and offshore wind-driven surface currents.

From November 8, 1996 to April 10, 1997 a bottom mounted 600 kHz Acoustic Doppler Current Profiler (ADCP) was installed at the proposed outfall site (station 2). From May 1 to October 21, 1997 a 1200 kHz RDI ADCP was installed at that location, and from May 2 to October 20 a similar ADCP was installed 10 km offshore to the east of the proposed outfall site at station 8, along with other temperature and meteorological moorings described below. The ADCP emits bursts of sound waves out from an array of four transducers oriented to point downward, or - as in these instances - upward through the water column. Doppler shift in the return signal frequency for signals reflected off of particles in the water are measured and analysed in a manner which yields a velocity for the reflecting object, and presumably the water, at that level. Accurate measurement of the delay time from transmission to return of the signal provides a measure of the distance to the reflecting particles. This concept is the basis whereby current velocities are determined for a number of levels, or bins at varying distances from the instrument. Within certain practical constraints, the number of bins and their thickness may be pre-defined by the user during instrument set-up. The maximum distance from the instrument for which reliable

readings are obtained depends to a large degree on water clarity. Obviously, sufficient reflective particles are required to ensure adequate return signal strength. This becomes an especially significant factor at offshore stations in winter when micro-organisms are at a minimum and the suspended inorganic sediment supply dwindles because resuspension in coastal waters is inhibited by shore-ice formation. Since the velocity of sound in a medium is temperature dependent, and temperature is measured only at the ADCP itself, the temperature stability of the water column in which the measurements are made is very important to the velocity calculations, and the bin determinations.

Temperature Measurements

As mentioned above, each VACM and ADCP current meter is equipped with a thermistor probe on the instrument housing, thereby providing a temperature reading which is recorded with each current reading.

Fixed temperature profile (FTP) moorings were installed at stations 4 and 8 from late April to mid-October 1997 to record time-series vertical profiles of temperature. Profilers consisted of typical U-shaped taut-wire moorings with self-contained single temperature recording loggers attached at selected vertical intervals below the subsurface buoy. Instruments installed shallower than about 10-m depth were attached to the recovery line below the mooring's surface buoy. At station 4 instruments were deployed at 2, 4.2, 6.2, 8.2, 11, 12, 14, 16, and 20-m. The installation depths at station 8 were 2, 6, 8, 11, 12, 14, 16, 20, 29, and 40-m. Sounding depths at stations 4 and 8 at installation time were 28.4 and 47.6-m, respectively.

Two types of temperature loggers were used. Most units were Richard Branckner Research (RBR) XL-105 temperature loggers which give an accuracy of ± 0.01°C in the sampling range of -5 to 35°C. These units have a memory capacity of 28,000 readings. Set-up and data transfer is achieved by direct serial cable connection between ports on the logger electronics board and a PC while the cylindrical pressure case is uncapped.

Three of the instruments at each station were Stowaway temperature loggers manufactured by Onset Computer Corporation. These are an economical sealed unit with an in-use battery life of about 5 years, and an accuracy of ± 0.5 degree over a sampling range of -20 to 50°C. Set-up and data recovery are accomplished with the 3 x 4 x 1.1 cm logger docked to a computer-linked bench top unit. Optically coded data pass back and forth between the logger and docking unit via a transparent window in the logger housing. The docking unit in turn communicates with the computer via standard RS232 serial connection. The shallowest and deepest locations were fitted with these units leaving the higher resolution loggers in the mid to upper part of the water column hoping to better capture the development of, and change in, thermal stratification.

Vertical temperature profiles were also taken at stations located over the study area from a launch during intensive measurement periods in 1997. These measurements are discussed below under "Temperature Surveys".

Meteorological Measurements

Meteorological observations - air temperature, relative humidity, average wind speed, vector-average wind speed, vector-average wind velocity, and near-surface water temperature - were only recorded at the NWRI tower on the pier along the Burlington Bay Ship Canal during 1996. In 1997 a pair of toroidal buoys with recording meteorological sensors were moored about 10 km east of the canal at station 8, in addition to continued measurements at the tower. All systems were equipped with the above named sensors; plus, during 1997, the tower also measured barometric pressure, and buoys measured incoming solar radiation. Wind sensors were mounted at a height of 10-m on the tower. On buoys they were mounted at a height of 3-m.

3.2 Intensive Study Periods

During 1996 the automated physical measurements were supplemented with a number of drifting buoy experiments conducted on a day-to-day basis in the vicinity of the proposed outfall. These experiments served to provide short-duration Lagrangian current trajectories; useful in their own rite, but also important as a pilot study into the practicality of using satellite-tracked drifters in this area.

In 1997 drifting buoy experiments were conducted using satellite-tracked/GPS drifters, thereby providing much longer data records over a much broader area. Drifters were released near the proposed outfall site during three 'intensive periods' in 1997 - May 5 to 16; July 21 to August 1; and September 15 to 26. During these periods, supplementary vessel based current and temperature measurements were also made, primarily along three shore-perpendicular transects shown as A, B, and C on the study map (Figure 1.1). The transects coincided with the proposed outfall site and many of the instrument moorings. Transects B and C essentially formed a boundary between the study area and the main body of Lake Ontario.

Two types of measurements of interest to this work were made along the 1997 transects. Vertical profiles of currents were measured using a 'downward-looking' launch-mounted ADCP, and vertical temperature-depth profiles were taken using a Hydrolab multi-sensor profiler at regular stations established along each of the transects. These measurements are discussed in greater detail below. The intensive measurement chronology is summarized in Table 3.2

Current Surveys

Vertical profiles of current were measured along the transects shown in Figure 1.1 during the intensive measurement periods in 1997. A launch was equipped with a 600 kHz ADCP current meter mounted in a well in the vessel's hull with the sensor head 'looking' down through the water column, and configured to measure forward, transverse, and vertical, current components at 1-m vertical intervals every thirty seconds. With the vessel maintaining a steady course at a near-constant speed - usually about 2 m/s (4 knots) - a horizontal sample interval of about 60-m was achieved.

Specialized computer software for the ADCP processed incoming signals from the ADCP and the onboard differential GPS navigation system to produce and record sample ensembles comprised of time, position, current velocity, vessel velocity, water temperature at the ADCP sensor, and various signal quality parameters for each sampling time interval. In order to accurately compute vessel speed which is separated from the gross measured velocity to derive the current velocity, the ADCP must be able to maintain bottom tracking - the detection of a signal echo from the lake bottom. Naturally, with increasing depth, bottom tracking deteriorates and eventually fails completely. The actual depth at which bottom tracking is lost depends on a number of factors including turbidity, temperature, and the degree of uniformity of density throughout the water column.

The depth at the convergence of the three sampling transects, which was about 43-m, was usually somewhat beyond that at which reliable bottom tracking could be maintained. Since, velocity values deteriorate drastically without it, bottom tracking was maintained throughout sampling by veering off the transect and following a depth contour at which it could be maintained until the next desired transect was reached where a shoreward course along that transect would be established in the usual manner.

Ideally, the three transects were measured twice each sampling day - out to the focal point of the transects along transect A, in and out along each of transects B and C, and back in along transect A. At times, bad weather resulted in reduced variations of this sample scheme; however, on all but five of the twenty-five days when sampling was attempted, at least one pass on each of the three transects was realized.

Temperature Surveys

Temperature surveys were carried out concurrent with many of the current transect surveys, using a second launch. Vertical profiles of temperature and depth, as well as dissolved oxygen, pH, and conductivity, were taken at numerous stations throughout the study area using a Hydrolab H_2O profiler. Since this sampling attempted to serve both the water quality interests, which are outside the scope of this report, and the physical interests of the project, the focus shifted between stations in a series of short nearshore water quality transects and those in the three long ADCP sample transects described above. On several occasions in July and September very extensive surveys were completed, including stations from both sample programs. The Hydrolab system samples all parameters at a rate of 1 Hz, logging the results, along with appropriate time and position information, in a file on an attached computer system. The vertical velocity of the probe is typically adjusted to something between ½ and 2 m/s, and may be increased or decreased to alter the spatial resolution of the samples.

Lagrangian (Drifting Buoy) Experiments

Drifting buoys have been used for many years by NWRI to measure currents in the Great Lakes including several other locations in Lake Ontario. In fact, such experiments conducted in 1989 in western Lake Ontario are the basis of the Lagrangian current analysis in Chapter 2.5. Two distinct forms of drifting buoys have been used extensively. Both forms are functionally similar:

a current follower is suspended from a surface float which serves as a means of tracking the device. The difference that divides drifters into two vastly different families is automation. The simpler form uses as small a float as practical with some form of vertical mast to aid relocation. The device's trajectory is determined by repeated fixes by observers in one or more vessels, using one of any number of methods including radar, GPS, etc. In contrast to this personnel and equipment intensive scheme, satellite-tracked, and combination satellite-tracked/GPS, drifting buoys contain transmitters designed to send an intermittent coded signal to the Argos satellite-tracking system receivers in NOAA satellites circling the earth in polar orbits. Measuring the Doppler shift in the accurately modulated signal enables the system to determine the signal's source location within about half a kilometre. Buoy data, including locations, are transmitted to tracking stations, and thence to central data centres, from which users can obtain data for their own systems by telephone or network link. The combined Argos/GPS systems additionally record regularly collected time/position data from the buoy's built-in GPS receiver, in an onboard data memory. This system combines the near real time monitoring capability of the Argos system for progress and recovery tracking with the increased accuracy of GPS for accurate post-mission trajectory analysis. Each buoy is fitted with a drogue of large surface area relative to the buoy cross-section. The drogue, in our case a 3.0-m wide by 2.4-m high heavy rubberised canvas sheet suspended from a top bar and stiffened with another bar at the bottom, is suspended below the buoy at the desired current measurement depth. The large surface area of the drogue relative to the cross-sectional area of the buoy presented to wind and surface currents ensures that the system trajectory accurately reflects the currents at the depth of interest. While this is not absolutely true, the uncorrected buoy trajectories still give a good representation of the circulation field at installation depth. Post-processing to improve the accuracy of GPS fixes, and to correct for drogue slippage was not performed on the data from the experiments described here.

In the case of western Lake Ontario the greatest concern with drifters is grounding. Since the area is essentially a bay, and one of the main interests of the work described here is with water movement at outfall depth, i.e., near the bottom, and within a kilometre of shore, drifter experiments required exceptional vigilance to ensure equipment safety and measurement validity. The presence of the ship canal and a high level of recreational traffic increased the risk of damage and/or personal injury due to collision with drifters.

Experience has shown that drifters caught in the zone of breaking waves near shore are fairly quickly driven ashore because the solid surface buoy is readily swept along by the surf, but the drogue, which by now is merely dragging horizontally along the bottom, offers little resistance to the return flow which might otherwise keep the whole device off the beach. In areas of sand beach the end result may be limited to superficial abrasion of the buoy; however, on rocky shores or developed areas with docks or seawalls the buoy is quickly demolished - sometimes to the extent that no trace is ever found. In order to help avoid such a fate, drifters used in these experiments were equipped with 5 kg navy anchors slung from the surface buoy by a separate cable in such a manner that the anchor would engage the bottom before any other part of the system. Under most conditions this kept the drifter beyond the breaker zone, at least long enough to effect a recovery.

4. Climatological Characteristics

4.1 Data Summary

The 1996-1997 experiments in western Lake Ontario yielded a large amount of physical limnological and meteorological data. Details of instrumentation and sample locations are given in Chapter 3. Two general categories of data were gathered: first, continuous time-series current, temperature, and meteorological data, as obtained by moored or fixed automatic data logging systems; and second, vertical and horizontal profiles of current and temperature, usually obtained from systems aboard ships or launches requiring intensive human participation. Data from satellite-tracked drifting buoys - drifters for short - could be argued to fall in either category. Drifters are released to follow currents and record time and position at regular intervals for several days or weeks; however, due to the unpredictability of their trajectory, and the constant threat of being cast up on a hostile shore, especially when used to track coastal currents in confined areas of lakes, frequent monitoring of their progress is required. The drifter data records obtained from 1997 experiments ranged from a few hours to about nine days in length.

Table 3.1 summarizes the time-series data gathered between May 1996 and October 1997. Table 3.2 similarly summarizes data from temperature, ADCP, and drifting buoy intensive studies. Time-series data records for moored instruments fall into one of three periods defined by the deployment/recovery cycle based on instrument battery life and data capacity; and, to some degree, ship schedules. The periods were: A) May to November, 1996; B) November, 1996 to April, 1997; and C) April to October, 1997. Exact start and stop times vary over a period of a few days reflecting the time required to carry out the task of deploying and recovering all of the equipment. In some instances data records are short due to premature instrument or battery failure. Much of the following climatological analysis, where statistics for long periods are calculated, was performed for each of the three original data periods to preserve the gross effects arising from differences in lake dynamics under winter isothermal conditions and those typical of summer stratified conditions.

Sampling periods of 15 minutes, 20 minutes, 30 minutes, and 1 hour were used in collecting the original time-series data. The setting was chosen based on a number of factors, including battery life, projected mission length, and instrument recording capacity. Unless otherwise stated the analyses described below were performed on hour-centred hourly series generated from the original data records by time-weighted averaging.

Data collected during the intensive study periods, in many cases, provides a tremendous increase in detail over that provided by the time-series data alone. The current transect data obtained using the launch-mounted ADCP provides excellent vertical and horizontal spatial coverage vastly superior to the sparse measurements provided by the moored instrument array. A serious caveat exists, however, in using the data collected from vessels to assist in the determination of "typical" characteristics of the lake, owing to the strong fair-weather bias in these data. The conditions most effective in driving lake dynamics are seldom, or never, observed for the simple reason that it is impossible to perform the measurements under these conditions.

Satellite-tracked drifter data can create somewhat the opposite effect. Data is collected in all kinds of conditions; however, trajectories where the drifter meanders in circles and basically goes nowhere are often cast aside and forgotten. In the western Lake Ontario experiments the release point was shallow and close to shore, so a substantial number of trajectories ended within a kilometre of the launch site after a few unimpressive loops that took several hours or even a couple of days. Bearing in mind that this work is addressed to the question of the ability of a water mass to disperse pollutants, these seemingly worthless drifter trajectories may be telling a very important part of the story; that is, that there may be significant periods of time that mixing is not adequate at this location. The type of drifter analysis described later on, requires trajectories of considerable length to render the analysis valid. Without exception the drifter tracks subjected to this analysis represent the stronger end of the current spectrum in the area.

This chapter is devoted in using the 1996-97 data to look at the 'big picture' in western Lake Ontario; that is, the generalities we can deduce from relatively long simultaneous records obtained from a number of different locations and depths - in short, the climate of the area. The data from 1996-97 covers a broad enough spectrum of seasonal and short-term events to provide a good insight into the type and range of physical processes that prevail in western Lake Ontario. The validity of this claim is somewhat confirmed by comparing the results from 1996-97 with those presented in Chapter 2 for previously conducted studies. The data are presented in the form of table summaries, time-series and vector plots, frequency of occurrence histograms, progressive vector diagrams, and speed and direction plots, many of which bear the same format as the figures presented in Chapter 2.

4.2 Wind and Current

Statistics for wind and current data have been assembled in a number of tables; some covering whole instrument deployment periods, and others breaking data records down by month. Note that for these and other tables directions are always given as direction toward, for both wind and current. 'U speed' and 'V speed' correspond to east-west speed and north-south speed, respectively. '% time in stagnation' is the percent of the total data record represented by periods over 12 hours in length during which speed values fail to exceed 3 cm/s. Mean scalar speed is given in many of the tables. Interpretation of this parameter requires extra caution, and must be considered without any inference to direction. The value is derived by simple arithmetic averaging of speed values and is of limited use for quick comparison of current magnitude at different stations.

Tables 4.1, 4.2, and 4.3 provide statistics for wind and VACM current meter locations for each of the three main sample periods, respectively. Tables 4.4, 4.5 and 4.6 give similar statistics for wind and each depth measured by ADCP current meters deployed at stations 2 and 8 for the deployment periods indicated. Table 4.7 provides monthly statistics for wind, and VACM current meters for all months for which measurements are available during 1996-97. Table 4.8, 4.9. and 4.10 provide monthly statistics for ADCP current meters at stations 2 and 8 for all months for which measurements are available.

The relevance of statistical data is often easier to grasp if presented in a graphical form which simplifies comparison of like values from different sources. We have prepared several types of graphic illustrations which present the statistics described above in different formats.

Figure 4.1 shows rose-plots of wind from station 99 (Burlington Pier) and currents from VACM current meter stations for the period May 23 to November 4, 1996. The rose-plots were created as described in detail in Chapter 2 by first dividing velocity values into speed and direction 'bins'. The percentage of values in each bin determine the length of the vector of that direction and speed range. Higher speeds at a given direction are drawn with increasing line width. The plots are positioned on the map at the approximate location of the station they represent. Figure 4.2 is a map prepared from the same data set as Figure 4.1, but instead of statistical values, it shows the progressive vector diagram (PVD) generated by joining, tail to head, each of the hourly vectors measured by a current meter and positioning the plot with its origin at the station represented. At the scale shown in the legend (not map scale) the plot represents the trajectory of a particle travelling at the measured velocities over the duration of the record. Comparing Figures 4.1 and 4.2 one can see similar features in the velocity data despite the very different method of analysis. Note the differences in dominant direction of currents at different depths at stations 1 and 2. In this relatively shallow restricted bay-like environment it appears that water with an onshore velocity component at locations closer to the surface, presumably generated by winds and/or large circulation systems is returned to the open lake by a relatively offshore component close to the bottom. Even stations relatively close in depth at a deeper location, such as station 4 (25-m and 29-m depth) show significant differences in trajectories. Figure 4.3 shows another method of comparing velocity data from different sites. Here the mean scalar speed - a simple average of all speed values - for each current meter record over the period discussed above is plotted to scale in the vector resultant direction for the period. The scalar mean speed gives a better indication of the magnitude of currents over the sample period than the vector mean which often almost vanishes for records from coastal areas experiencing a well balanced range of oscillating currents.

Figures 4.4 and 4.5 were created in a manner similar to Figure 4.1 for the other two previously defined sampling periods. Figures 4.6, 4.7, and 4.8 are stacked rose-plots generated from the full sampling period statistics for the three ADCP deployments in 1996-97. The plots in these figures have the appearance of being tilted because they have been vertically squeezed to enable assembling them all on a single page.

Figures 4.9 through 4.14 deal with the range of speed values and their distribution over time-factors which greatly affect the ability of a water mass to disperse pollutants. Figures 4.9, 4.10, and 4.11 summarize the data from VACM current meters for each of the main 1996-97 sample periods, respectively. In each figure the graphs on the left of the page show the frequency of occurrence of specific speed values and the cumulative percent of the total samples represented by speeds below given values as speed increases - one graph for each current sensor. On the right side of the page is a bar chart for each sensor, showing the number of occurrences of uninterrupted periods of stagnant currents (currents less than 3 cm/s), where the minimum stagnation period has been defined as 12 hours. A lengthier discussion of speed distribution and stagnation currents can be found in Chapter 2. Similar treatment of each depth of ADCP current

data is presented in Figures 4.12 to 4.14, which present speed occurrence graphs for all depths in each ADCP deployment period. Stagnation charts have not been included for ADCP data because they show very low occurrence of stagnation values as previously defined. The reason for this is not readily apparent, but is presumed to stem from the fact that the measurement volume of the ADCP is very large compared to VACM meters or mechanical current meters; hence, with the wider range of turbulent motion visible to the sensor, the likelihood of a 12-hour period passing without some kind of motion exceeding 3 cm/s is less likely.

Figures 4.15 and 4.16 show profiles of scaled arrows - one for each ADCP sampling depth - representing monthly mean scalar speed and directed in the direction of the vector mean velocity for the month. Note that arrows represented with broken lines are not to scale, and have, in most cases, been reduced to a fraction of the size of the values they represent. The accuracy of some of the ADCP data from very near the surface is highly suspect since it is difficult to assess the extent to which data is contaminated by the effects of waves.

In Chapter 2 we showed variance ellipses for the historical data (1982-83, 1990, and 1992) and explained their usefulness as graphic indicators of the dispersion characteristics of a location. Figures 4.17, 4.18, and 4.19 show similarly prepared variance ellipses for the VACM current meter data, and selected depths of ADCP data for each of the three sampling periods in 1996-97. The major axis of the variance ellipse, often called the principal axis, is the direction along which mixing is most effective. Axis length is proportional to the mixing effectiveness. In general the figures show that mixing is good in the shore parallel direction at nearshore stations with well defined shore parallel currents. Onshore offshore mixing is typically poor at these locations. Offshore locations typically indicate reasonably good mixing with much less tendency toward one particular narrow band of directions. This scenario is shown by ellipses which more closely resemble circles. The mean current vectors are also shown at the centre of the ellipses for comparison only, since at scale, they are almost too small to see. Mean current data is given in Tables 4.1 through 4.6. The results discussed here follow a similar pattern to those from the historical data, with frequent episodes of shore-parallel currents dominating most of the nearshore except for the extreme western end of the lake north of the ship canal, where weaker more erratic currents dominate.

Figure 4.20 shows drifter positions at 15-minute intervals for all the 1997 drifter missions superimposed on one another. This picture further indicates the tendency toward shore-parallel currents close to shore, with eddies of a wide variety of sizes dominating the open lake. All drifter releases took place within a relatively small area at the western end of the lake where the dot density is the greatest in the figure. Except for removal of a few 'wild' points there was virtually no editing of the data used for this figure.

4.3 Water Temperature

A statistical summary of the measured temperatures from all the available data averaged over each period is shown in Table 4.11. Only data for periods of comparable length have been included. The mean temperature measured by the current meters varied from 2.9°C during the

winter to 14.1°C during the summer and the respective standard deviations ranged from 1.4°C to 4.6°C. The FTP's at station 4 and 8 in 1997 had sensors typically about every two metres in the upper 10-m then increasing in separation with depth. The temperature shown as 0-m depth was the surface temperature collected at the meteorological buoy at station 8. The average temperature for the period from May 2 through October 20, 1997 from the two FTP stations ranged from 13.6°C at the surface to 5.0°C at 40-m. The statistical computations at the two stations (4 and 8) were within 0.5°C for comparable depths, thereby fostering reasonable confidence in the measurements. In general the standard deviation was slightly larger at station 8, possibly indicating greater temperature fluctuations than at station 4.

In Figure 4.21 all of the temperature data were plotted for whole measurement periods to provide a synoptic view of the thermal behaviour of the study area in space and time. Figures 4.22 and 4.23 are enlargements of station 4 and 8, 1997 data, respectively. In these figures only surface bottom and representative intermediate depths were plotted to provide a clearer picture of individual data traces.

5. Nearshore Currents and Exchange Processes

Locations of moored instruments in western Lake Ontario during 1996 and 1997 are shown in Figure 1.1, with details of instrument depth, data return, etc., summarized in Table 3.1. Time-series of these data were analysed to specifically investigate coastal physical processes under different seasonal and meteorological conditions. The relatively fine (1 m) vertical resolution of current data from the two bottom mounted broadband ADCPs, and the temperature profiles from the two FTP moorings which sampled the entire water column at substantially greater intervals, provided considerable insight into the physics of the study area. The single point current and temperature data from the VACM current meters allowed at least an inference about the horizontal patterns of motion and temperature fields. The data were hourly averaged for the analysis. Due to the curved shoreline around the western end of the lake, the orientation of local shoreline differs at each current meter location. Accordingly the unique alongshore and cross-shore components of velocity were computed for each VACM in a manner similar to that described in Chapter 2, and illustrated in Figure 2.18.

5.1 Summer (Stratified) Conditions

Nearshore Currents and Thermal Structure

As a part of the field program wind speed and direction were measured at Burlington Pier station and at an offshore location. Since the scale of the atmospheric weather systems is much larger than Lake Ontario, the wind field may be expected to be rather uniform over the lake (Simons and Schertzer, 1989). Wind data from the meteorological buoy located at station 8 - also an ADCP site - have been used for the analysis. The rotary spectra of wind speed during the 1997 summer season show a gradual decrease of energy density with increasing frequency (Figure 5.1). A broad peak is observed at a period of 6 to 8 days. The oscillations are mainly clockwise with a period of 3 days. A marginal peak at 1 day period shows day-to-day variations of wind speed.

The wind stress was obtained by conventional quadratic law given as $\tau = \rho_a C_d |W| W$, where ρ_a is the air density, and W is wind velocity. In general, drag coefficient C_d increases with the wind speed and is estimated as $C_d = (0.8 + 0.065\ W) \times 10^{-3}$ for W >1 m/s. Here the direction of wind stress is toward the reference station. Figures 5.2a and 5.2b show the low pass filtered (period > 24 hours) east-west and north-south wind stress components in dynes/cm^2 obtained from hourly wind measurements at the meteorological buoy. The wind stress shows the 6- to 8-day oscillations corresponding to the typical east-west and north-south wind reversals which influence upwelling and downwelling events in the lake. The mean components of the wind stress during this period were small, and were directed toward the north-east (0.0633 dynes/cm^2 east; 0.043 dynes/cm^2 north).

The position of isotherms in the range of 10 to 13°C are generally used to define upwelling and downwelling events in Lake Ontario (Simons and Schertzer, 1989). By taking the position of the 10°C isotherm as the depth of the thermocline, we identified upwelling (downwelling) events in

the data from the summer of 1997 when the thermocline sharply moved upwards (downwards) coinciding with favourable wind direction. Figures 5.3a and 5.3b show the daily averaged temperature (°C) derived from 20- and 30-minute data at FTP stations 4 and 8, located in 28.4-m and 46.7-m of water respectively. The mean temperature decreases with depth, and the time-series of temperature profiles show variability at a period of 10 to 12 days. The temperature data shows several episodes of upwelling and downwelling of isotherms. Table 5.1 shows selected upwelling and downwelling events, predominant wind direction and a range of wind speeds during these episodes.

The kinetic energy spectra averaged over the depth for the summer season at ADCP stations 2 and 8 exhibit oscillations at several frequencies (Figure 5.4). Both locations show a prominent peak corresponding to a period of 10 to 12 days. This was also observed in other previous studies along the north shore, and in the middle of the lake, and attributed to large-scale meteorological forcing. Also, it has been theoretically shown that during stratification, the Great Lakes have a predominantly baroclinic response in the form of a rotating Kelvin wave with an approximate period of 10 days (Csanady, 1972). The other pronounced peak was located close to the inertial period (~17 hours) and dominates the higher frequency band (0.05 cph to 0.1 cph) at both stations. At this frequency band we observe weak oscillations at the 14-hour and 11-hour period due to internal baroclinic seiches. The energy falls quite rapidly at the offshore location in the high frequency band. The spectral minimum observed at around 24 to 30 hours can be used as a transition between mean flow and fluctuations (Murthy and Dunbar, 1981); hence, we use a low-pass filter (Graham, 1963) with a cut-off period of 18 to 24 hours which will damp out inertial and high frequency oscillations leaving values attributable to the mean flow.

Figure 5.5 shows the daily variations of filtered currents over depth at ADCP stations 2 and 8. A strong wind toward the north-east beginning July 3, 1997 (Julian day 184) produced upwelling of isotherms at both locations. Near surface temperatures of 6-7^{0}C were observed for 2 to 3 days when temperatures dropped by nearly 10-11^{0}C within a period of about 12 hours coinciding with strong northward winds (Figure 5.2 and 5.3). During this period surface currents were predominantly north-eastward with eastward currents dominating at station 2 coinciding with prevailing winds. In the upper layers, slightly below the surface, though the average alongshore currents are toward the north. The onshore flow from Julian day (JD) 184 is seemingly responsible for the drop in temperature, probably because subsurface waters mixed with upper waters. This may be because in the surface Ekman layer, the strong winds towards the north-east would have caused an offshore transport. Coastal divergence requires this offshore flow to be compensated by an onshore adjustment drift current below the surface friction layer. During this episode the net currents were relatively weak and flowed in the opposite direction in the deeper layers. The weakening of currents coincided with near homogeneous conditions during that period. This particular upwelling event persisted for nearly 5 days, before temperatures started recovering to normal as the winds relaxed. Another strong upwelling event took place from August 7 to 12 (JD 219-224) under the moderate north-eastward wind stress (0.5-0.6 dynes/cm^2) from JD 218. The thermocline moved upward with the 13^{0}C isotherm at 6m depth. The surface alongshore currents changed to northward. Although the surface cross-shore flow was directed away from the coast, onshore flow developed at middle and lower levels as a return flow.

The persistent weak or moderate west or south-westward winds from July 19 (JD 200) caused a strong downwelling of the thermocline and the 13^0C isotherm moved to 20-m depth intersecting the bottom at station 2 by JD 205 (Figure 5.3). The near surface temperatures increased considerably to 20^0C because of warm currents coming from the north. The strong southward flow is visible at almost all depths. Although the cross-shore currents were toward the shore in surface layers they were almost in the opposite direction in middle and deeper layers. This particular downwelling event continued for nearly 6 days.

Another strong downwelling event occurred during August 18 to 24 (JD 230-236) due to strong westward winds (1.4 dynes/cm^2, wind stress). The thermocline intersected the bottom on JD 235 at station 8 with warm water of 20^0C throughout the entire water column. The alongshore currents changed from northward to southward sharply coinciding with the change in wind direction. The southward currents prevailed at all depths at both stations. Offshore flow developed in deeper layers during this event.

Each of these episodes on average lasted for about 4 to 6 days indicating the typical period of upwelling and downwelling in the lake. On some occasions it was seen that, although prevailing winds were weak and westward, downwelling was quite strong. Warm water intrusion from the north shore was probably due to the propagation of an internal Kelvin wave.

Plots of energy density at some important periods are shown in Figure 5.6 for ADCP stations 2 and 8. These frequencies were selected on the basis of the previously discussed significant peaks at meteorological forcing (255 hours), the inertial band (17.06 hours), and baroclinic seiches (14.1 hours and 11 hours). The figures show characteristics of current structure over depth at these frequencies. They reveal that spectral energy varies significantly throughout the water column. As expected the energy peaks are generally located in the near surface layer for alongshore currents at all periods. It seems meteorological forcing strongly influences surface alongshore currents, which gradually drop to small values near the bottom at coastal stations. The spectral energy in cross-shore flow in the low frequency band is generally less than in alongshore flow, however, it increases as we go to deeper layers. This may be because of the compensatory return flows generated during both upwelling and downwelling episodes. At near inertial frequency (ω=0.0586), the energy of alongshore flow is much higher in surface layers, but at other depths both components are comparable. The wind influences the surface layer to generate inertial currents, but at deeper layers these currents are affected by bottom friction. It may be noticed that the surface energy levels at 14.1 hours is comparable to the energy at inertial periods; however, these oscillations are damped just below the mixed layer. Although less energetic, the oscillations at the 11-hour period show similar pattern. The oscillations at 14 hours and 11 hours correspond to baroclinic internal Poincaré modes 5 and 3.

Exchange Processes

In the previous section we discussed the nature of nearshore currents and thermal structure during summer stratification with particular reference to upwelling and downwelling episodes in western Lake Ontario. It has been illustrated that the circulation consists of very complex eddy-like turbulent movements superimposed on the mean flows and are highly variable in intensity

and scales. These eddy-like motions exist in both horizontal and vertical directions. Although several studies on horizontal and vertical exchange of momentum and heat have been attempted for several episodes under different seasonal conditions, none of these studies have looked into the role of horizontal and vertical mixing processes during upwelling and downwelling episodes in the Great Lakes.

In order to develop a relationship between the horizontal exchange coefficient and current fluctuations observed at a fixed point, we followed earlier studies that used Taylor (1921) analysis (Gbah and Murthy, 1998). In a stationary and homogeneous field of turbulence with zero mean particle velocity, the Lagrangian particle displacement is given by

$$x(t) = \int_0^t u_l'(t')dt' \tag{5.1}$$

where u_l' are the Lagrangian current fluctuations. The horizontal exchange coefficient K_x is related to the variance of x(t) as

$$K_x = \frac{1}{2}\frac{\overline{dx^2}}{dt} = x\frac{dx}{dt} = \overline{\int_0^t u_l'(t')u_l'(t')dt'} \tag{5.2}$$

where the overbar denotes ensemble averaging. Introducing the Lagrangian correlation coefficient,

$$R_l(\tau) = \overline{u_l'(t)u_l'(t+\tau)} \,/\, \overline{u_l'^2} \tag{5.3}$$

we then have:

$$K_x = \overline{u_l'^2}\int_0^t R_l(\tau)d\tau \tag{5.4}$$

where $\tau_l = \int_0^\infty R_l(\tau)d\tau$ is called the Lagrangian time-scale. When diffusion time has elapsed beyond some lag time t_l (Lagrangian correlation time-scale), $R_l(\tau)$ will drop to zero. Physically t_l is the decay time-scale of the eddies which contribute to diffusion; therefore, for large time-scales $t > t_l$, the horizontal exchange coefficient attains a constant value

$$K_l = \overline{u_l'^2}\tau_l \tag{5.5}$$

Experimentally, it is difficult to measure Lagrangian current fluctuations and therefore the Lagrangian integral time-scale. It is known from Lumley and Panofsky (1964) that in a stationary and homogeneous turbulence, the Lagrangian variance $\overline{u_l'^2}$ can be assumed to be equivalent to Eulerian variance $\overline{u_e'^2}$. Hay and Pasquill (1959) also pointed out that the essential difference between Eulerian and Lagrangian velocities is that at a fixed point, velocity fluctuations appear to move rather quickly, as turbulent eddies are advected past the instrument. They argued that if

the fixed point velocity record is slowed down by a suitable factor, then it is possible to obtain the velocity history of a drifting particle in a Lagrangian framework. Further, it was argued that the Lagrangian correlation function $R_l(\tau)$ and the Eulerian counterpart $R_e(\tau)$ have similar shape but differ only by a factor β which is greater than unity.

$$R_e(\tau) = R_l(\beta\tau)$$

Introducing these assumptions, the horizontal exchange coefficient in terms of Eulerian statistics can be written as

$$K_e = \beta\overline{u_e'^2}\tau_e \qquad (5.6)$$

Schott and Quadfasel (1979) determined values of β to be in the range1.4±0.4 based on simultaneous Lagrangian and Eulerian measurements in the Baltic Sea. We have chosen β =1.4 for the present study, which although it may sometimes underestimate the horizontal exchange coefficient, is considered a reasonable estimate since our primary goal is not the precise quantification of the exchange coefficient but the general analysis of various turbulence exchange parameters. The mean and fluctuations of all variables were obtained by using a filter with 18 to 24-hour cut-off frequency (Graham, 1963). The filter retains all high frequency oscillations including inertial oscillations in the fluctuating turbulence part.

The turbulent levels in coastal waters can be characterized from root mean square (RMS) values as $\sqrt{\overline{u'^2}}$ and $\sqrt{\overline{v'^2}}$. Here, u' and v' are fluctuating velocities in cross-shore and alongshore direction. The RMS values plotted against depth at ADCP stations 2 and 8 in Figure 5.7 show near isotropic conditions in the middle and lower levels and non-isotropic conditions with alongshore variance dominating slightly in surface layers. The other current meters also show non-isotropy of horizontal turbulence. In Table 5.2 we present the characteristics of fluctuations from VACM current meter locations during the summer period. Here U, V, K_x and K_y denote the cross-shore and alongshore components of currents and diffusion. The peak of turbulence intensity is located in the upper 5-6-m during the summer season. The upwelling episode (JD 184-189) shows less turbulent activity, with substantial decrease in alongshore variance. The peak turbulence intensity is located at slightly shallower depth (~4m) indicating the shift of the thermocline and turbulence activity toward the surface. This is the time during which the thermocline has intersected the surface. Turbulence levels decreased with depth at both stations. Cross-shore variance increased from below the mixed layer indicating the onshore flow was also turbulent during upwelling. Both alongshore and cross-shore variances increased during the downwelling episode from JD 230-235. Slight increase in turbulence intensity near the bottom at stations 2 and 8 could be due to the effect of bottom friction on currents.

Figure 5.8 shows that mean flow kinetic energy (MKE) was generally higher than turbulent kinetic energy (TKE) over the summer period. Alongshore exchange coefficients were higher in the surface layer (6 m^2/s) in comparison to cross-shore exchange coefficients (2.5 m^2/s). Below the mixed layer both were more or less equal indicating near isotropy of turbulent currents. During the upwelling episode of JD184-189 the magnitude of TKE decreased slightly at the

surface, but was comparable to mean flow kinetic energy at 3-5-m below the surface. The MKE was nearly constant from 5-m to bottom indicating the near homogeneous nature of mean currents during this episode. The mean flow was generally weak during the upwelling period. The alongshore exchange coefficient, though still dominant in surface layers, was somewhat reduced to 4 m^2/s. The other important feature during this episode was the slight increase in cross-shore exchange coefficient just below mixed layer indicating onshore momentum exchange at those depths. At the off-shore station TKE dominated over MKE, because MKE has significantly decreased due to weak mean flow during upwelling. Horizontal exchange coefficients increased at the lower depths and were more or less equal in both directions.

During the downwelling episode of JD230-235 we observed an increase of TKE at surface levels which had fallen off rapidly within 6-m from the surface; however, the energy in the mean flow was considerably higher from 3.5 to 6.5-m then decreased to 7.5 cm^2/s^2 near the bottom. Mean flow kinetic energy was comparatively high at the off-shore station 8 at 35-m depth. Overall the energy levels were higher at the offshore location with a local maximum at about 2-3-m above bottom.

Table 5.2 presents properties of velocity fluctuations recorded from five VACM current meters for the whole summer period. These turbulence statistics supplement the ADCP data in western Lake Ontario. The magnitudes of the VACM turbulence parameters obtained here were comparable to the values obtained from ADCP station 2 at comparable depths. The alongshore turbulent variances and exchange coefficients were generally higher than cross-shore components, except at station 4 which was at 25-m depth. This probably indicates that some cross-shore exchanges taking place in the deeper layers in the corner of the lake.

Vertical mixing in lakes and coastal oceans can be due to many factors such as current shear, breaking of internal waves, convective overturns. Stable vertical stratification damps the turbulence. One of the measures of dynamic or shear stability is the gradient Richardson number which can be given as

$$Ri = \frac{N^2}{\left(\frac{\partial U}{\partial z}\right)^2 + \left(\frac{\partial V}{\partial z}\right)^2} \qquad (5.7)$$

N is the Brunt-Vaisala frequency, which gives the static stability of the water column and is written as

$$N^2 = -g / \rho_o \frac{\partial \rho}{\partial z} \qquad (5.8)$$

where z is the vertical co-ordinate positive upwards, U and V are cross-shore and alongshore currents, g is acceleration due to gravity and ρ_o is reference density. Some implications of Richardson number can be readily studied from the turbulent kinetic energy (q) equation, which

under the assumption of horizontal homogeneity and neglecting horizontal advection can be written in a simple form as

$$\frac{\partial q}{\partial t} = \frac{\partial}{\partial z}\left(\frac{K_z}{\sigma_k}\frac{\partial q}{\partial z}\right) + p_s\left(1 - \frac{1}{\sigma_t}Ri\right) - \varepsilon \qquad (5.9)$$

where σ_k and σ_t are Schmidt and Prandtl numbers, ε is the dissipation rate, p_s is production due to mean shear and K_z is vertical eddy viscosity. It was observed in the previous section that horizontal turbulence is isotropic at middle and lower depths; however by assuming the turbulence is isotropic over the whole water column, the dissipation, ε, can be given as

$$\varepsilon = \frac{15}{2}\vartheta\left[\overline{\left(\frac{\partial u'}{\partial z}\right)^2} + \overline{\left(\frac{\partial v'}{\partial z}\right)^2}\right] \qquad (5.10)$$

where ϑ is the kinematic viscosity which is given a value of 1.27×10^{-6} m^2/s.

It can be observed from equation (5.9), that by neglecting the vertical diffusion term, turbulence is damped if Richardson number becomes greater than 0 and for Ri <0, turbulent kinetic energy may increase. In this study we use a critical Richardson number of 0.25, as the transition point between laminar to turbulent flow (Omstedt and Murthy, 1994). Pacanowski and Philander (1981) related the eddy viscosity to the Richardson number and studied the modeling of temperature in the tropical ocean. Their formula was used by Omstedt and Murthy (1994) for Lake Ontario studies by reducing background viscosity, and has been adopted in this study. It can be given as

$$K_z = \frac{K_o}{(1+5Ri)^2} + K_b \qquad (5.11)$$

where K_o and K_b are equal to 10^{-2} m^2/s and 10^{-6} m^2/s, respectively.

The temperature profiles at FTP stations 4 and 8 show stable stratification over the summer period except in strong upwelling episodes. Although temperature and current profiles were obtained close to one another at station 8, ADCP station.2 and temperature station 4 were separated by nearly 2 km. Comparison of available transect measurements and temperature data obtained from nearby VACM current meters with values from station 4 show no major horizontal variations; hence, we used these measurements for calculating vertical mixing characteristics at ADCP Station 2. The thermistor data at different levels were smoothly interpolated using a cubic spline technique at ADCP current measurement levels. Since our main interest was not in studying diurnal variations of different parameters, we calculated daily averages of Brunt-Vaisala frequency (N), shear (Sh), Richardson number (Ri), and eddy viscosity (K_z) obtained by equation (5.11). These are presented in Figures 5.9a and 5.9b for ADCP stations 2 and 8, respectively.

Brunt-Vaisala frequency shows stable stratification and shallow thermocline from JD 178-184. Vertical shear was slightly more in the upper layers (4-5 m); however, during the strong upwelling period from JD 185-192, because of nearly homogeneous conditions, N dropped to small values ($< 2.0^{-2}$) and vertical shear was weak throughout the water column. With this weak shear Richardson numbers reduced to near critical values in the upper layer, turbulence declined in the thermocline region. Considerable increase in vertical viscosity coefficients (40 - 60 cm^2/s) was observed during this episode in the near surface layers. In the bottom layers at station 8, due to small Brunt-Vaisala frequency and considerable vertical shear, Richardson numbers were near critical values. This enhanced the turbulence as indicated by high vertical eddy coefficients.

The other upwelling event from JD 219-225 showed reduced Richardson numbers and increased turbulence in the surface layer. The shear was particularly strong in the upper mixed layer which was responsible for high eddy viscosity values in that region.

During the downwelling episodes from JD 204-210 and JD 230-235 we observed low values of N in the upper mixed layer and higher values nearer the bottom. This was due to deepening of the mixed layer and downward migration of the thermocline to its ultimate intersection with bottom at station 8 as is clearly shown in Figure 5.3b. Vertical current shear slightly increased at the base of the mixed layer (8-9-m depth) on JD 210 characterized by slightly reduced Richardson number and enhanced mixing at that level. Although shear was strong at station 8 in deeper layers, it was not sufficient to overcome the stable stratification. Higher Richardson numbers in deeper layers during these episodes indicate lower turbulence activity, which was reflected by low eddy viscosity coefficients.

Figure 5.10 shows the variation of turbulent kinetic energy (TKE) and dissipation rate at ADCP station 2. It may be noticed from the figure that during upwelling episodes both TKE and dissipation were relatively less. Turbulent activity and dissipation of turbulent energy peak near the surface due to proximity to the point of application of wind stress. Richardson numbers are typically low for this region. Dissipation decreases as we go deeper.

The downwelling event from JD 230-235 was characterized by high TKE in the surface layers associated with consistent westward wind stress; however, dissipation of TKE was not significant. In general the time-series of dissipation rate shows a decrease in dissipation with increasing static stability. It may be argued from these measurements that the source of vertical turbulence in western Lake Ontario is mainly from wind forcing with additional contributions from mean current shear and density gradients.

Vertical exchange coefficients obtained by Pacanowski and Philander (1981) formula closely relate to the dynamic stability of the water column. The range of K_z varied from 0.1 cm^2/s to 60 cm^2/s. The high values were usually obtained in the surface layers during upwelling events associated with enhanced vertical shear and small Brunt-Vaisala frequencies. Downwelling events did not show much variation in vertical eddy viscosity, although they were slightly larger in upper layers. Stable stratification due to thermocline intersection with bottom reduced K_z values in the bottom layers. K_z values obtained in this study were slightly higher than the general range of values obtained by Kullenberg et al. (1974) from dye diffusion studies; however, their

observations were confined to weak local wind conditions and were made in the thermocline and hypolimnion in deeper regions of the lake.

5.2 Winter (Isothermal) Conditions

Five VACM current meters and one ADCP were operational from 8 November 1996 to 10 April 1997. During this period no vertical temperature profiles were measured; however, temperature at each current meter was recorded with each current sample. The temperature data at these depths were fairly representative of thermal conditions because of the homogeneous conditions during winter. The wind data were obtained from the shore based station at Burlington Pier (station 99) from 29 January to 29 April 1997. Figure 5.11 shows the rotary spectra of wind speed at this location. The main characteristic of the winds during this season is a main peak at the 4-day period, which is mainly clockwise rotary. The wind stress was calculated in the conventional manner discussed in the previous section. Figure 5.12 shows the time-series of low pass filtered (period > 24 hours) east-west and north-south components of wind stress. The mean wind stress was very low, with a southward component of 0.08 dynes/cm^2 and an eastward (offshore) component of 0.006 dynes/cm^2 which shows that, although the observations show large day-to-day variations in the speed and direction, the net forcing nearly vanishes on the seasonal scale.

Figure 5.13 shows the low-pass filtered alongshore and cross-shore currents at all five VACM stations, indicating several episodes of current reversal associated with wind shifts. In general alongshore currents were much stronger than cross-shore currents. The kinetic energy spectra of currents at VACM station 3 and ADCP station 2 are presented in Figure 5.14. In general the spectral plots show a broad peak at a period of about 4 days (96 hours) indicating that low frequency currents are mainly influenced by large-scale wind events during this season. In essence the current fluctuations in the surface layer are caused by short local wind impulses, with large-scale circulation driven by wind induced topographic waves (Simons et al., 1985). The ADCP data also shows that currents are fairly uniform in the vertical. Spectral energy drops off rapidly at higher frequencies. The significant peak observed in the inertial frequency band during summer stratification is absent during this period due to the homogeneous conditions during winter.

The means of low-pass filtered currents during the 1996-97 winter show that the alongshore currents were directed towards the north at lower levels and cross-shore currents were directed toward the west (onshore), (Figure 5.15a). Mean vertical current shear was significant in upper layers due to the influence of surface winds. The root-mean-square values of fluctuating (turbulent) currents showed near isotropic conditions near the bottom (Figure 5.15b); however, close to the surface the cross-shore components were slightly higher than the alongshore values.

Figure 5.16a shows that the mean flow kinetic energy was generally higher than turbulent kinetic energy during winter. In the surface layer the magnitude of both TKE and MKE were comparable. The alongshore exchange coefficients (~2.5 m^2/s) in the surface layer were slightly higher than cross-shore values (1-1.5 m^2/s). At lower levels both were nearly equal indicating the

near-isotropy of the fluctuating currents (Figure 5.16b). Exchange coefficients during winter were somewhat smaller than the summer values.

5.3 Lagrangian Drifter Analysis

Lagrangian surface observations have been useful in the study of transport of particles and contaminants in the oceans (Strub et al., 1991) and lakes (Pal et al., 1998). In 1997, the National Water Research Institute (NWRI) conducted a series of experiments involving current meter and drifter deployments in the western end of Lake Ontario. The main objectives of this study were to examine the near-surface coastal circulation and the transport and mixing of sewage treatment plant effluent within the dynamic coastal waters of the lake. This section analyses the drifter trajectories using Lagrangian technique.

Observations and Database

Starting in mid-May through September 1997, GPS-tracked drifters were released at the western end of Lake Ontario and were tracked for about two weeks using Global Positioning System (GPS). The drifters used in this study were dual positioning (GPS and Argos satellite tracking) buoys and were manufactured by Seimac (Model 3206 GTB). The drifters were equipped with roller-blind type drogues made of heavy rubberised canvas with a dimension of 2.4-m x 3.0-m. The drogues were set at 6-m depth (waterline to centre of drogue).

Most of the drifters trajectories were of a short time duration with tracking period less than a day and they were not used in this analysis. About ten drifters were found to have position time-series 2-7 days long. Four position fixes per hour were recorded, with positioning error typically less than 30-m. Velocity errors associated with each velocity estimate have a magnitude less than 4 cm/s and are random in nature.

Preliminary processing of the data involved reformatting the data, removing extraneous characters from the data files, and plotting the drifter trajectories. In general, the unfiltered drifter trajectories were noisy. To help detect errors in the data, the position time-series were converted to a velocity time-series and were plotted. The velocity time-series of two drifters showed large horizontal spikes indicating errors in one or more record's time-stamp. The data were carefully edited to eliminate this effect. The velocity plot of one drifter showed step-function like behaviour and it was not included in the analysis. Figure 5.17 shows plots of two typical, fairly long duration drifter trajectories in the western part of the lake under conditions of clockwise shore-parallel currents. These are basically raw data plots, the removal of obviously wild data points was the only editing applied. The plot of the latter part of the trajectory of drifter number 5382 was omitted because of the onset of significant gaps in the data record, thereby casting doubt on the reliability of the data that was recorded. The contribution of wind to the resultant velocities of any of the drifters was not considered in this preliminary analysis. While there is no doubt that wind does influence the movement of drifters both through drag on the exposed part of the surface buoy, and through effects of waves on both the buoy and the drogue assembly, the

magnitude of that effect was not deemed sufficient for the scope of this work, to warrant the extra processing.

In general, the unfiltered drifter velocities were noisy because of the random positioning errors and other noises (e.g., interference due to close proximity of power lines, etc.) that appear as high frequency oscillations overriding the other components of motion. In order to remove these high frequency oscillations, the raw drifter velocities were filtered using an eighth order, band-pass Butterworth Filter. Phase shifts introduced during the filtering process were removed by running the data forward and then backward through the filter (Emery and Thomson, 1997). The filtered velocity records served as the basic data for further analysis.

Lagrangian Statistics

The 9 drifter trajectories gave about 35 drifter days of observations at 6-m depth in the western part of Lake Ontario. The ensemble-averaged zonal and meridional components of velocities (obtained from the 9 drifter trajectories) were approximately 5 cm/s and 1 cm/s, respectively (Table 5.3) which are comparable with the drifter observations of 6 cm/s and 1 reported by Pal et al. (1998) at 3.5-m depth and at 5-m depth. The root-mean-square (RMS) velocities were 7 cm/s along the zonal direction and 6 cm/s along the meridional direction. However, the computed speed appears to be strongly dependent on the duration of the observations.

Two important parameters that describe the characteristics of the eddy field are the Lagrangian integral time-scale T_i^L and length-scale L_i^L, defined as the time and the distance along the $i(=1,2)$ direction over which a drifter's motion remains correlated. The methods of computing Lagrangian time and length scales, and coefficients of eddy diffusivities, have been discussed by a number of authors including de Verdier (1983), Krauss and Böning (1987), Poulain and Niiler (1989), Paduan and Niiler (1993) and Pal et al. (1998) and are given by

$$T_i^L = \int_0^T R_{ii}^L(\tau)d\tau \qquad (5.12)$$

$$L_i^L = \sqrt{\langle u_i'^2 \rangle}\int_0^T R_{ii}^L(\tau)d\tau = \sqrt{\langle u_i'^2 \rangle}T_i^L \qquad (5.13)$$

where u′ is the residual velocity defined by u′ = u -< u >, < > denotes average over time, and R_{ii}^L is the auto correlation function defined as

$$R_{ii}^L(\tau) = \frac{1}{T}\frac{\int_0^{T-\tau} u_i'(t)u_i'(t+\tau)dt}{< u_i'^2 >} \qquad (5.14)$$

Division by T rather than T-t reduces the error at large lags (Beauchamp and Yuen, 1979).

Because of low frequency motions the Lagrangian integral time and length scales are generally time dependent and do not approach a constant limit (Poulain and Niiler, 1989; Pal and Sanderson, 1992). Most of the individual autocorrelation functions oscillate and have significant negative lobes which underestimate the integral time-scales as they are integrated over the duration of the time-series. To avoid this, we followed the usual practice of integrating from zero to the time of the first zero crossing (Poulain and Niiler, 1989; Thomson et al., 1990). This can be viewed as the upper bound to the true scales.

The de-correlation scales of subsurface motions were less than 12 hours and 7 kilometers (Table 5.3). The mean zonal time-scale was 7 hours which was similar to the mean meridional time-scale of 8 hours. The mean zonal and meridional length scales using all 9 drifters were 1.7 km and 1.5 km, respectively.

Single-Particle Dispersion

Derivation of statistically meaningful results requires averaging over a large number of independent drifter tracks, but the number of drifters available for analysis was small and of short time duration. In this situation, single-particle analysis is unlikely to give reliable estimates. Nevertheless, to get some idea of dispersion properties of the water mass in the experimental site, we attempted to calculate the single-particle statistics following the procedure described in Pal and Murthy, (1998). Assuming that the drifter velocities become decorrelated after about 25 hours (3 times the integral time-scale), the position time-series of individual drifters were split up into a number of time-series of 25 hours long with no overlap. End segments shorter than 25 hours were not used (by doing this we lost some data which has some implications on our analysis as discussed below). This yielded 28 pseudo drifter trajectories of 25 hours long.

Also calculated are the mean and RMS velocities and autocorrelation functions from the pseudo-drifter trajectories. The single-particle estimates of mean and RMS velocities (Table 5.3) are, respectively, 6.3, 0.9 and 12.0, 9.8 cm/s. These estimates are larger than those of individual trajectory estimates. The reason was that, considering our small database, a significant amount of the data were lost because the end segments shorter than 25 hours were not used. The zonal and meridional integral time-scales were found to be 7 hours and 4.6 hours, respectively; the corresponding eddy diffusivities were 3.5×10^6 and 1.6×10^6 cm^2/s.

The data selected for the analysis typically represents conditions of significant currents because such conditions tend to yield longer drifter trajectories without the drifters running aground because they have been carried too close to shore. These longer data records are more suitable for analysis; therefore, the results might give the impression of better mixing conditions overall than really exist. Figure 5.18 shows a drifter trajectory covering a time span of about six hours during which very little distance was covered. The mean speed calculated from the time and displacement works out to a little over 1 cm/s. The drifter was recovered because it was believed to be aground, but in fact was not. This example is just one of numerous similar trajectories, many of which did end up with the drifter aground after being slowly carried into shallow nearshore waters by very weak currents. If a contaminant source were present, such conditions

would provide poor mixing, and it appears from the drifter performance, would, in many cases, transport the higher concentration of contaminants toward shore.

5.4 Summary

Current and temperature measurements during 1996-97 in western Lake Ontario were analysed to study the summer and winter circulation. The data also provided an opportunity to study the coastal exchange characteristics during summer upwelling and downwelling events. The whole basin experienced upwelling and downwelling of the thermocline associated with northward and southward flowing surface currents under the influence of prevailing winds over the region. Each upwelling/downwelling episode lasted for about 4-6 days indicating the typical period of events in the lake. The peak energy at the high frequency end of the energy spectrum was mainly at the theoretical inertial frequency even at the nearshore station analysed; however, many other oscillations at much larger scale have significant energy indicating the presence of different baroclinic internal waves. During the summer season, although near-isotropic fluctuations were observed in middle and bottom layers, non-isotropic conditions were clearly seen in the surface layers. Alongshore horizontal exchange coefficients were much higher than cross-shore exchange coefficients; however, during upwelling events due to increased onshore transport below the mixed layer, cross-shore exchange coefficients increased. Cross-shore exchanges associated with offshore flow were dominant during downwelling events. Upwelling events were characterized by weak static stability and vertical current shear in surface layers. This was indicated by intense turbulence and increased vertical exchange coefficients. Near bottom layers were also characterized by intense turbulence associated with increased vertical shear. During the downwelling episodes due to migration and intersection of thermocline with the bottom, vertical exchange coefficients were relatively small due to weak turbulent activity.

Winter currents were mainly characterized by a 4-day period oscillation influenced by large-scale meteorological forcing. Currents were directed toward the north-west. Fluctuating coastal currents were less significant in winter than in summer and were nearly isotropic in the bottom layers. Alongshore exchange coefficients were slightly higher than cross-shore values near the surface, but values were comparable at depth.

6. Coastal Transport Modeling

Wastewaters are often discharged into coastal waters through long outfalls that terminate in a diffuser. The effluent is quickly and efficiently diluted by the diffuser and is then further dispersed by variable lake currents. These processes cause rapid reduction in contaminant concentrations and can restrict any environmental impact of the discharge to a small area. The fate and transport of an outfall discharge are usually modeled in terms of near- and far-field processes. This is because the length and time-scales of the dominant mixing processes vary over a too wide range to incorporate in a single model.

6.1 Near-Field Models

The primary goal of the outfall diffuser system is to accomplish a rapid initial mixing of the effluent with the receiving waters and thus minimize detrimental effects of the effluent discharge on the environment. In engineering practices, sea outfall systems with a submerged multiport diffuser have been found to be the most efficient way of maximizing near-field initial dilution by enhancing the rapid initial mixing of the effluent discharge with ambient waters.

Hydrodynamic mixing processes of effluent discharge depends primarily on the discharge condition, diffuser length, and the ambient current and density conditions. A waste field is established at the end of the initial mixing region, which drifts with the currents to be diffused by oceanic turbulence in the far-field. Mathematical mixing models have been developed (Winiarski and Frick, 1976; Teeter and Baumgartner, 1979; Muellenhoff et al., 1985) to predict the near-field characteristics of effluent discharges. As shown in Figure 6.1 the most important waste field parameters of submerged effluent discharges are the height to the top of the established waste field, Z_e, the height of the level of maximum concentration (minimum dilution), Z_m, and the thickness, h_e (Roberts, 1996). The minimum dilution at the end of initial mixing region (x_i) is S_m which is defined as the smallest value of the dilution observed in a vertical plane through the waste field at the end of the initial mixing region. There have been two different approaches for developing the prediction models: the first one is based on the jet integral theory, and the second approach is based on the dimensional length scale arguments. Jet integral models, which comprised most of the early mixing models, thus far have not been successful due to their limited applicability (Jirka et al., 1996). More recently, length scale models such as CORMIX (Cornell Mixing zone model; Jirka et al., 1996) and RSB (Roberts, Snyder and Baumgartner model; Roberts et al., 1989) have been widely used by U.S.EPA to determine near-field initial dilution for effluents in the mixing zone.

RSB Model

The initial mixing of wastewater discharged from a multiport diffuser depends on diffuser design and receiving water characteristics. The diffuser can be characterized by fluxes of volume, momentum, and buoyancy per unit diffuser length:

$$q = \frac{Q}{L} \qquad m = uq \qquad b = g_o' q \tag{6.1}$$

where Q is the total discharge, L the diffuser length, u the jet exit velocity, and $g_o' = g(r_a - r_o)/r_a$ is the reduced gravitational acceleration, g is the acceleration due to gravity, r_a is the ambient density at the level of the ports and r_o the effluent density. A linear density stratification can be characterized by the buoyancy frequency, N, also referred to as the Brunt-Vaisala frequency, usually expressed in units of sec^{-1}:

$$N = \pm\left(\frac{g}{\rho_a}\frac{|d\rho|}{dz}\right)^{1/2} \tag{6.2}$$

We define three length scales:

$$l_q = \frac{q^2}{m} \qquad l_b = \frac{b^{1/3}}{N} \qquad l_m = \frac{m}{b^{2/3}} \tag{6.3}$$

Note that these length scales are defined based on the *total* fluxes, rather than the flux from each side of the diffuser. The geometrical characteristics can then be expressed as:

$$z_e,\ h_e,\ z_m = f(q, b, m, s, u, N, \Theta) \tag{6.4}$$

which, by means of dimensional analysis, becomes:

$$\frac{z_e}{l_b},\ \frac{h_e}{l_b},\ \frac{z_m}{l_b} = f\left(\frac{l_m}{l_b},\ \frac{s}{l_b},\ F,\ \Theta\right) \tag{6.5}$$

where $F = u^3/b$ is a dynamic variable which is a type of Froude number. The corresponding normalized expression for dilution is:

$$\frac{S_m q N}{b^{2/3}} = f\left(\frac{l_m}{l_b},\ \frac{s}{l_b},\ F,\ \Theta\right) \tag{6.6}$$

where S_m is the minimum initial dilution, as previously defined. An average dilution S_a is computed as 1.15 S_m based on hydraulic model tests by Roberts et al. (1989).

The two length scale ratios l_m/l_b and s/l_b are diffuser parameters which characterize the significance of source momentum flux and port spacing respectively. Note that these length scale ratios encompass the jet exit velocity, port diameter, port spacing, effluent density, and ambient stratification. Based on consideration of actual operating conditions, the range of experiments was chosen to be $0.31 < s/l_b < 1.92$ and $0.078 < l_m/l_b < 0.5$. For $s/l_b < 0.3$ and $l_m/l_b < 0.2$, the discharge approximates a line plume, i.e., the individual plumes rapidly merge and the effect of source momentum flux is negligible. Many ocean outfalls operate in the regime in which

momentum is negligible; therefore the range of diffuser parameters can be considered to be $s/l_b <$ 1.92 and $l_m/l_b < 0.5$.

A more important parameter is F, which characterizes the importance of the current speed relative to the buoyancy flux of the source. Small values of F signify little effect of current; according to Roberts et al. (1989) the current exerts no effect on dilution if $F < 0.1$. Larger values of F denote situations where the plumes are rapidly swept downstream by the current; dilution is always increased by increased current speeds, although not always at the regulatory (critical) mixing zone boundary. The tests were run at differing current speeds to obtain $F = u^3/b$ in the range 0 (zero current speed) to 100. The effect of the current also depends on the direction of the current relative to the diffuser Q. For non linear stratification, RSB assumes that the density profile is linearized over the rise height. In RSB, the solution procedure is iterative, solving automatically for the rise height z_e.

The RSB model can be broadly classified as an updated model of ULINE (Roberts et al., 1989). It also accommodates the effects of varying source momentum flux and port spacing. It is based on the experimental results for merging plumes in linearly stratified cross-flows. The RSB model assumes that the density profile is linearized up to the top of the plume, and so can be used with non-linear stratification also. Because the RSB model is based on experiments, it will of course provide reliable estimates of minimum dilution, rise height and other waste field characteristics for these experiments. Independent comparisons of the RSB model predictions have been reported in several studies (Roberts and Wilson, 1990).

As described earlier, a proposed site for a new outfall for Skyway WWTP is 1200-m offshore in Lake Ontario to the east of the treatment plant. The mean local depth at this location is approximately 14-m with a bed slope of 1% eastward. Burlington's water intake is approximately 3.4 km northeast of the outfall site and Hamilton's is approximately 5.8 km to the south. For modeling purposes, a 200-m staged diffuser was used to provide a near-field dilution greater than 20:1 at 60-m for different lake current distributions. The nozzle spacing was defined as 10-m with port diameter of 180 mm. All of the nozzles were given a vertical angle of 30° above the horizontal and an alternating angle of 10° with respect to the line of the diffuser.

Field measurements of currents, winds, and temperature in western Lake Ontario were described earlier. From these observations the distribution of current speed and direction during summer and winter conditions were computed (Figures 6.2 and 6.3). The significant feature of these currents is their lack of coherency. Over nearly 80 percent of the period the mean currents were weak (<3 cm/s) to moderate (3-7 cm/s). In summer stratification typically developed at 5-8-m depth then decayed in the fall until temperature profiles became isothermal and remained so over the winter. From the results of drifter experiments conducted between May and October 1997 (Chapter 5.4), the ensemble averaged zonal and meridional components of drifter velocities were 5 and 10 cm/s, respectively. The root-mean-square values were 7 cm/s along the zonal and 6 cm/s along the meridional direction.

Table 6.1 presents mean monthly distribution of ambient and effluent temperatures throughout the year based on Skyway plant data from 1996-97. Generally, the effluent temperatures were

greater than the lake temperatures; however, there were large fluctuations in the lake temperature due to upwelling and downwelling events during summer stratification (Rao and Murthy, 2001). The RSB model was used to obtain near-field dilution characteristics for different flow conditions. For summer conditions we have taken the mean temperature profile obtained from thermistor chain data for August, and for winter simulations we assumed homogeneous condition with 4°C as the mean temperature. For ambient flow velocities we considered three different cases with currents perpendicular to the diffuser. The simulated outfall was as described above. In the simulations of near-field mixing we use faecal coliform bacteria as the tracer. In making the Burlington plant analysis it was assumed that time taken for 90% die off of bacteria (T_{90}) is 5 hours. The expected effluent (end-of-pipe) concentrations for the plant design flow of 2-3 m^3/s will be 200 col./100 ml for E. coli after disinfection of the effluent in the treatment plant. As per the Provincial Water Quality Objectives (Ontario Ministry of the Environment) the E. coli concentration at the beach should not exceed 100 col./100 ml. Table 6.2 shows the predicted results of waste field characteristics and dilution rates near the outfall for summer and winter conditions with different current speeds based on the frequency distribution of currents. In the RSB model the simulation of the dilution away from the initial mixing zone to 100-m from the outfall were calculated using Brooks (1960) formulation. The dilution rates predicted by the model for a flow of 2 m^3/s are in the range of 12.7 :1 to 28.3:1 during summer, and 21.5:1 to 96.9:1 during winter season. Since the ambient stratification during the summer is strong the waste field is trapped at 4-5-m depth. In the winter the buoyant jet rises and forms a stable layer at the surface due to homogeneous conditions. The dilution difference between summer and winter is very large mainly because of the effect of density stratification. The objective of less than 100 faecal coliforms per 100 ml was met within the simulated near-field of the diffuser even for very weak currents.

If the outfall capacity were increased to 600,000 m^3/day by combining the Hamilton and Burlington discharge into this location the initial dilution rates would be expected to decrease considerably. By taking the same ambient current speeds and vertical density profiles in the previous section, we carried out the RSB near-field model simulations for a waste discharge rate of 6.94 m^3/s (Table 6.3). We assume that the end of pipe concentrations would be the same with enhanced treatment capacity. Table 6.3 shows the summary of the predicted results. It was predicted that near-field dilution rates during the summer season would be reduced to nearly half of the values calculated for the present discharge conditions. Even under strong ambient currents (10 cm/s), the dilution rates would be decreased from 28.3:1 to 13.8:1 during summer and from 97:1 to 28.3:1 in winter.

In another simulation the proposed outfall was relocated from 1200-m offshore to 2000-m from the shore (Table 6.4). The local depth at this location is 20-m and the bed slope is toward east. In this simulation the ambient density profiles were computed with the temperature data obtained from the thermistor chain located at station 4 and currents from ADCP station 2. With a flow rate of 2 m^3/s, the initial dilution in the near-field marginally increased from 17.9:1 to 20.4:1 for moderate current speeds (5 cm/s), and from 28.3:1 to 31.8:1 for high current speed (10 cm/s).

Rerunning the model for the offshore (2000 m) outfall location with an increased flow rate of 6.94 m^3/s, the model predicted results showed a marginal increase in the initial dilution in the near-field zone from that at the location 1200-m offshore.

6.2 Far-Field Models

Modeling the behaviour of sewage plumes beyond near-field in a coastal environment is fraught with difficulty. In this region, often called the 'far-field' the waste field is diffused by turbulence as it drifts with lake currents. In this report we use a Gaussian plume model that uses mean currents and assumes that effluent is distributed uniformly over the local depths. The second model is a non-linear two-dimensional numerical model that uses objectively analysed currents for hydrodynamics. In this section, hydrodynamic mixing characteristics of submerged effluent discharging into western Lake Ontario from a proposed Skyway WWTP outfall were investigated using the RSB model.

Gaussian Plume Model

The analytic equations describing the diffusion mechanisms and average concentration field of an effluent plume in a steady current in the wake of a line source diffuser are readily available in the literature (Fischer et al. 1979). Following Brooks (1960), the advection diffusion equation of a non-conservative tracer with an exponential decay rate in a field of homogeneous turbulence is

$$\frac{\partial c}{\partial t}+u\frac{\partial c}{\partial x}+v\frac{\partial c}{\partial y}+w\frac{\partial c}{\partial z}=\frac{\partial}{\partial x}\left(K_x\frac{\partial c}{\partial x}\right)+\frac{\partial}{\partial y}\left(K_y\frac{\partial c}{\partial y}\right)+\frac{\partial}{\partial z}\left(K_z\frac{\partial c}{\partial z}\right)-\lambda c \quad (6.7)$$

where c(x,y,z) is the tracer concentration, (u,v,w) are velocity components in (x,y,z) directions, (K_x, K_y, K_z) are the corresponding eddy diffusivities, λ is the decay life time or dieoff constant of the tracer. Consider now a steady and continuous effluent line source of length 'b' kept perpendicular to a uniform and steady shore parallel current of speed U. To allow for initial jet mixing it is assumed that the effluent has been diluted to concentration c_o prior to release from the ideal line source. Under these conditions equation (6.7) reduces to

$$u\frac{\partial c}{\partial x}=\frac{\partial}{\partial x}\left(K_x\frac{\partial c}{\partial x}\right)+\frac{\partial}{\partial y}\left(K_y\frac{\partial c}{\partial y}\right)+\frac{\partial}{\partial z}\left(K_z\frac{\partial c}{\partial z}\right)-\lambda c \quad (6.8)$$

The following assumptions simplify the analysis:

(1) It is assumed that the effluent field formed by the line source moves downstream in the x-direction at the same rate as the prevailing current and without disturbing the existing flow pattern of the coastal zone.
(2) The diffusion in the flow direction is negligible in comparison to the advection ($K_x \sim 0$).
(3) Vertical diffusion is negligible compared to the lateral horizontal diffusion ($K_y >> K_z \sim 0$). This is due to the large difference between the width and depth scales of the coastal zone.

(4) The effluent is distributed uniformly over the available depth, which is assumed to be constant, so that mixing can be described by a two-dimensional depth integrated analysis.
(5) The lateral eddy diffusivity K_y is a function of L, the plume width, which with the preceding assumptions is only a function of x, the distance from the source, and not of y. The assumption implies that $K_y/K = g[L(x)]/g(b) = f(x)$, so that if an eddy diffusivity $K = g(b)$ is associated with the length b of the diffuser then $K_y = g[L(x)] = f(x)$, where L(x), g(x), and f(x) are functional relationships.
(6) The outfall is located sufficiently far offshore that the spread of effluent in the coastal zone is not restricted by the shore boundary.

With the above assumptions the advection-diffusion equation reduces to

$$\frac{\partial c}{\partial x} = \left(K_y \frac{\partial^2 c}{\partial y^2} \right) - \lambda c \qquad (6.9)$$

Equation (6.9) can be solved in the half plane $x \geq 0$, the boundary conditions of $x = 0$ being

$$\begin{aligned} c &= c_o \quad \text{for } |y| \leq b/2 \\ c &= 0 \qquad \text{for } |y| > b/2 \end{aligned} \qquad (6.10)$$

The dieoff term is eliminated by the variable change

$$c = Ce^{-\lambda x/u} \qquad (6.11)$$

which simplifies equation (6.3) to the form

$$u \frac{\partial C}{\partial x} = \left(K_y \frac{\partial^2 C}{\partial y^2} \right) \qquad (6.12)$$

where C(x,y) is the concentration with no dieoff and x/u is the travel time to any distance x. Thus the diffusion problem can be solved without dieoff and then multiplied by the decay factor. The spatial dependence of the eddy diffusivity is eliminated by the transformation

$$dX/dx = K_y/K = g(L)/g(b) = f(x) \qquad (6.13)$$

which reduces the equation (6.12) to the form

$$u \frac{\partial C}{\partial x} = \left(K \frac{\partial^2 C}{\partial y^2} \right) \qquad (6.14)$$

The solution of this equation with standard integral techniques is found to be

$$c(x,y) = C(x,y)e^{-\lambda x/u} = C(X,y)e^{-\lambda x/u} \qquad (6.15a)$$

$$= c_o e^{-\lambda x/u} / \sqrt{4\pi KX/u} \int_{-b/2}^{b/2} \exp\{-(y-\beta)^2 / 4KX/u\} d\beta \qquad (6.15b)$$

$$= \frac{1}{2} c_o e^{-\lambda x/u} \left\{ erf\left[\frac{y+b/2}{\sqrt{4KX/u}}\right] - erf\left[\frac{y-b/2}{\sqrt{4KX/u}}\right] \right\} \qquad (6.15c)$$

where

$$erf(z) = \frac{2}{\sqrt{\pi}} \int_0^z e^{-\alpha^2} d\alpha = \frac{1}{\sqrt{\pi}} \int_{-z}^{z} e^{-\alpha^2} d\alpha \qquad (6.16)$$

Before equation (6.15) can be utilized the functional relationship between X and x must be specified. This is accomplished as follows. Set

$$L = 2\sqrt{3}\,\sigma \qquad (6.17)$$

where σ is the standard deviation of cross-plume distribution function, i.e.

$$\sigma^2 = \frac{1}{C_o b} \int_{-\infty}^{\infty} y^2 C(x,y) dy = \frac{1}{C_o b} \int_{-\infty}^{\infty} y^2 C(X,y) dy \qquad (6.18)$$

With these definitions L = b at x = 0 and equation (6.18) can be integrated to yield

$$\left(\frac{L}{b}\right)^2 = 3\left(\frac{2\sigma}{b}\right)^2 = \left[1 + \left(\frac{4KX}{u}\right)\frac{6}{b^2}\right] \qquad (6.19)$$

Now from the preceding section the standard diffusion mechanisms relating to the lateral eddy diffusivity K_y to the scale or width L of the effluent plume are:

(1) Fickian diffusion	K_y = const.	f(x)=1	(6.20a)
(2) Shear diffusion	$K_y \alpha L$	f(x)=L/b	(6.20b)
(3) Inertial subrange diffusion	$K_y \alpha L^{4/3}$	$f(x)=(L/b)^{4/3}$	(6.20c)

Substituting equation (6.19) and any one of the functional relationships of equation (6.20) into equation (6.13), integrating, and rearranging the result then gives

$$\left(\frac{4KX}{u}\right) = \frac{b^2}{6}\left\{\left[1 + \frac{1}{n}\left(\frac{4Kx}{u}\right)\frac{6}{b^2}\right]^n - 1\right\} \qquad (6.21)$$

where the diffusion model index n=1,2, or 3 for Fickian, lateral shear, and inertial sub-range diffusion, respectively. The most useful form of equation (6.15c) refers all concentrations to the effluent concentration c_s before release from the diffuser. Introducing the dilution factors:

$\eta = c/c_s$; effluent field to source dilution factor; and
$\eta_{so} = c_o/c_s$; jet or near-field to source dilution factor,
allows equation (6.15c) to be written as

$$\eta_{(x,y)} = \frac{1}{2}\eta_{so} e^{-\lambda x/u}\left\{erf\left[\frac{y+b/2}{\sqrt{4KX/u}}\right] - erf\left[\frac{y-b/2}{\sqrt{4KX/u}}\right]\right\} \qquad (6.22)$$

Equations (6.21) and (6.22) are basic equations describing the average concentration field of an effluent plume in a steady current in the wake of a line diffuser.

The input parameters of the Gaussian Plume model are those of an ideal line source of fixed strength lying perpendicular to a steady current in a homogeneous field of turbulence. After the initial jet mixing the effluent field stabilizes and moves with the speed of the ambient lake currents. The parameters that define the near-field solution in the previous section are the ones used as input parameters for this model. The decay constant for the present simulations was assumed to be similar to the value used for coliform bacteria in the near-field simulations. The selection of initial value and growth law is crucial for diffusion in the far-field. The average alongshore and cross-shore current values obtained at ADCP station 2 were used for the present calculations. In all the computations of far-field concentrations the background concentration was set to zero.

Two simulations for western Lake Ontario were carried out using shore parallel currents of 5 cm/s and 10 cm/s for illustrative purposes. Figure 6.4 shows the plot of the output concentration distributions for north-easterly directed currents. The input parameters for this simulation - diffusivity (0.5 m^2/s), source concentration, and diffuser width - were taken from the near-field model described in the previous section. Given that diffusivity increases as the 4/3 power of the scale of the diffusion field, the effluent was carried nearly 3 km from the source by 10 cm/s currents. Similar results for southward flowing shore parallel currents, with diffusivity of 1 m^2/s, are shown in Figure 6.5.

Kuehnel et al. (1981) calculated the average dilution by including the effects of current speed fluctuations and direction in a shore parallel episode by calculating the equilibrium or steady concentration field produced by all unique current speed and direction events. Here the time-series data (U, θ) is divided into Q segments so that speed and direction may be considered constant during the segment. They defined speed-direction frequency distribution f_{mn} of the current episode into m x n bins of a speed direction histogram and then dividing by Q so that $\Sigma f_{mn} = 1$. In Figures 6.2 and 6.3 we presented frequency of occurrence diagrams for currents, speeds and directions during 1996-97. In the present study the average dilution was estimated by first calculating the average sector monthly velocity and direction from different current speed and direction histograms. Figure 6.6(a) shows the concentration distributions for two representative months, August (summer) and January (winter), for a wastewater discharge rate of 2 m^3/s. The initial concentrations and plume widths were taken from the near-field model. The diffusion coefficients were calculated from the hourly values of currents at ADCP station 2.

Figure 6.6(b) presents the far-field effluent concentration for the simulation outfall capacity increased to 6.94 m^3/s. For simplicity and to compare the results with previous computations, we used the same flow field and diffusion parameters. The model results show that, even with increased treatment capacity, no significant contamination of beaches or the water intake region would be likely; however, with significant onshore currents or shore parallel currents, conditions could deteriorate due to the advection of pollutants.

A Simple Transport And Diffusion Model

In view of the limitations of the Gaussian Plume model and the inadequacy of the information regarding the flow field, a simple transport and diffusion model was developed for western Lake Ontario. For the present case, a two-dimensional (x,y) model is found to be adequate, if we assume that the effluents are contained and vertically mixed in the top few meters during summer stratification, and well-mixed during the winter season.

The two-dimensional transport equation for a moving patch of pollutant is given as

$$\frac{\partial c}{\partial t} + u\frac{\partial c}{\partial x} + v\frac{\partial c}{\partial y} = K_x\left(\frac{\partial^2 c}{\partial x^2}\right) + K_y\left(\frac{\partial^2 c}{\partial y^2}\right) - kc + S_c \qquad (6.23)$$

where c is the concentration, u and v are velocity components, K_x and K_y are eddy diffusivities, S_c is the pollutant source and k is decay constant. The boundary conditions completing the model impose a no-flux condition at a solid boundary, and at open boundaries the diffusive flux is assumed to be zero. At the pollutant source the input concentrations are taken from the output of the RSB near-field model. A central difference scheme is applied for the diffusion terms, and advection terms are solved by an upstream finite difference scheme. Thus the distribution of an effluent can be obtained by solving equation (6.23) for a sufficiently long period until the steady state is reached.

In these experiments the modelled area extends over a region of 10.5 km in the x-direction (east-west) and 11.4 km in y-direction (north-south) with a grid resolution of 300 x 300 m. For this grid interval a time step of 30 sec is found to be consistent with computational stability. A decay rate of T_{90}=5 hr was used in the simulations. The choice of horizontal diffusion coefficients is very important to the prediction of model concentrations. As discussed in Chapter 5 the horizontal diffusion varied during episodic events. Eddy diffusivity values also varied in space and time. Accordingly, we have used the average values of diffusion coefficients for K_x (0.48 m^2/s) and K_y (1.02 m^2/s) for these experiments. A simple objective analysis method was found to be adequate to define the flow field for the model. It consists of interpolation of currents by defining radii of influence around the observed points. The daily averaged observed currents at 5 VACM and two ADCP stations were used to generate the u and v components at the grid interval.

Several numerical experiments were conducted for different outfall locations and discharge conditions. In the first experiment, as in the Gaussian Plume model the outfall location was assumed to be 1200-m offshore. For a discharge rate of 2 m^3/s the near-field mixing model

yielded initial dilution of 17.9:1 which is equivalent to a concentration of 11.74 coliforms/100 ml. By introducing this input as a continuous source the model was run for a typical shore parallel episode occurring August 1 to 5, 1997. Figures 6.7(a) and 6.7(b) show the concentration distributions on 1st and 5th August, respectively, with current vectors at the model grid points superimposed. The area affected by the effluent was confined to the region near the outfall. These results also suggest that, with a flow of 2 m^3/s, the pollutants may not extend beyond 2-3 km from the outfall.

The next experiment, using the same discharge conditions, simulated the concentration distribution during a typical current reversal episode from August 11 to 13, 1997. Results are shown in Figures 6.8(a) to 6.8(c). During the first day the weak north-easterly currents trapped the pollutants near the outfall with concentrations reaching a high of 11 coliforms/100 ml. Although the current direction shifted toward the offshore on 12th August, the current speeds were still small; hence, the pollutants were not dispersed offshore. With the increase of the magnitude of south-easterly currents the next day, the pollutants were transported to nearly 2.5 km south of the outfall; however, they were shown to be unlikely to influence the region near the Hamilton water intake, even after integrating the model for a few more days.

In order to study the likely spread of effluent from an outfall located 2 km from the shore we used the initial dilution obtained from the appropriate near-field model run, and calculated for 5 cm/s currents flowing perpendicular to the outfall. Figures 6.9a and 6.9b show the concentration distributions for a discharge of 2 m^3/s at this location for August 12 and 13, 1997. As observed in the near-field zone no significant increase in dilution of the effluent was observed by shifting the location offshore to 20-m depth. The area influenced by the effluent was further offshore and only a trace amount (<0.1 coliforms/100 ml) were observed near the shore line.

In the final numerical experiment we considered a sewage outfall discharging at a new location just south of the Burlington canal in 14-m of water, roughly 3 km north of Hamilton municipal water intake. The model was run with two discharge conditions for southward flowing currents during August 12 and 13, 1997. In the first case we considered the treated effluent equivalent to that of Skyway Plant alone (2 m^3/s), while the second scenario dealt with combined Burlington and Hamilton discharges (6.94 m^3/s) released at the same location. Figures 6.10a and 6.10b show concentration contours for the Skyway-only simulation. Weak currents during 12th August trapped the pollutants near the source, however, with the increase in southward flow, the effluent dispersed over a much larger region. The effluent patch of 0.1 coliforms/100 ml extended toward the Hamilton beach.

Similar concentration distributions for the combined Burlington and Hamilton discharge are shown in Figures 6.11a and 6.11b. This simulation shows a trace amount of concentration reaching the water intake area. The computed concentrations near the beach were well below the exceedance limits set for contamination of beaches; however, these values could increase considerably during certain conditions, particularly during strong downwelling episodes.

Nutrients

One of the advantages of lake discharges would be lower nutrient levels in Hamilton Harbour. It has been observed from E. coli simulations that the area affected by outfall plumes is significantly smaller than the harbour area. Several experiments have been conducted to compute the distance where lake background nutrients are achieved from the proposed outfall location. In this case the expected phosphorus concentration for the plant design flow of 2 m^3/s would be 300 µgP/l. In these calculations we consider phosphorus as a conservative substance and simulate the conditions for typical currents during summer stratification. In Tables 6.5 to 6.8 we summarize the results for near and far field simulations. As expected the initial dilutions have not varied from earlier E. coli simulations. The far-field calculations show that for the present outfall location and flow conditions (2 m^3/s) concentrations would attain lake levels (10 µgP/l) within 510-m from the diffuser for weak to moderate currents. However, when the outfall capacity was increased to 6.94 m^3/s, it is expected that the concentrations be higher than 10 µgP/l near the beaches. In another numerical experiment the proposed outfall was relocated to 2 km (20-m depth) from shore. The results show that dilutions at 100-m and beyond improved considerably by relocating the discharge location to offshore.

7. Summary and Conclusions

The coastal zones of large lakes and oceans are the areas of most immediate concern to the general public. Understanding the circulation and mixing in the nearshore region is very important for the loading, pathways and fate of pollutants in lakes and for locating water intakes and wastewater treatment plants. The western Lake Ontario shore is rapidly becoming one continuous urban community that heavily depends on the lake for drinking water and discharge of wastewater. Population and development estimates for Halton Region predict that by the year 2011 a 50% increase in capacity will be required at the Skyway Wastewater Treatment Plant. One proposal to stay within the permissible effluent limits would involve shifting the Skyway outfall from Hamilton Harbour to the western end of Lake Ontario. Although substantial advances have been made in regulating the outfall locations, the ever increasing total volumes of wastewater, heighten the need to understand coastal physical processes in much more detail due to the complications introduced by basin shape and bathymetry at the western end of the lake. Historical current and temperature data show high variability of currents with several occurrences of current stagnation periods. In consideration of these water quality concerns and with a long-term interest in sustainable use of nearshore waters, National Water Research Institute undertook a comprehensive study of physical characteristics of the area near the proposed outfall. The main results from this study are summarized below.

Summer Circulation

- The alongshore currents are stronger than cross-shore currents, and the currents show a primary peak at 10-12 days corresponding to the large-scale response of meteorological forcing. Another major peak is located near the near-inertial frequency band.
- Eastward winds induce upwelling, and during these events currents flow in the eastward direction with a slight offshore drift in the surface levels.
- Westward winds induce downwelling, and during these events currents are stronger than during upwelling events.
- The Root Mean Square (RMS) values of fluctuating currents show non-isotropic conditions in the surface levels and nearly isotropic conditions in the middle and bottom depths.
- Upwelling episodes show less turbulent activity due to the reduction of near-inertial oscillations.
- During the downwelling events turbulence intensity increases in the bottom layers.
- During the summer season the mean flow kinetic energy is significantly higher than turbulent kinetic energy.
- Average alongshore exchange coefficients are higher than cross-shore values during the summer season, but upwelling events reduce both alongshore and cross-shore turbulent exchange coefficients.
- Upwelling events show decreased static stability and increased vertical current shear resulting in higher vertical exchange coefficients.
- Downwelling events reduce the vertical exchange coefficients.

Winter Circulation

- The winter currents are mainly characterized by a 4-day period oscillation influenced by large-scale wind forcing.
- The mean currents are mainly directed towards the north-west, with several episodes of alongshore and cross-shore current reversals.
- The fluctuating currents are less significant than summer values, and are nearly isotropic in the bottom layers.
- The alongshore exchange coefficients are slightly higher than cross-shore values in the surface layers, but comparable in the bottom depths.

Near- And Far-Field Models

- Near-field dilutions obtained from a mixing zone model show that for treated effluents with existing discharge conditions (2 m^3/s) at the proposed outfall site at Burlington, the dilution ratios are in the range of 13:1 to 28:1 for weak to moderate currents during summer stratification. Winter dilution ratios increased to 21:1 for weak currents and to 96:1 for moderate currents.
- By shifting the proposed Burlington outfall location to 2 km from the shore initial dilution increased marginally.
- With the proposed Burlington outfall location and discharge conditions no far-field contamination is observed near the beaches or at drinking water intakes of Hamilton and Burlington for typical summer and winter current regimes.
- With increased treatment capacity to 6.94 m3/s (representing the combined flow from Burlington and Hamilton outfalls) the near-field dilution ratios decreased considerably. However the concentrations are below the prescribed exceedance limits of water quality.
- The far-field models have not shown any significant contamination near the beaches or water intakes even with increased treatment capacity of 6.94 m3/s (representing the combined flow from Burlington and Hamilton outfalls) for a typical summer current distribution.

Acknowledgements

Planning, conducting, and analysing the data from a study of this magnitude requires support of individuals far too numerous to list individually. The authors extend sincere thanks to all who have contributed, especially those of NWRI Engineering services, Technical Operations, and Computing Information Services. The authors wish to express their thanks to Murray Charlton for his keen interest during the course of the study. We thank M.G. Skafel for his careful review of the manuscript.

References

Akima, H., 1972. Interpolation and smooth curve fitting based on local procedures. Communication of the ACM 15(10): 914-918.

Anderson, R.V., 1985. Mid Halton Water Pollution Control Plant and Operation Centre, preliminary engineering update report.

Beauchamp, K. and C. Yuen, 1979. Digital Method for Signal Analysis. George Allen and Unwin, London.

Brooks, N.H., 1960. Diffusion of sewage effluent in an ocean-current. Proc. of the 1st Int. Conf. on Waste Disposal in the Marine Environment. E.A. Pearson (ed.), Univ. of California, Berkely.

Bull, J., Farooqui et al, 1976. Coastal Zone Limnological Observations in Lake Huron at Bruce Nuclear Power Development. Environment Canada, Canada Centre for Inland Waters, Burlington, Ontario, Paper No. 17.

Csanady, G.T., 1972. The coastal boundary layer in Lake Ontario, Part 2: The summer-fall regime. J. Phys. Oceanogr. 2: 168-176.

de Verdiere, C.A., 1983. Lagrangian eddy statistics from surface drifters in the eastern North Atlantic. J. Mar. Res. 41: 375-398.

Dick, T.M. and J. Marsalek, 1973. Exchange flow between Lake Ontario and Hamilton Harbour. Environment Canada, Canada Centre for Inland Waters, Burlington, Ontario. Scientific Series No. 36.

Emery, W.S. and R.E. Thomson, 1997. Data Analysis Methods in Physical Oceanography. Pergamon Press, Oxford.

Fischer, H.B., E.J. List, R.C.Y. Koh, J. Imberger and N.H. Brooks, 1979. Mixing in Inland and Coastal Waters. Academic Press.

Gbah, M.D. and C.R. Murthy, 1998. Characteristics of turbulent cross and alongshore momentum exchanges during a thermal bar episode in Lake Ontario. Nordic Hydrology 29: 57-72.

Graham, R.J., 1963. Determination and analysis of numerical smoothing weights. NASA Tech. & Res. No. 179.

Hay, J.S. and F. Pasquill, 1959. Diffusion from a continuous source in relation to spectrum and scale of turbulence. Adv. In Geophysics 6: 345-365.

He, C. and P.F. Hamblin, 2000. Visualization of model results and field observations in irregular coastal regions. Estuar. Coast. Shelf Sci. 50: 73-80.

Jirka, G.H., R.L. Donekar and S.W. Hinton, 1996. Users Manual for CORMIX U.S. EPA, Washington, D.C.

Jordan, D.E. and J.A. Bull, 1977. Coastal Zone Limnological Observations in Lake Ontario at Bronte, June 1973-March 1974. Climatology Report, Environment Canada, Canada Centre for Inland Waters, Burlington, Ontario, Paper No. 18.

Krauss W. and C.W. Böning, 1987. Lagrangian properties of eddy fields in the northern North Atlantic as deduced from satellite-tracked buoys. J. Mar. Res. 45: 259-291.

Kuehnel, R.O.W, C.R. Murthy, K.C. Miners, B. Kohli and Y. Hamdy, 1981. A coastal dispersion model for effluent plumes. Environment Canada, Canada Centre for Inland Waters, Burlington, Ontario, pp. 128.

Kullenberg, G., C.R. Murthy and H. Westerberg, 1974. Vertical mixing characteristics in the thermocline and hyplomnion regions of Lake Ontario (IFYGL). Proc. 17th Conf. Great Lakes Res. 425-434.

Lumley, L. and H.A. Panofsky, 1964. The Structure of Atmospheric Turbulence, Interscience, NewYork.

Mortimer, C.H., 1975. Physical characteristics of Lake Michigan and its response to applied forces. Argonne Nat. Lab., Env. Status of Lake Michigan Region, Vol. 2, Pt. 1.

Muellenhoff, W.P., A.M. Soldate, D.J. Baumgartner and W.E. Frick, 1985. Initial mixing characteristics of municipal ocean discharges. U.S. EPA, EPA-600/3-85-073.

Murthy, C.R. and J.O. Blanton, 1975. Coastal zone climatological studies of the Laurentian Great Lakes. Proceedings Second World Congress, Int. Water Res. Ass., New Delhi, December 1975, Vol. V, pp. 431-448.

Murthy, C.R. and D.S. Dunbar, 1981. Structure of flow within the coastal boundary layer of the Great Lakes. J. Phys. Oceanogr. 11: 1567-1577.

Murthy, C.R., and K.C. Miners, 1989. Mixing characteristics of the Niagara River Plume in Lake Ontario. Water Poll. Res. J. Canada 24: 143-162.

Omstedt, A. and C.R. Murthy, 1994. On currents and vertical mixing in Lake Ontario during summer stratification. Nordic Hydrology 25: 213-232.

Ontario Ministry of the Environment, 1974. Hamilton Harbour Study. Water Quality Branch, 135 St. Clair Avenue West, Toronto, Ontario.

Pacanowski, R.C. and S.G.H. Philander, 1981. Parametrization of vertical mixing in numerical models of tropical oceans J. Phys. Oceanogr. 11: 1443-1451.

Paduan, J.D. and P.P.Niiler, 1993. Structure of velocity and temperature in the north-east Pacific as measured with Lagrangian drifters in fall 1987. J. Phys. Oceanogr. 23: 585-600.

Pal, B.K. and B.G. Sanderson, 1992. Measurements of drifter cluster dispersion. Atmosphere-Ocean. 30: 621-651.

Pal, B. K., C.R. Murthy, and R.E. Thomson, 1998. Lagrangian measurements in Lake Ontario. J. Great Lakes Res. 24(3): 681-697.

Poulain, P.M. and P.P. Niiler, 1989. Statistical analysis of the surface circulation of the California current system using satellite-tracked drifters. J. Phys. Oceanogr. 19: 1588-1603.

Poulton, D.J., B. Kohli, R.R. Weiler, I.W. Heathcote and K.J. Simpson, 1986. Impact of Hamilton Harbour on western Lake Ontario. Water Resources Branch, MOE Report.

Rao, Y.R. and C.R. Murthy, 2001. Nearshore currents and turbulent exchange characteristics during upwelling and downwelling events in Lake Ontario. J. Geophysical Research 106, C2: 2667-2678.

Roberts, P.J.W, W.H. Snyder and D.H. Baumgartner, 1989. Ocean outfalls, I: Submerged waste field formation, II: Spatial evolution of submerged outfields, III: Effect of diffuser design on submerged wastefields. J. Hydraul. Div., ASCE 115: 1-70.

Roberts, P.J.W., 1996. Sea outfalls. In Environmental Hydraulics, V.P. Singh and Willi H. Hager, eds. Kluwer Academic Publishers, pp. 63-110.

Roberts, P.J.W. and D. Wilson, 1990. Field and model studies of ocean outfalls. Nat. Conf. Hydraul. Eng., San Diego, California.

Rukavina N.A., 1969. Nearshore sediment survey of western Lake Ontario, Methods and Preliminary Results. Proc. 12th Conf. Great Lakes Res. 1969: 317-324. Internat. Assoc. Great Lakes Res.

Schott, F. and D. Quadfasel, 1979. Lagrangian and Eulerian measurements of horizontal mixing in the Baltic. Tellus 31: 138-144.

Simons, T.J. and W.M. Schertzer, 1989. The circulation of Lake Ontario during summer of 1982 and the winter of 1982/83. Scientific Series, 171, Environment Canada, Canada Centre for Inland Waters, Burlington, Ontario, pp. 191.

Simons, T.J., C.R. Murthy and J.E. Campbell, 1985. Winter circulation in Lake Ontario. J. Great Lakes Res. 11(4): 423-433.

Strub, P.T., P.M. Kosro and A. Huyer, 1991. The nature of the cold filaments in the California Current System. J. Geophysical Research 96(C8): 14743-14768.

Taylor G.I., 1921. Diffusion by continuous movements. Proc. London Math Soc. 20: 196-212.

Teeter, A.M. and D.J. Baumgartner, 1979. Prediction of the initial mixing for municipal ocean discharges. CERL Publ. 043, U.S. EPA, Corvallis, Oregon.

Thomson, R.E., P.H. LeBlond and W.J. Emery, 1990. Analysis of deep-drogued satellite-tracked drifter measurements in the northeast Pacific. Atmosphere-Ocean. 28: 409-443.

Winiarski, L.D. and W.E. Frick, 1976. Cooling tower plume model. U.S. EPA, Ecological Research Series EPA-600/3-76-100.

Wu J., I.K. Tsanis and F. Chiocchio, 1996. Observed currents and water levels in Hamilton Harbour. J.Great Lakes Res. 22(2): 224-240.

List of Tables

Table 2.1 Table summary of historical data in western Lake Ontario.

___ Current meter/drifter data ----- Wind data

Station Number	Sensor Depth (m)	Water Depth (m)
174	3	12.2
175	3	12.2
176	6	18.3
177	4	14.6
1	---	----
9	---	----
13	5	12.1
13	10	12.1
9	---	----
29	5	25.5
29	10	25.5
9	---	----
Drifter Number		
5380	3.5	
5381	3.5	
5385	3.5	
5387	3.5	
5388	3.5	
5389	3.5	
5396	3.5	
5397	3.5	

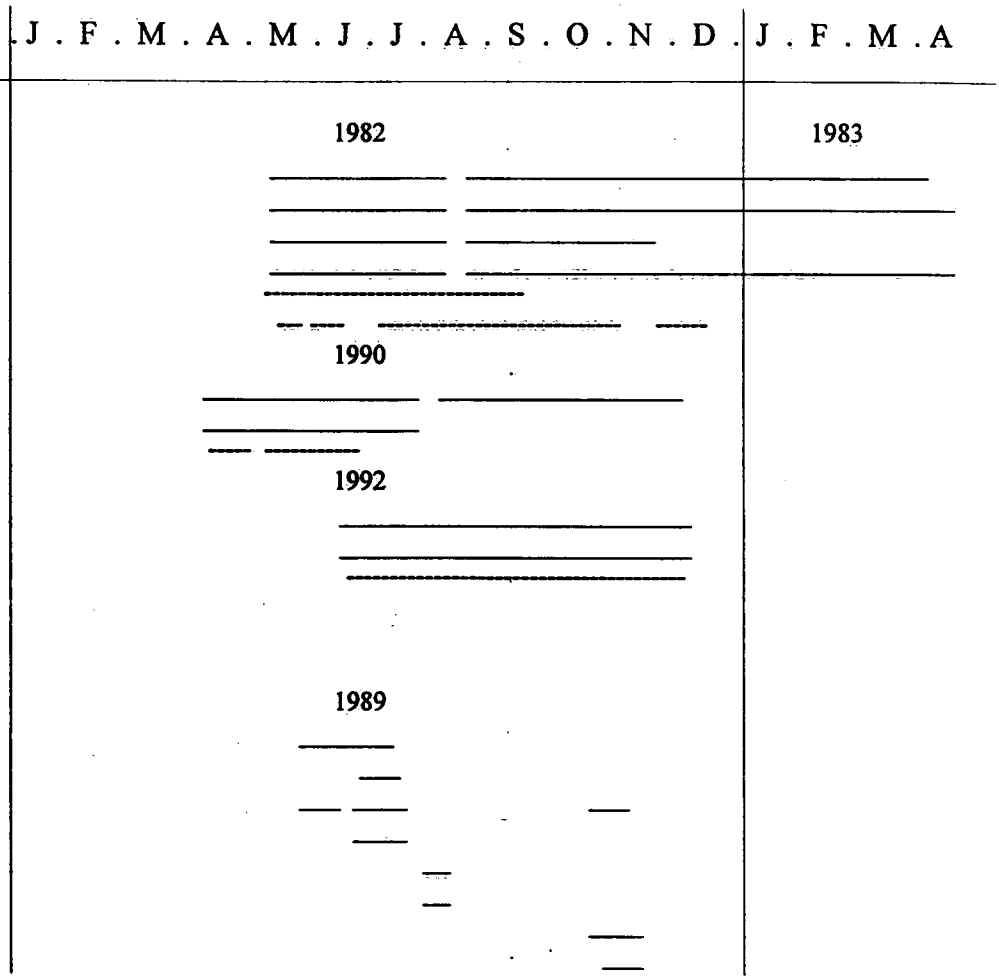

Table 2.2 Statistic summaries of historical data, wind and current, 1982-83, 1990, 1992 in western Lake Ontario.

	1982					1990			1992		
	9	174(3m)	175(3m)	176(6m)	177(4m)	9	13(5m)	13(10m)	9	29(5m)	29(10m)
Mean Velocity (a)	0.7	1.1	1.3	3.0	0.4	1.0	1.0	1.4	0.6	0.8	0.7
Resultant Direction (0 Deg as North)	126	210	141	106	237	88	265	226	141	250	229
Mean Temperature (Deg C)	12.1	6.3	6.6	11.1	4.3	13.5	10.2	7.1	13.9	12.5	10.9
Mean Scalar Speed (a)	3.4	3.5	5.0	8.1	4.8	3.5	3.1	3.1	3.6	3.2	3.6
Mean square Speed (b)	15.3	23.5	43.0	86.3	39.0	15.8	14.2	15.0	16.8	16.0	20.1
Mean Square U Speed (b)	8.0	5.0	17.2	63.0	16.0	7.9	3.8	6.7	10.3	9.0	13.2
Mean Square V Speed (b)	7.3	18.5	25.8	23.2	23.0	7.8	10.3	8.3	6.5	7.0	6.9
Variance (U,V) (b)	7.4	11.1	20.7	38.6	19.4	7.4	6.6	6.5	8.2	7.7	9.8
Persistence Factor	0.2	0.3	0.3	0.4	0.1	0.3	0.3	0.5	0.2	0.3	0.2
% Time in Stagnation(>=12 hours)		77	58	16	56		38	38		41	34
% Speeds 0 - 3 (a)	47.6	64.3	39.8	12.3	40.8	47.4	58.9	60.3	45.1	57.0	50.9
% Speeds 3 - 7 (a)	47.3	24.2	39.8	32.8	38.9	46.3	35.8	33.1	48.8	35.1	37.1
% Speeds >= 7 (a)	5.1	11.5	20.3	54.9	20.3	6.3	5.3	6.6	6.1	7.9	12.0
Total Hours	4194	7867	8036	4647	8128	1908	5509	2687	4368	4368	4368

(a) cm/s for current; m/s for wind

(b) $(cm/s)^2$ for current; $(m/s)^2$ for wind

Table 2.3. Statistics from satellite-tracked drifter trajectories in western Lake Ontario.

Time of Experiment	ID	Mean U (cm/s)	Mean V (cm/s)	RMS u (cm/s)	RMS v (cm/s)
May/Jun.	5380	2.89	-1.54	9.21	3.66
	5380	3.16	-0.75	6.60	4.98
	5381	8.21	0.71	8.31	6.32
	5385	3.00	-1.57	9.42	5.41
	5385	6.93	0.47	9.60	7.80
	5387	1.14	-1.11	7.00	5.33
July	5388	0.93	-0.57	4.35	3.65
	5389	1.02	-0.61	4.41	3.22
Sept./Oct.	5380	15.70	1.05	18.60	14.00
	5385	18.50	0.71	21.09	17.50
	5396	3.91	-0.04	6.73	6.19
	5397	6.98	-0.93	5.03	6.46

Table 3.1 Data summary western Lake Ontario 1996-97.

Stn No	Instr. Depth (M)	Lat (North)	Lon (West)	Snd (M)	From Gmt DyMoYr	To Gmt DyMoYr
	Current Meter Data					
1	9	43-18-45	79-47-06	14.1	23/05/96	04/11/96
		43-18-39	79-47-00	15.7	30/04/97	21/10/97
	13				23/05/96	04/11/96
					08/11/96	24/04/97
					30/04/97	29/06/97
2	11	43-18-45	79-47-00	16.1	23/05/96	04/11/96
					08/11/96	09/01/97
	15				23/05/96	04/11/96
					08/11/96	24/04/97
3	8	43-20-03	79-45-34	12.7	30/04/97	24/09/97
	12	43-19-59	79-45-38	12.5	23/05/96	04/11/96
					08/11/96	24/04/97
4	25	43-18-56	79-44-31	30.0	23/05/96	04/11/96
		43-18-32	79-44-20	28.4	30/04/97	20/10/97
	29				23/05/96	04/11/96
5	5	43-17-12	79-46-37	10.1	23/05/96	25/09/96
	9				23/05/96	28/09/96
					08/11/96	24/04/97
	12	43-17-13	79-46-30	12.5	30/04/97	21/10/97
6	7	43-16-00	79-44-26	11.5	23/05/96	04/11/96
	11				08/11/96	24/04/97
9	9	43-21-11	79-44-02	10.2	30/04/97	21/10/97
	Meteorological Data					
	Moor					
99	9A	43-17-50	79-47-30		02/05/96	29/12/96
					27/01/97	29/04/97
8	20A	43-18-50	79-40-31	43.5	09/05/97	14/05/97
8					09/06/97	25/10/97
8	21A	43-18-58	79-40-29	43.5	22/04/97	24/10/97
	ADCP Current Profiler					
	Moor					
2	01A	43-18-49	79-47-00	16.2	08/11/96	10/04/97
2	01A	43-18-42	79-47-02	16.2	01/05/97	21/10/97
8	18A	43-18-54	79-40-26	48.1	02/05/97	20/10/97
	Fixed Temperature Profiler					
	Moor					
4	16A	43-18-32	79-44-20	28.4	30/04/97	20/10/97
8	19A	43-18-59	79-40-38	47.6	29/04/97	20/10/97
	Three Weeks of Intensive Period					

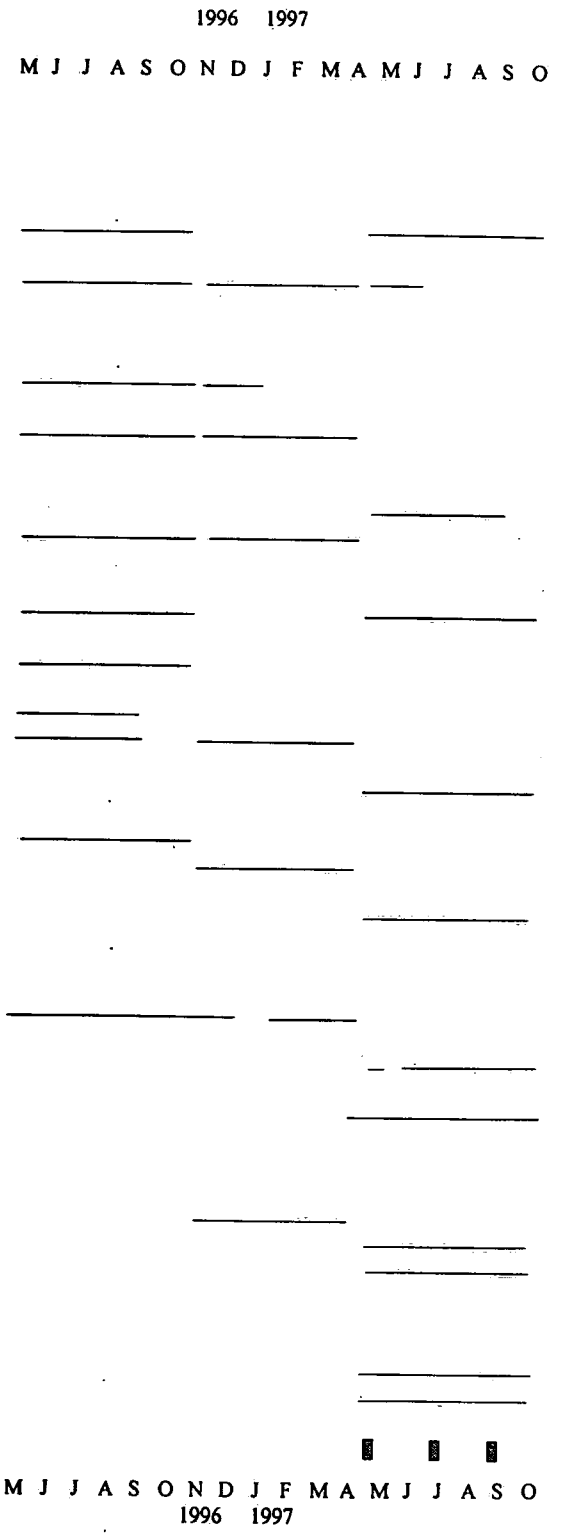

Table 3.2 Intensive periods in 1997 (ADCP transects, temperature surveys and drifting buoys experiments).

ADCP Sampling transects in 1997

Date	From	To	Transect
First Intensive Period			
May 05	1428	1618	A
May 07	1409	1917	ABBCCA
May 08	1342	1839	ACCBBA
May 09	1452	1839	CCBBA
May 12	1351	1559	AC
May 13	1354	1852	ABBCCA
May 14	1427	1919	ACCBBA
May 15	1343	1512	AA
Second Intensive Period			
July 21	1413	1642	ABBCC
July 22	1301	1817	ACCBBA
July 23	1258	1722	ABBCC
July 24	1357	1913	ACBBA
July 25	1304	1822	ACCBBA
July 28	1456	1832	ACB
July 29	1341	1930	ABBCC
July 30	1259	1945	ACCBB1/2A
July 31	1329	2024	ABBCCA
Third Intensive Period			
Sep 15	1312	2011	ACCBBA
Sep 16	1243	2001	ACCBBA
Sep 17	1228	1439	AB
Sep 18	1223	1913	ABBCCA
Sep 19	1227	1458	AC
Sep 22	1313	2009	ABBCCA
Sep 23	1242	1936	ACCBBA
Sep 24	1319	1945	ABBCCA

Temperature Surveys

May 07	
May 08	
May 09	
May 12	
May 13	
July 22	
July 23	
July 24	
July 25	ABC
July 28	A
July 29	ABC
July 30	ABC
July 31	ABC
Sep 15	
Sep 16	
Sep 17	
Sep 18	
Sep 22	C
Sep 23	ABC
Sep 24	

Drifter buoy data in 1997 (depth of 6 m)

No	Mission	SN	Launched	Retrieved	Temp (7 m)
First Intensive Period					
9	7	23828	97 05 05 2110	97 05 08 2031	
15	13	5382	97 05 05 2110	97 05 08 2031	
33	28	5384	97 05 05 2153	97 05 12 1600	
16	14	5382	97 05 07 1332	97 05 12 1616	
25	21	5383	97 05 07 1526	97 05 10 1431	
10	8	23828	97 05 12 1327	97 05 16 1300	
17	15	5382	97 05 13 1337	97 05 13 1930	
34	29	5384	97 05 13 1343	97 05 15 1745	
26	22	5383	97 05 13 1601	97 05 17 1302	
1	1	23827	97 05 14 1407	97 05 15 1345	
11	9	5381	97 05 14 1414	97 05 15 1345	
Second Intensive Period					
7	5	23827	97 07 21 1432	97 07 23 1501	109798
18	16	5382	97 07 22 1355	97 07 23 1425	
12	10	5381	97 07 22 1401	97 07 22 2146	
13	11	5381	97 07 23 1431	97 07 23 2231	
19	17	5382	97 07 23 1727	97 07 24 1524	
35	30	5384	97 07 24 1458	97 07 25 1313	
27	23	5383	97 07 24 1515	97 07 25 1215	109810
28	2301	5383	97 07 25 1330	97 07 25 1830	109810
36	3001	5384	97 07 25 1343	97 07 25 1825	
29	24	5383	97 07 28 1326	97 08 06 1630	109810
37	31	5384	97 07 28 1325	97 08 01 2013	
2	2	23827	97 07 29 1336	97 07 30 1401	109789
20	18	5382	97 07 29 1334	97 07 30 1340	
21	1801	5382	97 07 30 1358	97 07 31 1254	
3	201	23827	97 07 30 1416	97 07 31 1331	109789
4	202	23827	97 07 31 1346	97 08 01 1315	109789
22	1802	5382	97 07 31 1440	97 08 01 1324	
Third Intensive Period					
5	3	23827	97 09 15 1349	97 09 18 1716	
23	19	5382	97 09 15 1349	97 09 18 0246	
30	25	5383	97 09 16 1327	97 09 18 1845	
38	32	5384	97 09 16 1335	97 09 18 1817	
6	4	23827	97 09 22 1443	97 09 24 1517	
24	20	5382	97 09 22 1450	97 09 22 1715	
31	26	5383	97 09 22 1453	97 09 24 1430	
39	33	5384	97 09 22 1434	97 09 24 1516	
14	12	5381	97 09 24 1502	97 09 26 1325	
32	27	5383	97 09 24 1502	97 10 02 1844	
8	6	23827	97 09 24 1602	97 09 26 1346	
40	34	5384	97 09 24 1601	97 09 26 1331	

Table 4.1 VACM current and wind statistics, May 23 to November 4, 1996.

Station No.	99	1	1	2	2	3	4	4	5	5	6
Depth		9m	13m	11m	15m	12m	25m	29m	5m	9m	7m
Mean Vector Speed (a)	0.7	1.4	1.2	1.1	1.0	0.6	0.5	0.4	1.1	0.6	1.1
Resultant Direction (Degrees True)	178	218	82	220	119	16	28	149	192	163	180
Mean Temperature (Deg C)		12.6	11.5	12.2	11.1	12.1	8.5	7.7	14.9	13.0	14.2
Mean Scalar Speed (a)	3.4	3.5	3.5	3.3	3.0	3.7	4.0	3.7	5.6	4.1	5.1
Mean Square Speed (a)	15.7	18.4	19.3	17.3	13.8	20.2	27.5	23.8	48.6	26.7	41.5
Mean Square U Speed (b)	9.3	5.8	8.9	5.7	7.1	11.1	18.3	16.1	8.9	12.8	12.9
Mean Square V Speed (b)	6.4	12.6	10.3	11.6	6.7	9.1	9.1	7.7	39.7	13.8	28.5
Variance (U,V) (b)	7.6	8.3	8.9	8.1	6.3	9.9	13.6	11.8	23.7	13.1	20.1
Persistence Factor	0.2	0.4	0.3	0.3	0.3	0.2	0.1	0.1	0.2	0.1	0.2
% Time in Stagnation (>-12 hours)		22.9	20.1	30.9	32.0	20.6	23.4	25.7	11.4	14.0	17.8
% Speeds 0.0 - 3.0 (a)	52.1	51.8	54.1	56.1	61.6	48.9	47.9	51.0	32.5	45.3	36.8
% Speeds 3.0 - 7.0 (a)	41.7	39.0	37.0	34.6	32.4	41.9	38.2	37.5	35.8	40.0	37.5
% Speeds >-7.0 (a)	6.2	9.2	8.9	9.3	5.9	9.1	14.0	11.5	31.8	14.8	25.7
Total Hours	3962	3962	3962	3962	3962	3962	3962	3962	2995	3065	3963

Table 4.2 VACM current and wind statistics, November 8, 1996 to April 24, 1997.

Station No.	99	1	2	3	5	6
Depth		13m	15m	12m	9m	11m
Mean Vector Speed (a)	1.2	3.1	0.6	2.0	0.2	0.8
Resultant Direction (Degrees True)	139	251	316	60	239	166
Mean Temperature (Deg C)		3.0	13.7	3.0	12.5	2.9
Mean Scalar Speed (a)	3.9	4.8	3.6	4.6	3.2	3.4
Mean Square Speed (a)	20.2	34.6	20.7	33.6	18.9	19.3
Mean Square U Speed (b)	13.2	21.4	7.1	18.3	6.4	7.4
Mean Square V Speed (b)	7.0	13.2	13.7	15.3	12.5	11.9
Variance (U,V) (b)	9.3	12.5	10.2	14.9	9.4	9.4
Persistence Factor	0.3	0.6	0.2	0.4	0.1	0.2
% Time in Stagnation (>-12 hours)		14.3	26.8	20.2	43.7	35.5
% Speeds 0.0 - 3.0 (a)	38.7	33.2	49.7	38.4	60.4	56.7
% Speeds 3.0 - 7.0 (a)	52.8	46.2	41.4	42.9	32.0	34.6
% Speeds >-7.0 (a)	8.5	20.7	8.9	18.7	7.6	8.8
Total Hours	3314	4006	4008	4008	4011	4007

Table 4.3 VACM current and wind statistics, April 30 to October 24, 1997.

Station No.	8	1	3	4	5	9
Depth		9m	8m	25m	12m	9m
Mean Vector Speed (a)	1.3	0.4	2.7	0.9	2.7	1.4
Resultant Direction (Degrees True)	68	197	54	115	133	53
Mean Temperature (Deg C)	13.5	10.0	10.6	7.8	9.9	10.1
Mean Scalar Speed (a)	3.7	2.7	6.0	4.0	3.9	3.6
Mean Square Speed (a)	15.6	11.7	51.0	27.2	22.1	21.6
Mean Square U Speed (b)	10.7	4.6	32.4	19.3	9.0	8.2
Mean Square V Speed (b)	5.0	7.2	18.6	7.8	13.0	13.4
Variance (U,V) (b)	7.1	5.8	21.8	13.2	7.5	9.8
Persistence Factor	0.4	0.1	0.5	0.2	0.7	0.4
% Time in Stagnation (>-12 hours)		43.9	3.8	22.3	16.2	27.5
% Speeds 0.0 - 3.0 (a)	47.1	67.9	21.3	45.4	43.9	51.1
% Speeds 3.0 - 7.0 (a)	47.2	27.3	47.0	40.6	45.7	38.8
% Speeds >-7.0 (a)	5.7	4.8	31.7	14.0	10.4	10.1
Total Hours	4176	4176	3537	4153	4175	4175

(a) cm/s for current; m/s for wind

(b) $(cm/s)^2$ for currents;$(m/s)^2$ for wind

Table 4.4 ADCP station 2 current and wind statistics, November 8, 1996 to April 10 1997.

ADCP Station No. (Depth m)	% time in time in Stagnation >=12 hours	Mean Scalar Speed (cm/s)	Square Speed (cm/s)**2	Mean U**2 Speed (cm/s)**2	V**2 Speed (cm/s)**2	Mean Velocity (cm/s)	Direction to Deg true	Variance (U,V) (cm/s)**2	% Speeds 0.0 - 3.0 (cm/s)	% Speeds 3.0 - 7.0 (cm/s)	% Speeds >= 7.0 (cm/s)	Total Hours	Mean Temp Deg C
2 (00.0)		36.8	1694.6	1089.4	605.2	12.1	118	774.3	3.5	4.1	92.5	3529	
2 (00.3)		48.9	2698.8	1840.2	858.6	19.2	110	1165.4	2.2	3.8	94.0	3670	
2 (00.8)		47.4	2522.7	1723.2	799.5	19.8	110	1064.8	2.2	3.1	94.7	3670	
2 (01.3)		28.1	948.7	657.8	290.9	10.1	111	423.6	4.0	2.6	93.4	3670	
2 (01.8)		8.7	111.4	77.9	33.4	0.8	150	55.4	17.5	29.3	53.2	3670	
2 (02.3)	2.2	4.3	29.7	14.6	15.1	0.2	250	14.8	42.3	42.4	15.4	3670	
2 (02.8)	1.9	4.0	24.0	10.1	13.9	0.2	275	12.0	45.4	42.6	12.0	3670	
2 (03.3)	4.3	3.8	22.7	9.1	13.6	0.3	281	11.3	46.4	42.1	11.5	3670	
2 (03.8)	3.1	3.8	22.2	8.7	13.5	0.4	289	11.0	47.1	41.7	11.3	3670	
2 (04.3)	4.9	3.7	21.3	8.3	13.0	0.6	292	10.4	47.9	42.0	10.1	3670	
2 (04.8)	5.0	3.7	21.0	8.1	13.0	0.7	293	10.2	48.2	41.6	10.1	3670	
2 (05.3)	5.7	3.7	20.7	8.2	12.5	0.9	290	10.0	48.6	41.6	9.8	3670	
2 (05.8)	4.5	3.6	20.3	8.1	12.1	0.9	295	9.7	49.3	41.0	9.6	3670	
2 (06.3)	4.0	3.6	20.0	8.1	11.9	1.0	294	9.5	48.5	42.1	9.4	3670	
2 (06.8)	6.4	3.6	20.1	8.2	11.9	1.1	294	9.4	49.0	41.6	9.4	3670	
2 (07.3)	5.1	3.7	20.7	8.6	12.2	1.2	295	9.7	46.9	43.9	9.2	3670	
2 (07.8)	3.7	3.7	20.7	8.6	12.1	1.3	296	9.5	47.3	43.1	9.6	3670	
2 (08.3)	5.9	3.7	20.6	8.7	11.9	1.4	295	9.4	46.8	43.7	9.5	3670	
2 (08.8)	3.6	3.7	20.7	8.7	11.9	1.4	296	9.4	45.3	45.2	9.5	3670	
2 (09.3)	4.6	3.8	21.1	9.2	11.9	1.5	296	9.5	45.2	45.0	9.8	3670	
2 (09.8)	5.5	3.8	20.7	9.2	11.5	1.5	296	9.3	45.4	45.4	9.2	3670	
2 (10.3)	5.7	3.8	20.7	9.2	11.5	1.5	296	9.2	44.4	46.2	9.4	3670	
2 (10.8)	4.6	3.9	21.6	9.9	11.7	1.5	296	9.7	42.9	46.8	10.3	3670	
2 (11.3)	4.5	3.9	21.6	10.0	11.6	1.6	294	9.5	42.6	47.1	10.3	3670	
2 (11.8)	4.1	3.9	21.8	10.1	11.7	1.5	294	9.7	41.6	48.1	10.2	3670	
2 (12.3)	3.1	4.0	22.2	10.5	11.7	1.6	294	9.9	41.1	47.9	11.0	3670	
2 (12.8)	3.1	4.0	22.4	10.7	11.6	1.6	293	9.9	40.6	48.7	10.7	3670	
2 (13.3)	3.2	4.0	22.3	10.4	11.9	1.5	293	10.0	39.8	49.7	10.5	3670	
2 (13.8)	3.2	4.0	22.6	11.0	11.6	1.6	287	10.1	37.7	51.9	10.4	3670	
2 (14.3)	2.4	4.1	22.1	11.0	11.1	1.6	281	9.7	35.6	55.2	9.3	3490	2.9
*9 Wind to (m/s)		4.0	20.7	13.7	7.0	1.2	136	9.6	37.0	54.2	8.7	2976	

Table 4.5 ADCP station 2 current and wind statistics, May 1 to October 21, 1997.

2 (00.3)		37.7	1829.3	970.0	858.0	11.3	75	851.0	2.7	7.0	90.4	4169	
2 (01.3)		29.1	1203.8	563.7	640.1	7.2	82	576.2	5.5	9.9	84.6	4169	
2 (02.3)	8.4	6.2	56.3	17.0	39.4	1.2	356	27.4	25.0	41.4	33.7	4169	
2 (03.3)	10.7	4.9	36.7	8.6	28.1	1.4	341	17.4	34.9	43.9	21.1	4169	
2 (04.3)	16.0	4.2	26.5	6.2	20.2	1.1	320	12.7	40.9	44.3	14.8	4169	
2 (05.3)	18.7	3.8	21.7	5.8	16.0	0.9	295	10.5	46.2	42.3	11.4	4169	
2 (06.3)	22.5	3.6	18.7	5.6	13.1	0.8	271	9.0	51.2	39.3	9.5	4169	
2 (07.3)	27.7	3.3	16.1	5.5	10.6	0.9	251	7.7	54.8	37.9	7.3	4169	
2 (08.3)	25.8	3.2	14.5	5.3	9.2	0.9	235	6.8	56.8	37.1	6.0	4169	
2 (09.3)	31.8	3.1	13.9	5.4	8.5	1.0	226	6.5	58.6	35.6	5.8	4169	
2 (10.3)	32.2	3.0	13.4	5.5	7.9	1.0	221	6.2	59.2	35.8	5.0	4169	
2 (11.3)	30.0	3.0	13.2	5.6	7.6	1.0	217	6.1	59.0	36.5	4.5	4169	
2 (12.3)	30.8	3.0	12.8	5.7	7.1	1.0	212	5.9	58.2	37.4	4.4	4169	
2 (13.3)	31.4	3.0	12.8	6.0	6.8	1.0	208	5.9	58.0	37.9	4.1	4169	
2 (14.3)	26.9	2.9	12.4	6.2	6.2	0.9	199	5.7	59.0	36.7	4.3	4169	8.6
*9 Wind to (m/s)		3.4	15.7	10.7	5.0	1.2	68	7.1	47.1	47.2	5.7	4169	13.5

Table 4.6 ADCP station 8 current and wind statistics, May 2 to October 20, 1997.

8 (31.5)		4.9	33.2	13.2	20.0	1.0	175	16.1	27.7	51.6	20.7	3193	
8 (32.5)	0.6	4.7	30.1	12.3	17.8	0.9	171	14.7	30.2	50.8	19.0	3853	
8 (33.5)	0.7	4.5	27.8	11.9	15.9	0.8	178	13.6	32.2	51.1	16.7	4086	
8 (34.5)	0.7	4.4	26.4	11.4	15.0	0.7	175	13.0	33.8	51.0	15.2	4106	
8 (35.5)	0.6	4.4	25.8	11.2	14.6	0.8	175	12.6	34.0	51.0	15.0	4106	
8 (36.5)	1.6	4.3	25.1	10.8	14.3	0.7	173	12.3	35.2	50.5	14.3	4106	
8 (37.5)	1.9	4.2	24.8	11.1	13.7	0.6	184	12.2	35.8	50.7	13.5	4106	
8 (38.5)	1.9	4.2	24.7	11.1	13.6	0.6	178	12.1	35.6	51.2	13.2	4106	
8 (39.5)	0.3	4.3	24.9	11.4	13.5	0.5	194	12.3	36.0	50.4	15.5	4106	
8 (40.5)	1.4	4.2	25.0	11.6	13.4	0.6	182	12.3	36.2	50.1	13.7	4106	
8 (41.5)	0.3	4.3	25.2	12.0	13.2	0.4	193	12.5	36.3	49.3	14.4	4106	
8 (42.5)	0.3	4.3	25.3	12.2	13.1	0.5	222	12.5	35.0	51.5	13.5	4106	
8 (43.5)	1.1	4.2	25.1	12.3	12.7	0.3	207	12.5	36.4	50.0	13.6	4106	
8 (44.5)	1.4	4.2	24.6	12.3	12.3	0.5	228	12.2	36.0	50.3	13.7	4106	
8 (45.5)	1.3	4.1	22.7	11.3	11.4	0.5	244	11.2	38.8	49.3	11.9	4106	
8 (46.5)	0.3	4.3	23.8	13.4	10.4	1.8	254	10.3	31.1	57.1	11.8	4106	4.5
8 Wind to (m/s)		3.4	15.0	10.1	4.9	1.2	67	6.8	47.1	47.2	5.7	4106	13.6

Table 4.7 VACM current and wind monthly statistics, May 1996 to October 1997.

Month	Mon	Year	Station No.	Depth (m)	Mean Scalar Speed cm/s	Mean Vector Speed cm/s	Resultant Direction TO deg True	Variance (U,V) cm/s**2	% Speeds 0-3	3-7	>7
										cm/s	
May	5	1996	99	-4	3.3	2.0	267	5.4	55.9	38.7	5.4
Jun	6	1996	99	-4	2.9	0.6	229	5.6	57.1	41.3	1.7
Jul	7	1996	99	-4	3.0	1.4	151	5.4	59.0	35.5	5.5
Aug	8	1996	99	-4	2.7	0.4	167	4.5	64.8	34.3	0.9
Sep	9	1996	99	-4	4.0	0.7	216	11.5	45.7	38.6	15.7
Oct	10	1996	99	-4	4.1	0.9	168	10.2	38.6	53.6	7.8
Nov	11	1996	99	-4	3.9	1.8	139	7.4	32.1	63.1	4.9
Dec	12	1996	99	-4	4.0	0.9	81	10.4	40.3	50.8	8.9
Jan	1	1997	99	-4	3.4	0.9	111	6.9	38.6	60.4	1.0
Feb	2	1997	99	-4	4.0	1.6	117	9.1	39.0	51.0	10.0
Mar	3	1997	99	-4	4.3	1.4	177	11.2	33.1	54.8	12.1
Apr	4	1997	99	-4	3.6	1.5	148	7.7	46.0	46.3	7.7
May	5	1997	8	-4	3.7	2.0	84	7.6	46.9	41.7	11.4
Jun	6	1997	8	-4	2.8	0.7	31	4.8	57.8	40.6	1.7
Jul	7	1997	8	-4	3.0	1.0	55	5.5	53.5	44.1	2.4
Aug	8	1997	8	-4	3.4	0.9	61	6.9	45.2	51.3	3.5
Sep	9	1997	8	-4	4.2	1.9	69	9.0	30.6	60.0	9.4
Oct	10	1997	8	-4	3.1	0.9	89	5.4	55.0	43.3	1.7
May	5	1996	1	9	4.6	2.1	193	12.6	36.8	40.2	23.0
May	5	1996	1	13	3.8	1.0	52	9.0	41.2	50.5	8.3
Jun	6	1996	1	9	3.5	1.1	233	7.9	50.7	40.7	8.6
Jun	6	1996	1	13	3.0	1.5	35	5.2	57.8	38.5	3.8
Jul	7	1996	1	9	3.3	1.6	252	6.9	59.8	34.0	6.2
Jul	7	1996	1	13	2.8	1.4	41	5.1	65.7	30.9	3.4
Aug	8	1996	1	9	3.5	1.9	191	7.2	53.2	36.7	10.1
Aug	8	1996	1	13	3.2	1.3	104	6.9	57.5	35.5	7.0
Sep	9	1996	1	9	3.3	1.4	190	8.4	56.1	35.8	8.1
Sep	9	1996	1	13	4.0	1.8	125	12.0	49.4	35.7	14.9
Oct	10	1996	1	9	3.6	1.5	218	7.7	47.7	43.8	8.5
Oct	10	1996	1	13	4.2	2.1	108	12.1	47.8	35.9	16.3
Nov	11	1996	1	13	3.8	2.2	281	6.6	33.2	63.1	3.7
Dec	12	1996	1	13	4.3	2.3	238	12.3	40.1	46.0	14.0
Jan	1	1997	1	13	6.6	4.5	262	17.3	17.3	36.2	46.5
Feb	2	1997	1	13	5.7	4.4	253	11.9	19.5	52.3	28.1
Mar	3	1997	1	13	4.7	2.9	231	13.6	32.7	51.2	16.1
Apr	4	1997	1	13	3.3	2.3	249	6.6	59.3	32.1	8.6
May	5	1997	1	9	2.5	1.1	279	4.3	71.6	25.7	2.7
Jun	6	1997	1	9	2.2	0.4	184	4.8	76.8	19.9	3.3
Jul	7	1997	1	9	2.7	0.8	197	5.3	65.5	30.0	4.6
Aug	8	1997	1	9	3.1	0.7	127	7.9	62.6	27.9	9.5
Sep	9	1997	1	9	3.1	0.5	185	7.1	58.2	36.4	5.4
Oct	10	1997	1	9	2.2	0.7	164	3.6	75.9	21.9	2.2
May	5	1996	2	11	4.3	1.8	199	12.6	39.2	41.7	19.1
May	5	1996	2	15	3.5	1.2	109	7.6	46.6	46.1	7.4

Table 4.7 (cont.) VACM current and wind monthly statistics, May 1996 to October 1997

Month	Mon	Year	Station No.	Depth (m)	Mean Scalar Speed cm/s	Mean Vector Speed cm/s	Resultant Direction TO deg True	Variance (U,V) cm/s**2	% Speeds 0-3	3-7	>7
									cm/s		
Jun	6	1996	2	11	3.0	0.6	237	7.2	59.0	32.8	8.2
Jun	6	1996	2	15	2.6	1.0	67	4.2	66.9	31.1	1.9
Jul	7	1996	2	11	2.5	0.7	243	6.0	72.4	22.3	5.2
Jul	7	1996	2	15	2.5	1.3	96	3.8	70.4	27.2	2.4
Aug	8	1996	2	11	3.3	1.9	207	6.7	53.1	37.8	9.1
Aug	8	1996	2	15	2.9	1.1	121	5.8	62.6	32.8	4.6
Sep	9	1996	2	11	3.5	1.0	207	9.1	51.7	38.9	9.4
Sep	9	1996	2	15	3.4	1.5	140	8.3	56.1	32.8	11.1
Oct	10	1996	2	11	3.4	1.2	212	8.4	53.9	35.1	11.0
Oct	10	1996	2	15	3.3	1.3	147	7.8	58.5	32.0	9.5
Nov	11	1996	2	11	3.2	1.1	260	6.6	56.1	39.1	4.8
Nov	11	1996	2	15	3.0	1.2	332	5.8	57.8	38.5	3.7
Dec	12	1996	2	11	3.8	2.0	229	9.0	45.3	45.2	9.5
Dec	12	1996	2	15	3.5	0.1	308	10.0	53.0	38.8	8.2
Jan	1	1997	2	11	4.5	1.7	244	12.6	29.2	54.4	16.4
Jan	1	1997	2	15	4.9	1.8	314	14.5	23.0	59.5	17.5
Feb	2	1997	2	15	3.9	1.0	318	10.0	38.7	51.6	9.7
Mar	3	1997	2	15	3.4	0.7	176	10.8	56.7	35.3	7.9
Apr	4	1997	2	15	2.4	0.1	315	6.1	73.7	22.3	4.0
Nov	11	1996	2	5.3	3.0	0.6	279	6.1	58.0	38.8	3.2
Dec	12	1996	2	5.3	3.7	0.8	318	10.6	48.3	42.1	9.7
Jan	1	1997	2	5.3	4.3	1.1	324	12.4	39.0	44.9	16.1
Feb	2	1997	2	5.3	3.8	1.3	286	10.3	49.7	38.1	12.2
Mar	3	1997	2	5.3	3.6	1.1	245	10.1	49.2	42.7	8.1
Apr	4	1997	2	5.3	3.0	1.1	283	5.7	54.5	41.6	3.9
May	5	1997	2	5.3	2.5	0.9	247	4.7	73.5	21.9	4.6
Jun	6	1997	2	5.3	3.6	0.9	293	8.5	44.3	49.6	6.1
Jul	7	1997	2	5.3	3.7	0.9	395	8.7	43.7	48.4	7.9
Aug	8	1997	2	5.3	4.3	0.7	254	13.2	37.8	45.2	17.1
Sep	9	1997	2	5.3	5.2	2.5	331	17.0	30.7	43.8	25.6
Oct	10	1997	2	5.3	3.5	0.5	253	7.9	47.3	47.1	5.6
Nov	11	1996	2	7.3	3.0	0.9	299	6.0	57.0	39.6	3.4
Dec	12	1996	2	7.3	3.7	1.0	310	10.4	49.2	41.3	9.5
Jan	1	1997	2	7.3	4.4	1.5	311	12.1	33.3	52.2	14.5
Feb	2	1997	2	7.3	3.8	1.6	294	10.3	44.6	45.5	9.8
Mar	3	1997	2	7.3	3.6	1.1	258	9.3	51.5	40.3	8.2
Apr	4	1997	2	7.3	3.2	1.4	296	5.9	51.9	42.5	5.6
May	5	1997	2	7.3	2.6	1.2	258	3.9	73.1	24.1	2.8
Jun	6	1997	2	7.3	2.9	0.7	244	6.2	64.9	30.6	4.6
Jul	7	1997	2	7.3	3.2	0.9	234	6.4	52.2	43.8	4.0
Aug	8	1997	2	7.3	3.9	1.2	217	11.4	49.5	34.0	16.5
Sep	9	1997	2	7.3	4.3	1.3	306	11.0	31.8	55.7	12.5
Oct	10	1997	2	7.3	3.0	0.6	230	5.6	57.9	40.4	1.6

Table 4.7 (cont.) VACM current and wind monthly statistics, May 1996 to October 1997

Month	Mon	Year	Station No.	Depth (m)	Mean Scalar Speed cm/s	Mean Vector Speed cm/s	Resultant Direction TO deg True	Variance (U,V) cm/s**2	% Speeds 0-3	3-7	>7
										cm/s	
Nov	11	1996	2	9.3	3.2	1.2	308	6.3	53.3	43.2	3.6
Dec	12	1996	2	9.3	3.7	1.2	294	10.2	46.2	45.3	8.5
Jan	1	1997	2	9.3	4.5	2.0	304	11.8	32.5	50.5	16.5
Feb	2	1997	2	9.3	3.9	1.9	297	9.1	42.3	46.7	11.0
Mar	3	1997	2	9.3	3.6	1.1	276	9.8	50.4	40.7	8.9
Apr	4	1997	2	9.3	3.1	1.4	289	6.0	55.8	38.2	6.0
May	5	1997	2	9.3	2.6	1.5	262	3.6	66.5	31.5	2.0
Jun	6	1997	2	9.3	2.5	0.7	213	4.8	72.6	24.3	3.1
Jul	7	1997	2	9.3	3.1	1.2	214	6.2	55.4	40.1	4.6
Aug	8	1997	2	9.3	3.7	1.0	206	10.0	50.3	36.0	13.7
Sep	9	1997	2	9.3	3.6	0.9	236	8.3	45.4	46.1	8.5
Oct	10	1997	2	9.3	2.8	0.9	198	4.9	62.4	36.0	1.6
Nov	11	1996	2	11.3	3.3	1.2	309	6.8	48.6	45.8	5.6
Dec	12	1996	2	11.3	3.7	1.2	291	9.6	45.8	45.4	8.7
Jan	1	1997	2	11.3	4.6	2.3	301	11.7	30.1	52.7	17.2
Feb	2	1997	2	11.3	4.1	2.1	299	9.4	37.5	50.7	11.8
Mar	3	1997	2	11.3	3.6	1.1	267	9.6	50.0	41.9	8.1
Apr	4	1997	2	11.3	3.4	1.7	290	6.6	52.0	43.2	4.9
May	5	1997	2	11.3	2.8	1.6	269	3.8	63.0	35.2	1.7
Jun	6	1997	2	11.3	2.4	0.7	200	4.6	73.1	24.3	2.6
Jul	7	1997	2	11.3	3.1	1.2	215	6.0	54.2	41.8	4.0
Aug	8	1997	2	11.3	3.5	1.0	191	8.6	52.7	38.4	8.9
Sep	9	1997	2	11.3	3.4	1.2	205	7.4	47.9	46.0	6.1
Oct	10	1997	2	11.3	2.8	1.1	184	4.9	65.4	31.4	3.2
Nov	11	1996	2	14.3	3.5	1.3	293	7.4	43.0	52.5	4.5
Dec	12	1996	2	14.3	3.9	1.2	267	9.8	39.3	53.1	7.7
Jan	1	1997	2	14.3	4.7	2.6	293	10.8	23.9	60.8	15.2
Feb	2	1997	2	14.3	4.6	2.6	286	9.8	23.0	64.4	12.6
Mar	3	1997	2	14.3	3.8	1.1	245	10.0	43.8	48.1	8.1
Apr	4	1997	2	14.3	3.3	1.5	288	5.8	46.4	51.1	2.6
May	5	1997	2	14.3	3.0	1.7	269	4.2	53.0	45.2	1.9
Jun	6	1997	2	14.3	2.5	0.8	174	4.4	70.8	26.4	2.8
Jul	7	1997	2	14.3	2.9	1.0	216	5.3	60.5	36.0	3.5
Aug	8	1997	2	14.3	3.1	1.4	169	6.4	58.3	34.1	7.5
Sep	9	1997	2	14.3	3.4	1.3	184	6.9	49.2	45.3	5.6
Oct	10	1997	2	14.3	2.8	1.3	160	5.0	64.0	31.6	9.2
May	5	1996	3	12	3.4	1.4	291	7.5	52.5	42.2	5.4
Jun	6	1996	3	12	3.5	1.0	20	7.8	50.3	42.4	7.4
July	7	1996	3	12	2.9	1.2	22	5.3	60.9	35.3	3.8
Aug	8	1996	3	12	3.2	0.6	37	7.7	59.5	33.2	7.3
Sep	9	1996	3	12	4.4	0.3	297	14.7	36.5	50.0	12.6
Oct	10	1996	3	12	4.1	0.2	288	12.1	41.7	45.6	12.8
Nov	11	1996	3	12	3.6	1.9	50	7.2	46.6	46.2	7.2

Table 4.7 (cont.) VACM current and wind monthly statistics, May 1996 to October 1997

Month	Mon	Year	Station No.	Depth (m)	Mean Scalar Speed cm/s	Mean Vector Speed cm/s	Resultant Direction TO deg True	Variance (U,V) cm/s**2	% Speeds 0-3	3-7	>7
									cm/s		
Dec	12	1996	3	12	5.2	2.4	68	16.9	30.9	43.7	25.4
Jan	1	1997	3	12	6.8	4.2	55	24.0	17.6	43.0	39.4
Feb	2	1997	3	12	4.7	2.5	47	14.4	30.1	53.4	16.5
Mar	3	1997	3	12	3.9	0.7	124	11.8	47.6	38.6	13.8
Apr	4	1997	3	12	3.2	1.0	67	7.1	58.8	34.2	7.0
May	5	1997	3	8	6.2	4.0	55	19.5	22.6	37.4	40.1
Jun	6	1997	3	8	5.6	2.6	70	16.7	18.9	54.2	26.9
Jul	7	1997	3	8	5.6	1.5	62	18.7	18.3	56.0	25.7
Aug	8	1997	3	8	5.9	1.9	39	24.0	27.2	43.3	29.6
Sep	9	1997	3	8	7.1	4.1	46	28.5	19.3	42.5	38.2
May	5	1996	4	25	2.8	0.2	356	5.7	62.7	32.4	4.9
May	5	1996	4	29	2.6	0.3	77	4.9	70.6	26.5	2.9
Jun	6	1996	4	25	3.2	1.1	333	6.4	53.6	41.7	4.7
Jun	6	1996	4	29	2.7	0.4	237	4.9	61.4	36.8	1.8
Jul	7	1996	4	25	3.1	0.8	9	7.9	59.9	34.3	5.8
Jul	7	1996	4	29	2.7	0.6	280	6.0	62.8	33.5	3.8
Aug	8	1996	4	25	4.2	1.3	68	14.0	46.5	37.0	16.5
Aug	8	1996	4	29	4.2	1.7	95	13.3	44.9	42.1	13.0
Sep	9	1996	4	25	4.6	0.5	100	18.8	45.1	35.7	19.2
Sep	9	1996	4	29	4.7	0.8	128	17.9	42.4	36.9	20.7
Oct	10	1996	4	25	5.0	0.5	42	19.7	34.5	43.4	22.0
Oct	10	1996	4	29	4.4	0.5	182	15.2	43.0	39.7	17.3
May	5	1997	4	25	3.3	1.1	260	7.9	51.5	41.5	7.0
Jun	6	1997	4	25	3.7	0.4	215	10.2	47.5	39.6	12.9
Jul	7	1997	4	25	4.1	1.1	104	11.7	41.9	44.4	13.7
Aug	8	1997	4	25	4.8	2.0	111	17.8	41.8	35.2	23.0
Sep	9	1997	4	25	3.9	1.1	100	12.3	45.6	42.5	11.9
Oct	10	1997	4	25	4.7	2.8	103	16.5	43.9	39.3	16.8
May	5	1996	5	5	7.3	6.4	172	11.2	10.5	31.0	58.5
May	5	1996	5	9	4.3	2.2	153	10.5	35.5	50.5	14.0
Jun	6	1996	5	5	5.7	0.8	258	23.1	28.3	40.6	31.1
Jun	6	1996	5	9	4.2	0.8	273	12.9	46.8	34.6	18.6
Jul	7	1996	5	5	4.5	1.3	203	16.4	45.8	34.0	20.2
Jul	7	1996	5	9	3.8	1.8	289	8.7	41.4	50.0	8.6
Aug	8	1996	5	5	5.7	0.8	218	22.2	29.6	35.6	34.8
Aug	8	1996	5	9	3.5	1.2	143	8.3	51.9	37.8	10.3
Sep	9	1996	5	5	6.5	1.1	142	33.7	31.7	33.9	34.4
Sep	9	1996	5	9	4.9	3.1	127	17.1	43.6	34.0	22.4
Nov	10	1996	5	9	2.5	0.7	190	4.0	73.1	24.8	2.1
Dec	10	1996	5	9	3.2	0.6	327	9.5	62.1	30.9	7.0
Jan	1	1997	5	9	4.1	1.3	300	11.3	37.8	50.1	12.1
Feb	2	1997	5	9	3.5	0.6	195	9.8	57.7	51.7	10.7
Mar	3	1997	5	9	3.3	0.9	133	12.6	64.2	28.2	7.5

Table 4.7 (cont.) VACM current and wind monthly statistics, May 1996 to October 1997

Month	Mon	Year	Station No.	Depth (m)	Mean Scalar Speed cm/s	Mean Vector Speed cm/s	Resultant Direction TO deg True	Variance (U,V) cm/s**2	% Speeds 0-3	3-7	>7
									cm/s		
Apr	4	1997	5	9	2.4	0.3	100	5.4	73.9	22.1	4.0
May	5	1997	5	12	4.8	3.9	144	9.7	30.2	53.6	16.1
Jun	6	1997	5	12	3.5	2.9	128	4.7	50.1	43.9	6.0
Jul	7	1997	5	12	3.6	2.6	128	6.6	43.7	49.5	6.9
Aug	8	1997	5	12	3.7	1.9	126	8.0	44.8	44.9	10.3
Sep	9	1997	5	12	4.1	2.2	135	10.1	44.2	41.5	14.3
Oct	10	1997	5	12	3.3	2.6	127	4.4	53.2	38.9	7.9
May	5	1996	6	7	6.2	5.5	151	9.4	19.1	39.2	41.7
Jun	6	1996	6	7	4.9	0.8	193	18.2	36.4	42.6	21.0
Jul	7	1996	6	7	4.2	2.2	165	12.3	46.2	34.1	19.6
Aug	8	1996	6	7	5.4	1.5	192	20.1	34.7	36.4	28.9
Sep	9	1996	6	7	6.3	0.4	171	33.5	28.1	35.8	36.1
Oct	10	1996	6	7	4.2	0.4	230	14.8	46.4	37.1	16.5
Nov	11	1996	6	11	2.4	0.9	155	3.5	73.7	25.7	0.6
Dec	12	1996	6	11	3.2	1.2	337	9.1	65.1	26.9	8.1
Jan	1	1997	6	11	4.1	1.3	132	10.6	34.5	55.5	9.9
Feb	2	1997	6	11	3.5	2.1	172	7.1	52.5	36.2	11.3
Mar	3	1997	6	11	3.9	1.7	128	13.0	53.4	34.1	12.5
Apr	4	1997	6	11	2.8	1.3	143	6.0	67.7	24.3	7.9
May	5	1997	8	31.5	3.8	2.1	312	7.0	38.0	56.2	5.8
Jun	6	1997	8	31.5	4.3	0.8	168	11.6	32.8	53.1	14.2
Jul	7	1997	8	31.5	5.0	0.6	161	17.1	27.7	50.5	21.9
Aug	8	1997	8	31.5	5.7	2.0	177	20.9	23.1	48.0	28.9
Sep	9	1997	8	31.5	5.0	2.5	159	13.1	24.4	54.6	21.0
Oct	10	1997	8	31.5	6.3	3.2	153	19.8	15.6	45.2	39.2
May	5	1997	8	45.5	3.6	2.5	306	5.4	43.2	51.3	5.5
Jun	6	1997	8	45.5	3.6	1.0	277	7.9	44.7	48.9	6.4
Jul	7	1997	8	45.5	4.0	0.7	271	11.1	39.7	48.8	11.6
Aug	8	1997	8	45.5	4.4	0.6	195	12.2	30.5	54.6	14.9
Sep	9	1997	8	45.5	3.8	1.4	180	8.4	39.3	52.6	8.1
Oct	10	1997	8	45.5	5.5	2.4	129	17.6	25.2	44.8	30.1
May	5	1997	9	9	5.0	3.2	30	16.1	33.7	45.6	20.7
Jun	6	1997	9	9	2.6	0.3	76	5.8	69.6	24.7	5.7
Jul	7	1997	9	9	3.5	1.0	57	8.7	49.7	41.0	9.3
Aug	8	1997	9	9	3.6	1.5	73	8.8	49.7	41.0	9.3
Sep	9	1997	9	9	4.0	2.5	54	8.9	42.6	45.6	11.8
Oct	10	1997	9	9	2.4	0.8	153	4.0	67.9	31.3	0.8

Table 4.8 ADCP station 2 current and wind monthly statistics, November 1996 to April 1997.

	Nov 96			Dec-96			Jan-97			Feb 97			Mar 97			Apr 97		
Station (Depth) (m)	Mean Scalar Speed (cm/s)	Average Velocity (cm/s)	Direction to Deg True	Mean Scalar Speed (cm/s)	Average Velocity (cm/s)	Direction to Deg True	Mean Scalar Speed (cm/s)	Average Velocity (cm/s)	Direction to Deg True	Mean Scalar Speed (cm/s)	Average Velocity (cm/s)	Direction to Deg True	Mean Scalar Speed (cm/s)	Average Velocity (cm/s)	Direction to Deg True	Mean Scalar Speed (cm/s)	Average Velocity (cm/s)	Direction to Deg True
#2 (0.0)	36.3	21.0	141	32.3	9.7	93	34.3	13.4	89	38.9	16.4	110	40.5	8.9	166	43.3	14.9	117
0.3	47.4	23.3	134	47.3	14.0	77	49.5	22.9	89	50.1	25.8	108	49.6	18.6	142	50.3	23.2	117
0.8	53.5	32.4	131	48.0	17.9	89	47.6	24.1	91	47.2	23.8	103	44.8	13.5	147	39.6	14.9	124
1.3	39.5	22.1	128	32.8	8.9	81	28.6	12.2	96	24.7	10.8	104	22.1	5.7	155	14.7	4.1	126
1.8	14.3	6.7	129	11.0	1.0	28	9.6	1.1	76	6.0	1.2	248	5.7	2.4	247	3.6	0.5	259
2.3	3.8	0.3	227	4.5	0.6	314	5.1	0.7	35	4.1	0.3	213	4.1	1.1	213	3.2	0.4	226
2.8	3.4	0.3	210	4.0	0.6	357	4.7	0.8	28	3.9	0.4	247	3.8	1.0	215	3.2	0.9	263
3.3	3.3	0.2	241	3.8	0.5	345	4.5	0.6	10	3.8	0.5	271	3.7	1.0	221	3.0	0.7	265
3.8	3.1	0.3	260	3.9	0.6	335	4.5	0.6	357	3.7	0.7	280	3.7	0.9	228	3.0	0.8	284
4.3	3.1	0.4	268	3.9	0.7	333	4.3	0.8	340	3.7	0.8	288	3.6	1.0	235	3.3	0.9	281
4.8	3.1	0.6	292	3.8	0.8	328	4.3	0.9	333	3.7	1.1	288	3.6	1.1	234	3.1	1.0	284
5.3	3.0	0.6	279	3.7	0.8	318	4.3	1.1	324	3.8	1.3	286	3.6	1.1	245	3.0	1.1	283
5.8	3.0	0.6	299	3.7	0.9	315	4.2	1.1	321	3.7	1.2	289	3.6	1.0	249	3.0	1.3	294
6.3	2.9	0.7	302	3.7	1.0	317	4.3	1.3	312	3.6	1.4	290	3.6	1.1	251	3.0	1.4	283
6.8	3.0	0.8	297	3.7	1.0	308	4.2	1.3	313	3.7	1.5	295	3.6	1.1	255	3.1	1.4	287
7.3	3.0	0.9	299	3.7	1.0	310	4.4	1.5	311	3.8	1.6	294	3.6	1.1	258	3.2	1.4	296
7.8	3.1	0.9	304	3.8	1.1	307	4.4	1.7	308	3.8	1.6	295	3.5	1.2	261	3.1	1.4	293
8.3	3.1	1.0	302	3.8	1.2	301	4.4	1.8	306	3.8	1.8	297	3.5	1.2	264	3.2	1.4	293
8.8	3.1	1.0	310	3.7	1.1	298	4.4	1.9	306	3.9	1.8	300	3.6	1.2	266	3.2	1.5	290
9.3	3.2	1.2	308	3.7	1.2	294	4.5	2.0	304	3.9	1.9	297	3.6	1.1	276	3.1	1.4	289
9.8	3.2	1.2	310	3.7	1.2	296	4.5	2.1	303	3.9	1.9	299	3.6	1.2	271	3.1	1.5	292
10.3	3.2	1.3	309	3.6	1.2	297	4.5	2.1	303	4.0	2.0	298	3.6	1.2	269	3.2	1.5	293
10.8	3.3	1.2	312	3.7	1.2	296	4.6	2.2	303	4.2	2.0	300	3.6	1.1	265	3.4	1.5	290
11.3	3.3	1.2	309	3.7	1.2	291	4.6	2.3	301	4.1	2.1	299	3.6	1.1	267	3.4	1.7	290
11.8	3.2	1.1	309	3.7	1.1	290	4.7	2.3	302	4.2	2.1	299	3.6	1.1	265	3.4	1.7	291
12.3	3.2	1.2	310	3.7	1.2	287	4.9	2.5	302	4.3	2.1	299	3.7	1.1	262	3.3	1.5	290
12.8	3.2	1.2	309	3.7	1.2	286	4.9	2.5	300	4.3	2.1	299	3.7	1.1	262	3.4	1.6	293
13.3	3.3	1.2	310	3.5	1.0	277	4.9	2.5	302	4.3	2.1	300	3.8	1.0	259	3.6	1.8	287
13.8	3.4	1.3	301	3.7	1.1	272	4.9	2.4	297	4.4	2.1	294	3.8	1.2	256	3.6	1.8	291
14.3	3.5	1.3	293	3.9	1.2	267	4.7	2.6	293	4.6	2.6	286	3.8	1.1	245	3.3	1.5	288
#99 (Wind m/s)	3.7	2.0	152	4.0	0.9	81	3.4	0.9	111	4.0	1.6	117	4.3	1.4	177	4.1	2.0	127

Table 4.9 ADCP station 2 current and wind monthly statistics, May to October 1977.

	May			Jun			Jul			Aug			Sep			Oct		
Station (Depth) (m)	Mean Scalar Speed (cm/s)	Average Velocity (cm/s)	Direction to Deg True	Mean Scalar Speed (cm/s)	Average Velocity (cm/s)	Direction to Deg True	Mean Scalar Speed (cm/s)	Average Velocity (cm/s)	Direction to Deg True	Mean Scalar Speed (cm/s)	Average Velocity (cm/s)	Direction to Deg True	Mean Scalar Speed (cm/s)	Average Velocity (cm/s)	Direction to Deg True	Mean Scalar Speed (cm/s)	Average Velocity (cm/s)	Direction to Deg True
#2 (0.3)	43.3	19.6	92	27.9	7.5	16	39.8	11.8	64	39.8	9.7	31	40.9	15.3	72	32.4	7.9	102
1.3	16.6	5.9	100	13.1	4.7	3	26.3	4.7	71	36.6	8.5	93	46.2	16.0	77	39.0	9.3	113
2.3	3.2	0.5	210	6.4	3.2	355	5.7	1.5	0	7.1	1.3	345	8.5	2.0	14	6.4	0.6	185
3.3	2.9	0.6	230	5.0	2.3	342	4.7	1.3	349	5.9	1.4	342	6.5	2.8	350	4.3	0.4	310
4.3	2.6	0.7	239	4.1	1.5	324	4.1	1.0	321	4.7	0.7	311	5.7	2.8	340	1.9	0.5	281
5.3	2.5	0.9	247	3.6	0.9	293	3.7	0.9	395	4.3	0.7	254	5.2	2.5	331	3.5	0.5	253
6.3	2.5	1.0	252	3.2	0.8	264	3.3	0.8	263	4.2	1.1	227	4.8	1.9	323	3.2	0.6	244
7.3	2.6	1.2	258	2.9	0.7	244	3.2	0.9	234	3.9	1.2	217	4.3	1.3	306	3.0	0.6	230
8.3	2.6	1.3	261	2.6	0.7	225	3.1	1.1	216	3.8	1.1	212	3.8	0.9	273	2.9	0.7	214
9.3	2.6	1.5	262	2.5	0.7	213	3.1	1.2	214	3.7	1.0	206	3.6	0.9	236	2.8	0.9	198
10.3	2.7	1.6	265	2.4	0.6	206	3.1	1.2	213	3.6	0.9	199	3.5	1.0	215	2.8	1.1	191
11.3	2.8	1.6	269	2.4	0.7	200	3.1	1.2	215	3.5	1.0	191	3.4	1.2	205	2.8	1.1	184
12.3	3.8	1.7	271	2.4	0.7	193	3.0	1.1	215	3.3	1.1	187	3.5	1.3	195	2.8	1.1	178
13.3	2.9	1.7	272	2.4	0.8	192	3.0	1.1	216	3.2	1.3	176	3.5	1.3	191	2.9	1.2	173
14.3	3.0	1.7	269	2.5	0.8	174	2.9	1.0	216	3.1	1.4	169	3.4	1.3	184	2.8	1.3	160
#8 (Wind m/s)	3.7	2.0	84	2.8	0.7	31	3.0	1.0	55	3.4	0.9	61	4.2	1.9	69	3.1	0.9	89

Table 4.10 ADCP station 8 current and wind monthly statistics, May to October 1997.

	May			Jun			Jul			Aug			Sep			Oct		
Station (Depth) (m)	Mean Scalar Speed (cm/s)	Average Velocity (cm/s)	Direction to Deg True	Mean Scalar Speed (cm/s)	Average Velocity (cm/s)	Direction to Deg True	Mean Scalar Speed (cm/s)	Average Velocity (cm/s)	Direction to Deg True	Mean Scalar Speed (cm/s)	Average Velocity (cm/s)	Direction to Deg True	Mean Scalar Speed (cm/s)	Average Velocity (cm/s)	Direction to Deg True	Mean Scalar Speed (cm/s)	Average Velocity (cm/s)	Direction to Deg True
#8 (31.5)	3.8	2.1	312	4.3	0.8	168	5.0	0.6	161	5.7	2.0	177	5.0	2.5	159	6.3	3.2	153
32.5	3.7	1.8	307	4.1	0.4	166	4.7	0.6	143	5.2	1.4	179	5.0	2.3	155	6.2	3.0	153
33.5	3.5	1.8	310	3.9	0.4	248	4.6	0.4	151	5.0	1.2	178	4.7	2.2	161	6.2	3.0	152
34.5	3.6	2.0	310	3.8	0.3	219	4.4	0.2	141	4.6	1.1	174	4.5	2.1	161	6.1	3.3	150
35.5	3.3	1.8	308	3.8	0.3	252	4.4	0.3	154	4.7	1.2	173	4.4	2.2	161	6.2	3.2	150
36.5	3.3	1.9	308	3.7	0.3	225	4.5	0.2	136	4.5	1.0	171	4.2	2.0	162	6.2	3.3	148
37.5	3.4	2.0	308	3.6	0.3	248	4.3	0.2	164	4.5	1.0	183	4.1	2.0	167	6.1	3.0	145
38.5	3.3	1.9	309	3.6	0.3	233	4.4	0.4	148	4.5	0.7	189	4.2	2.0	165	6.0	3.0	143
39.5	3.4	2.0	309	3.6	0.4	280	4.4	0.1	216	4.6	0.7	195	4.1	1.9	169	6.0	3.0	144
40.5	3.4	2.0	307	3.6	0.3	254	4.3	0.2	183	4.6	8.0	185	4.1	2.1	166	6.1	3.1	138
41.5	3.6	2.3	312	3.7	0.6	280	4.4	0.1	263	4.6	0.7	179	4.0	1.7	164	5.9	3.1	137
42.5	3.5	2.3	308	3.8	0.8	279	4.3	0.5	283	4.7	0.7	191	4.0	1.7	176	5.9	2.8	136
43.5	3.6	2.4	309	3.7	0.7	290	4.2	0.3	292	4.6	0.6	175	4.0	1.6	164	6.0	2.9	130
44.5	3.6	2.4	306	3.8	1.0	272	4.1	0.6	269	4.6	0.6	186	4.0	1.6	175	5.7	2.7	132
45.5	3.6	2.5	306	3.6	1.0	277	4.0	0.7	271	4.4	0.6	195	3.8	1.4	180	5.5	2.4	129
46.5	3.8	3.0	291	4.1	2.2	265	4.3	1.9	263	4.5	1.5	237	4.0	2.3	231	5.5	1.8	175
#8 (Wind m/s)	3.7	2.0	84	2.8	0.7	31	3.0	1.0	55	3.4	0.9	61	4.2	1.9	69	3.1	0.9	89

Table 4.11 Temperature summaries from FTP and current meters, 1996-97.

		#1 (9m) Deg C	#1 (13m) Deg C	#2 (11m) Deg C	#2 (15m) Deg C	#3 (12m) Deg C	#4 (25m) Deg C	#4 (29m) Deg C	#5 (9m) Deg C	#6 (7m) Deg C	#6 (11m) Deg C
12:00/23/5/96 to 13:00/4/11/1996											
Current Meters	Avg	12.6	11.5	12.2	11.1	12.1	8.5	7.7		14.1	
	Std Dev	5.0	4.8	4.9	4.7	5.0	4.3	3.9		4.6	
	Max	22.9	22.3	22.6	22.3	22.5	22.2	22.2		23.2	
	Min	4.2	4.2	4.3	4.2	4.3	4.1	4.1		5.7	
	Count	3962	3962	3962	3962	3962	3962	3962		3958	
17:00/8/11/96 to 14:00/24/4/97											
Current Meters	Avg		3.0		3.0	3.0			2.9		2.9
Winter	Std Dev		1.4		1.3	1.4			1.6		1.6
	Max		9.3		9.2	9.1			9.4		8.8
	Min		0.8		0.8	0.5			0.5		0.7
	Count		4006		4006	4006			4006		4006

17:00/30/4/97 to 13:00/21/10/97						
Current Meters		#1 (9m) Deg C	#3 (8m) Deg C	#4 (25m) Deg C	#5 (12m) Deg C	#9 (9m) Deg C
	Avg	10.0	10.6	6.6	9.9	10.1
	Std Dev	4.8	5.4	3.3	4.7	4.8
	Max	19.7	20.5	17.7	19.5	19.5
	Min	4.2	3.8	3.8	4.3	4.3
	Count	4173	3533	4150	4173	4173

Station #4 (12:00/2/5/97 to 15:00/10/20/97)) Temperatures (Deg C)

FTP	Depth (M)	20 m	16 m	14 m	12 m	11 m	8.2 m	6.2 m	4.2 m	2 m
	Avg	7.9	9.0	9.5	10.0	10.4	11.5	11.9	12.8	13.2
	Std Dev	4.0	4.6	4.7	4.8	4.9	4.9	5.1	5.2	5.3
	Max	18.9	19.1	19.0	19.0	19.1	20.1	20.1	20.8	21.1
	Min	3.9	3.9	3.9	3.9	3.9	4.3	3.9	3.9	3.8
	Count	4108	4108	4108	4108	4108	4108	4108	4108	4108

Station #8 (12:00/2/5/97 to 15:00/10/20/97)) Temperatures (Deg C)

FTP	Depth (M)	40m	29 m	20m	16 m	14 m	12 m	11 m	8 m	6 m	2m	Surface 0 m
	AVG	5.0	6.0	7.9	9.1	9.8	10.5	10.8	11.4	12.1	13.4	13.6
	STD DEV	2.1	3.0	4.3	4.8	5.1	5.3	5.4	5.4	5.5	5.6	5.5
	MAX	16.3	17.6	18.8	19.0	19.2	19.3	19.5	19.7	20.3	21.8	23.4
	MIN	3.4	3.5	3.5	3.5	3.5	3.5	3.5	3.5	3.5	3.5	3.2
	COUNT	4107	4107	4107	4107	4107	4107	4107	4107	4107	4107	4107

Table 5.1 Selected upwelling/downwelling episodes in 1997.

Dates	Julian Days	Episode	Predominant Wind Direction (Toward)	Range of Mean Wind Speed (m/s)
3 July 97-8 July 97	184-189	Upwelling	North-East	4-6
23 July 97-29 July 97	204-210	Downwelling	South,SW	3-4
30 July 97-3 Aug 97	211-215	Upwelling	North-West	3-5
4 Aug 97-6 Aug 97	216-218	Downwelling	West	3-4
8 Aug 97-13 Aug97	219-225	Upwelling	North-East	3-3.5
18 Aug97-23 Aug97	230-235	Downwelling	West	4-5
24 Aug97-28 Aug97	236-240	Upwelling	North-East	2-3

Table 5.2 VACM current meter statistics for the summer season.

Current meter	RMS u'	RMS v'	Kx(10^4 cm^2/s)	Ky (10^4 cm^2/s)	MKE (cm^2/s^2)	TKE (cm^2/s^2)
1	1.90	2.29	1.576	2.644	17.396	4.685
5	1.39	1.49	0.775	1.032	4.1154	2.142
4	1.69	1.50	1.267	1.003	6.0547	2.663
3	2.11	1.79	2.563	1.918	10.481	4.046
9	1.55	1.60	0.958	1.157	6.4250	2.624

Table 5.3 Mean and RMS velocities, Lagrangian integral time and length scales, and horizontal exchange coefficients derived from single particle analysis.

ID	Duration (Hours)	U-Mean1 (cm/s)	V-Mean (cm/s)	URMS (cm/s)	VRMS (cm/s)	Tx (Hours)	Ty (Hours)	Lx (Km)	Ly (Km)	Kx (cm^2/s)	Ky (cm^2/s)
3	75	8.1	2.4	14.6	12.7	11.7	6.4	6.2	2.9	9.0E+06	3.7E+06
19	24	17.0	11.2	19.1	13.5	12.3	8.9	8.4	4.3	1.6E+07	5.9E+06
21	71	6.8	-2.4	15.3	11.4	6.3	4.8	3.5	2.0	5.3E+06	2.2E+06
22	93	3.0	3.1	7.9	9.9	8.4	2.4	2.4	0.9	1.9E+06	8.4E+05
24	219	2.3	3.2	11.6	16.4	4.3	0.2	1.8	0.1	2.1E+06	1.5E+05
30	23	3.9	-8.4	6.7	16.3	4.2	2.9	1.0	1.7	6.8E+05	2.8E+06
32	28	2.3	-3.3	8.3	9.6	2.3	0.2	0.7	0.1	5.8E+05	5.6E+04

Table 6.1 Monthly Skyway WWTP effluent and Lake Ontario temperatures near the proposed outfall.

Temp. (°C)	Jan	Feb	Mar	Apr	May	Jun	Jul	Aug	Sep	Oct	Nov	Dec
Lake	2.2	1.5	2.1	3.4	5.3	8.2	11.1	15.8	16.1	11.0	5.6	4.0
Effluent	11.5	11.0	10.0	11.0	12.0	11.9	16.6	19.6	20.5	18.8	15.6	14.5

Table 6.2 Waste field characteristics and near-field dilution rates for the present discharge conditions (2 m^3/s) during the summer and winter seasons predicted by the RSB model.

Season	Current speed (cm/s)	IMR (x_i)	Z_e (m)	Z_m(m)	h_e(m)	S_m	Dilution at 100 m
	3	11.5	5.1	3.4	4.6	12.7	14.7
Summer	5	19.2	5.0	3.3	4.4	17.9	20.3
	10	39.4	3.9	2.6	3.7	28.3	30.1
	3	21.4	14.0	9.4	10.5	21.5	29.8
Winter	5	78.9	14.0	9.4	12.5	49.4	49.4
	10	204.8	14.0	9.4	13.3	96.9	96.9

Table 6.3 Waste field characteristics and near-field dilution rates with treatment capacity increased to 6.94 m^3/s.

Season	Current speed (cm/s)	IMR (x_i)	Z_e (m)	Z_m(m)	h_e(m)	S_m	Dilution at 100 m
	3	5.9	7.6	5.1	5.7	6.2	7.4
Summer	5	18.5	7.6	5.1	6.8	8.7	9.8
	10	37.4	6.6	4.4	6.9	13.8	14.7
	3	10.8	14.0	9.4	10.5	8.4	9.8
Winter	5	44.9	14.0	9.4	12.4	14.2	15.0
	10	115.8	14.0	9.4	12.5	28.3	32.5

Table 6.4 Waste field characteristics and near-field dilution rates for outfall site 2000 m offshore.

Flow rate m^3/s	Current speed (cm/s)	IMR (x_i)	Z_e (m)	Z_m(m)	h_e(m)	S_m	Dilution at 100 m
2.00	5	22.8	6.5	4.4	5.8	20.4	26.2
	10	46.2	5.1	3.4	4.5	31.8	38.2
6.94	5	21.7	9.5	6.4	8.4	9.7	12.5
	10	43.9	8.5	5.7	7.6	15.5	18.7

Table 6.5 Waste field characteristics and near-field dilutions during summer with 2 m^3/s (Phosphorus concentration of 300 µg/l from pipe).

Current speed cm/s	IMR (m)	Z_c (m)	h_c(m)	Z_m(m)	Initial Dilution S_m	Dilution at 100 m	Distance of 10 µg/l (m)
3	10.5	5.7	5.1	3.8	12.3	14.9	510 m
5	17.5	5.7	5.1	3.8	17.6	20.3	470 m
10	35.2	4.5	4.0	3.0	27.3	31.4	<100 m
15	39.8					40.0	<75 m

Table 6.6 Waste field characteristics and near-field dilutions during summer with 6.94 m^3/s (Phosphorus concentration of 300 µg/l from pipe).

Current speed cm/s	IMR (m)	Z_c (m)	h_c(m)	Z_m(m)	Initial Dilution S_m	Dilution at 100 m	Distance of 10 µg/l (m)
5	18.1	8.6	7.6	5.8	8.7	10.0	1150 m
10	37.2	7.9	7.0	5.3	13.9	15.2	1300 m
15	52.6	6.9	6.2	4.6	18.3	21.0	<1300 m

Table 6.7 Waste field characteristics and near-field dilutions during summer with 2 m^3/s (Phosphorus concentration of 300 µg/l from pipe).The outfall is shifted to 20 m depth (2 km from shore).

Current speed cm/s	IMR (m)	Z_c (m)	h_c(m)	Z_m(m)	Initial Dilution S_m	Dilution at 100 m	Distance of 10 µg/l (m)
5	23.9	6.7	5.8	4.4	20.6	25.5	<100 m
10	46.2	5.1	4.5	3.4	32.1	38.4	<100 m

Table 6.8 Waste field characteristics and near-field dilutions during summer with 6.94 m^3/s (Phosphorus concentration of 300 µg/l from pipe).The outfall is shifted to 20 m depth (2 km from shore).

Current speed cm/s	IMR (m)	Z_c (m)	h_c(m)	Z_m(m)	Initial Dilution S_m	Dilution at 100 m	Distance of 10 µg/l (m)
5	23.3	9.7	8.3	6.4	9.9	13.7	840 m
10	47.8	8.5	7.6	5.7	15.5	22.0	700 m

List of Figures

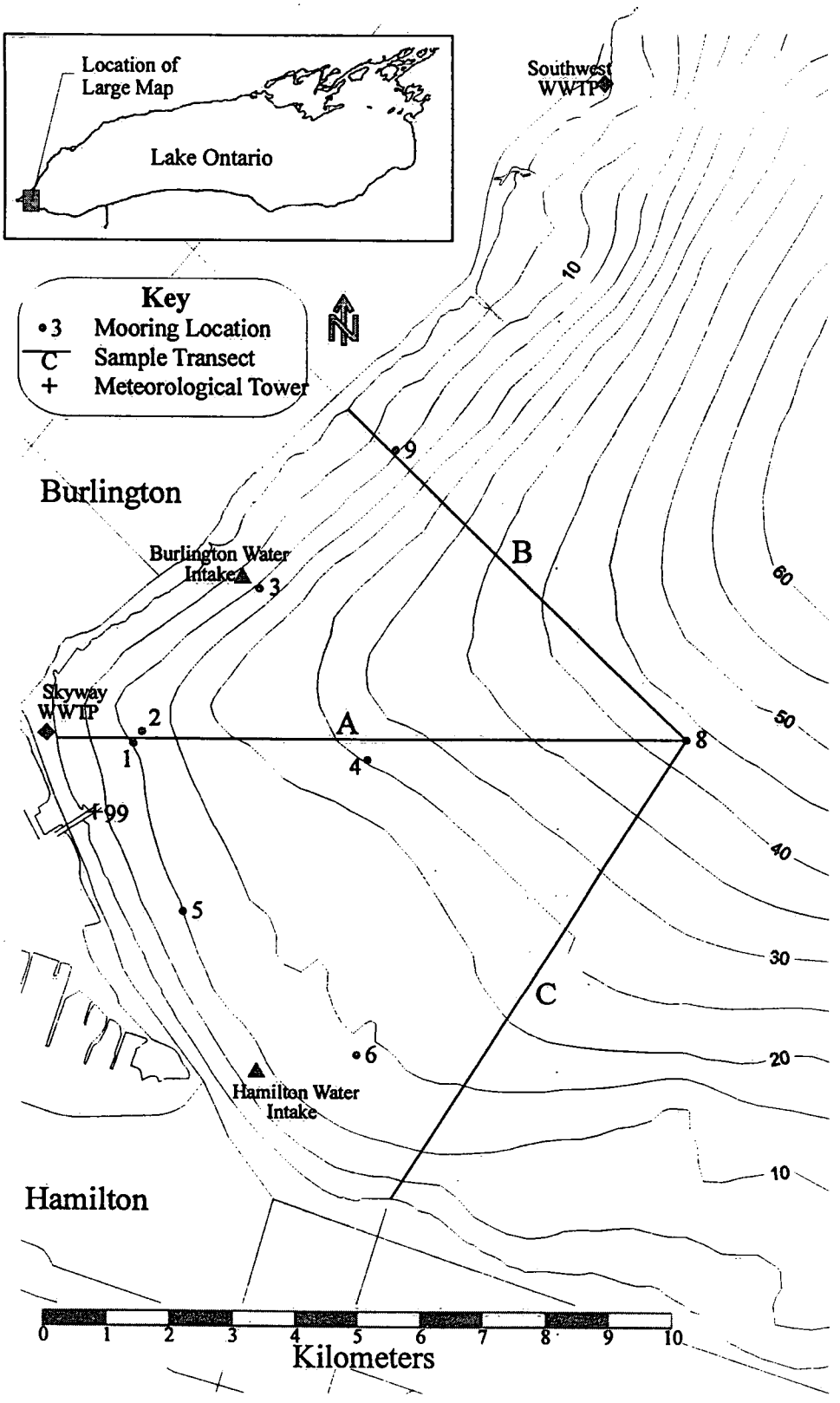

Figure 1.1 Map of 1996-97 study area and station locations.

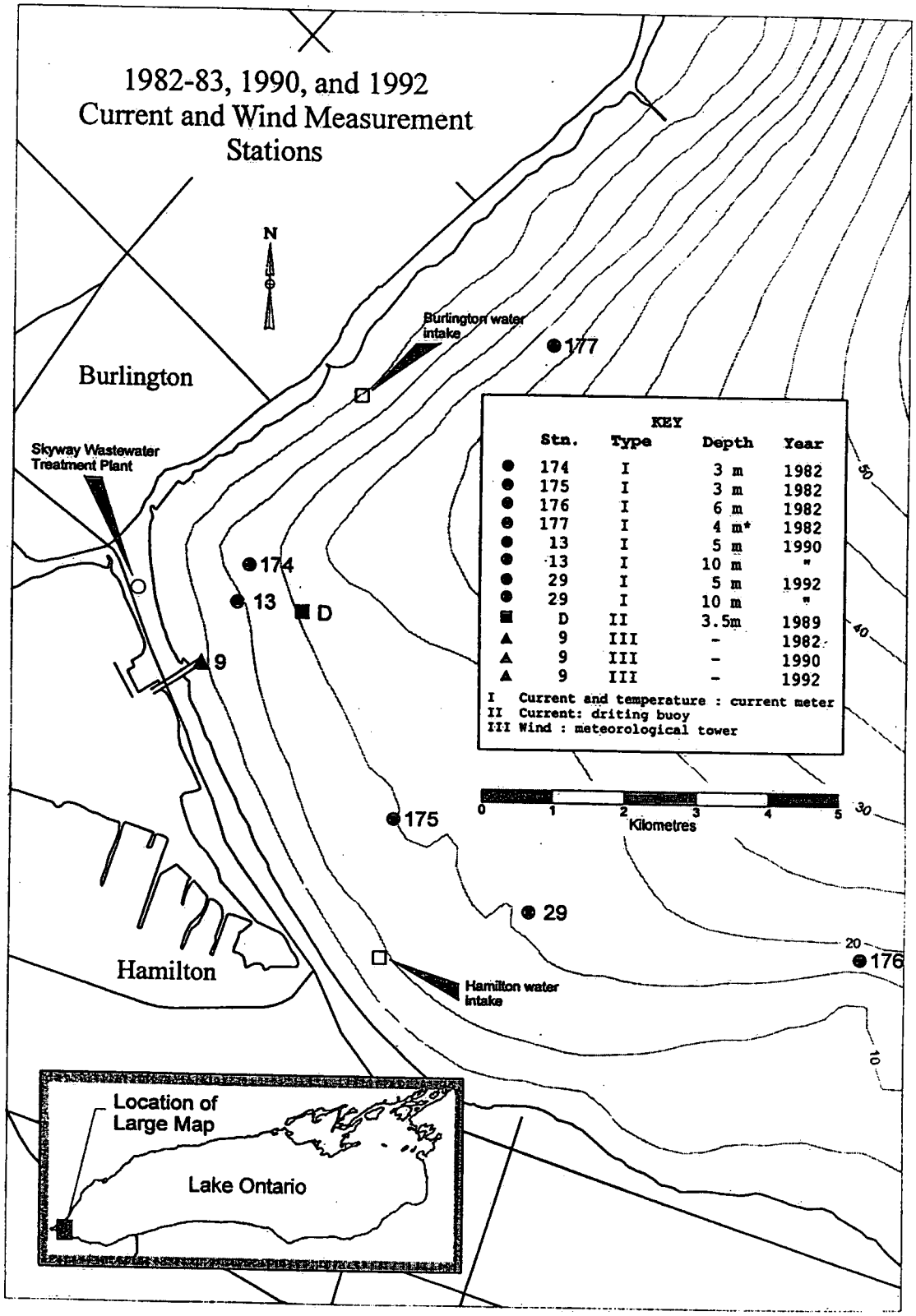

Figure 2.1 Map of historical data sample stations.

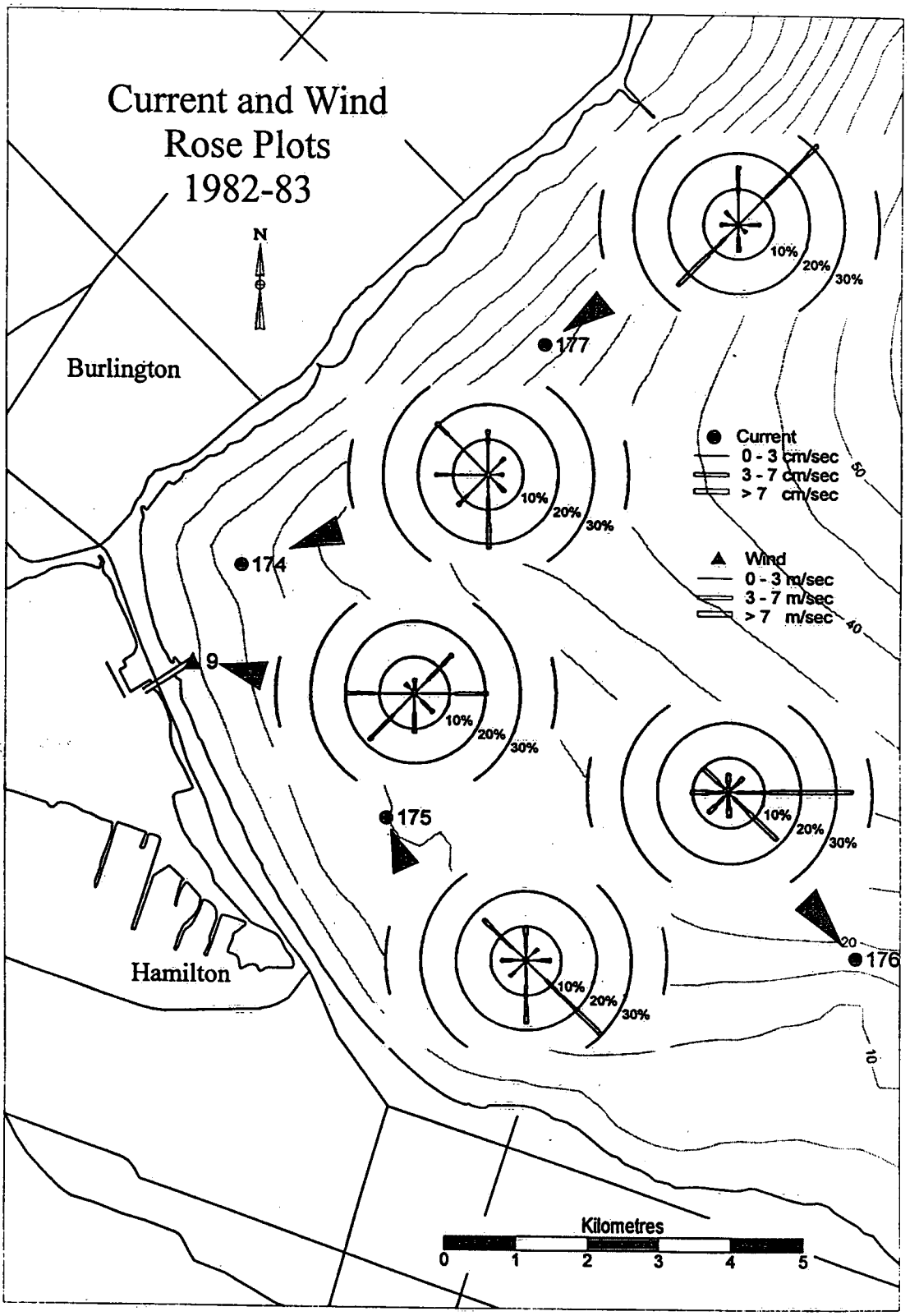

Figure 2.2 Rose histogram plots of hourly wind and current data for 1982-83.

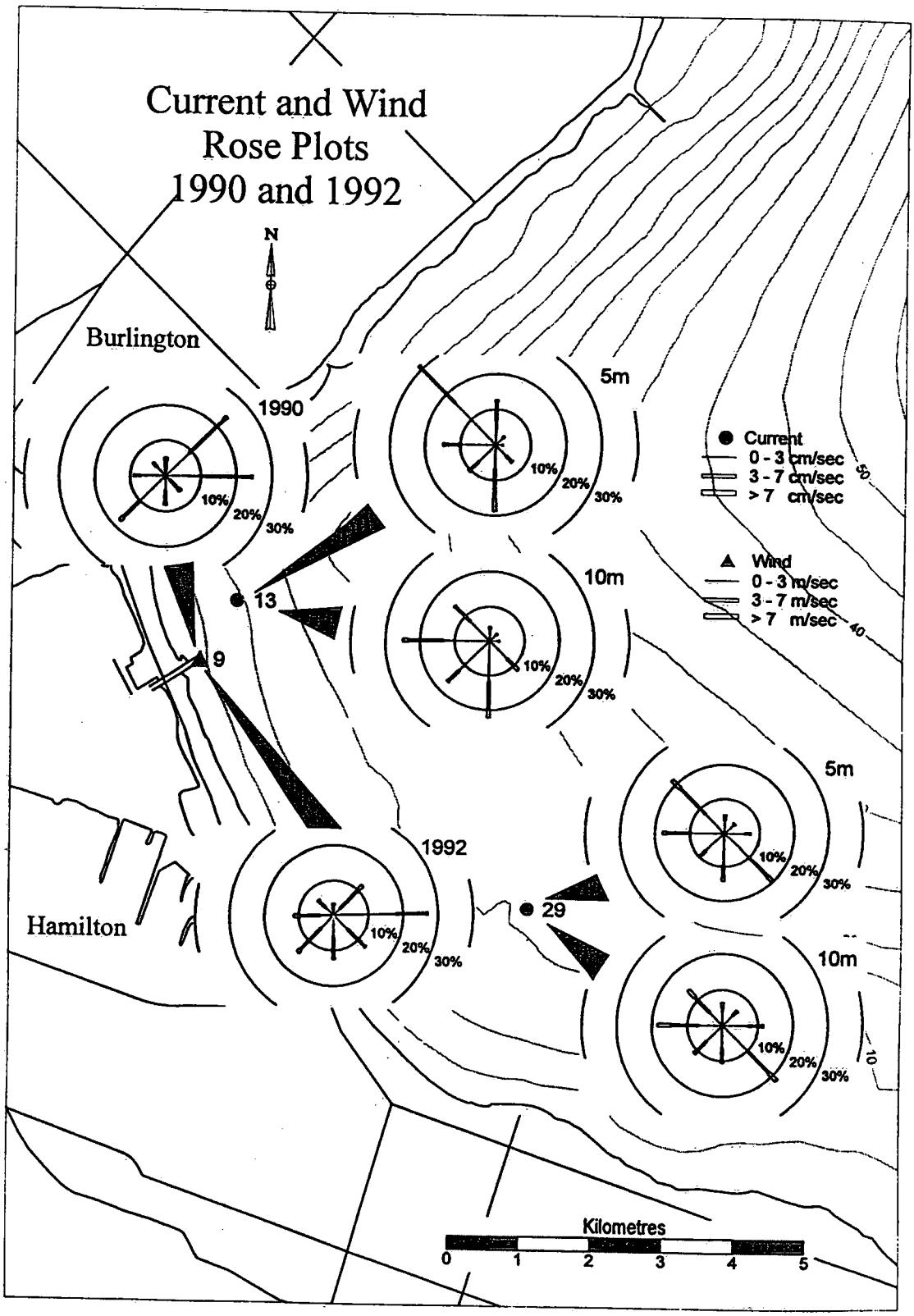

Figure 2.3 Rose histogram plots of hourly wind and current data for 1990, 1992.

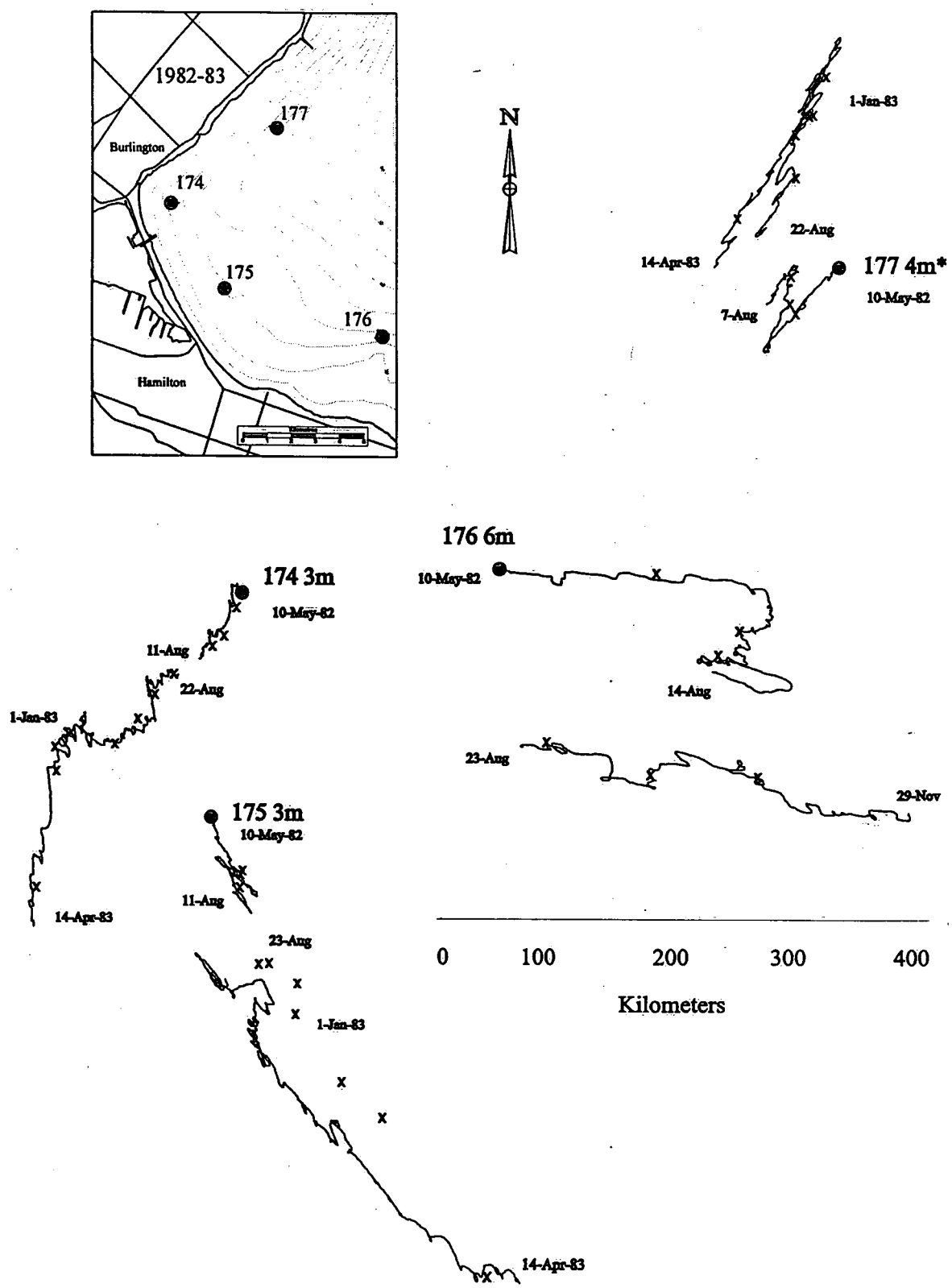

Figure 2.4 Current progressive vector diagrams 1982-83.

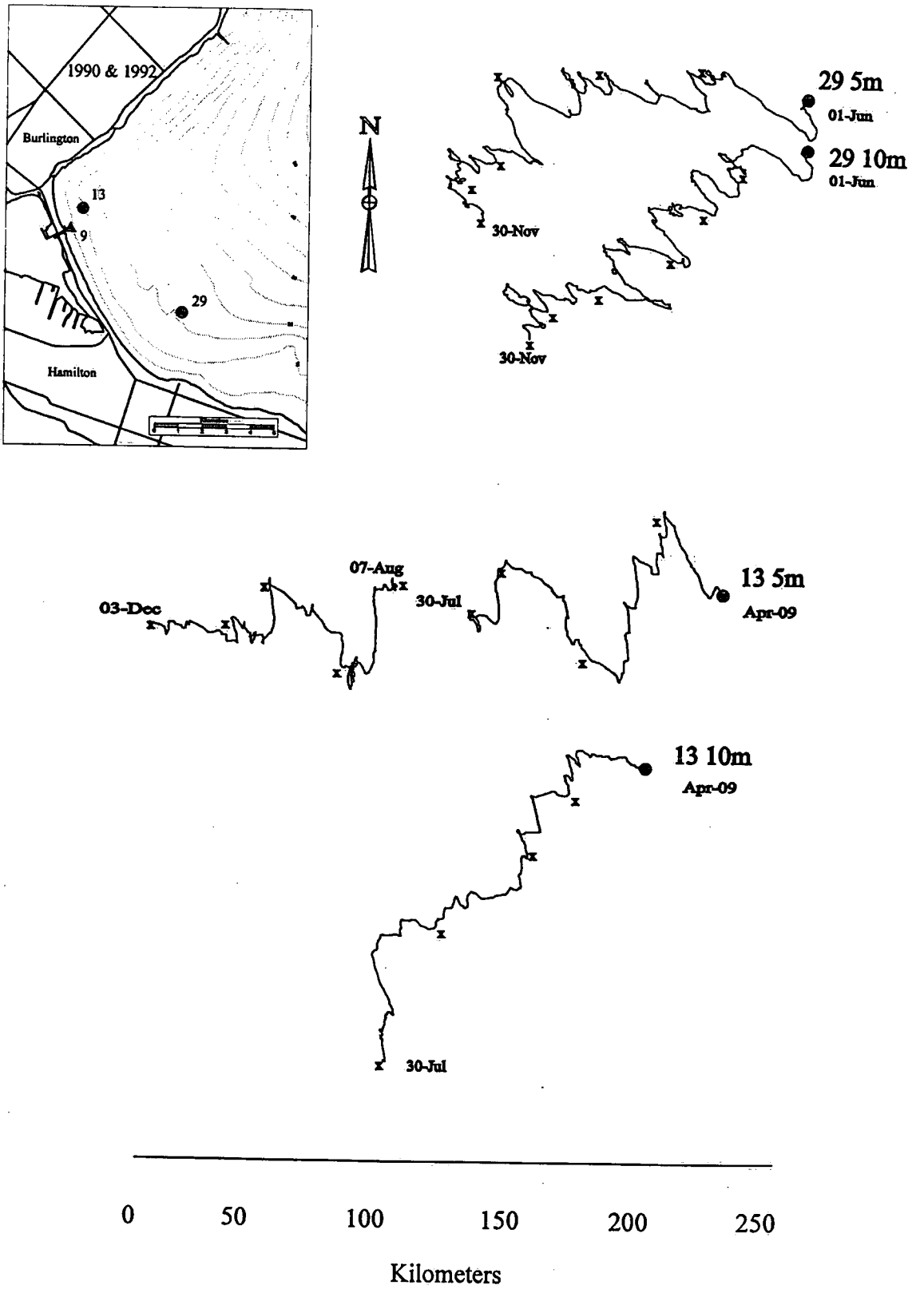

Figure 2.5. Current progressive vector diagrams 1990, 1992.

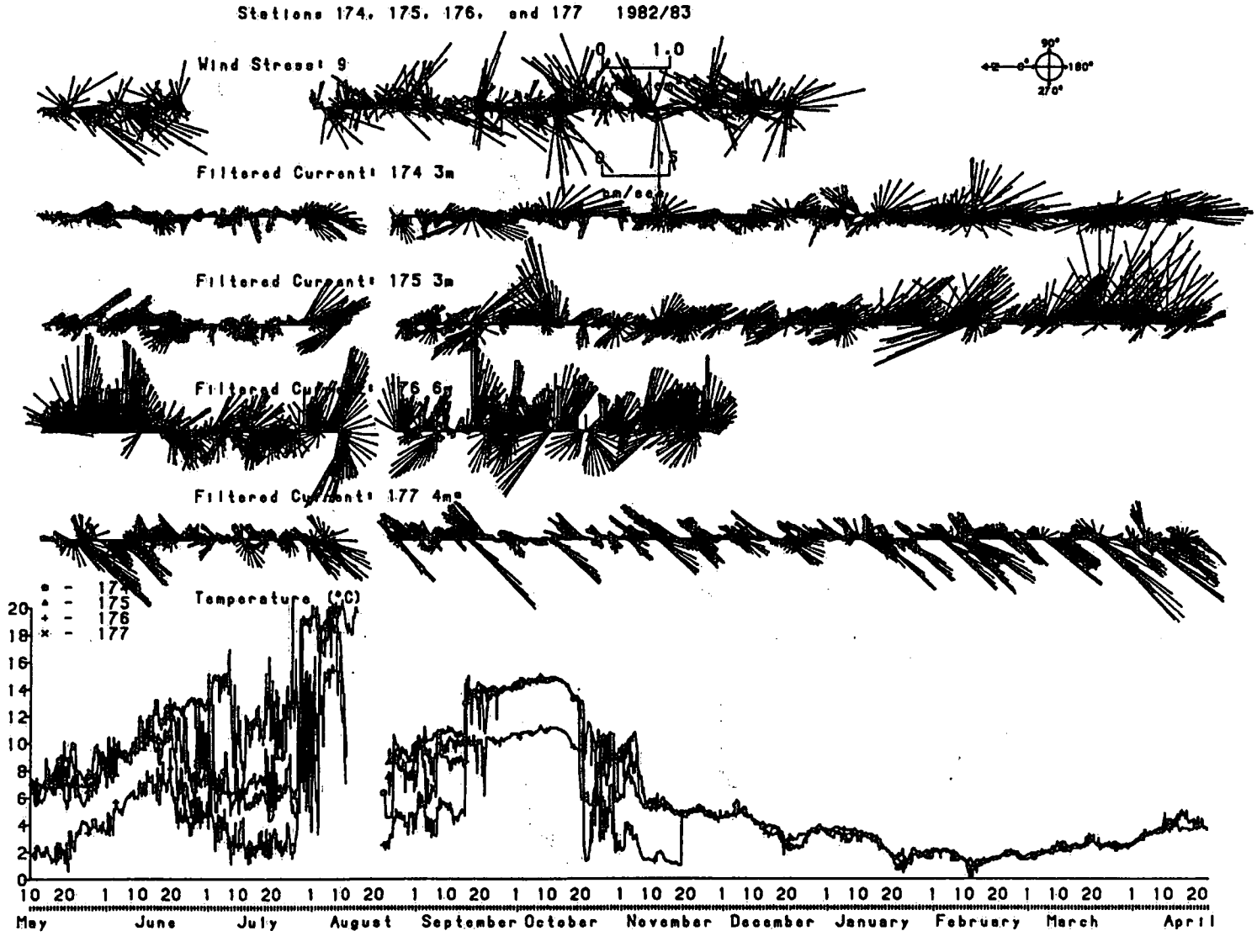

Figure 2.6 Wind stress, current stick plots and temperature 1982-83.

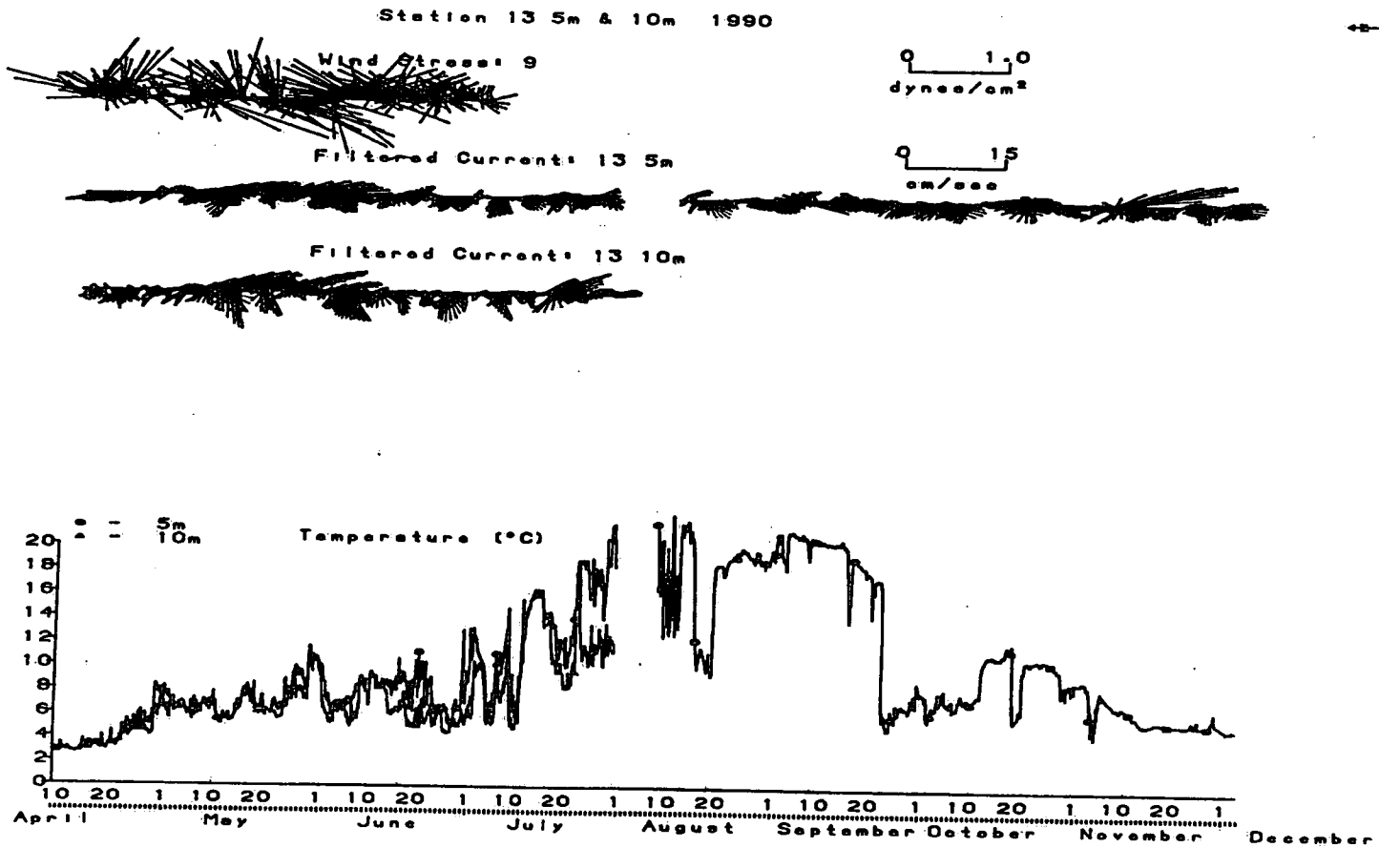

Figure 2.7 Wind stress, current stick plots and temperature 1990.

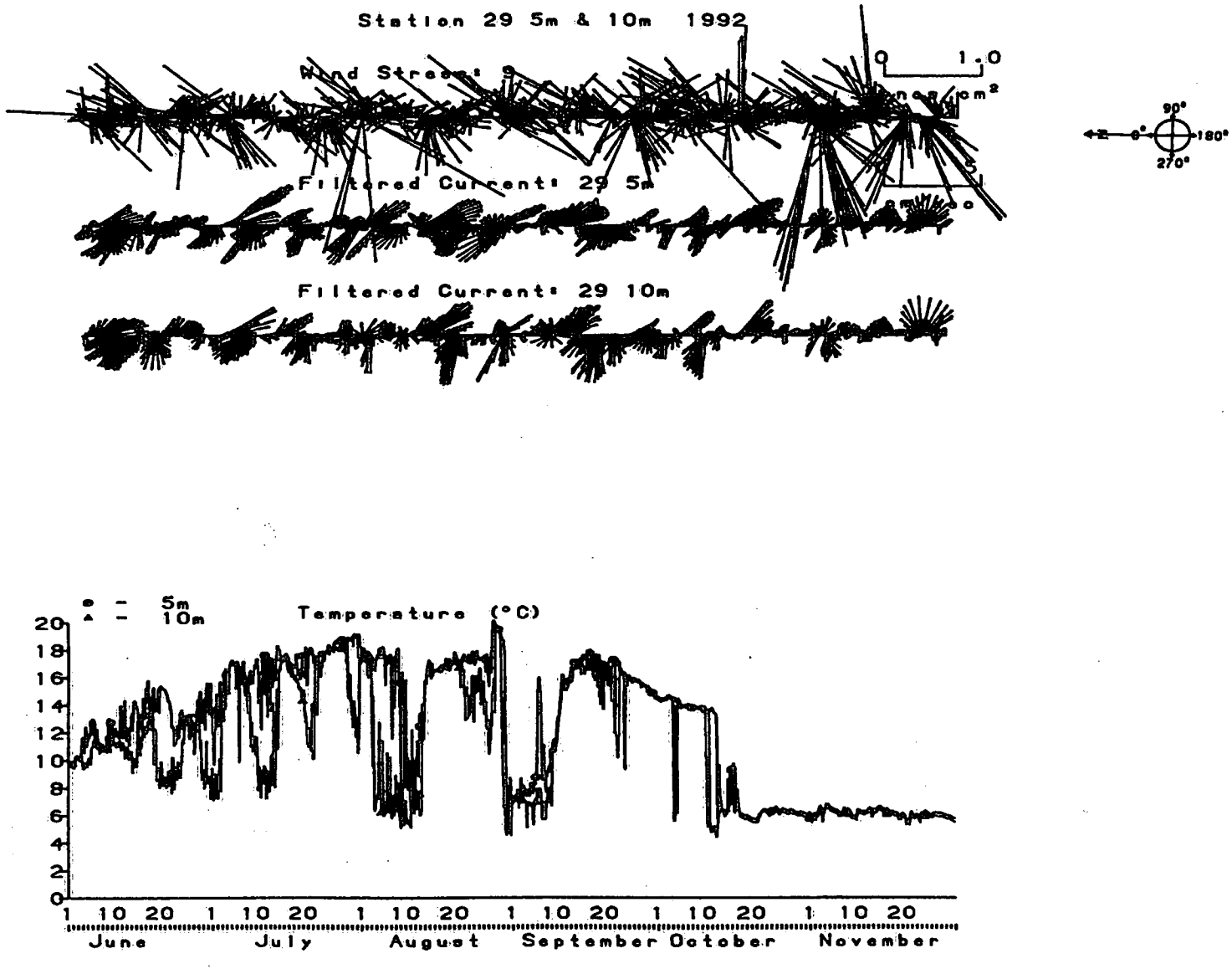

Figure 2.8 Wind stress, current stick plots and temperature 1992.

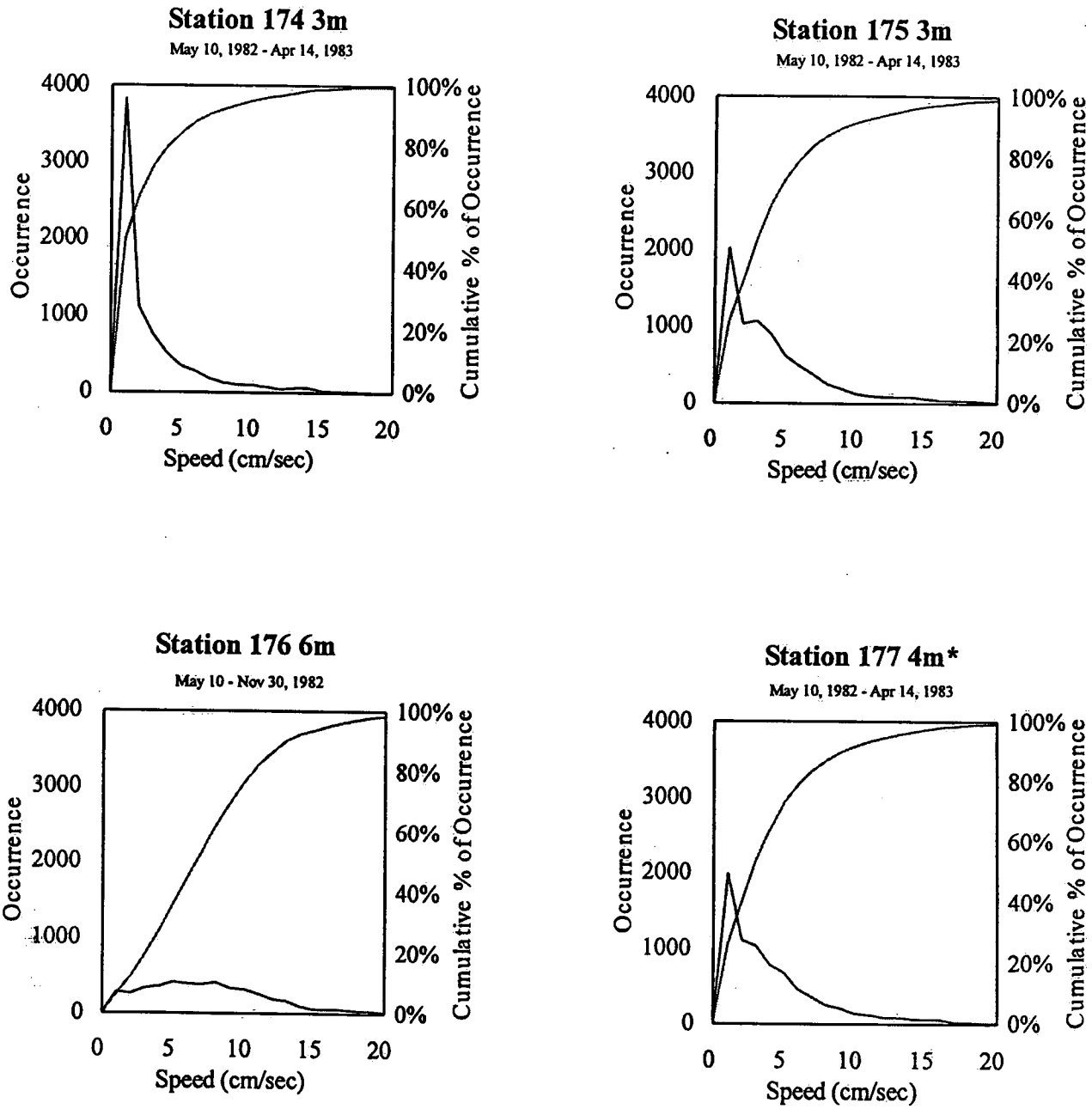

Figure 2.9 Distribution of velocity occurrences 1982-83.

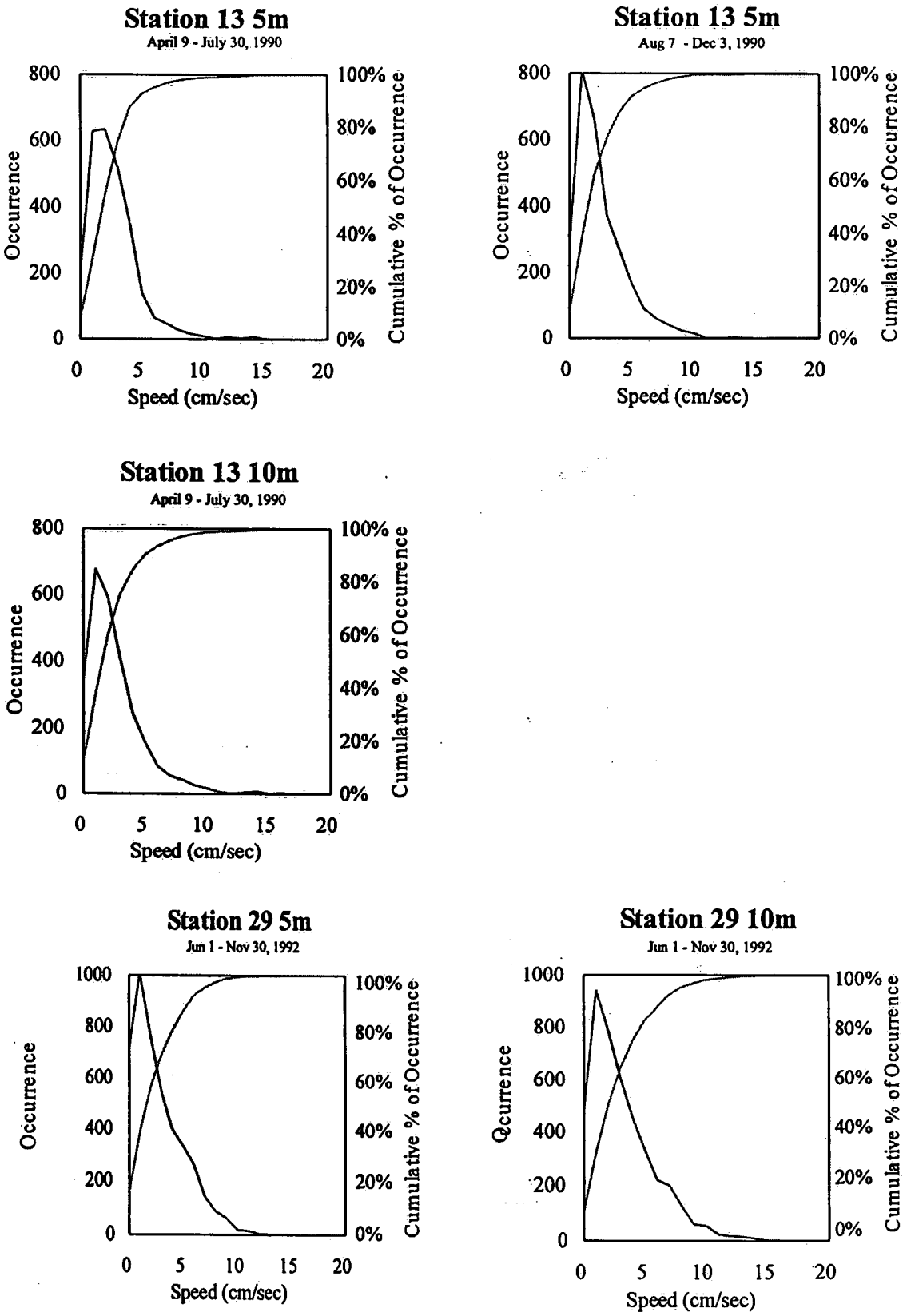

Figure 2.10 Distribution of velocity occurrences 1990 and 1992.

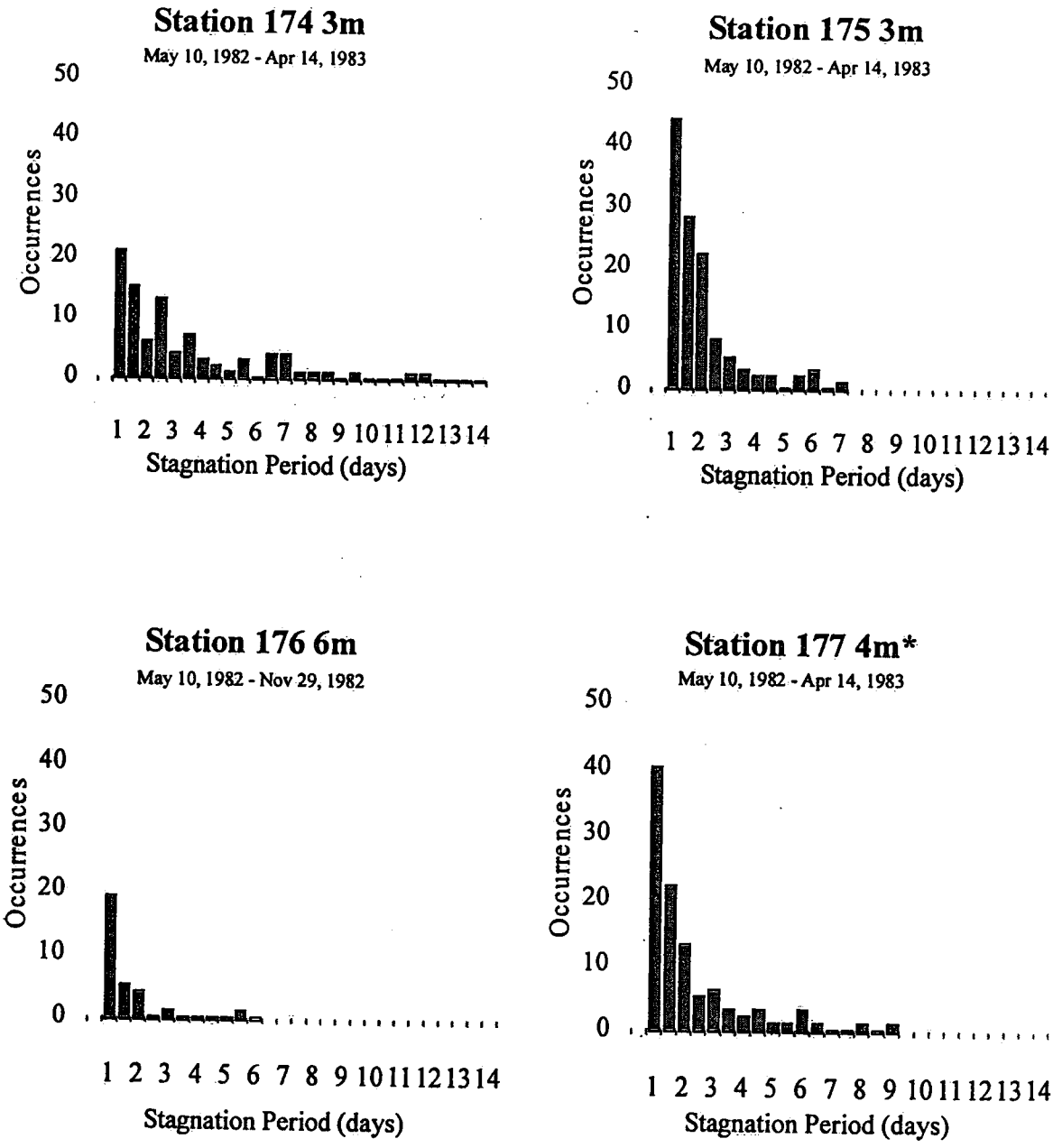

Figure 2.11 Frequency and duration of stagnation periods 1982-83.

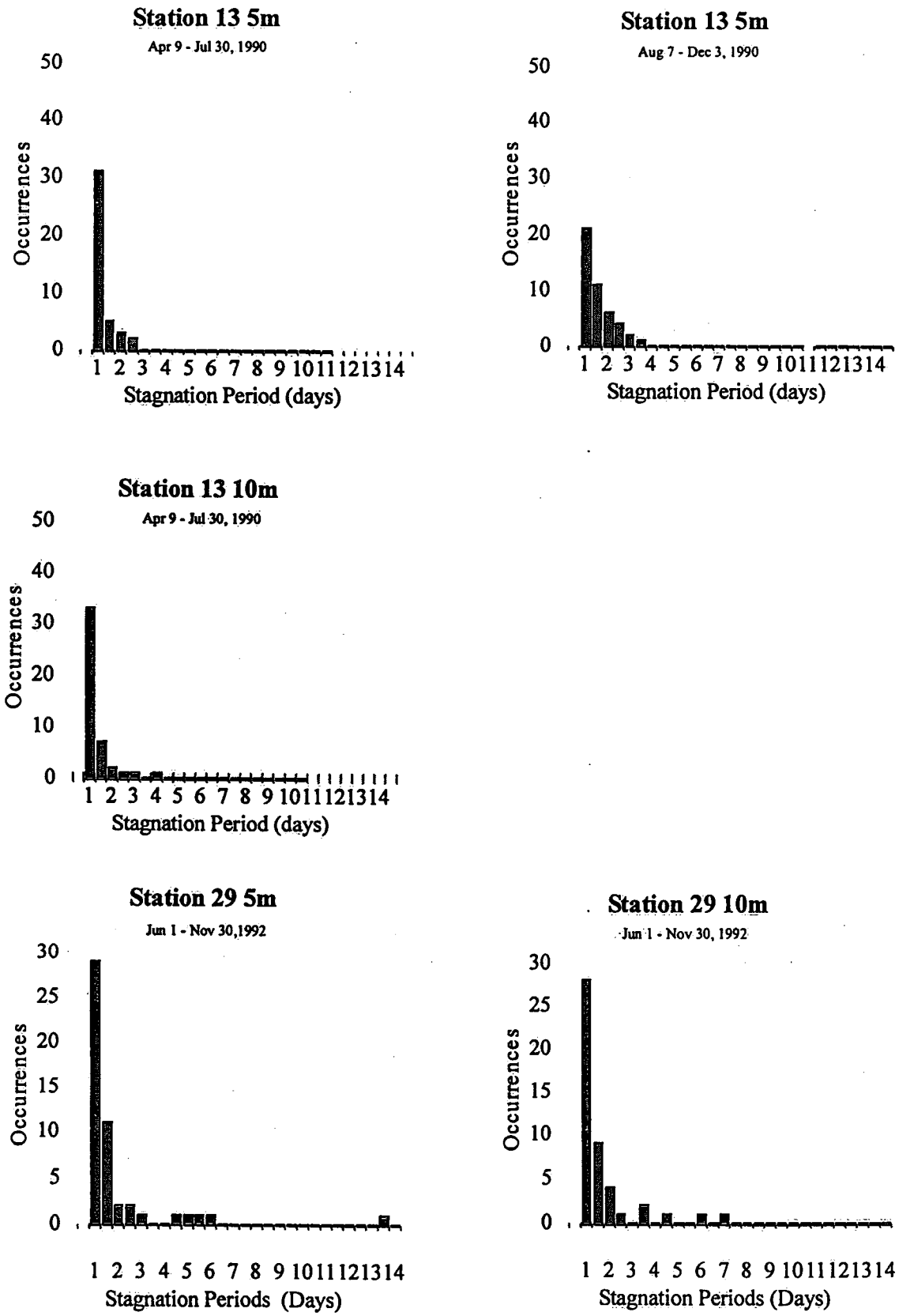

Figure 2.12 Frequency and duration of stagnation periods 1990 and 1992.

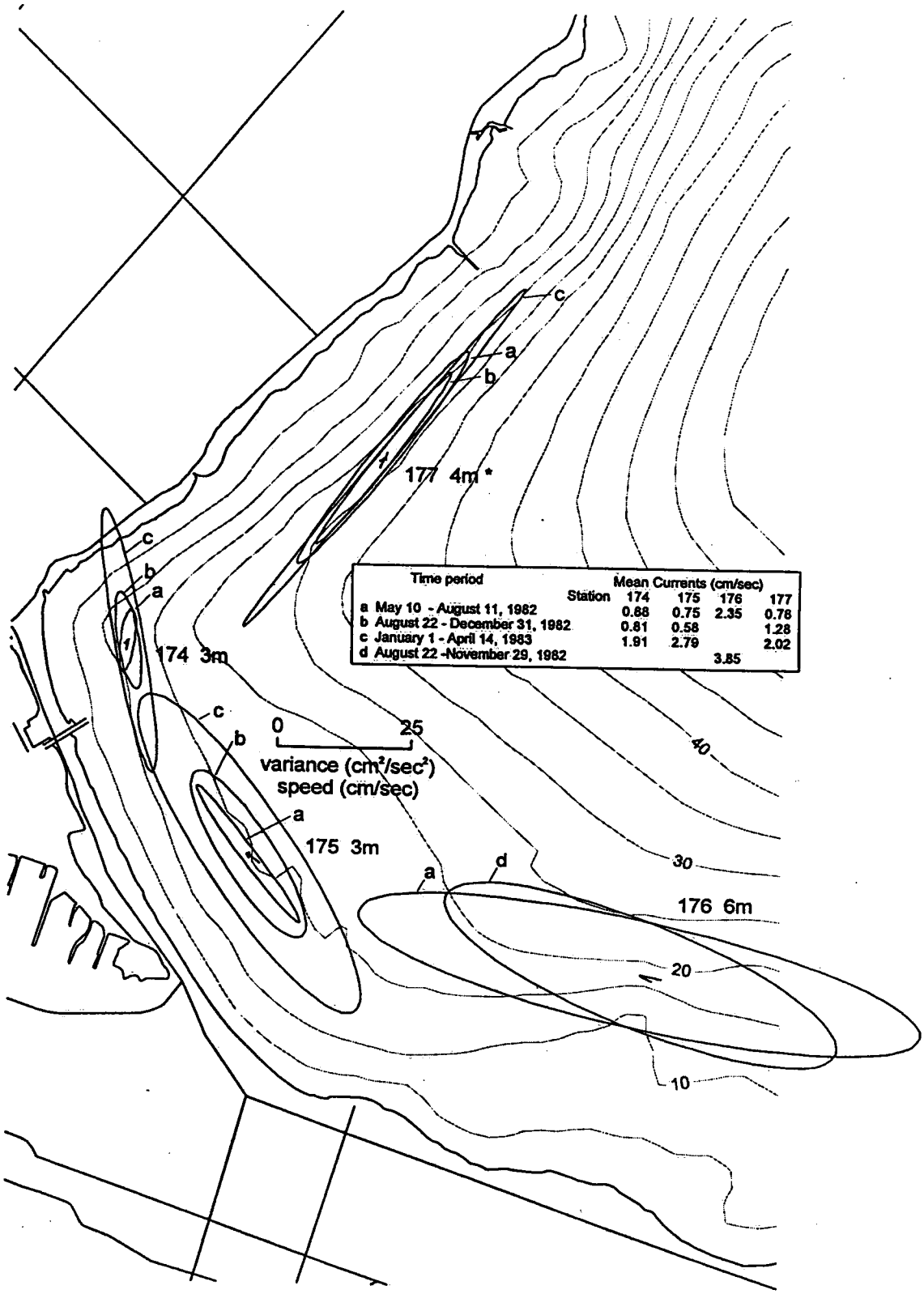

Figure 2.13 Variance ellipses and mean velocity vectors, 1982-83.

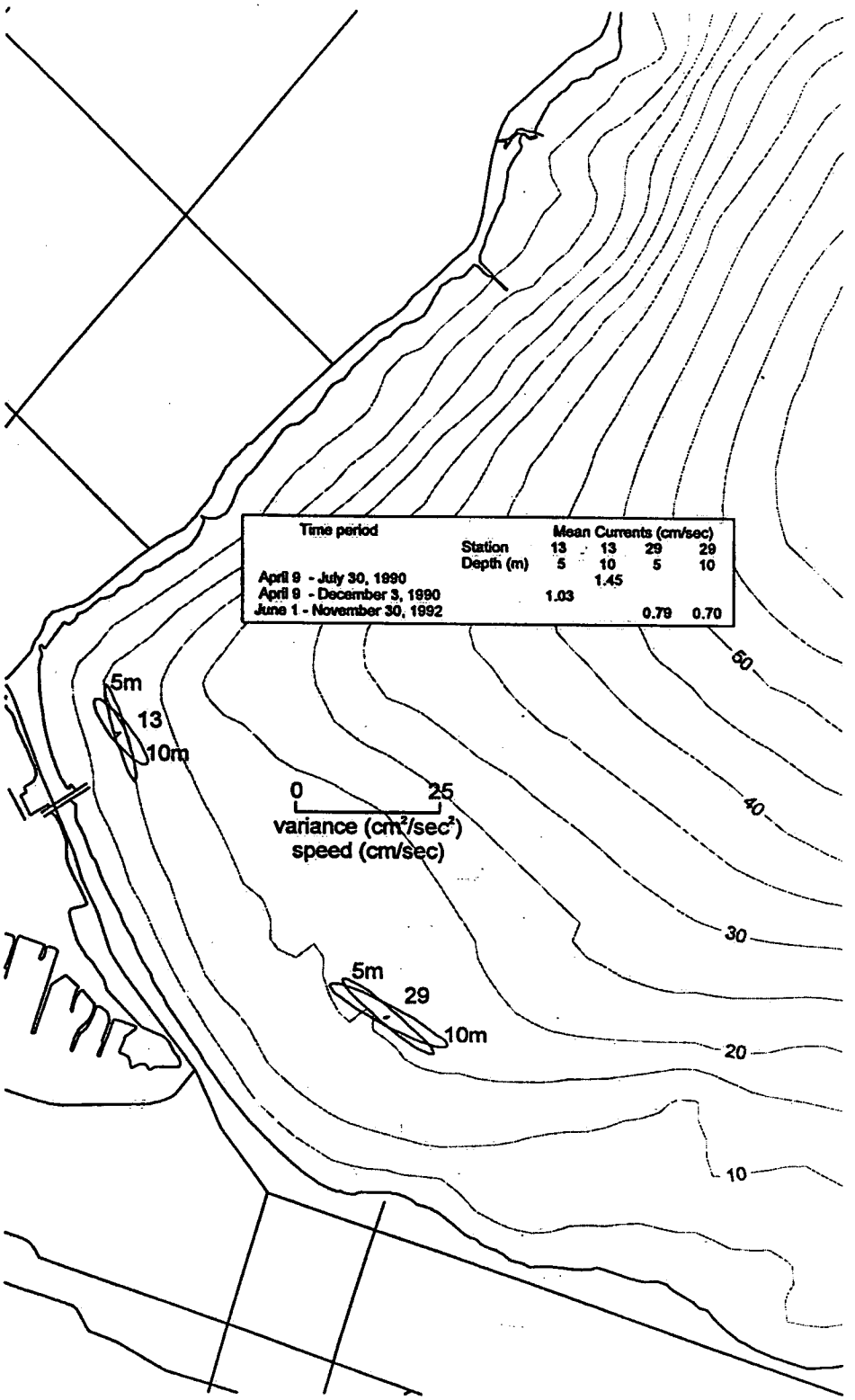

Figure 2.14 Variance ellipses and mean velocity vectors, 1990 and 1992.

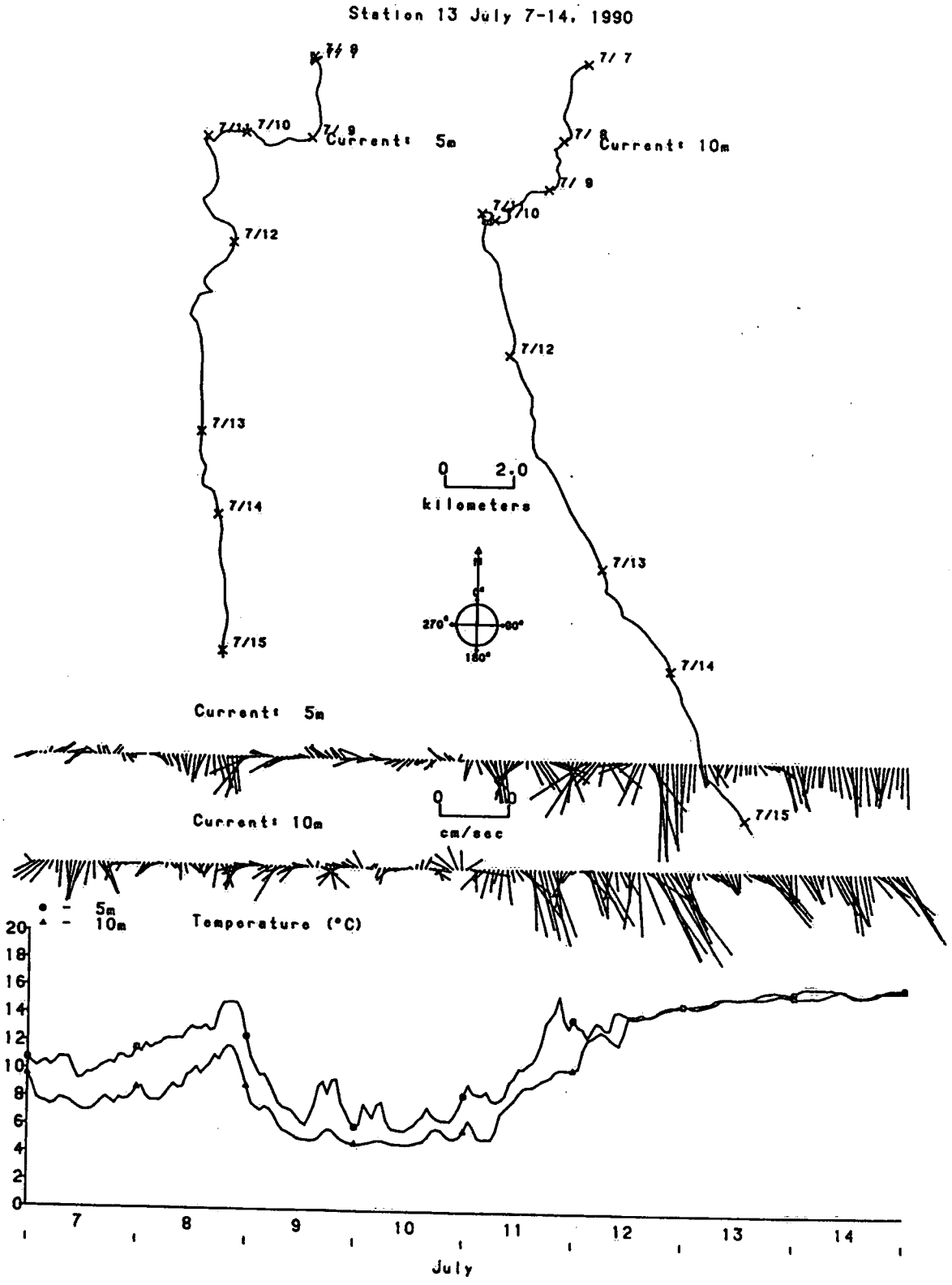

Figure 2.15 Upwelling and downwelling episode, station 13, July 7 to 14, 1990.

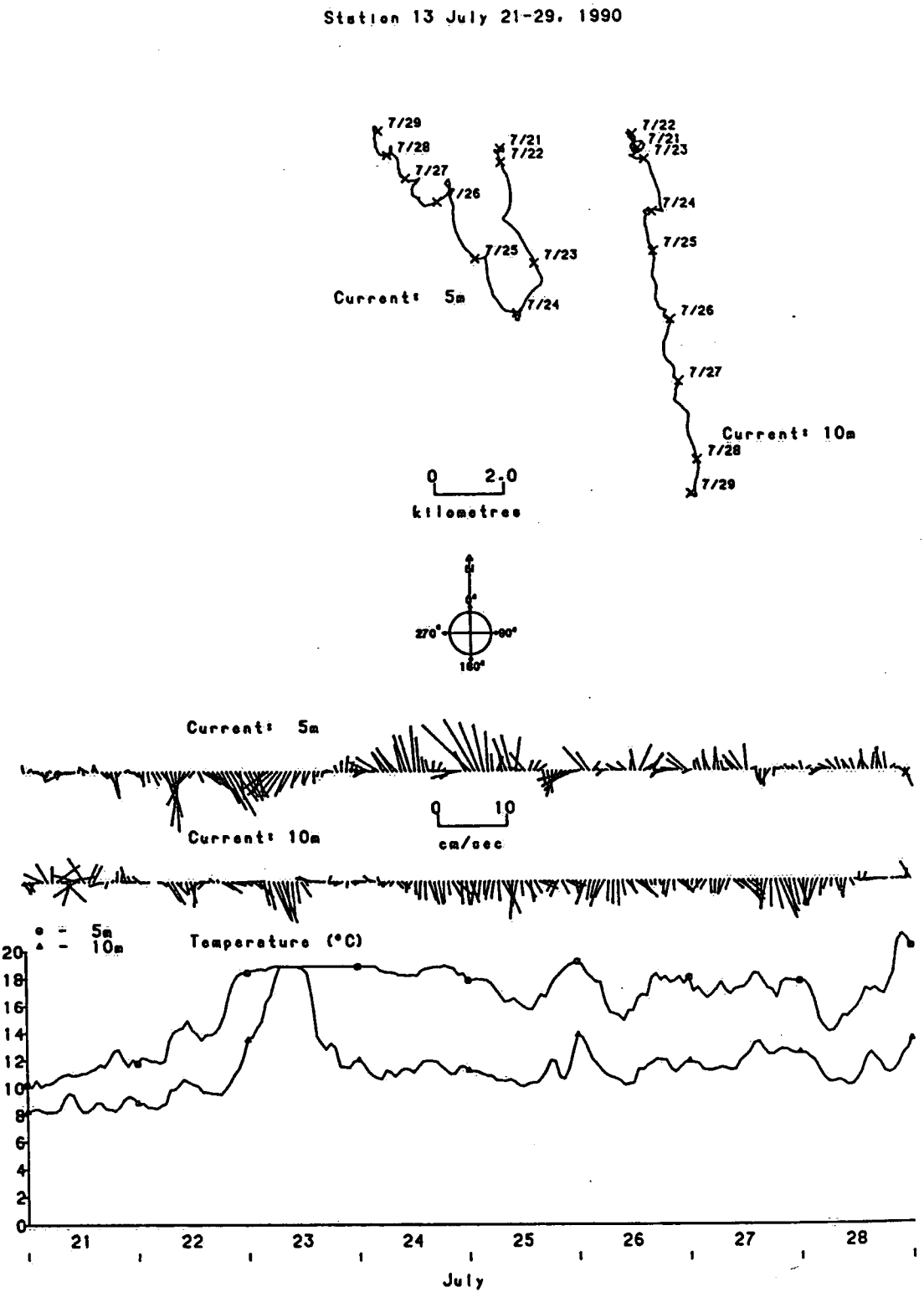

Figure 2.16 Evidence and effects of internal waves, July 22 to 29, 1990.

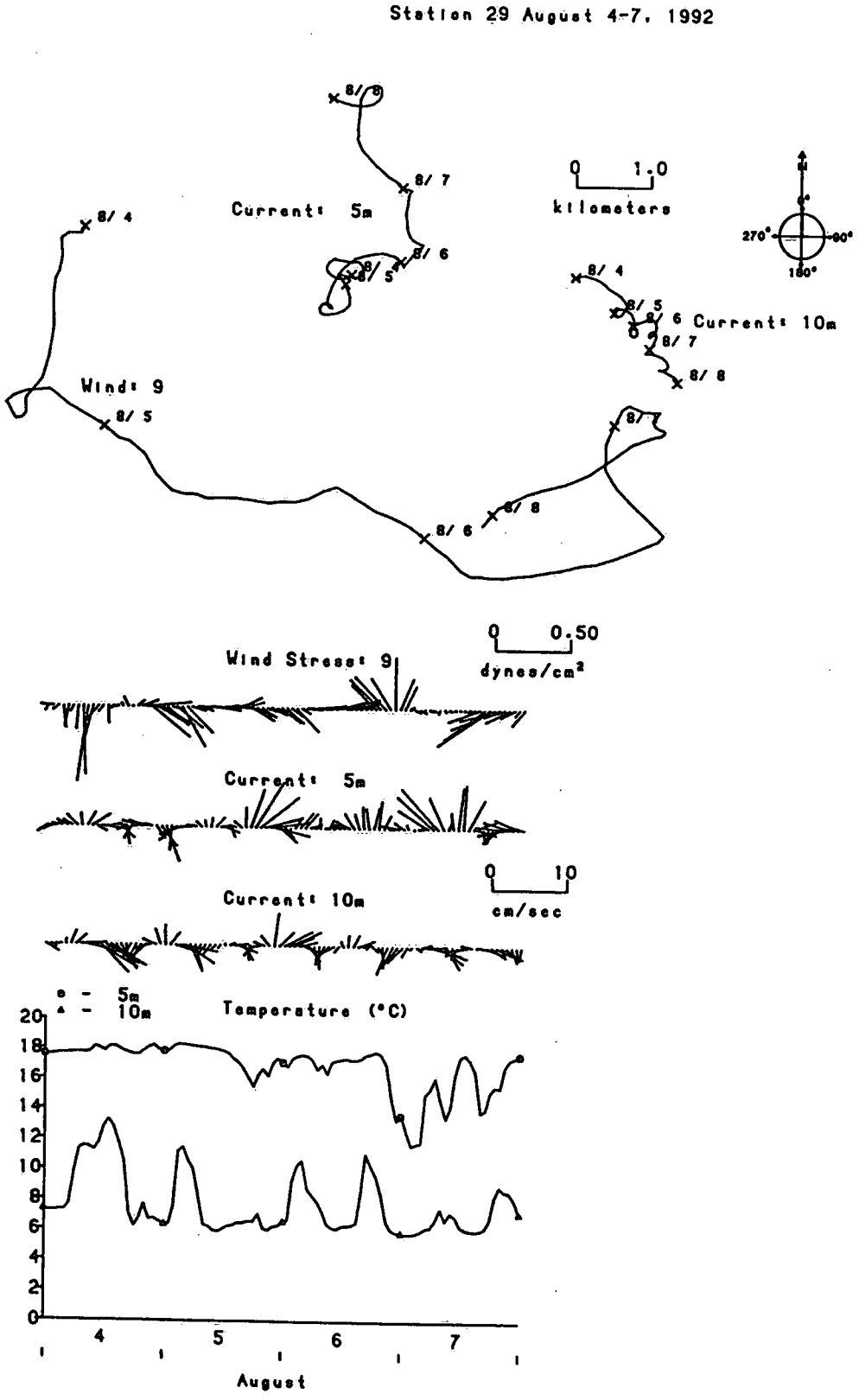

Figure 2.17 Episode of current shear at station 29, August 4 to 7, 1992.

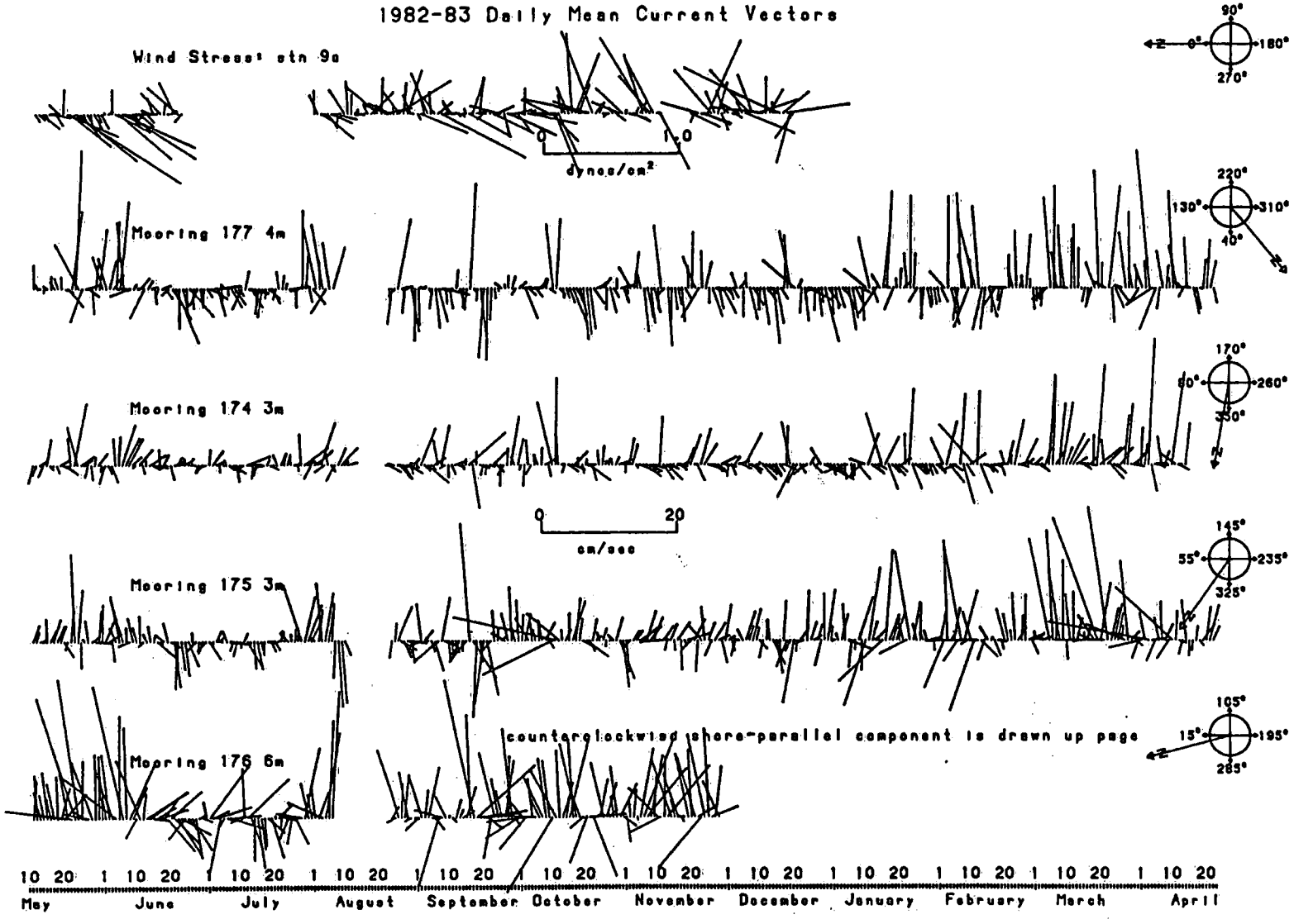

Figure 2.18 Rotated daily mean current vector plots 1982-83.

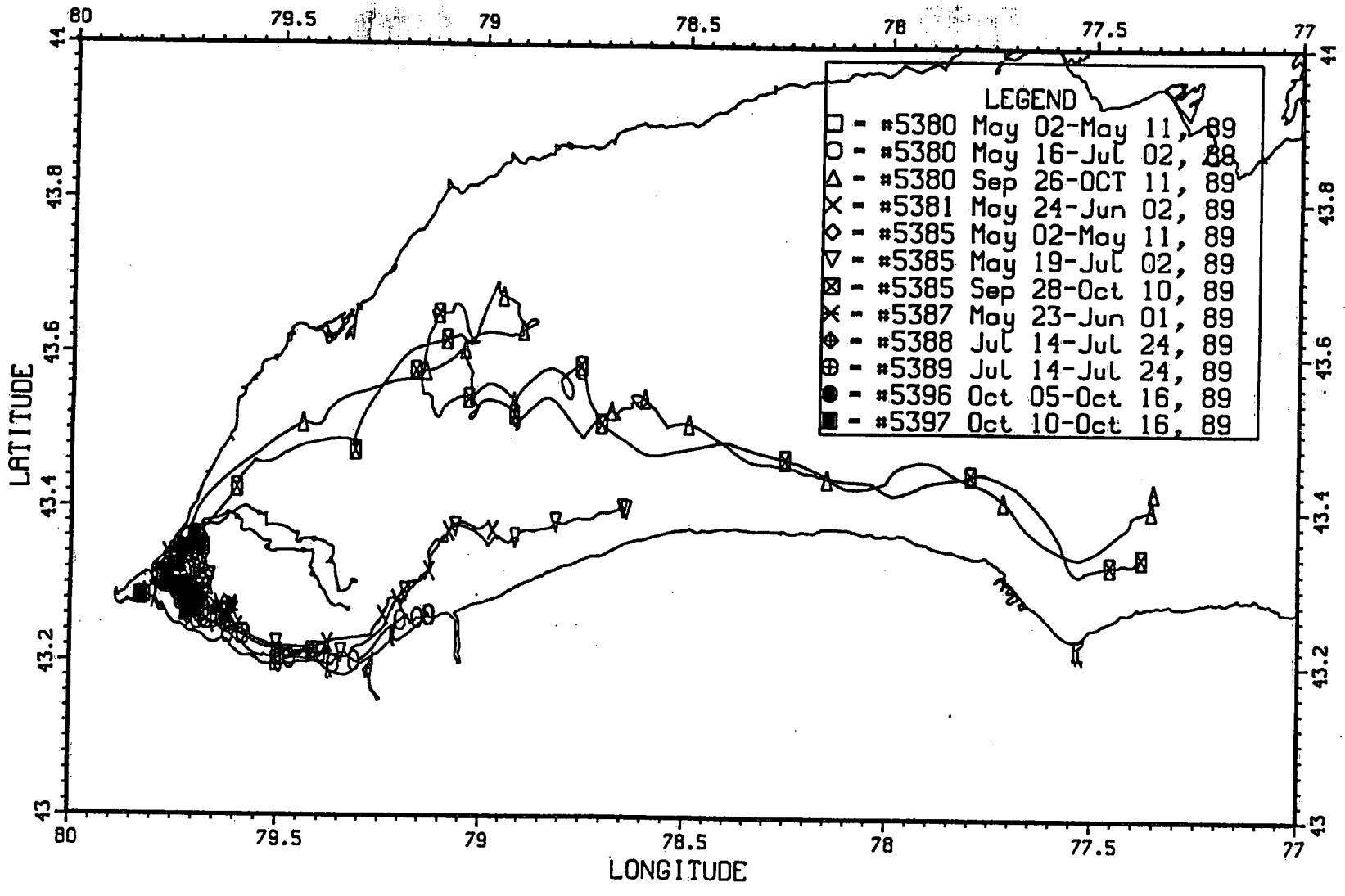

Figure 2.19 Superimposed Lagrangian drifter trajectories from 1989.

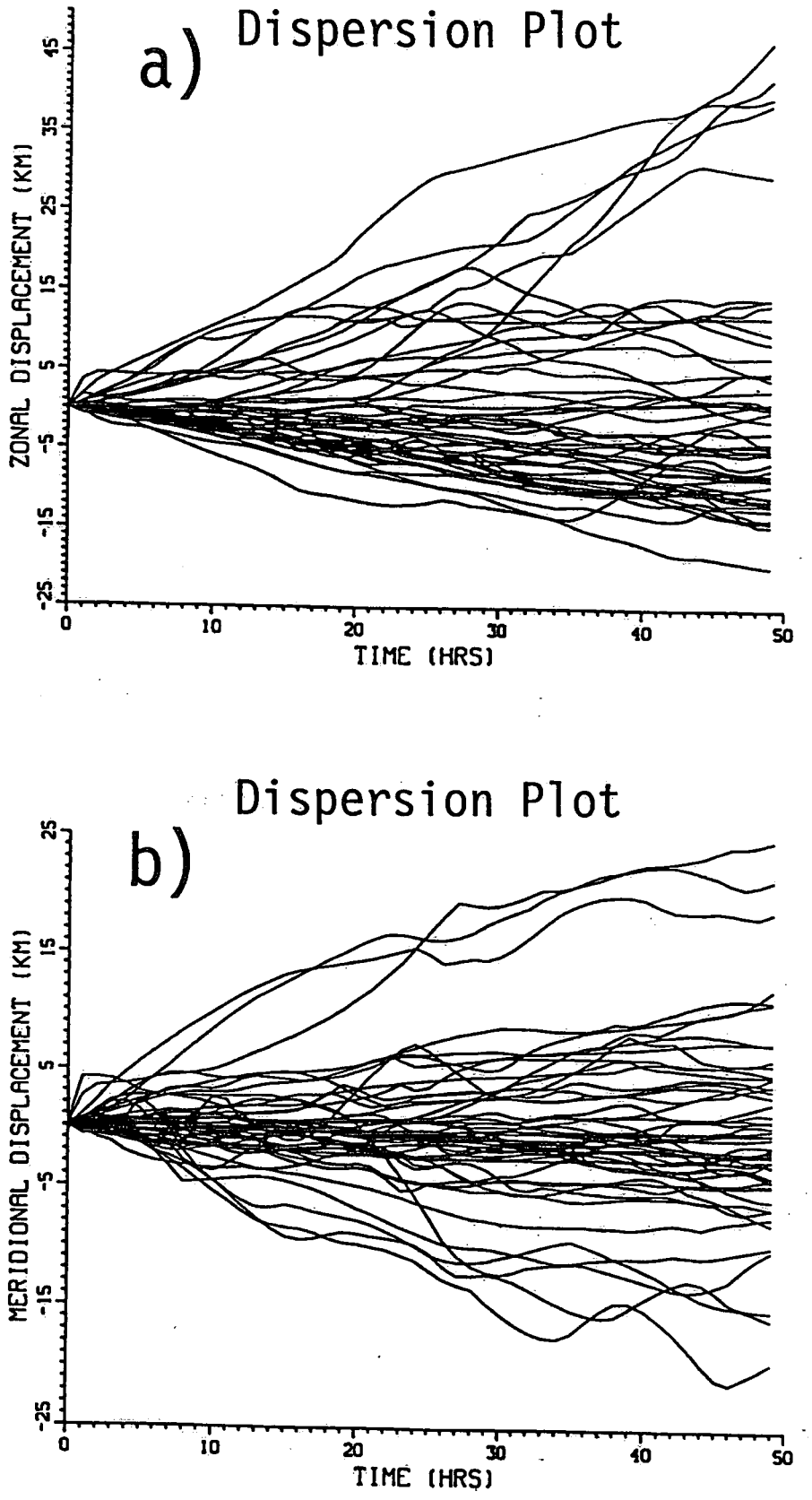

Figure 2.20 Dispersion plots from drifter trajectories.

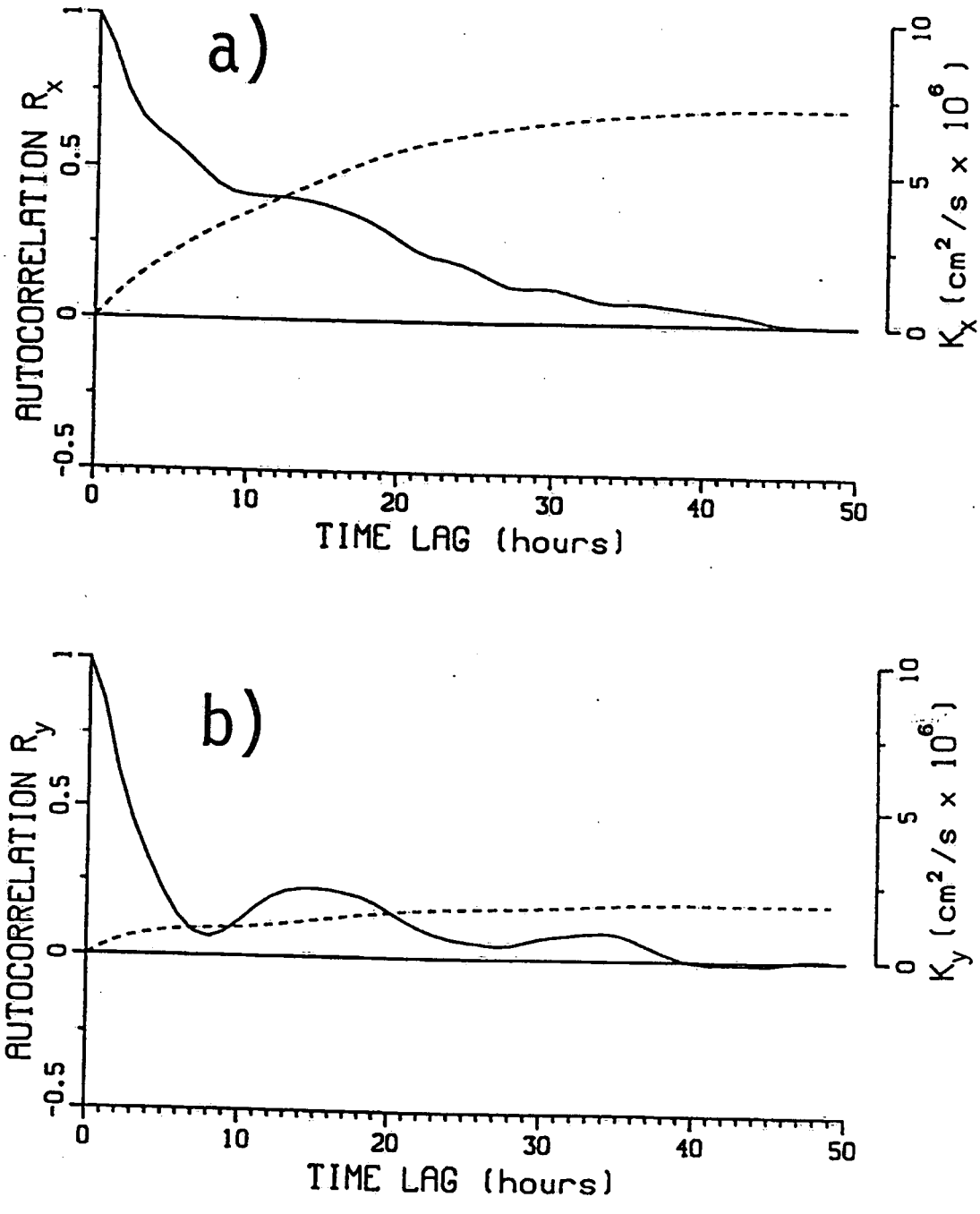

Figure 2.21 Autocorrelation and dispersion coefficient for drifter data, 1989.

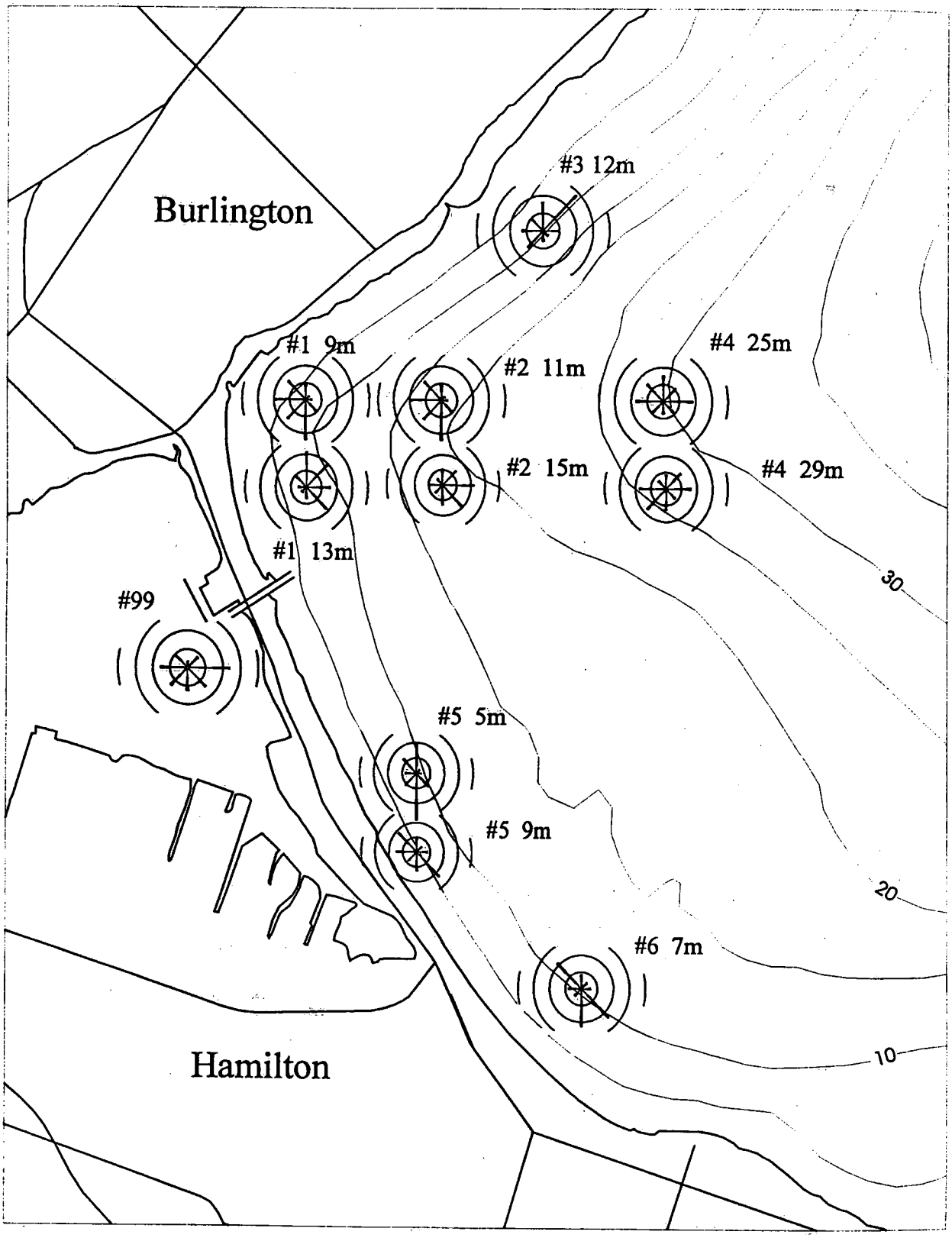

Figure 4.1 Rose histogram plots of hourly wind and VACM current data, May 23 to November 4, 1996.

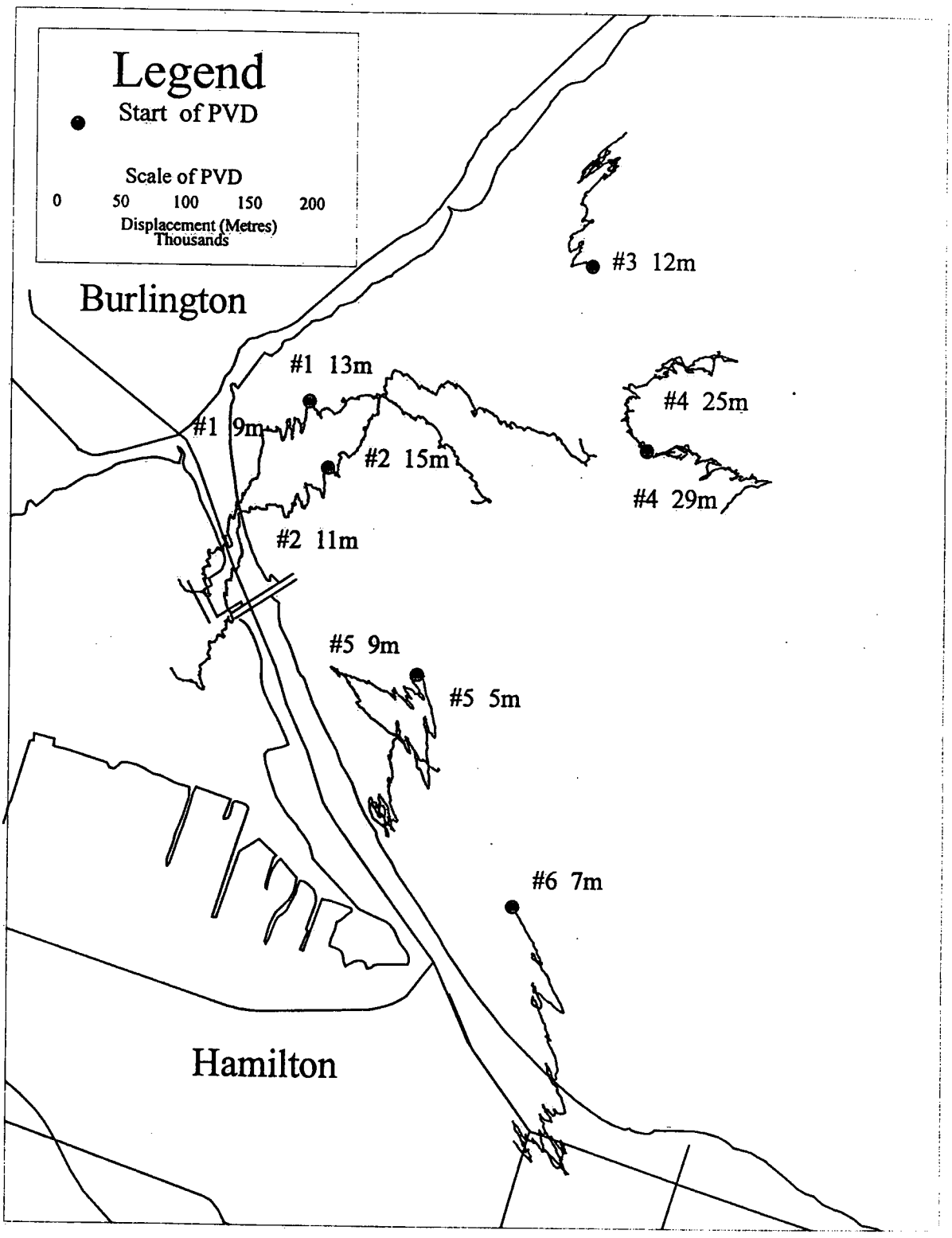

Figure 4.2 Current meter progressive vector diagrams, May 23 to November 4, 1996.

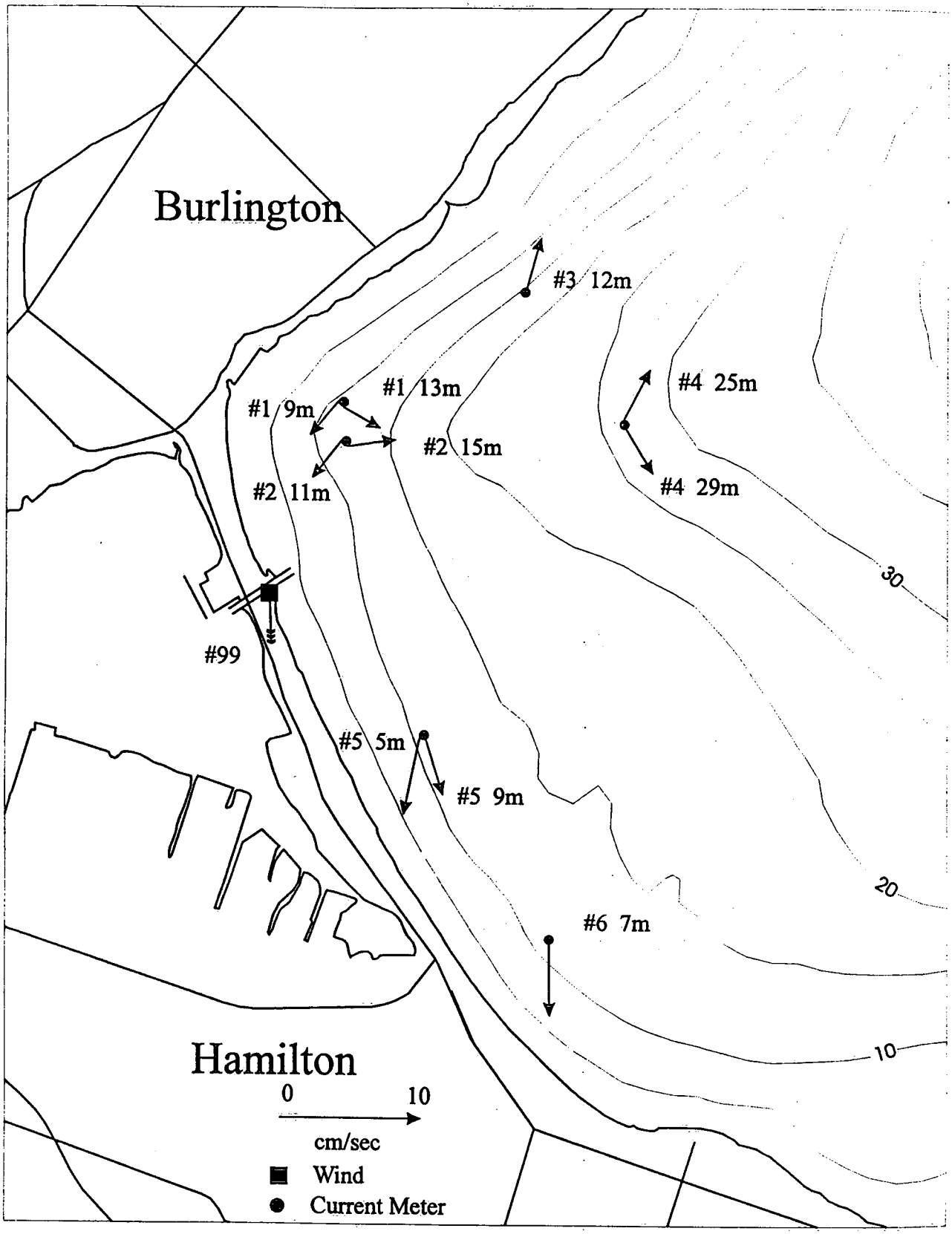

Figure 4.3 Plots of scalar speed and direction, May 23 to November 4, 1996.

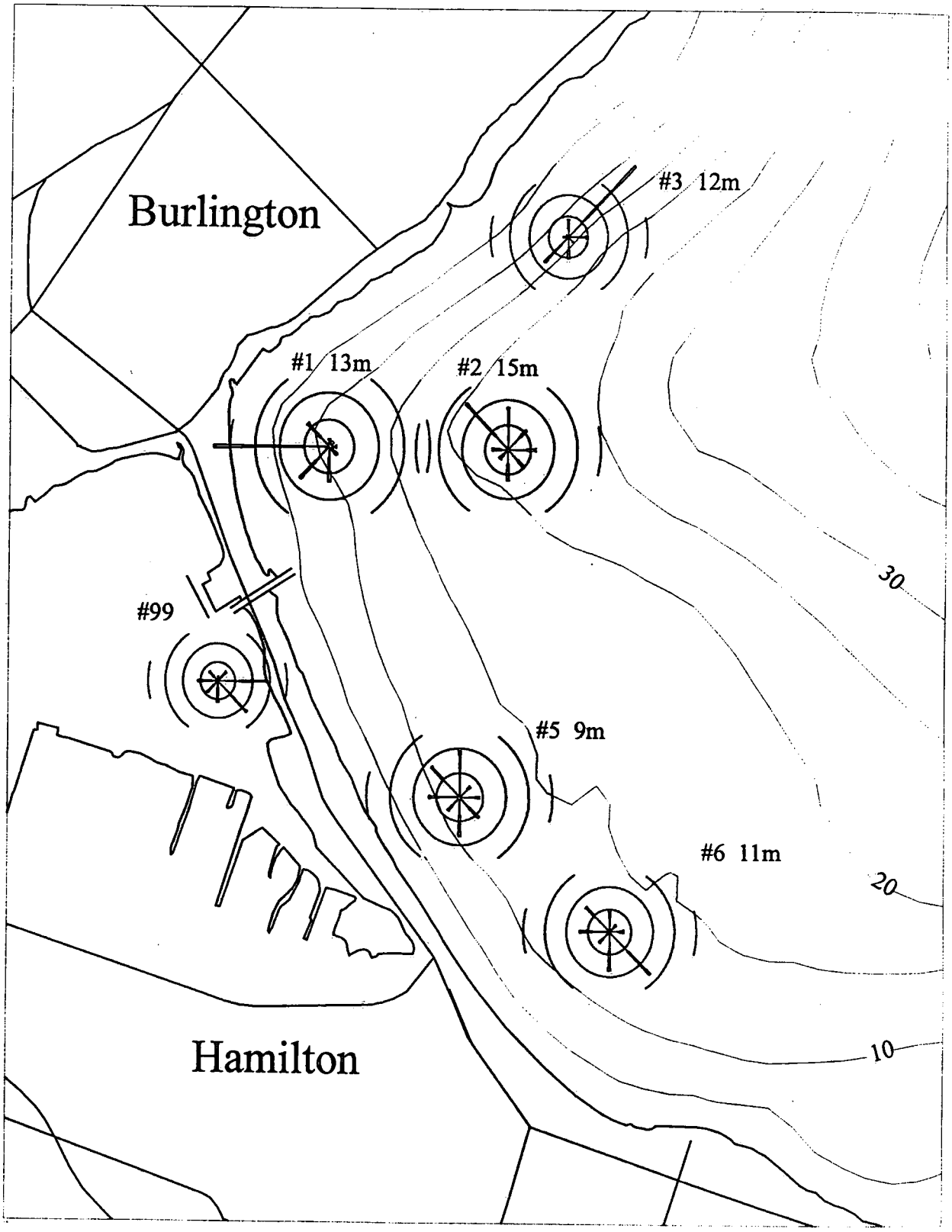

Figure 4.4 Rose histogram plots of wind and VACM current data, November 8, 1996 to April 24, 1997.

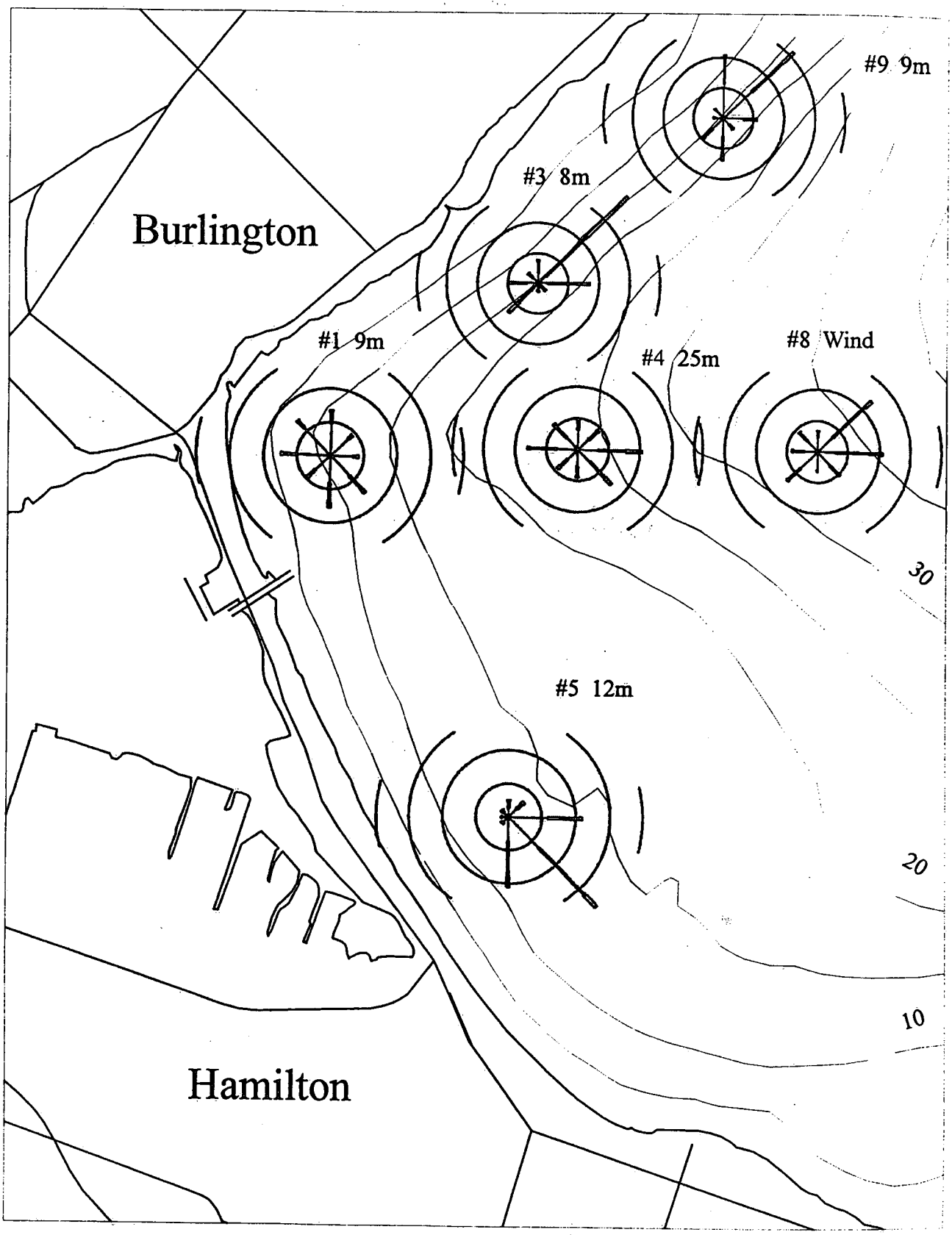

Figure 4.5 Rose histogram plots of wind and VACM current data, April 30 to October 21, 1997.

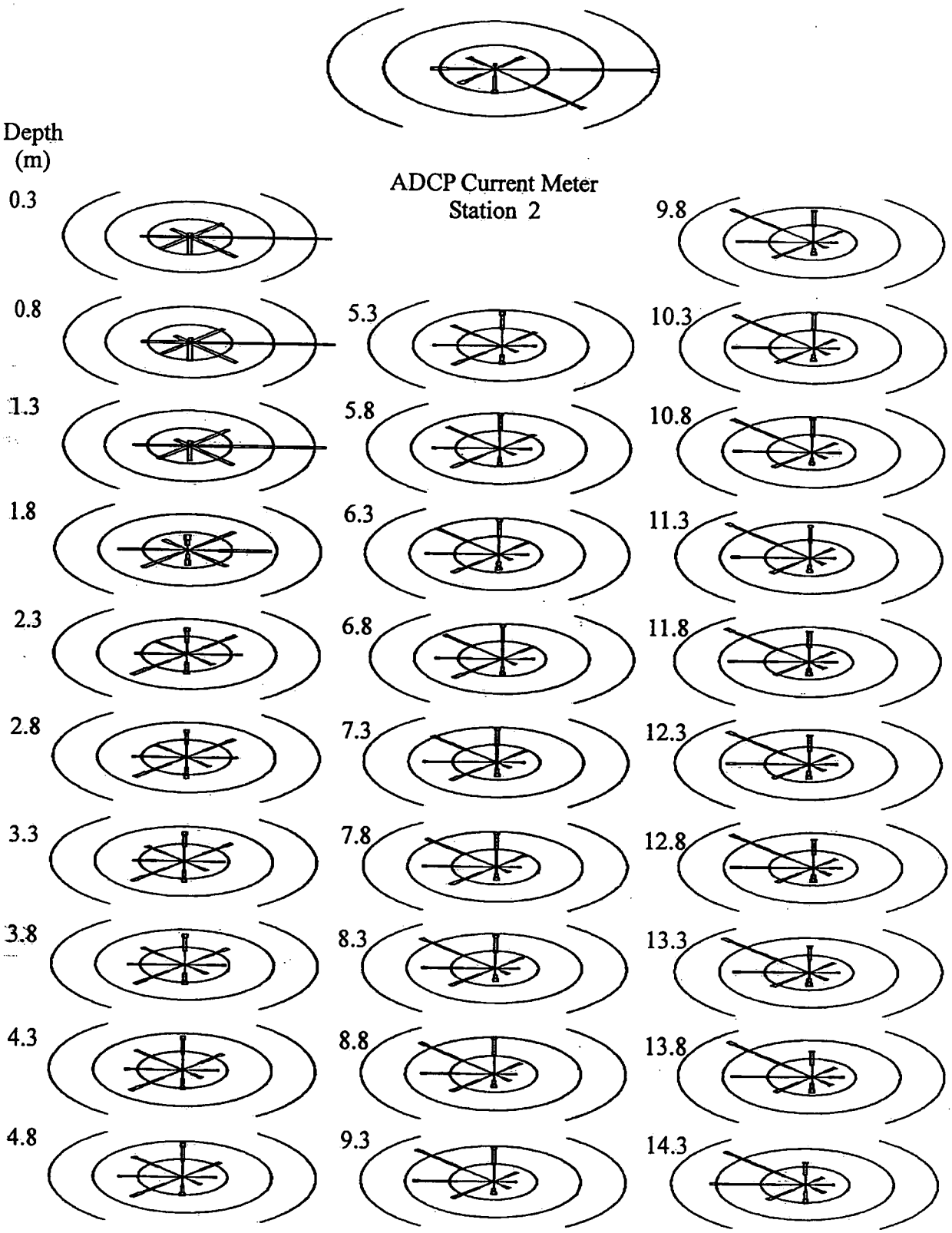

Figure 4.6 Rose plot summaries of wind and ADCP current meter data at station 2, November 8, 1996 to April 10, 1997.

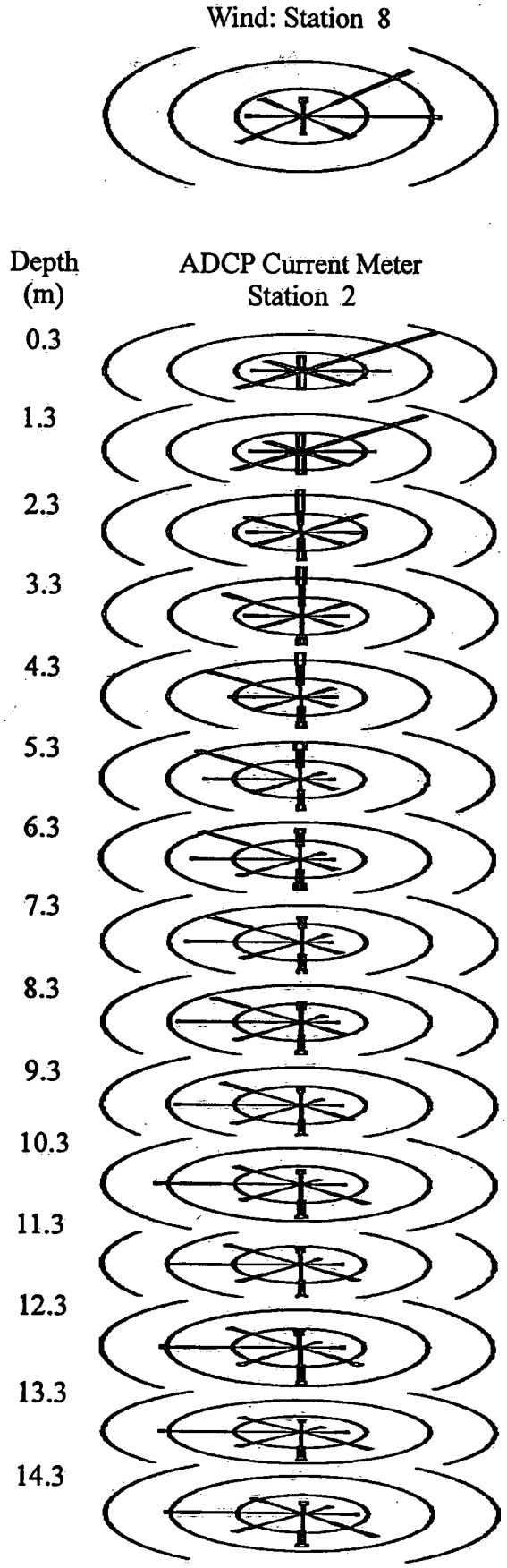

Figure 4.7 Rose plot summaries of wind and ADCP current meter data at station 2, May 1 to October 21, 1997.

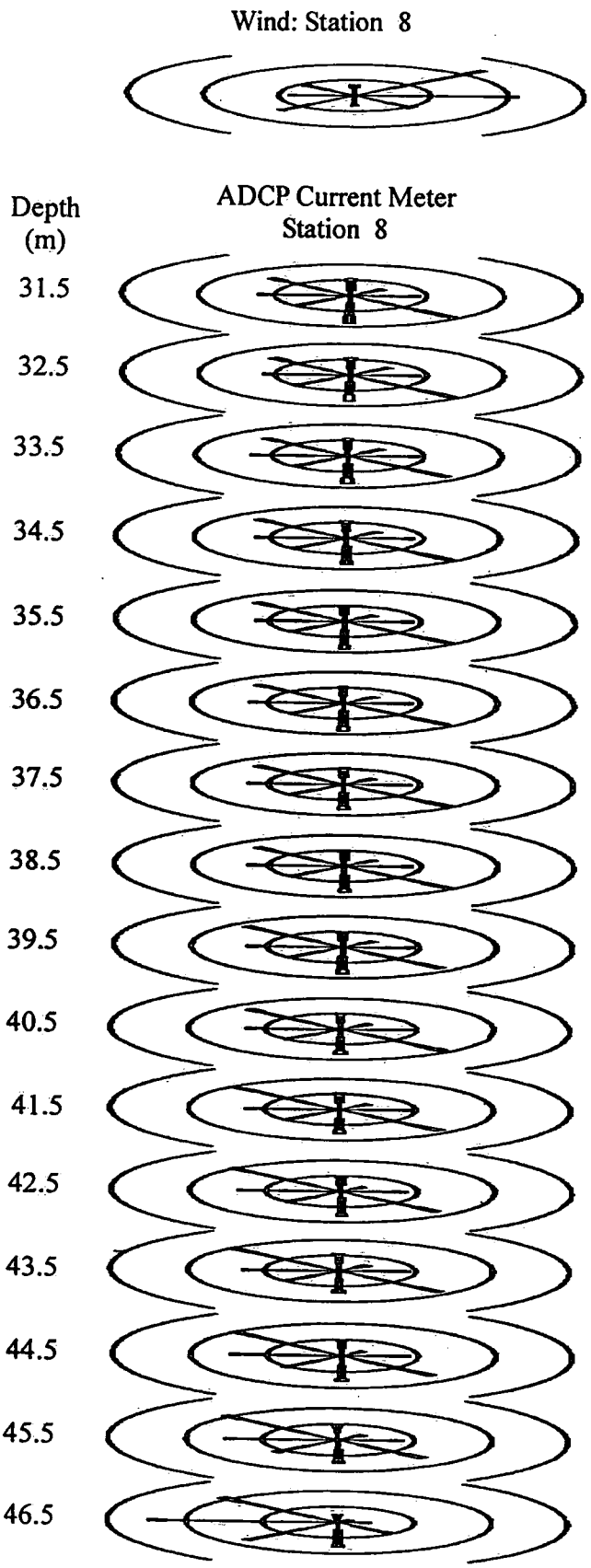

Figure 4.8 Rose plot summaries of wind and ADCP current meter data at station 8, May 2 to October 20, 1997.

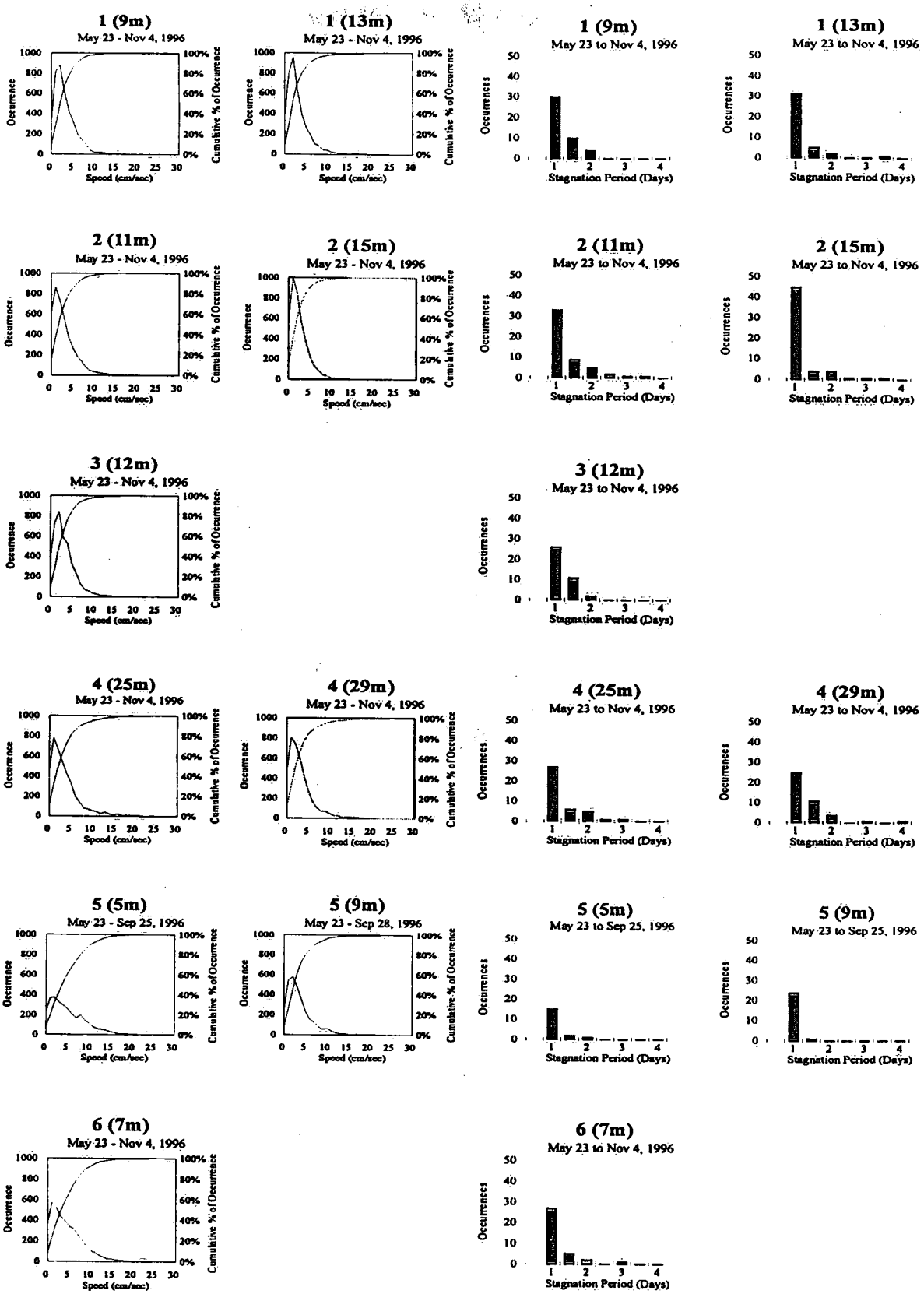

Figure 4.9 Frequency of occurrence vs. current speed and stagnation period, May 23 to November 7, 1996.

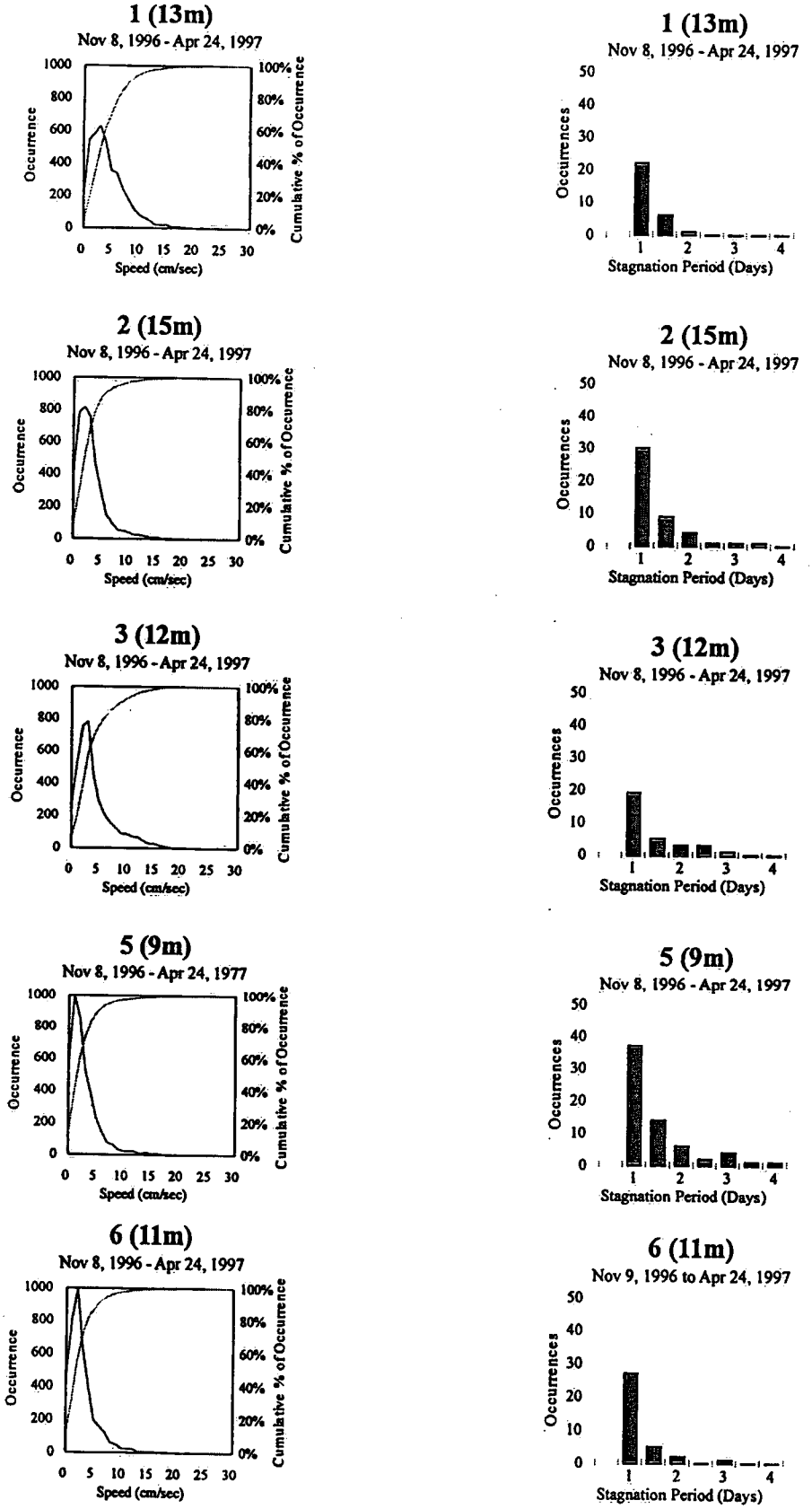

Figure 4.10 Frequency of occurrence vs. current speed and stagnation period, November 8, 1996 to April 24, 1997.

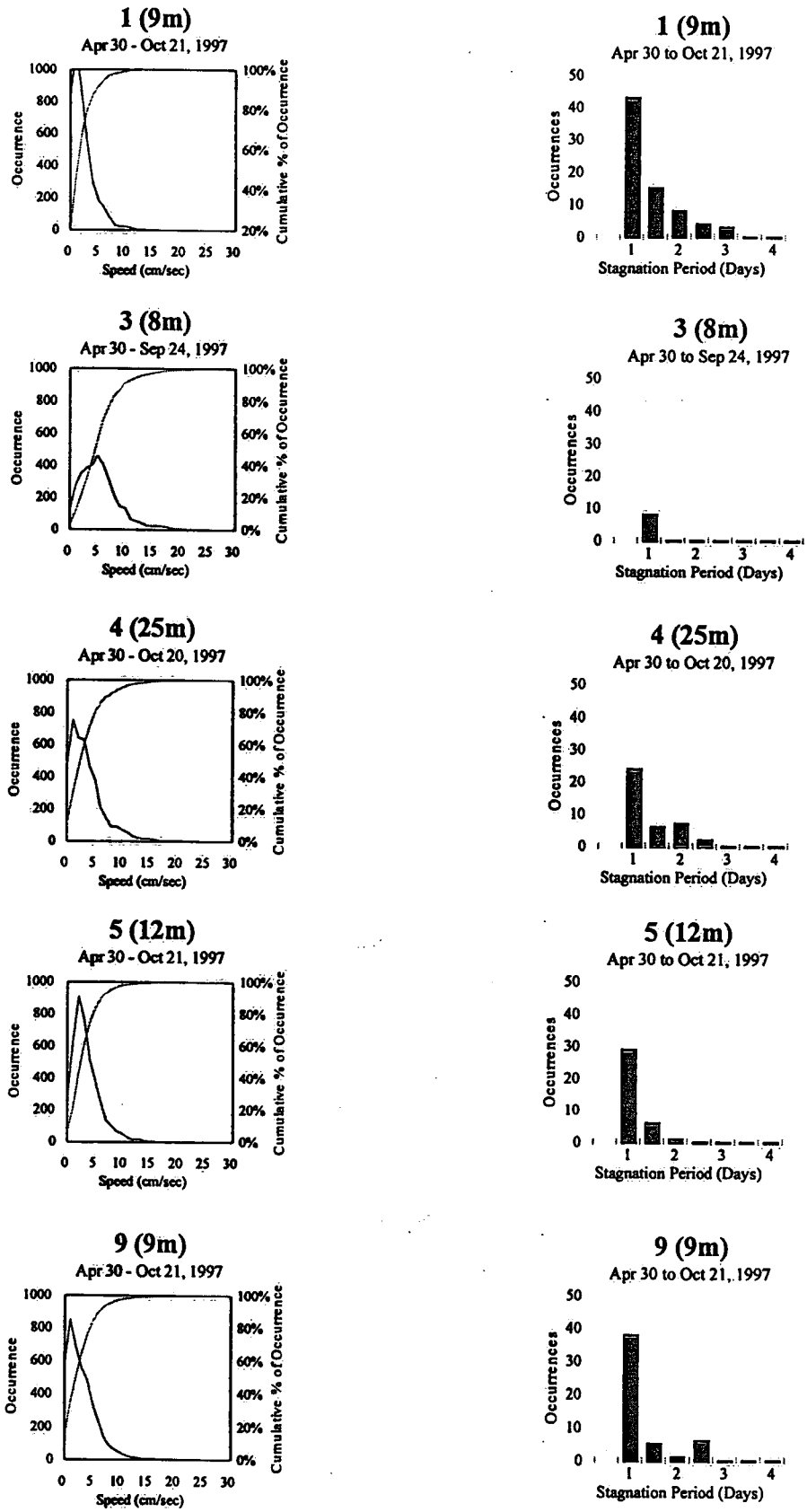

Figure 4.11 Frequency of occurrence vs. current speed and stagnation period, April 30 to October 21, 1997.

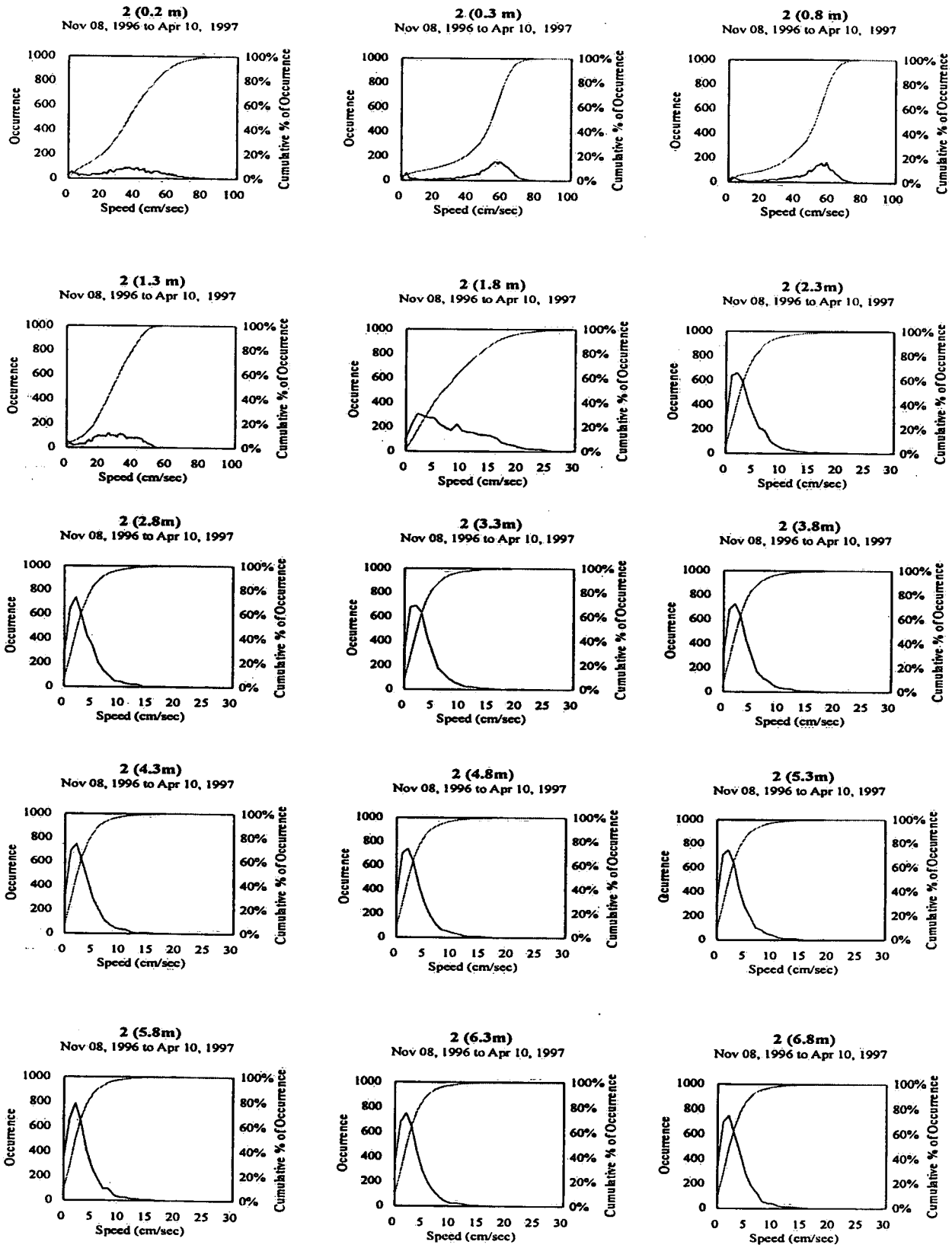

Figure 4.12 Frequency of occurrence vs. current speed for the ADCP station 2, November 8, 1996 to April 10, 1997.

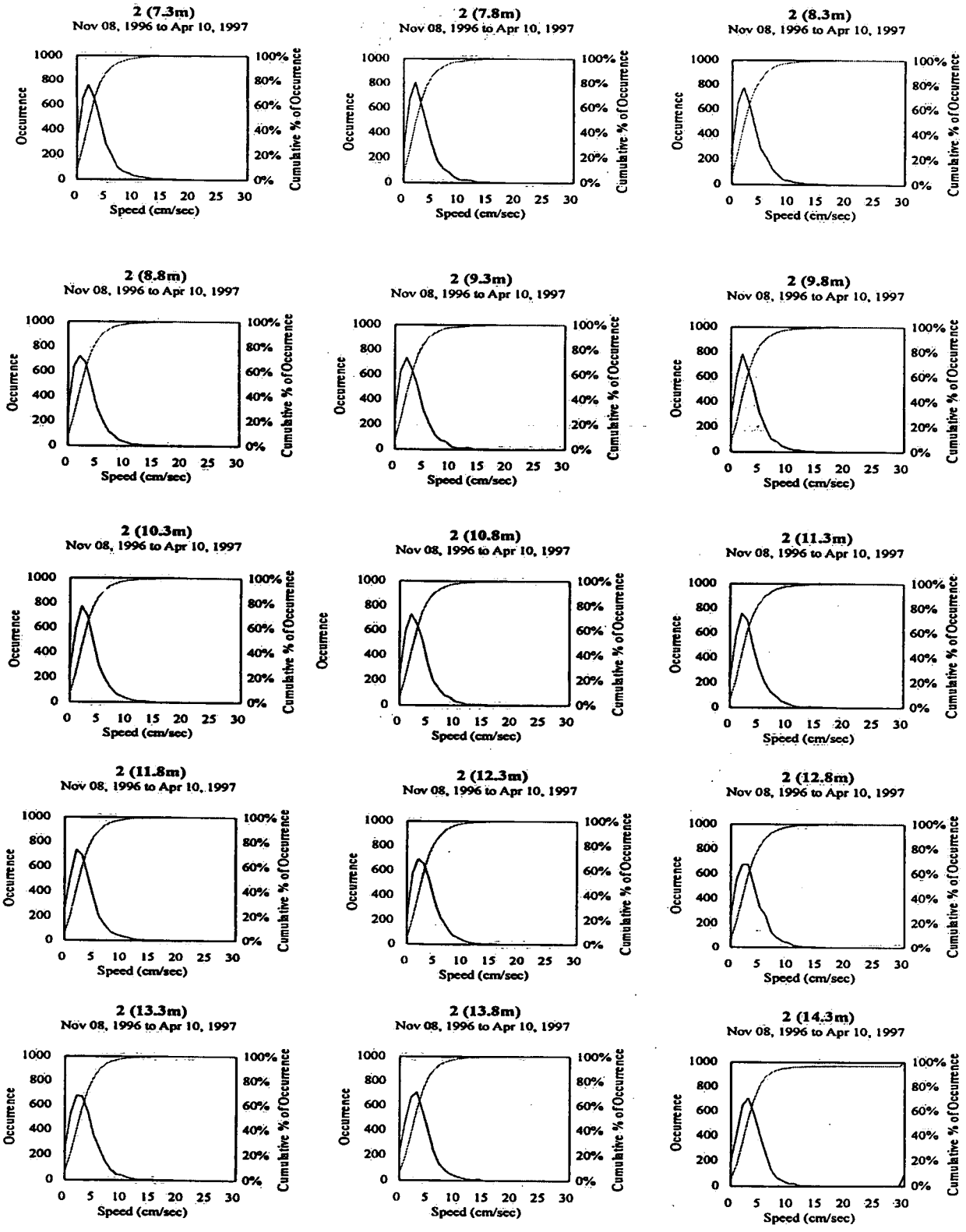

Figure 4.12 (cont'd) Frequency of occurrence vs. current speed for the ADCP station 2, November 8, 1996 to April 10, 1997.

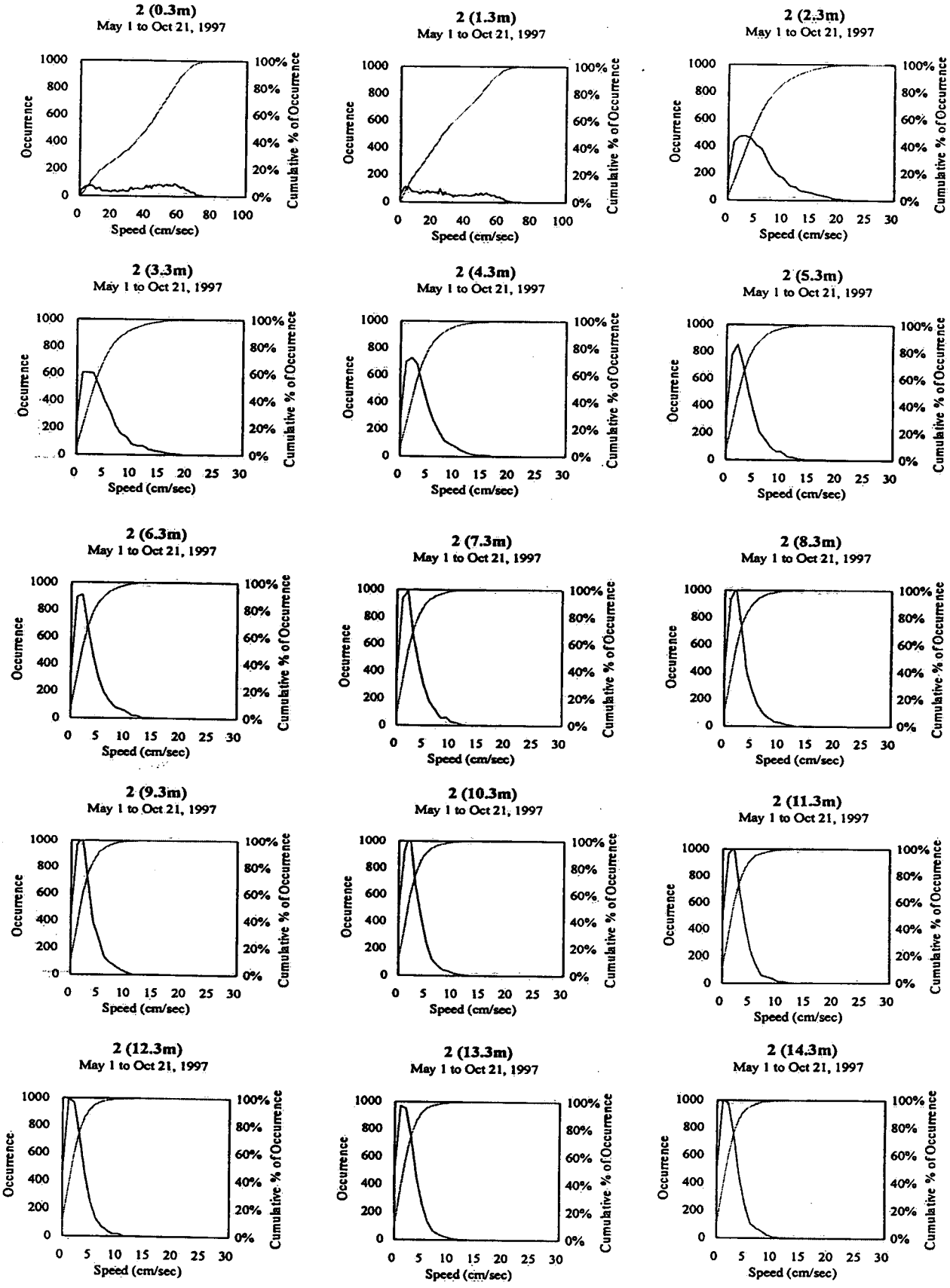

Figure 4.13 Frequency of occurrence vs. speed for the ADCP station 2, May 1 to October 21, 1997.

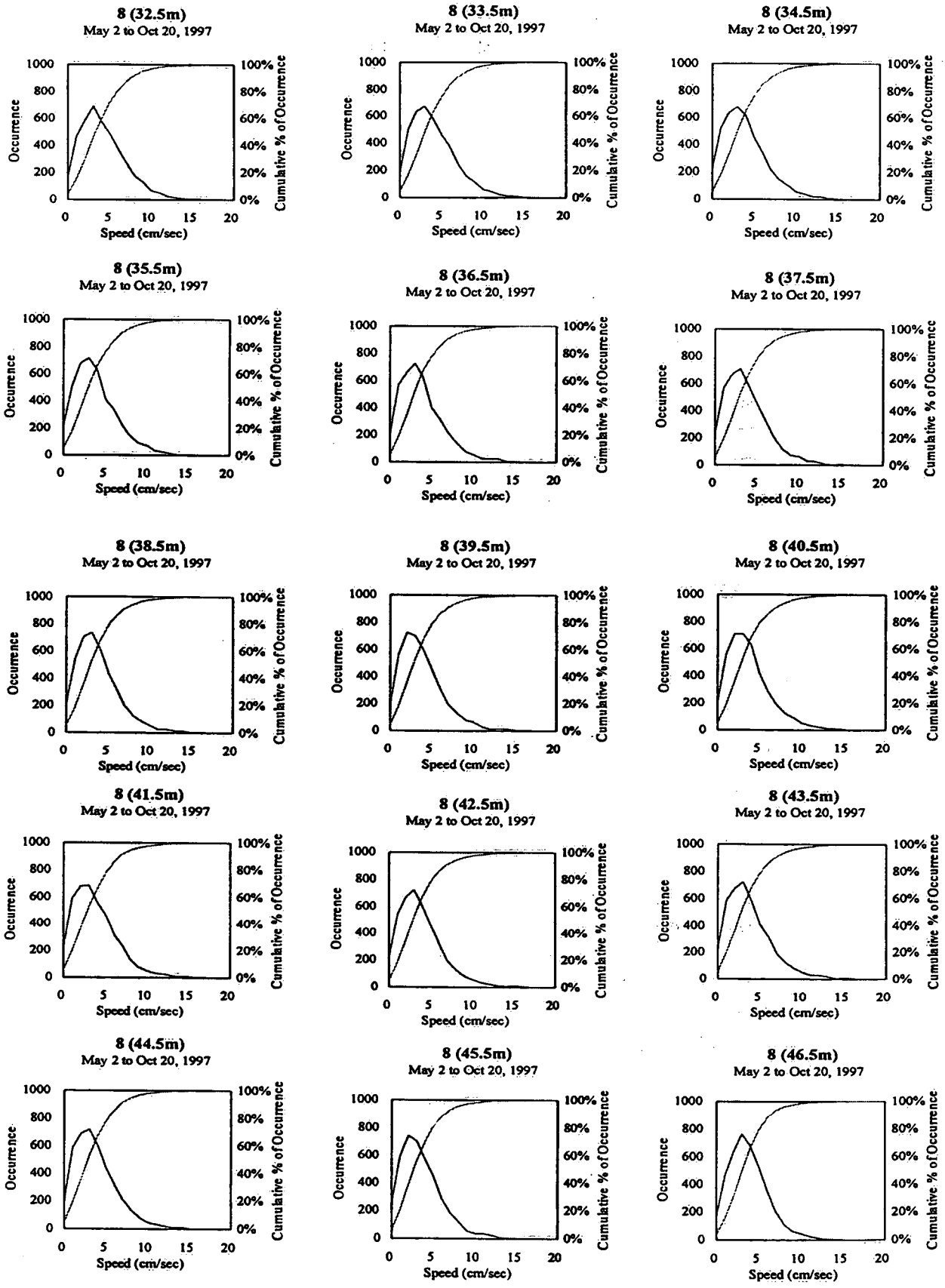

Figure 4.14 Frequency of occurrence vs. speed for the ADCP station 8, May 1 to October 20, 1997.

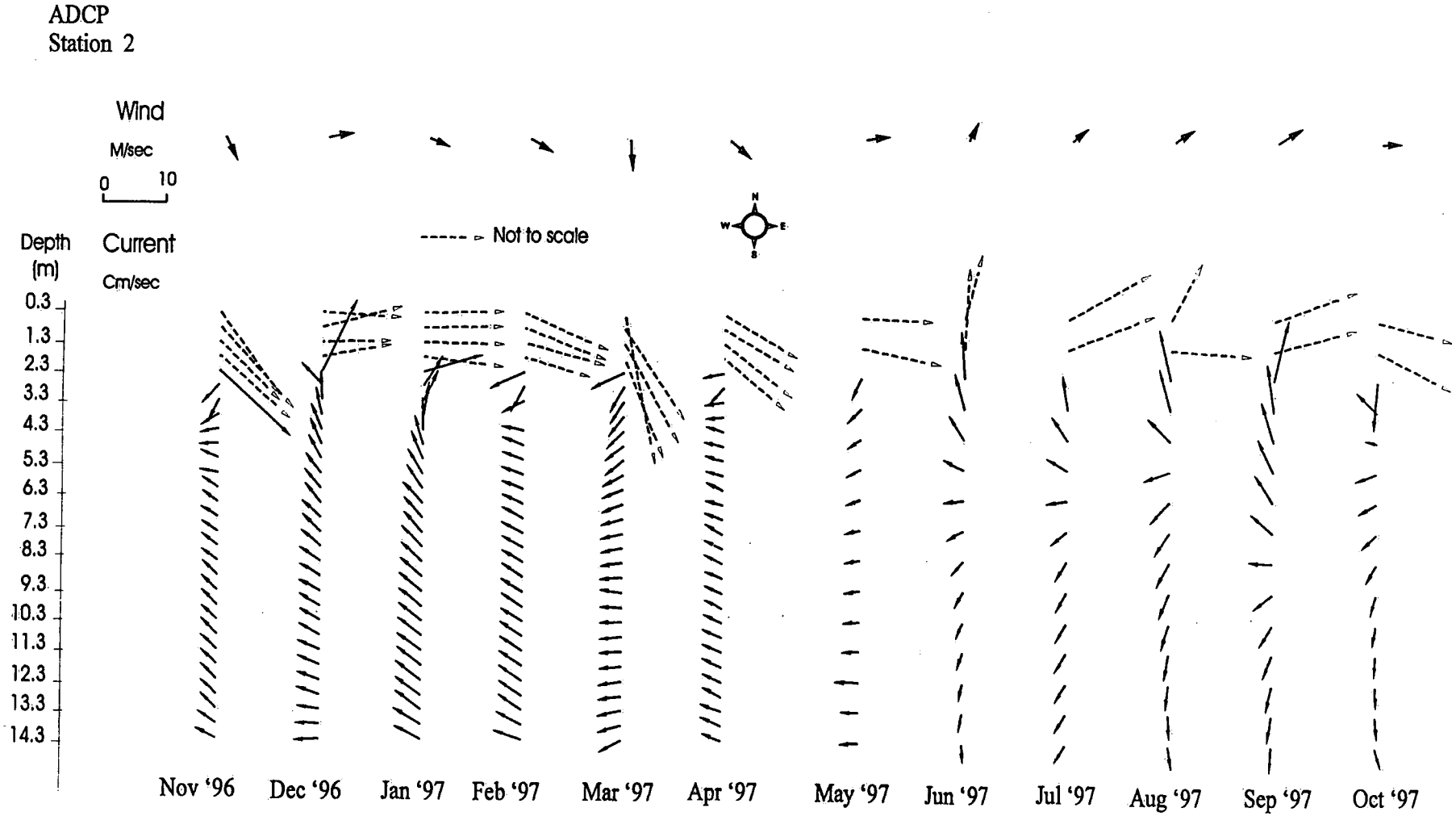

Figure 4.15 Monthly scalar speed stick plots for wind and ADCP current data at station 2, November 1996 to October 1997.

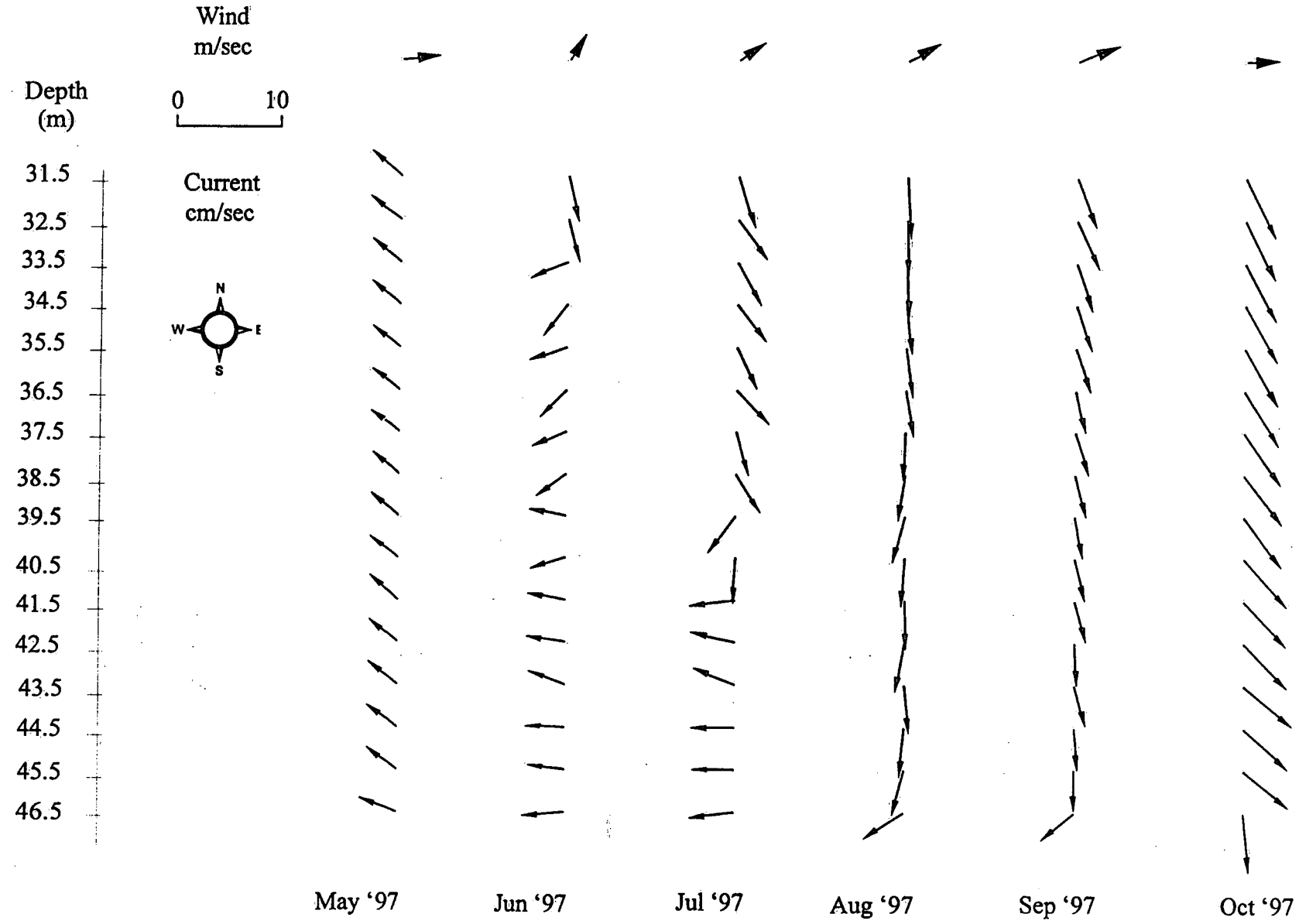

Figure 4.16 Monthly scalar speed stick plots for wind and ADCP current data at station 8, May to October 1997.

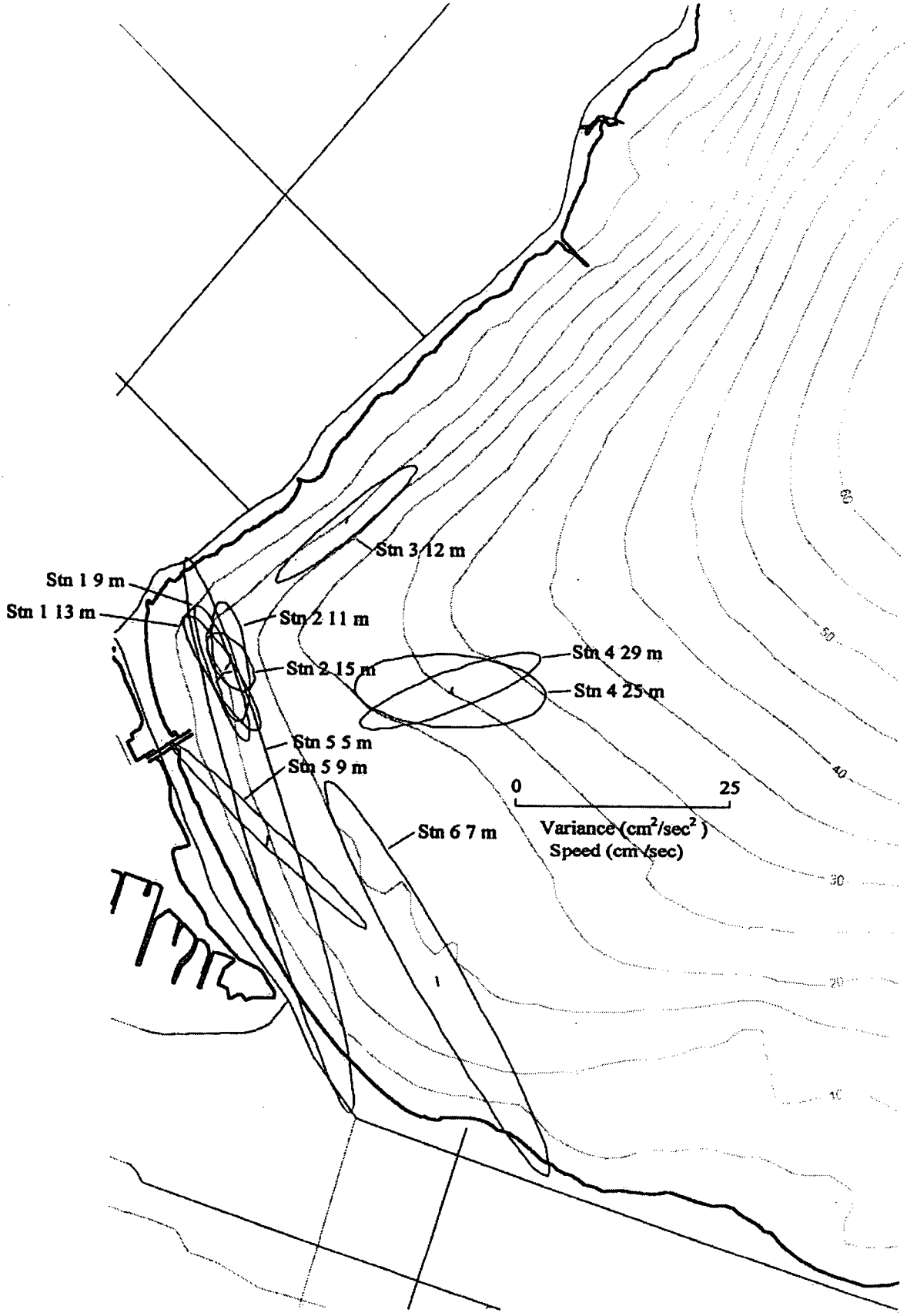

Figure 4.17 Velocity variance ellipses and mean speeds, May to November 1996.

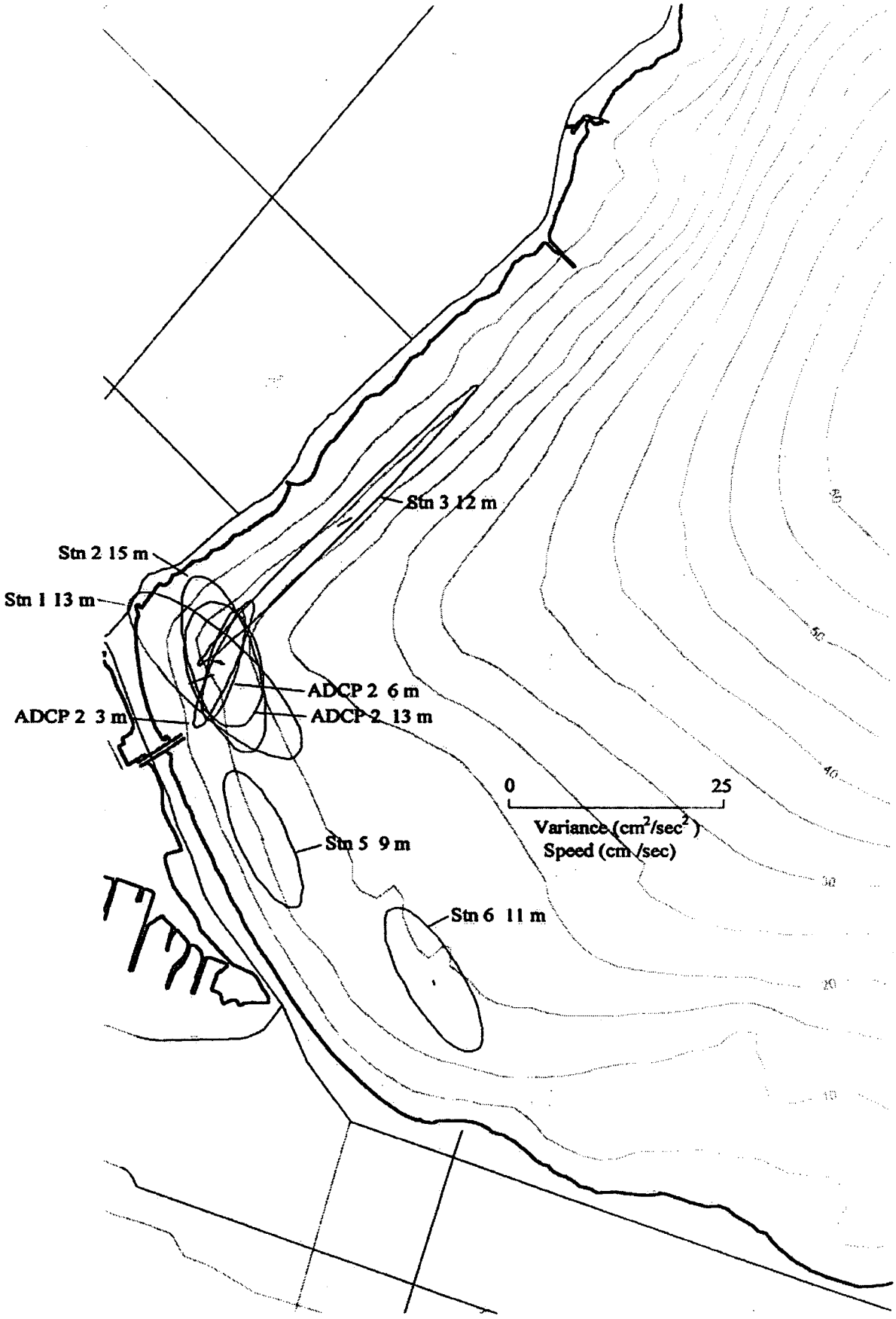

Figure 4.18 Velocity variance ellipses and mean speeds, November 1996 to April 1997.

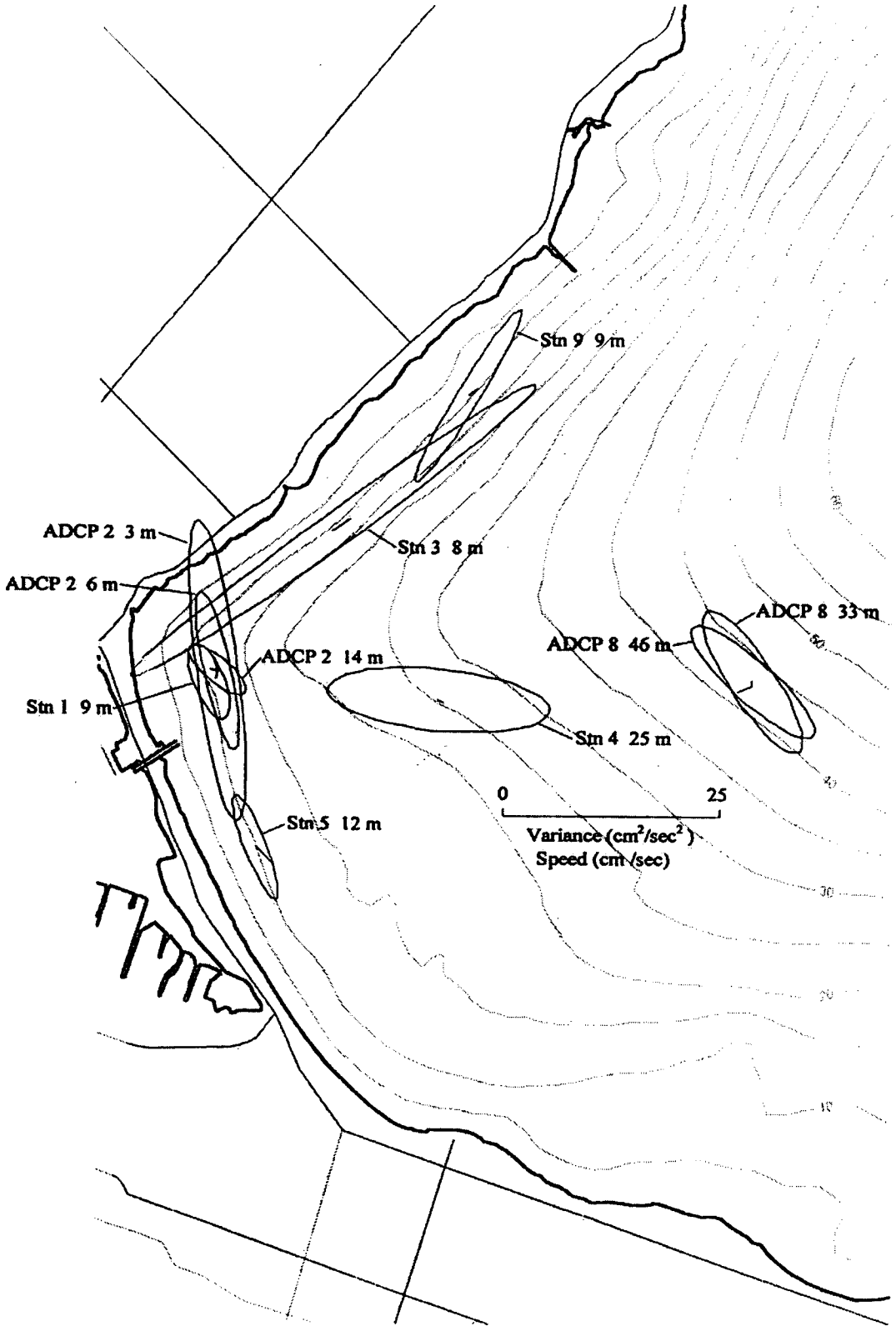

Figure 4.19 Velocity variance ellipses and mean speed, April to October 1997.

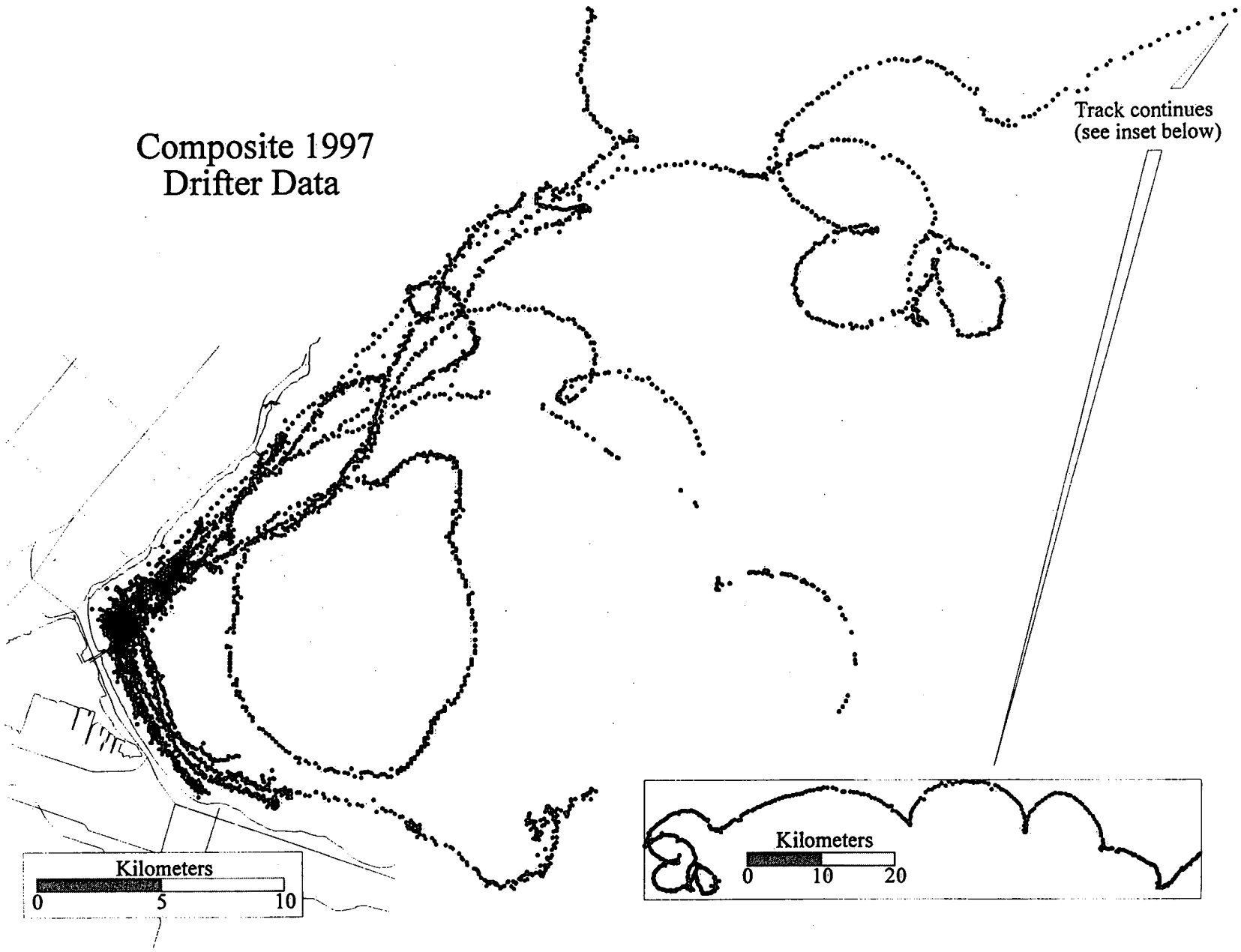

Figure 4.20 Composite of all 1997 drifter data at 15-minute intervals.

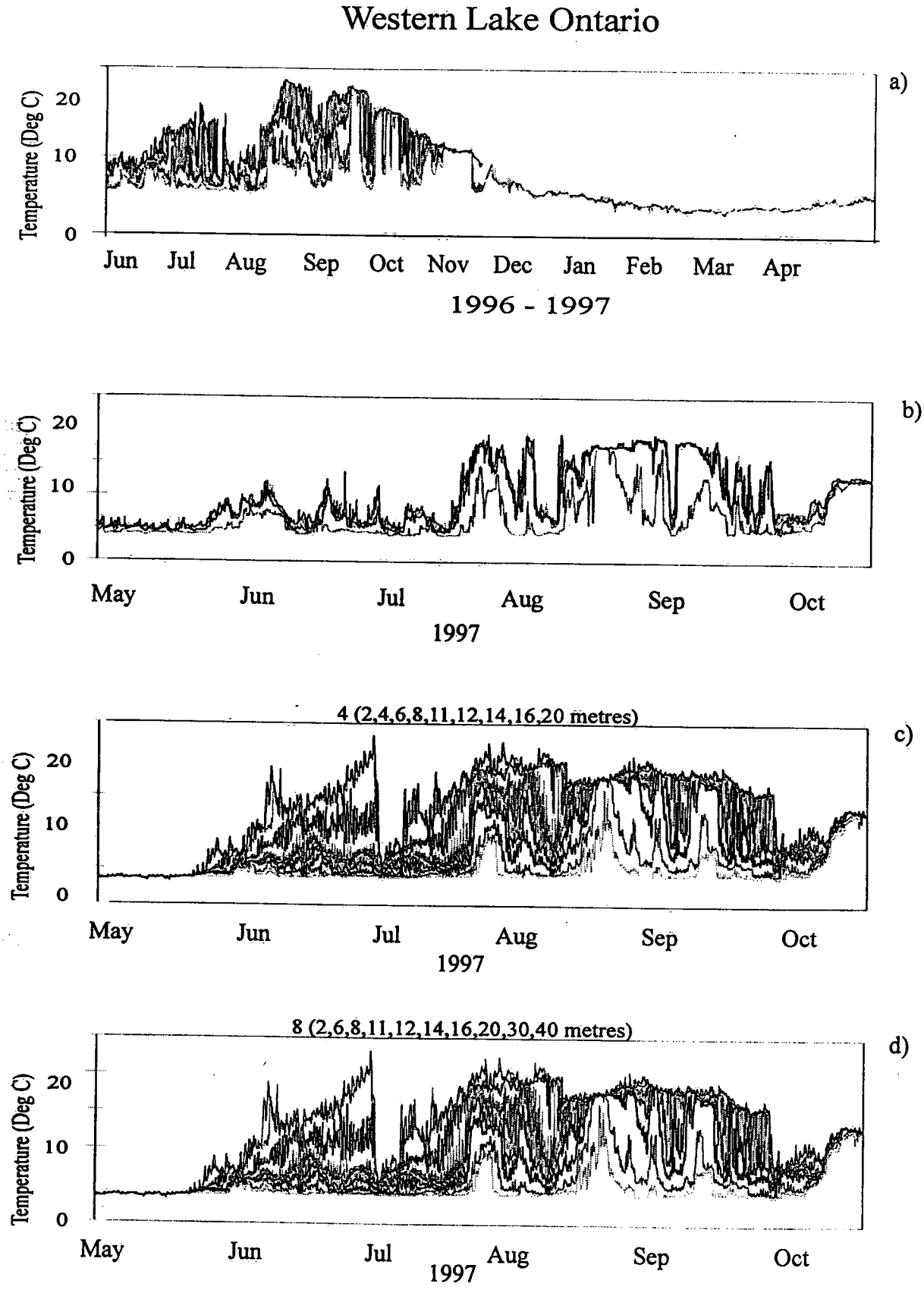

Figure 4.21 Temperature plots from a) Current meters, May 23, 1966 - April 24, 1997; b) Current meters, May 1 - October 21, 1997; c) FTP station 4, May 2 - October 20, 1997; d) FTP station 8, May 2 - October 20, 1997.

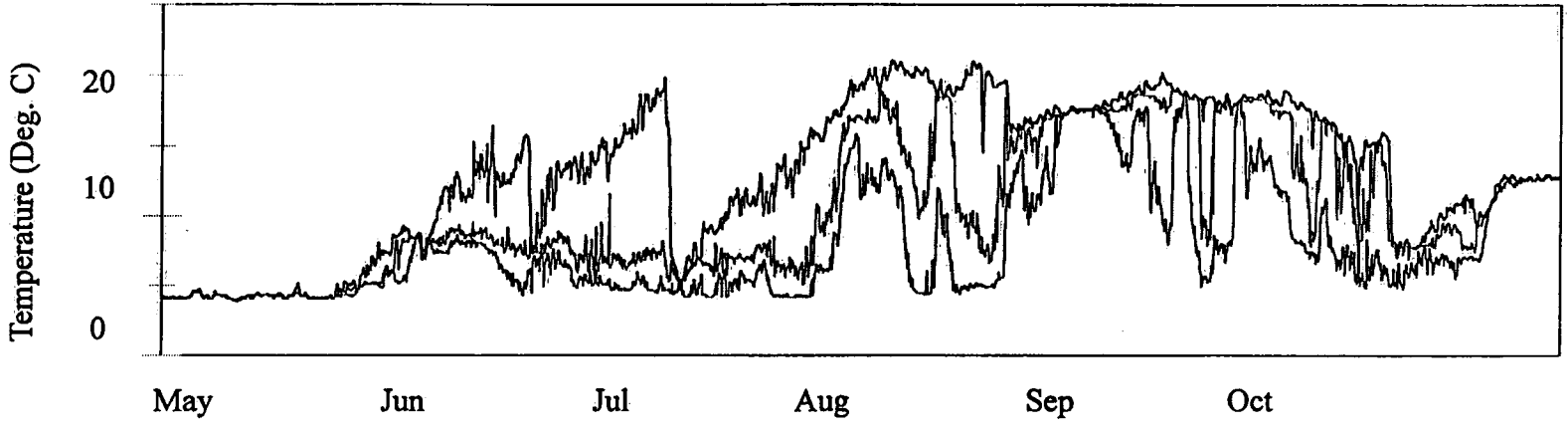

Figure 4.22 Temperature at station 4 at 2m, 10m and 20m, May 2 to October 20, 1997.

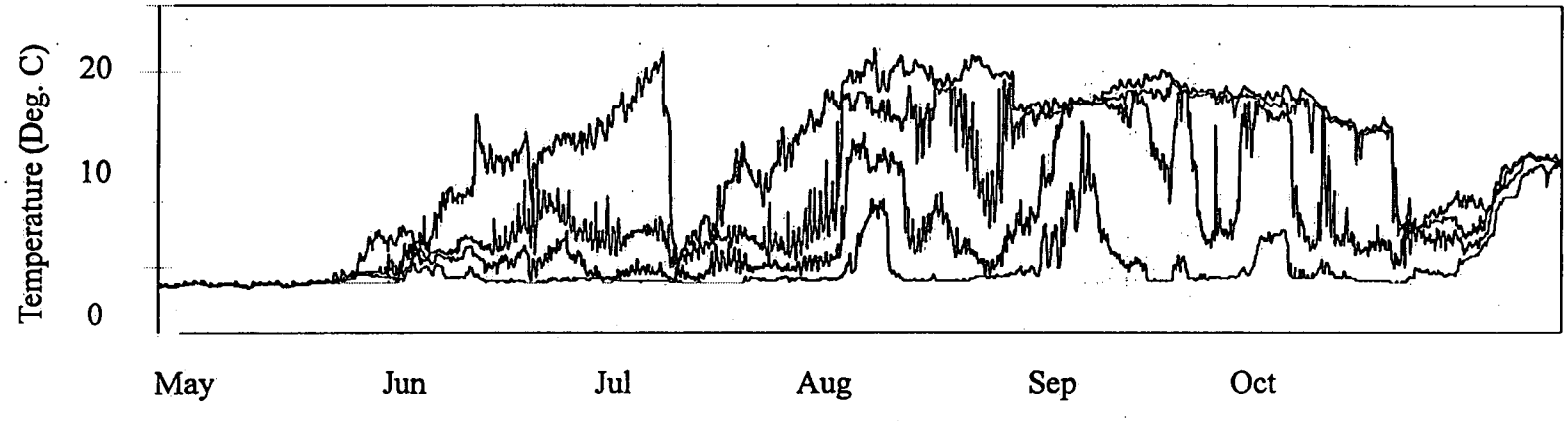

Figure 4.23 Temperature at station 8 at 2m, 10m, 20m, 40m, May 2 to October 20, 1997.

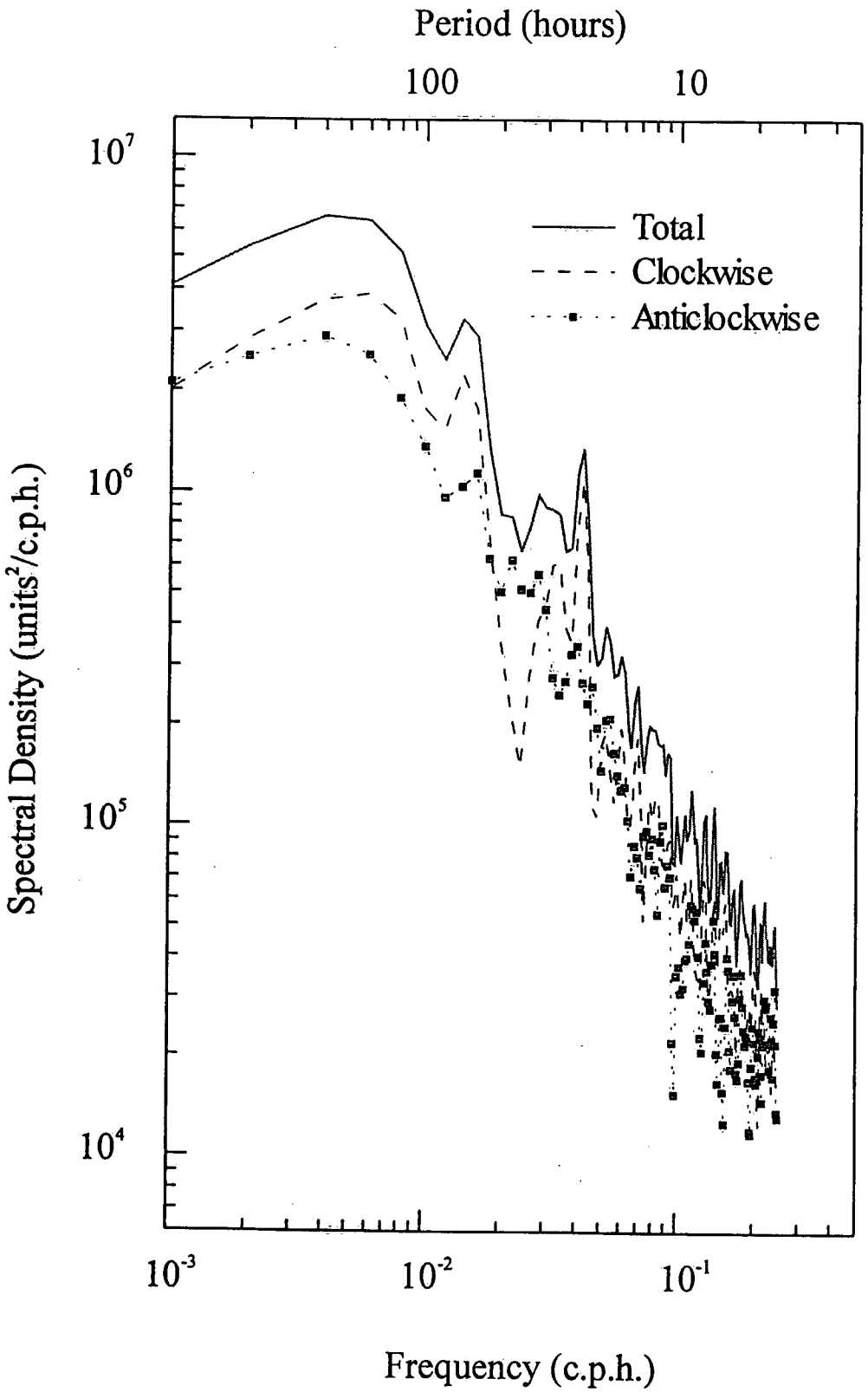

Figure 5.1 Spectra of wind speed at station 8, July 1 to August 31, 1997.

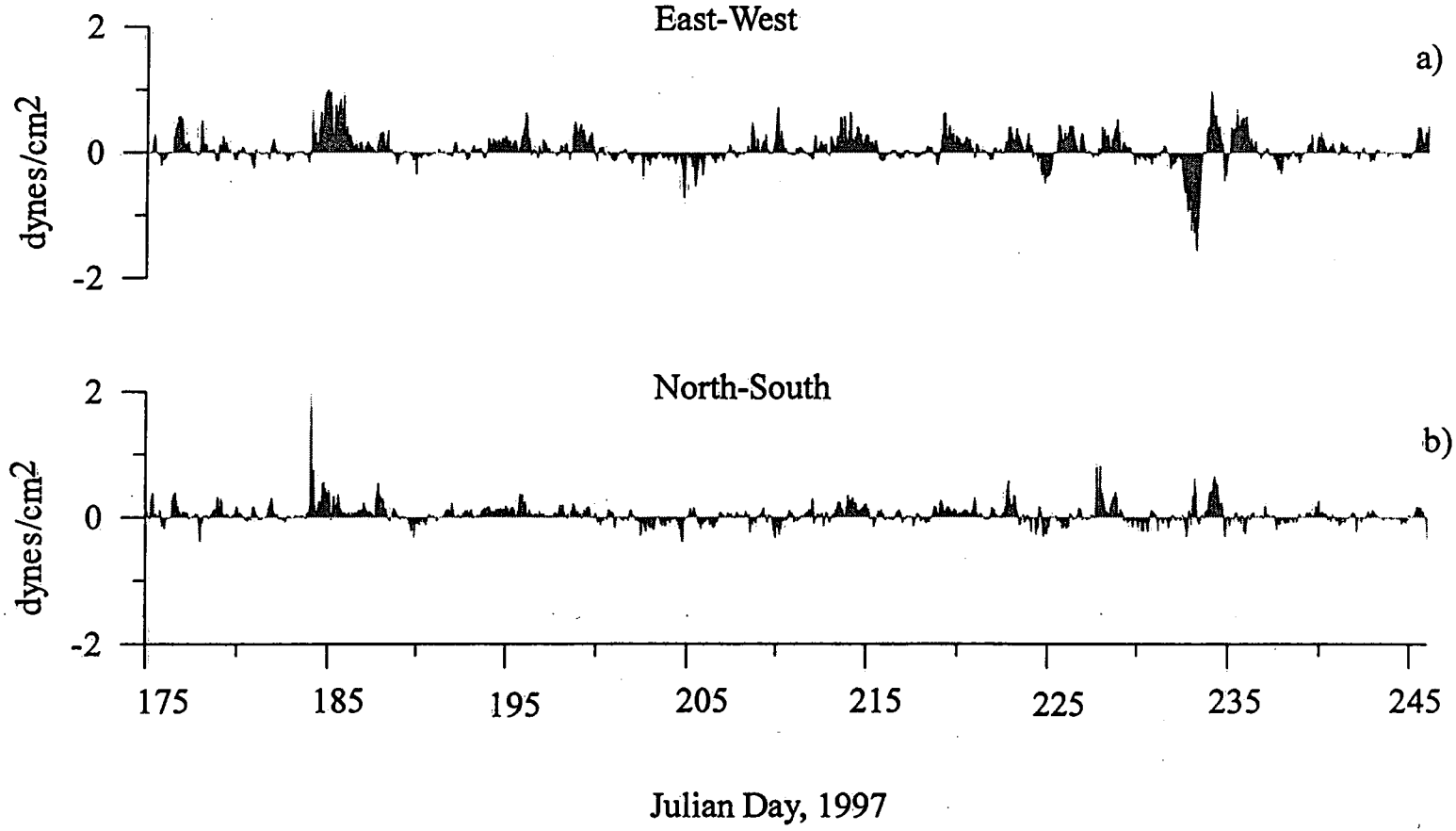

Figure 5.2 East-west and north-south wind stress components at station 8 (summer - 1997).

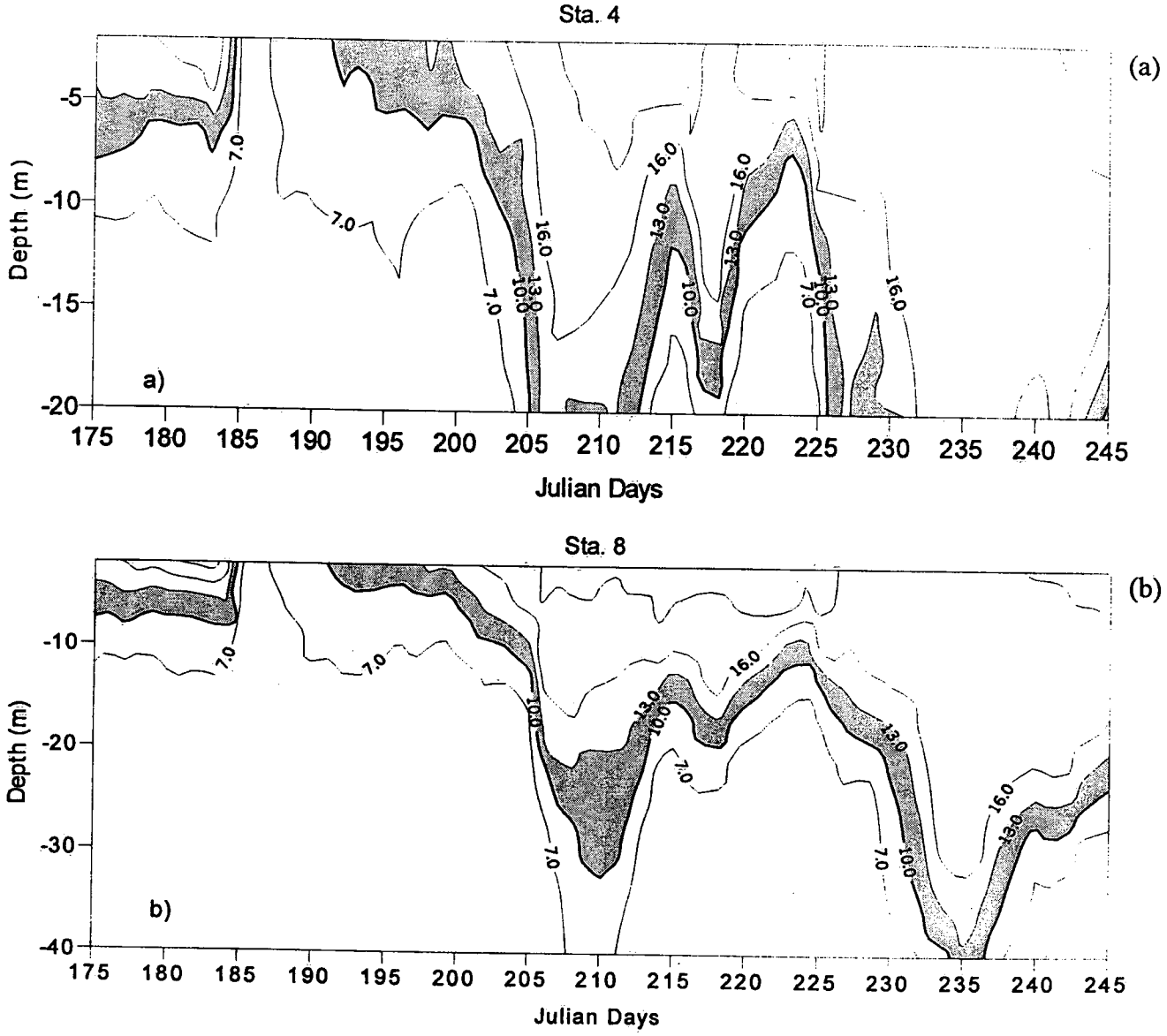

Figure 5.3 Daily averaged temperatures at a) station 4 and b) station 8, June 24 to September 2, 1997.

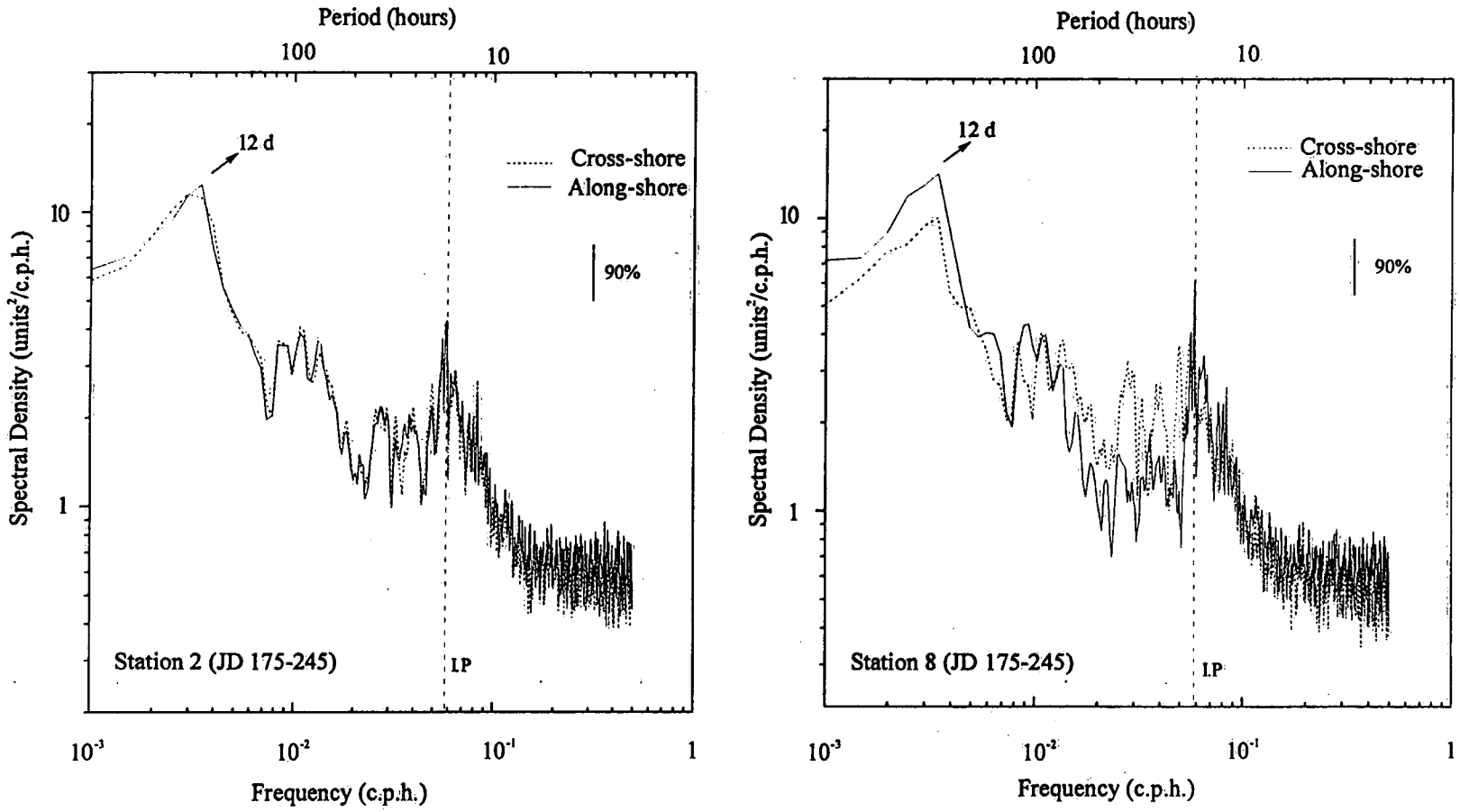

Figure 5.4 Kinetic energy spectra (depth-averaged) at station 2 and station 8 during the summer 1997.

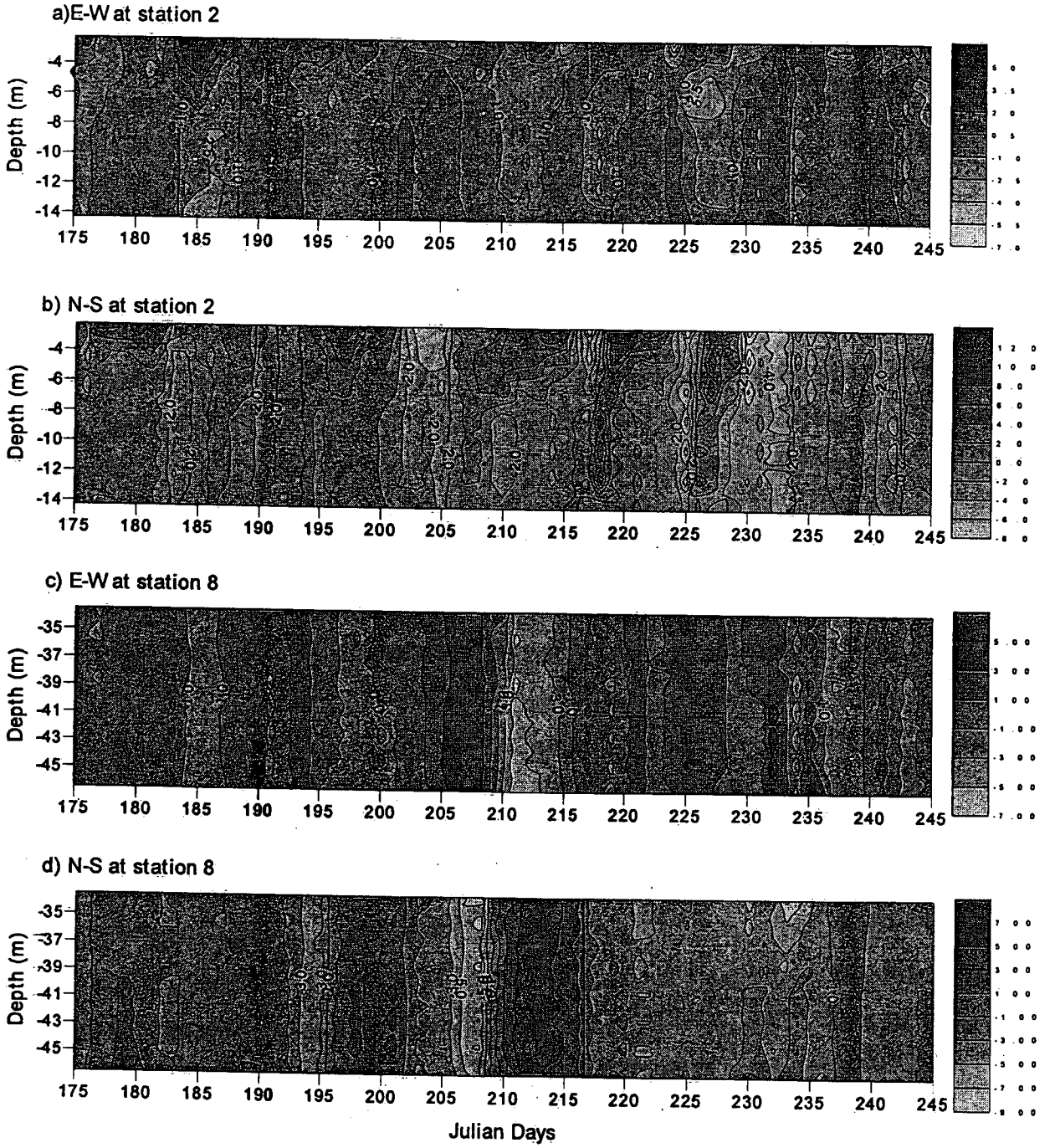

Figure 5.5 Current speed distribution at station 2 and station 8 (June 24 to September 2, 1997).

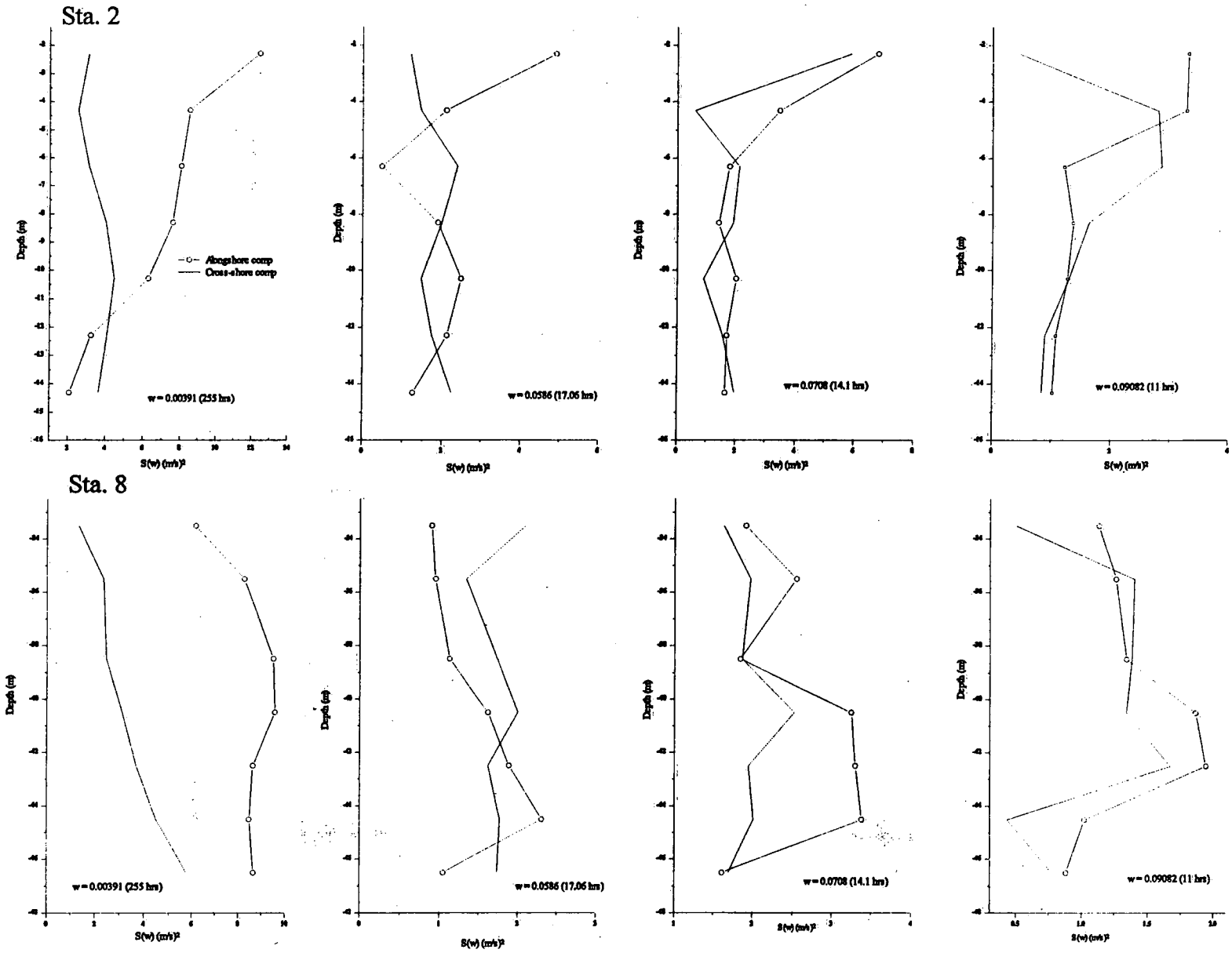

Figure 5.6 Spectral density at important frequencies of the cross-shore component (solid curve) and alongshore component (open circles) plotted against selected depths (top panel station 2, lower panel station 8).

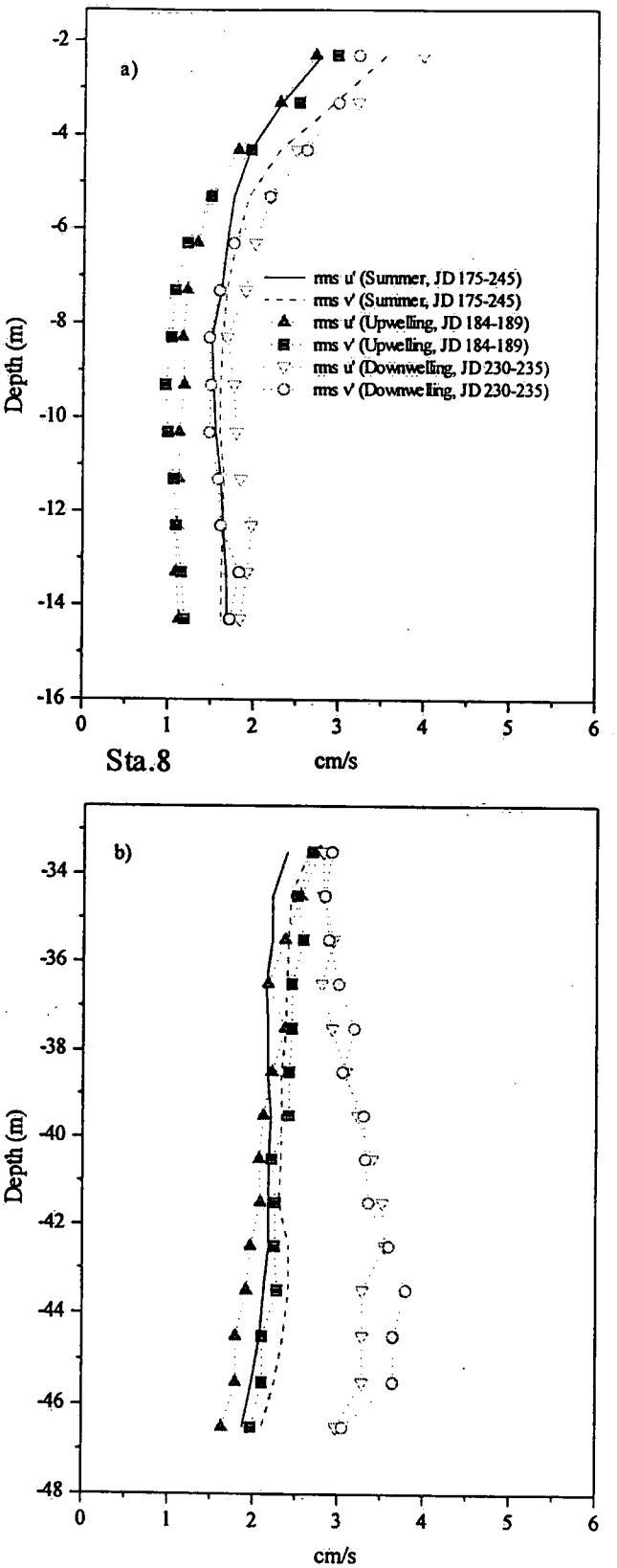

Figure 5.7 RMS velocity components from station 2 and station 8 during summer season and episodic events.

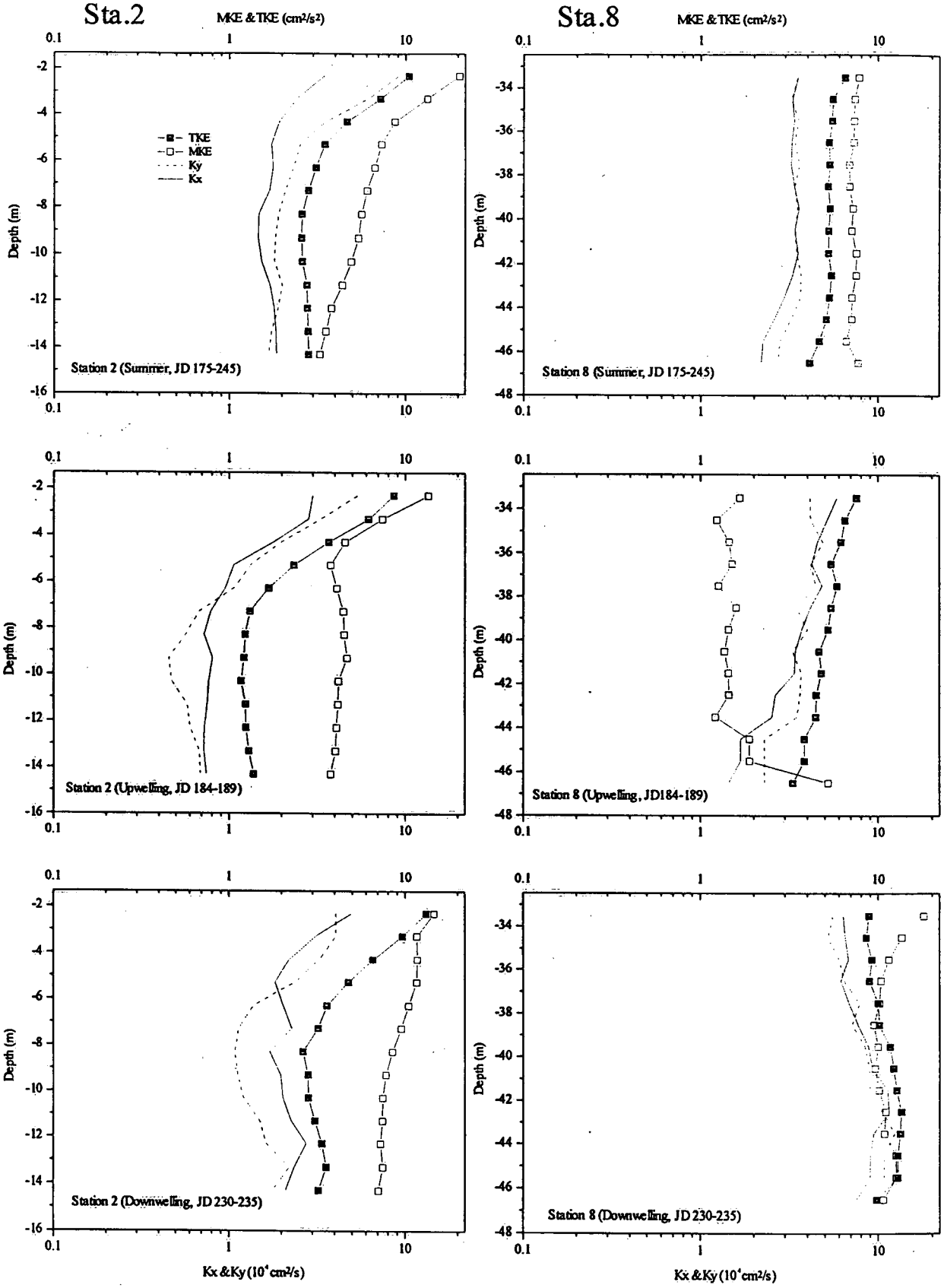

Figure 5.8 MKE, TKE and horizontal exchange coefficients during summer season and during the episodic events.

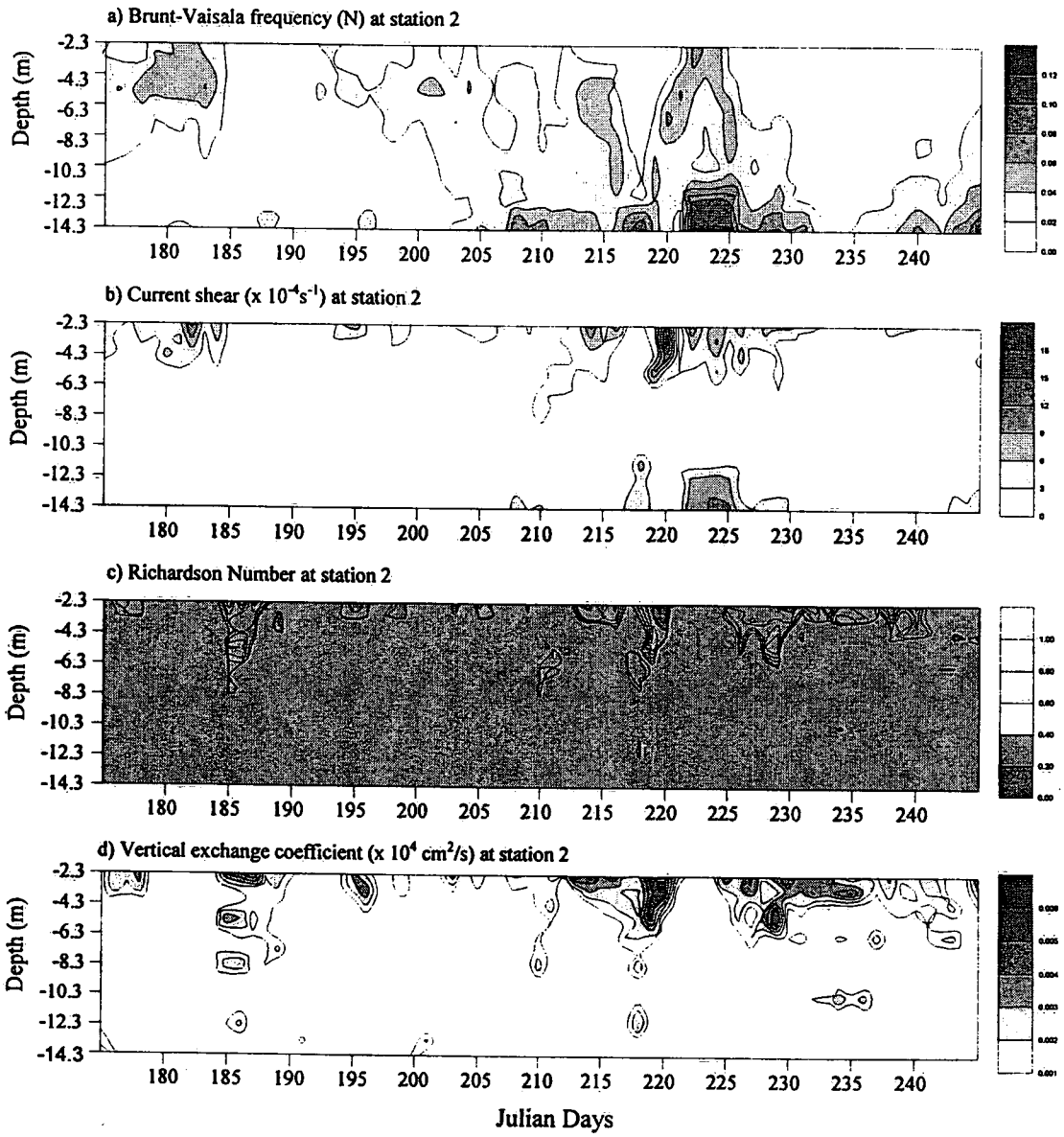

Figure 5.9a Brunt-Vaisala frequency, current shear, Richardson number and vertical exchange coefficient at station 2.

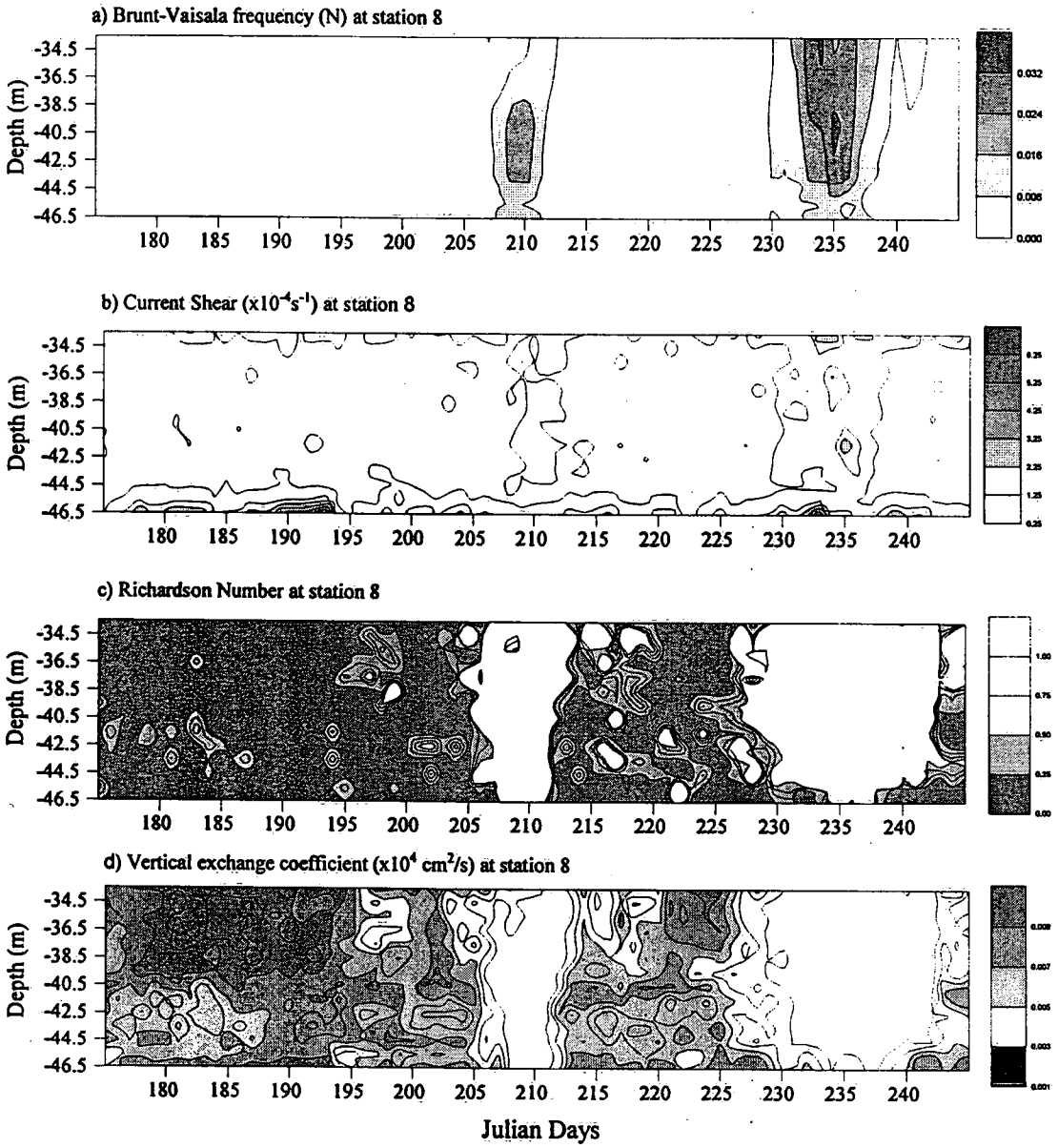

Figure 5.9b Brunt-Vaisala frequency, current shear, Richardson number and vertical exchange coefficient at station 8.

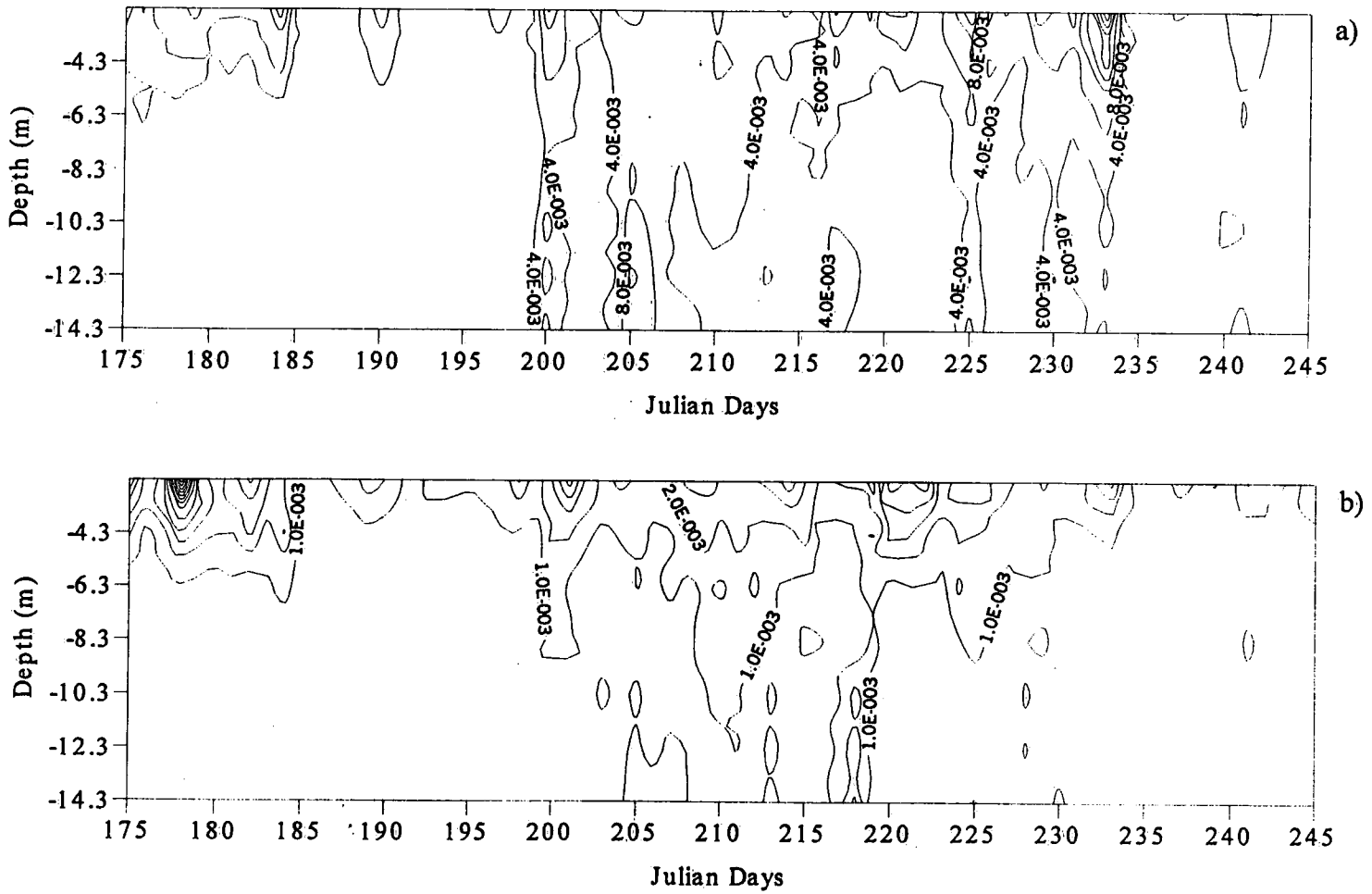

Figure 5.10 Daily variation of turbulent kinetic energy (TKE) and dissipation at ADCP station 2.

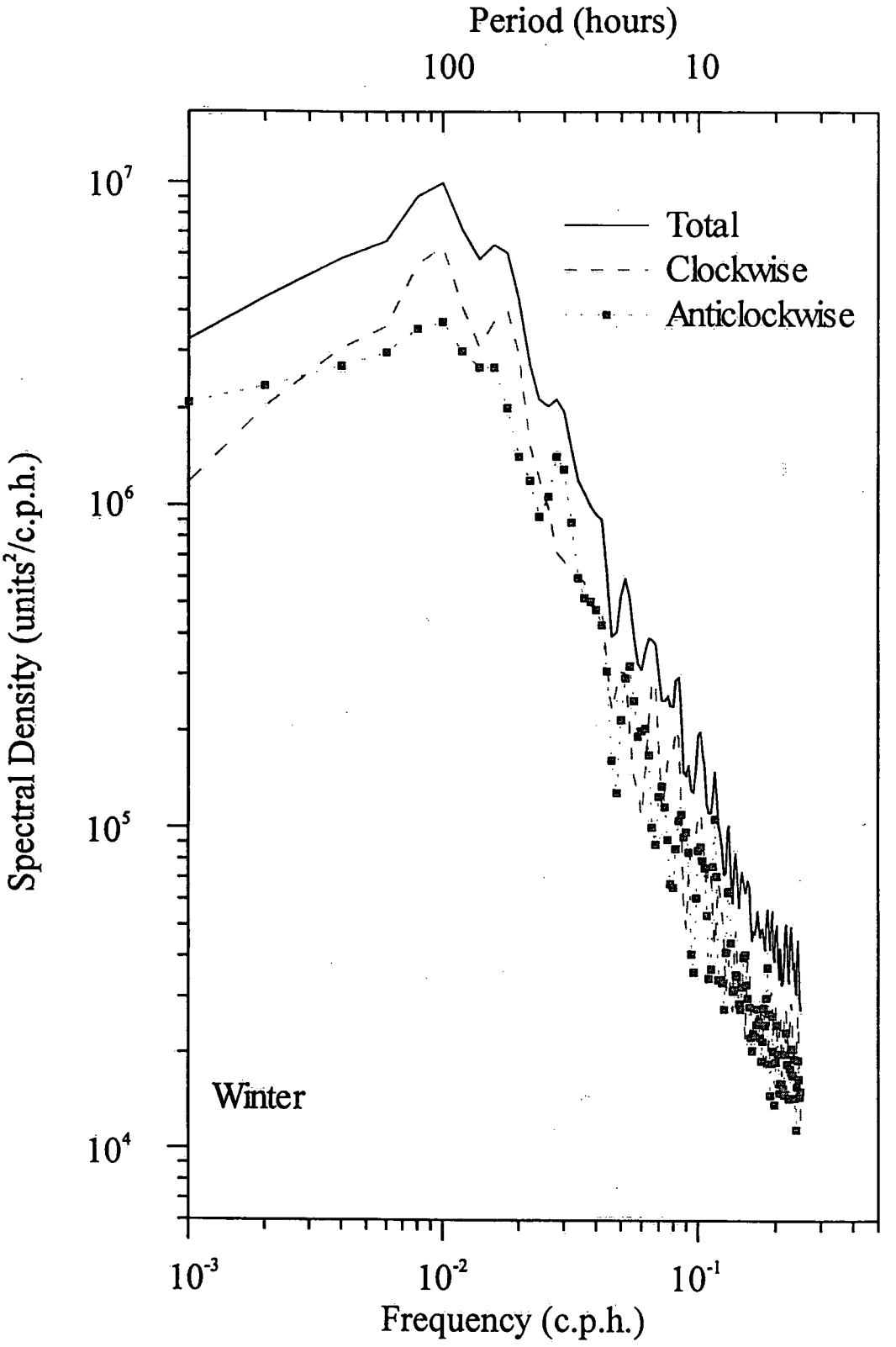

Figure 5.11 Rotary spectra of wind speed at Burlington Pier during the winter season (January 29 to April 29, 1997).

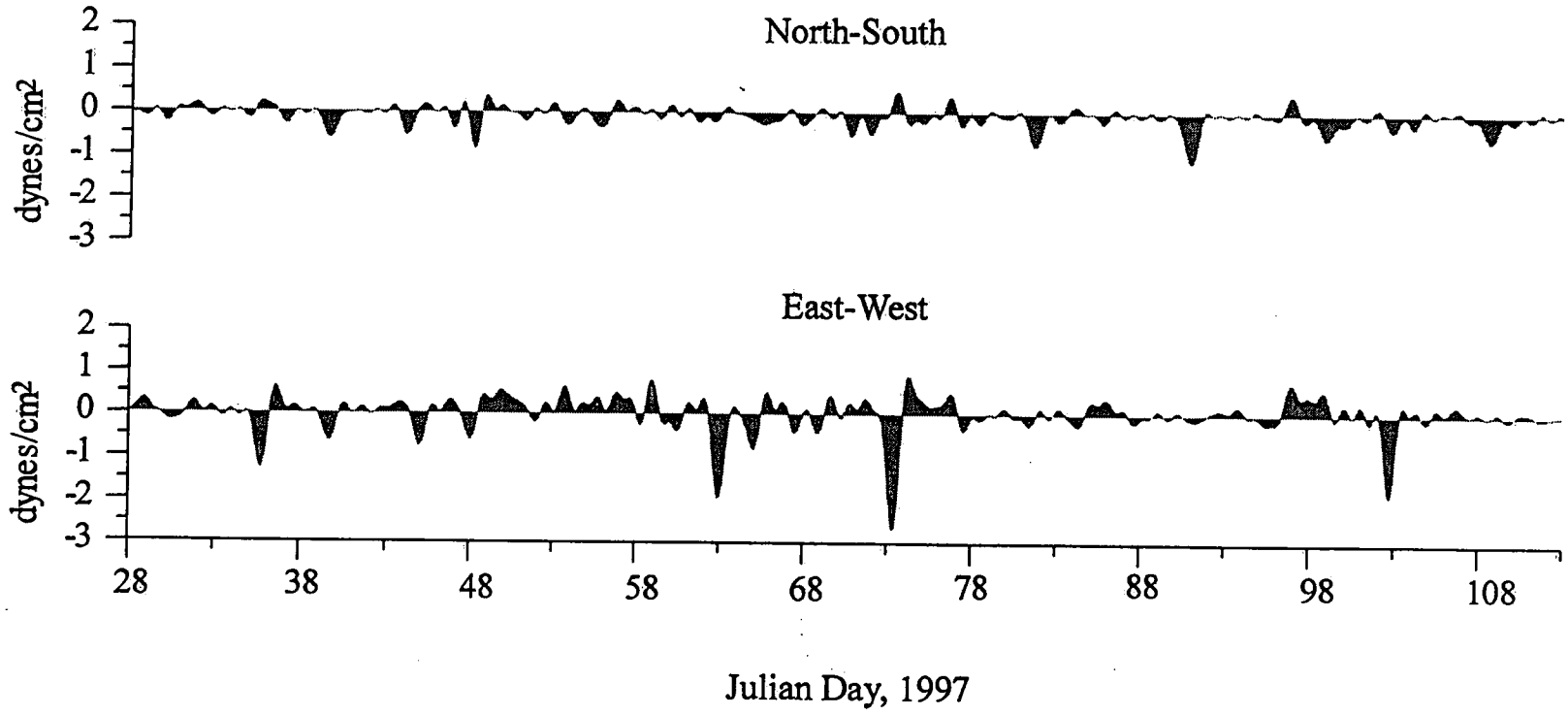

Figure 5.12. North-south and east-west wind stress components during the winter season

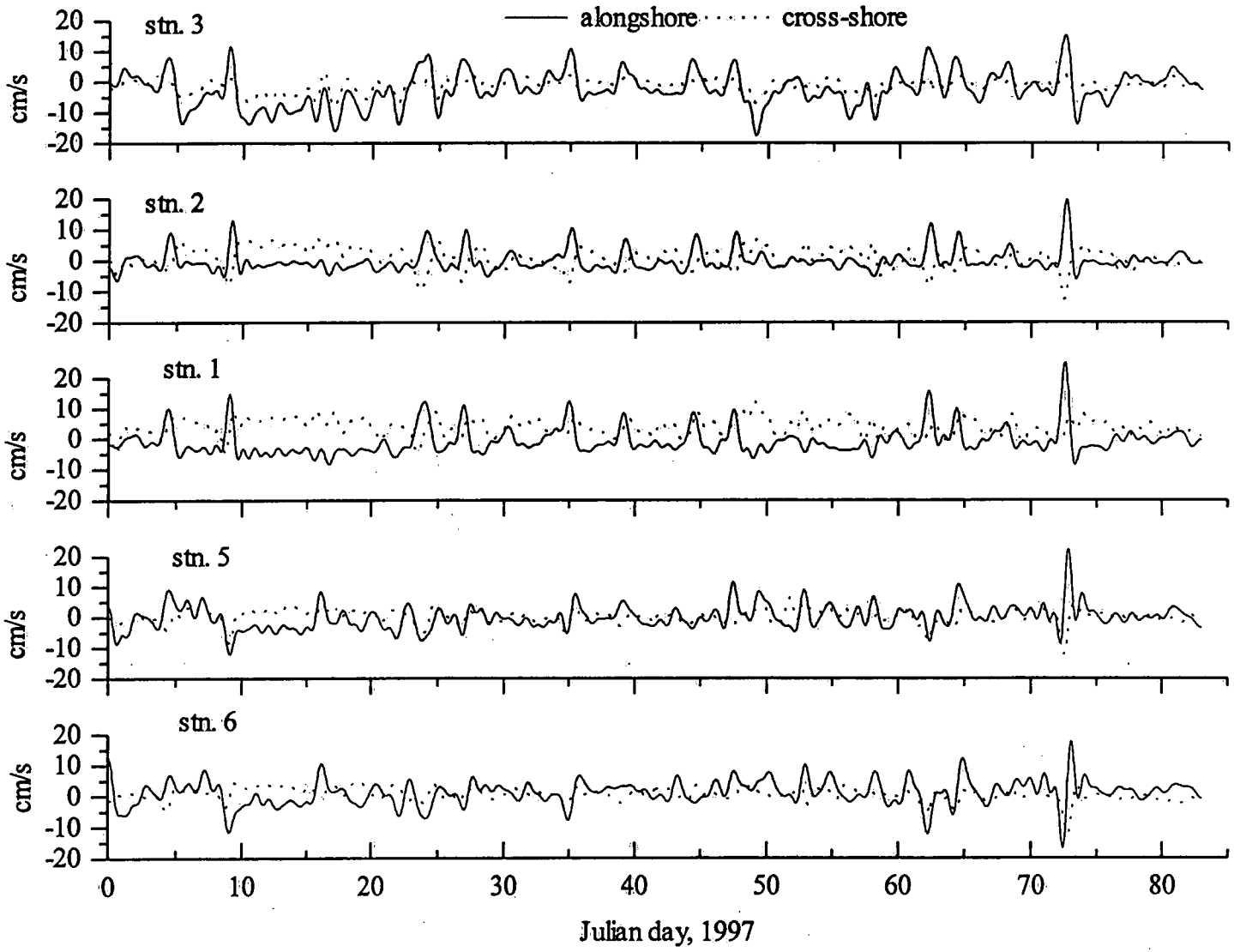

Figure 5.13 Time series of low-pass filtered currents at five VACM stations.

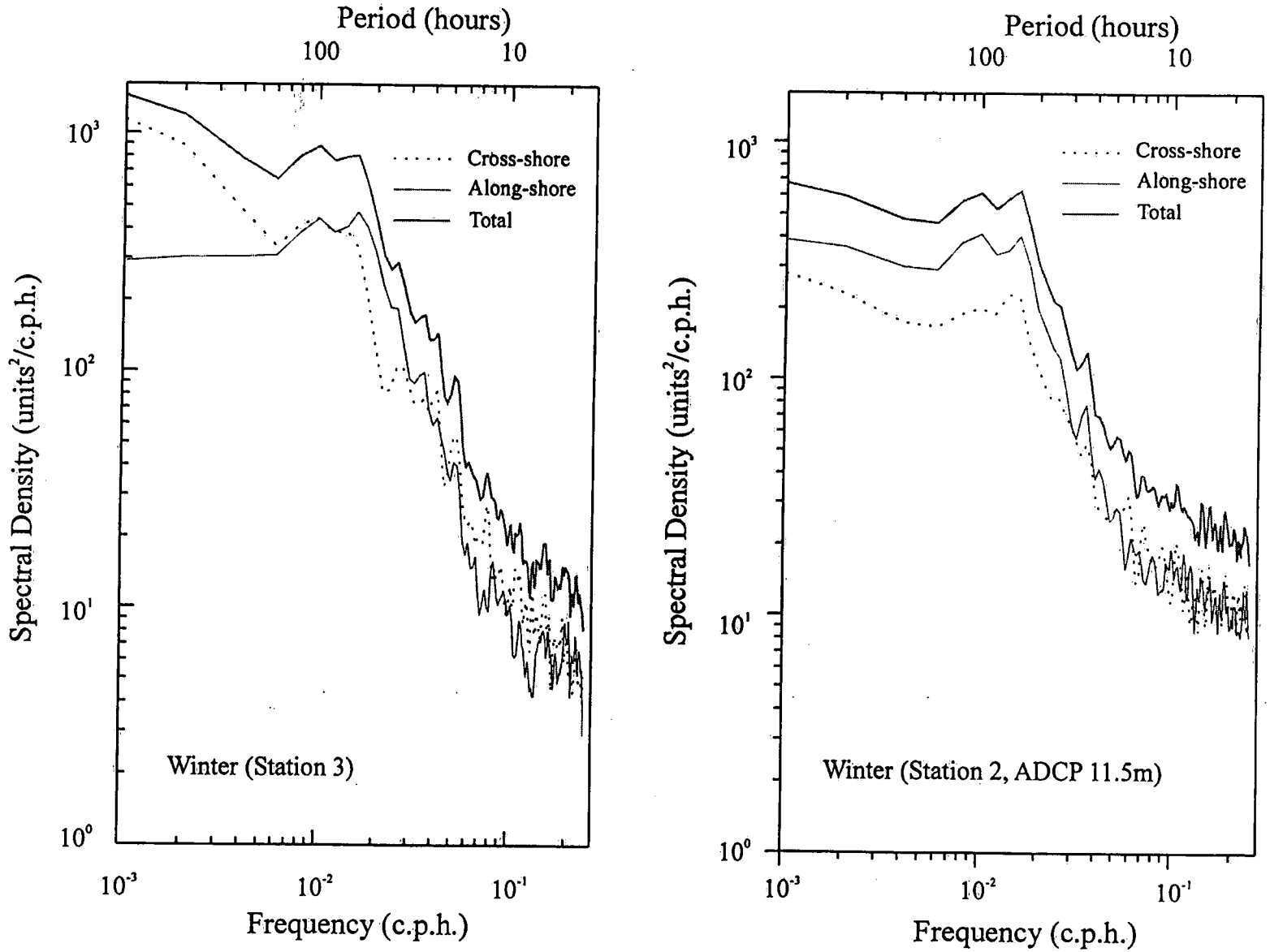

Figure 5.14 Kinetic energy spectra of currents at station 3 and station 2 during winter.

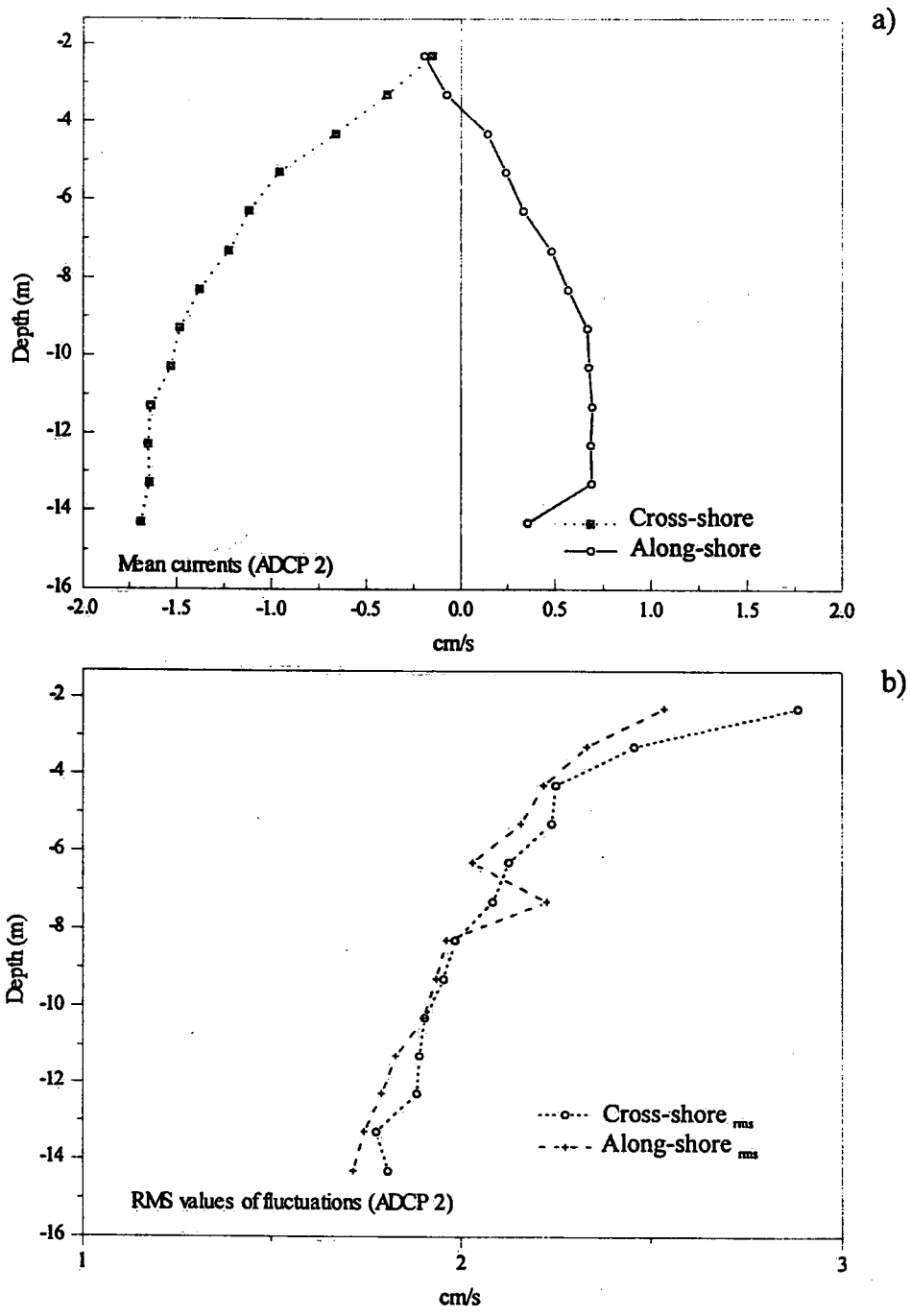

Figure 5.15 Mean currents and RMS values of fluctuations during winter at station 2.

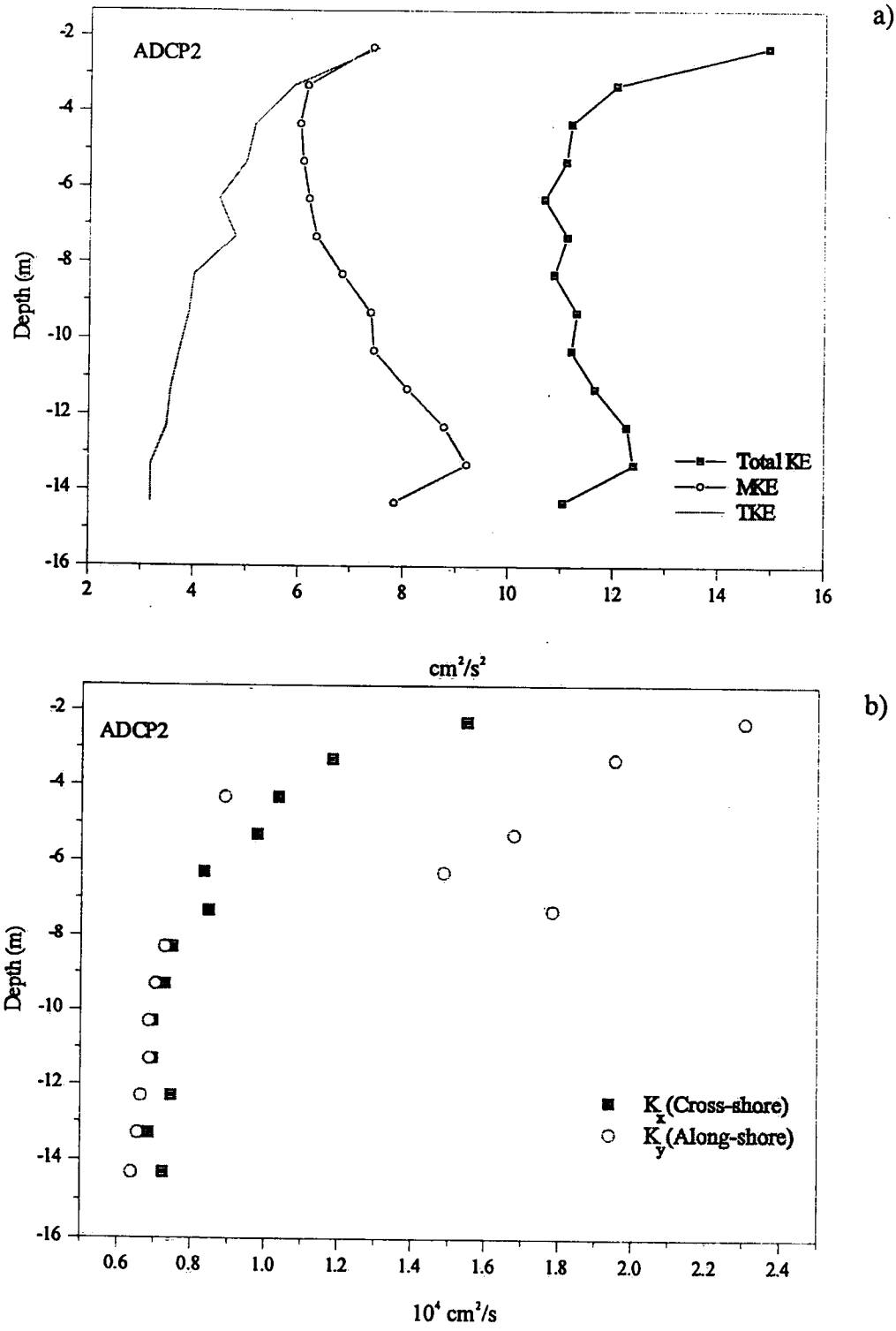

Figure 5.16 Plots of mean and turbulent kinetic energy and horizontal exchange coefficients during winter season at station 2.

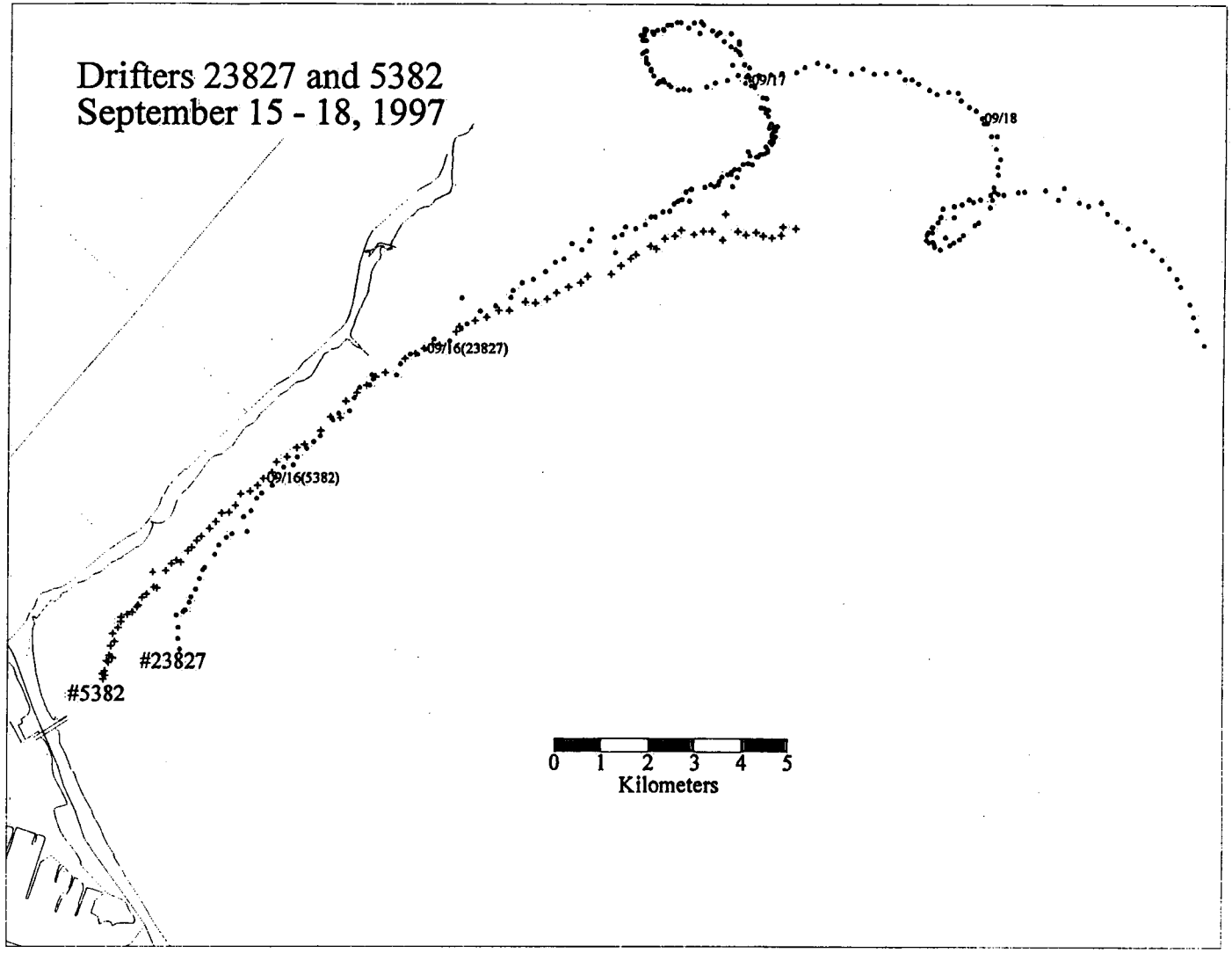

Figure 5.17 Examples of simultaneous long drifter trajectories (#5382 data truncated).

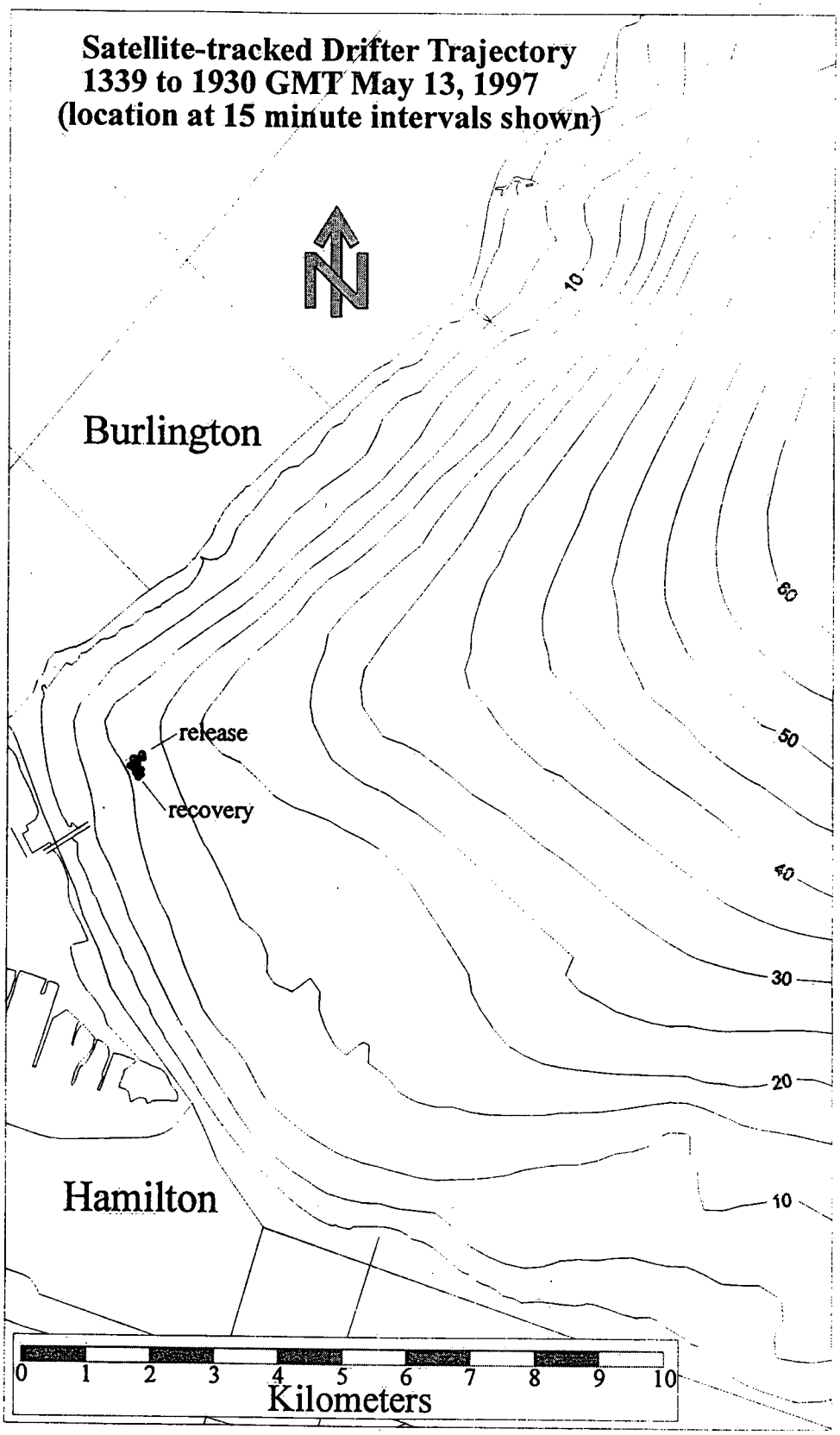

Figure 5.18 Example of short drifter trajectory in very low currents (~1.2 cm/sec).

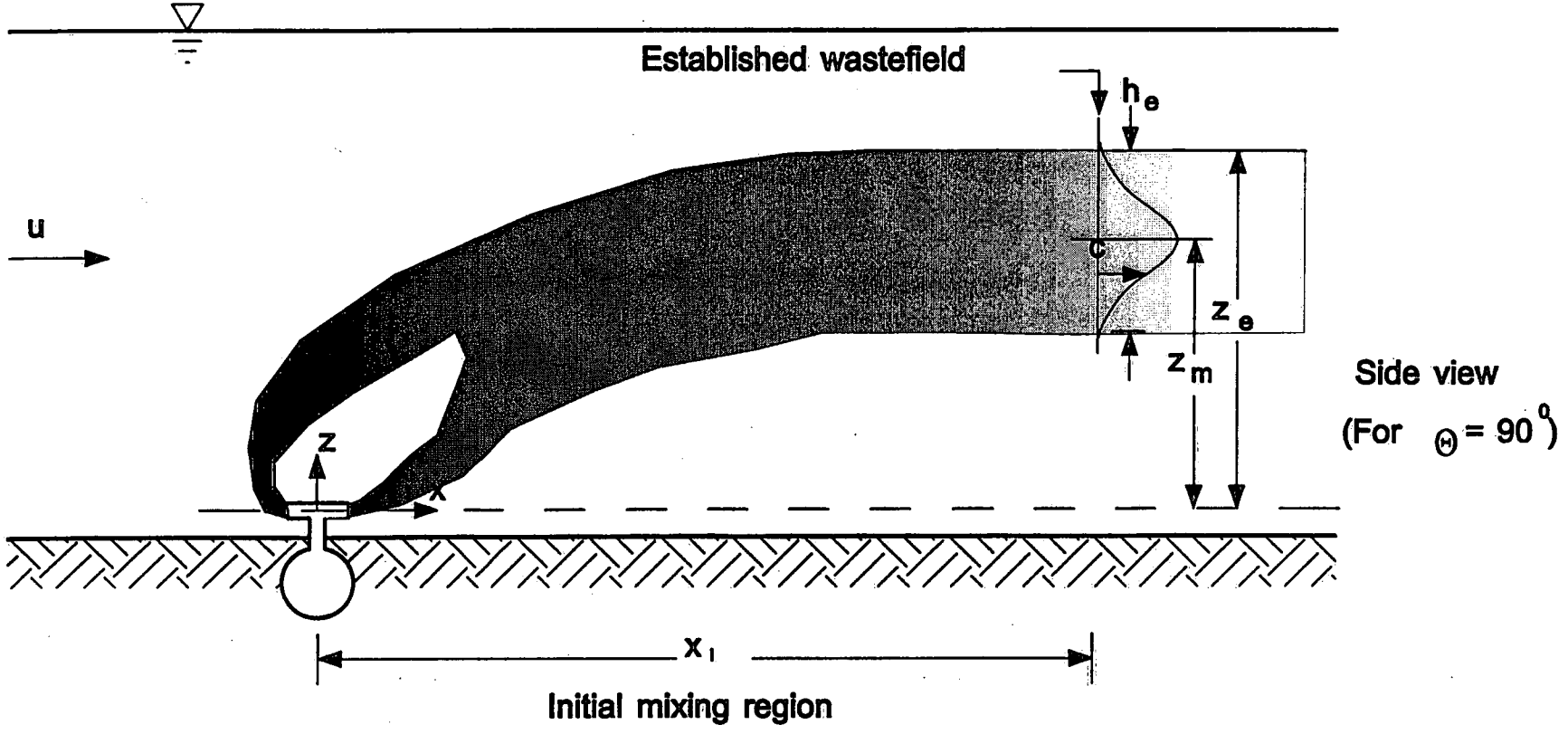

Figure 6.1 Waste field characteristics discharged from a submerged diffuser.

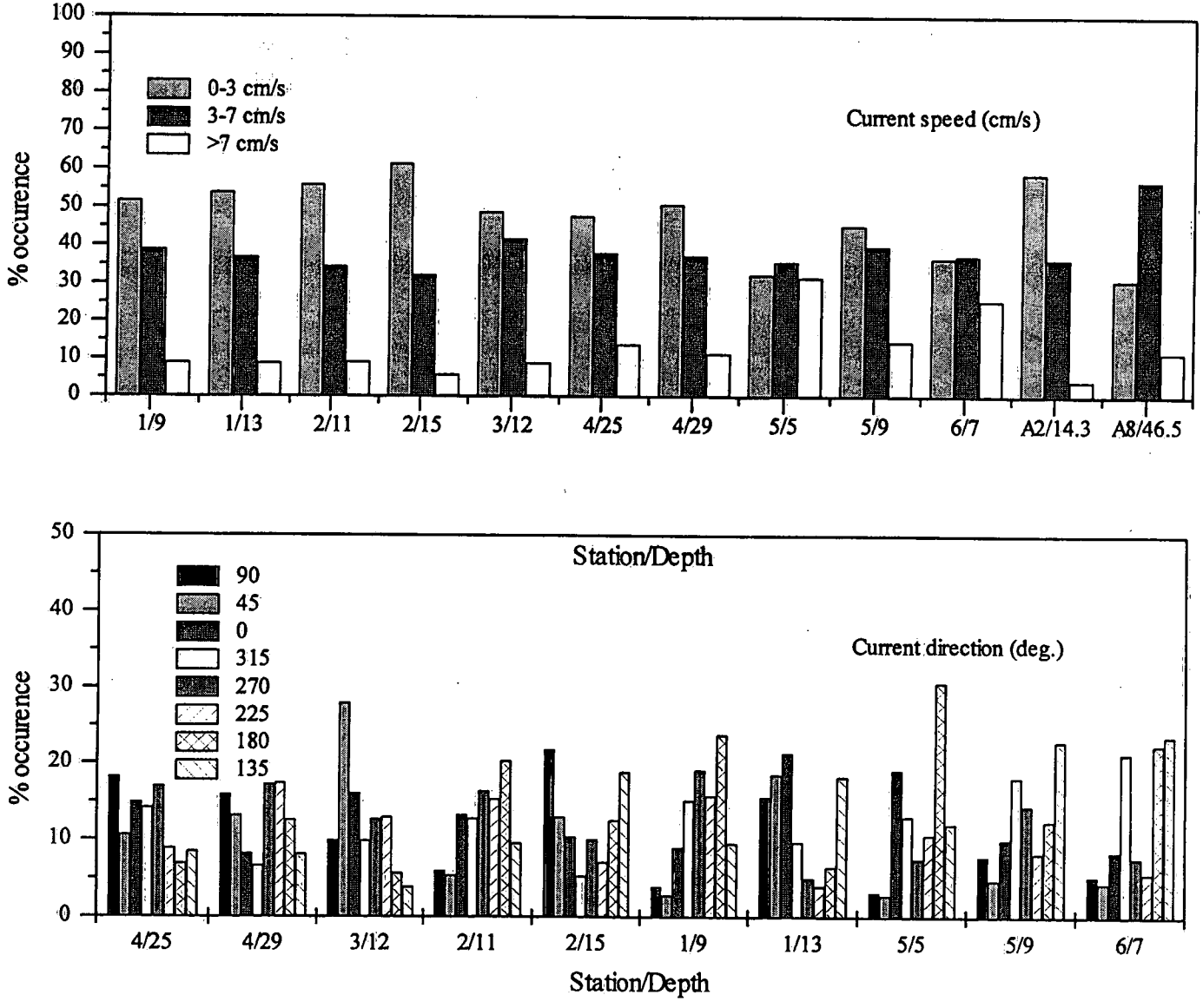

Figure 6.2 Distribution of current speed and direction during the summer season.

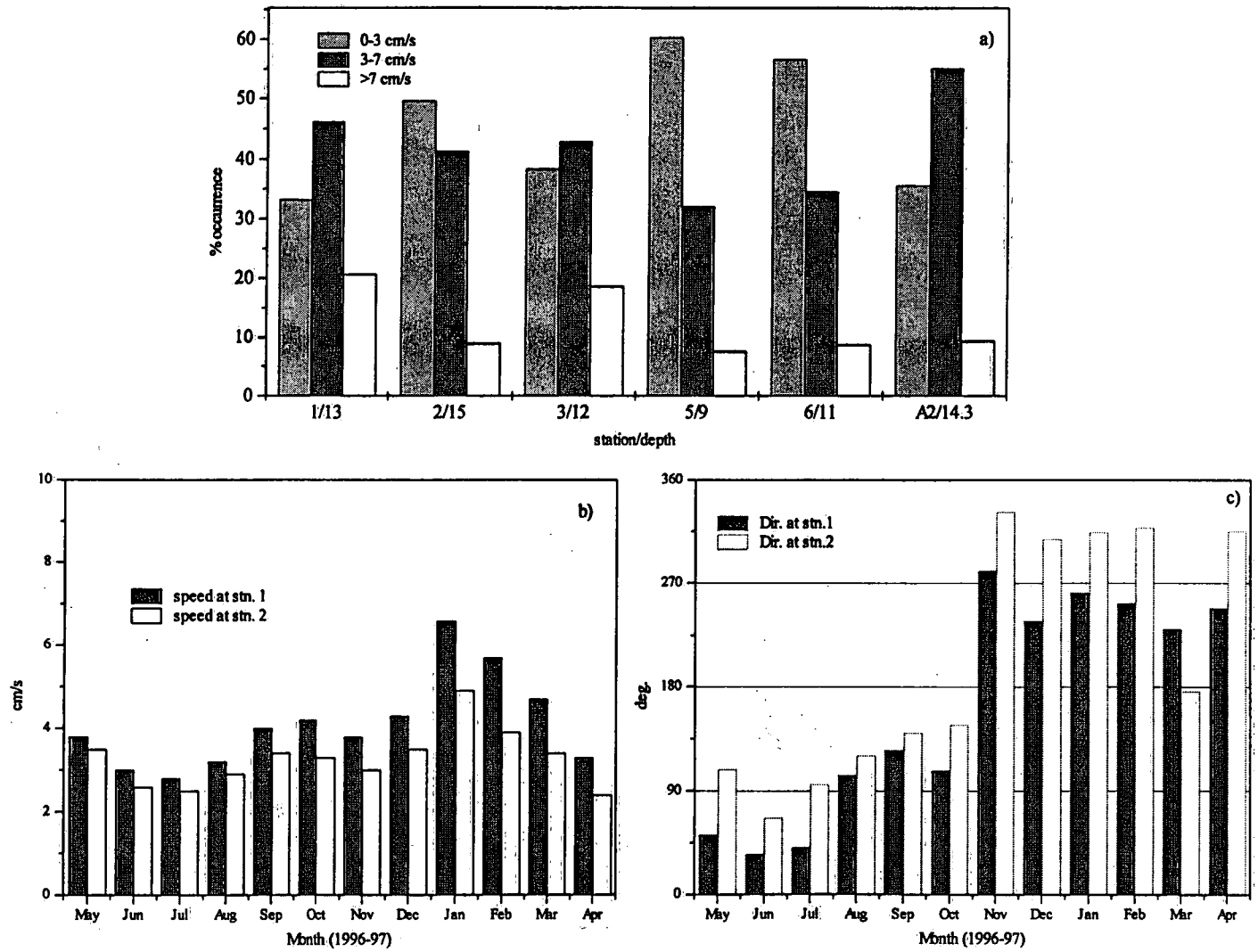

Figure 6.3 Distribution of a) current speed during winter season, b) annual distribution of current speed and c) current directions at stations 1 and 2.

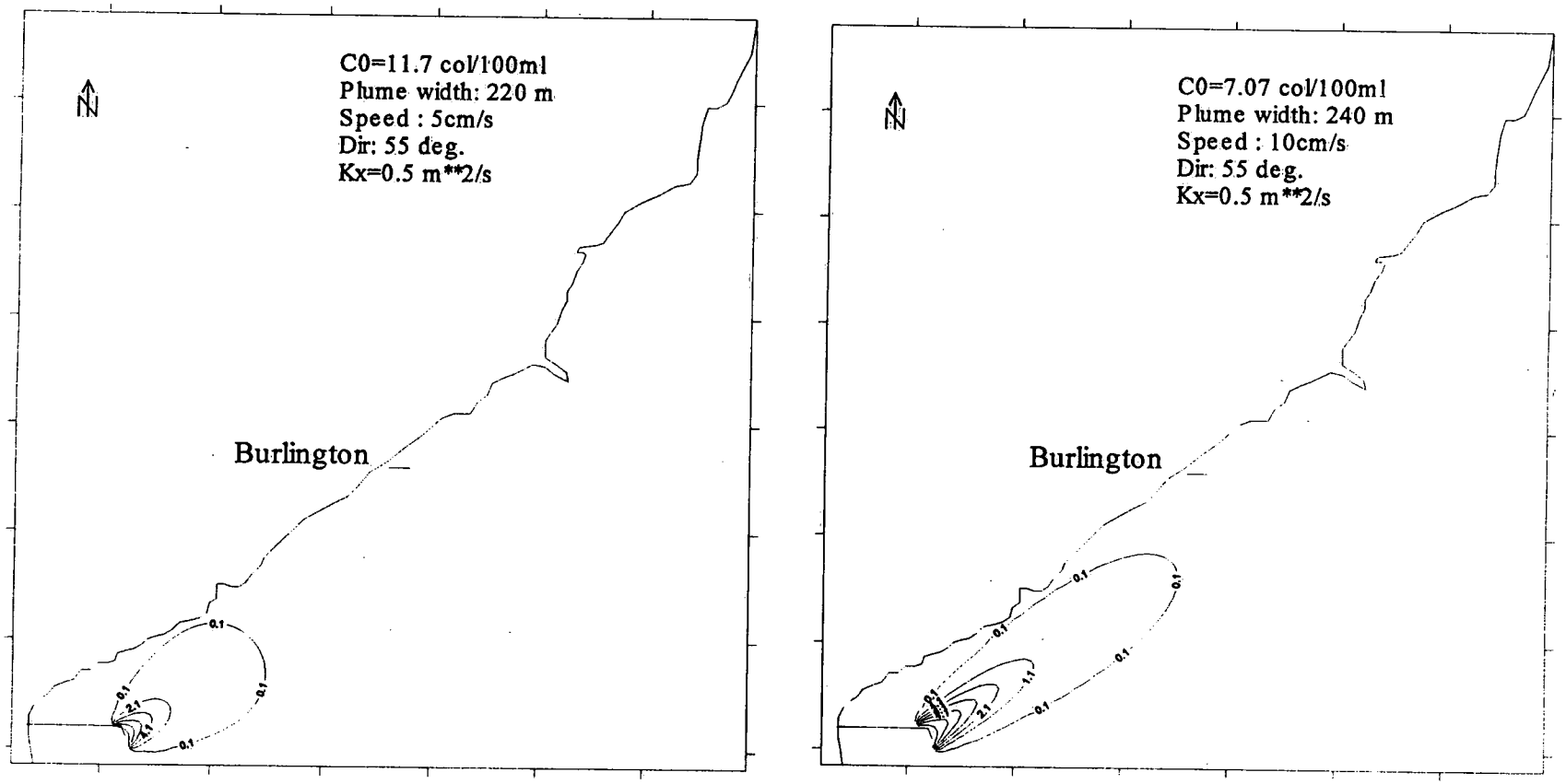

Figure 6.4 Contours of concentration field obtained from Gaussian plume model during a constant north-easterly current episode.

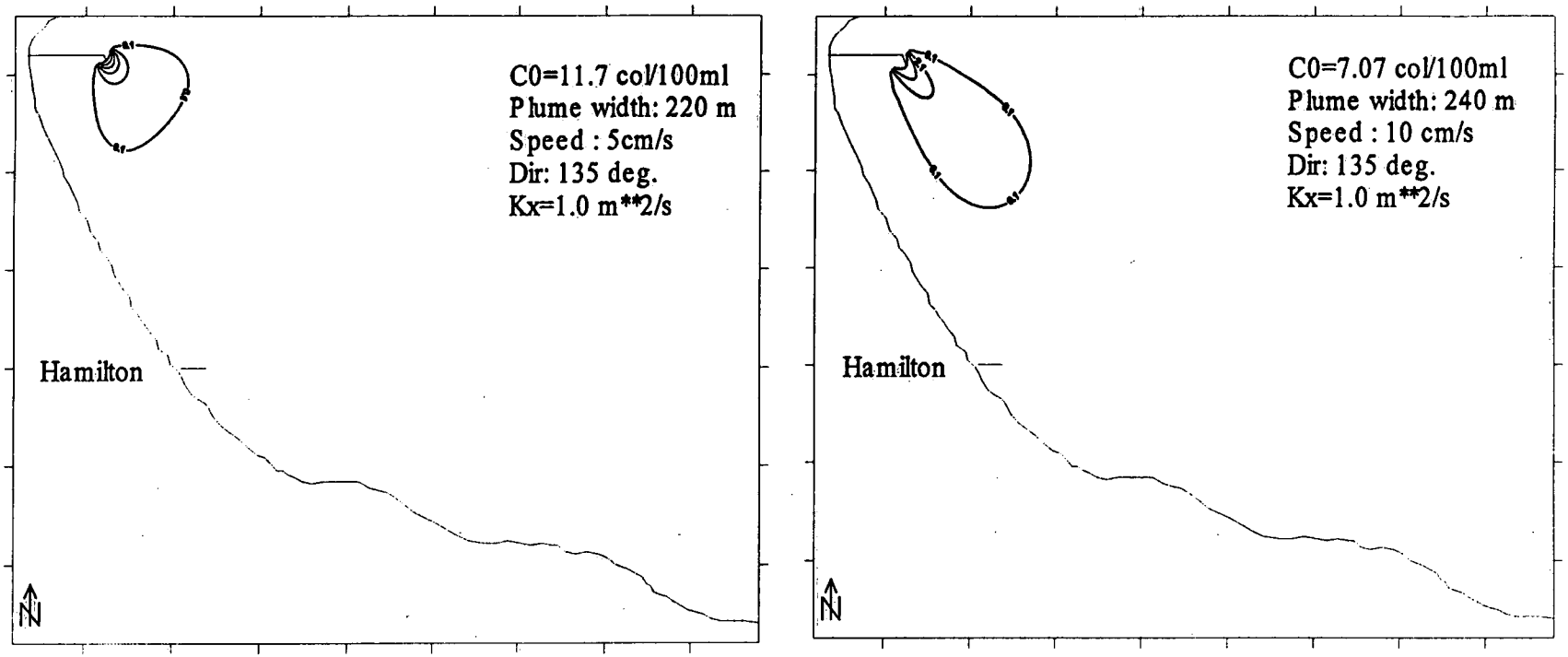

Figure 6. 5 Same as in Figure 6.4, but for south-easterly wind episode.

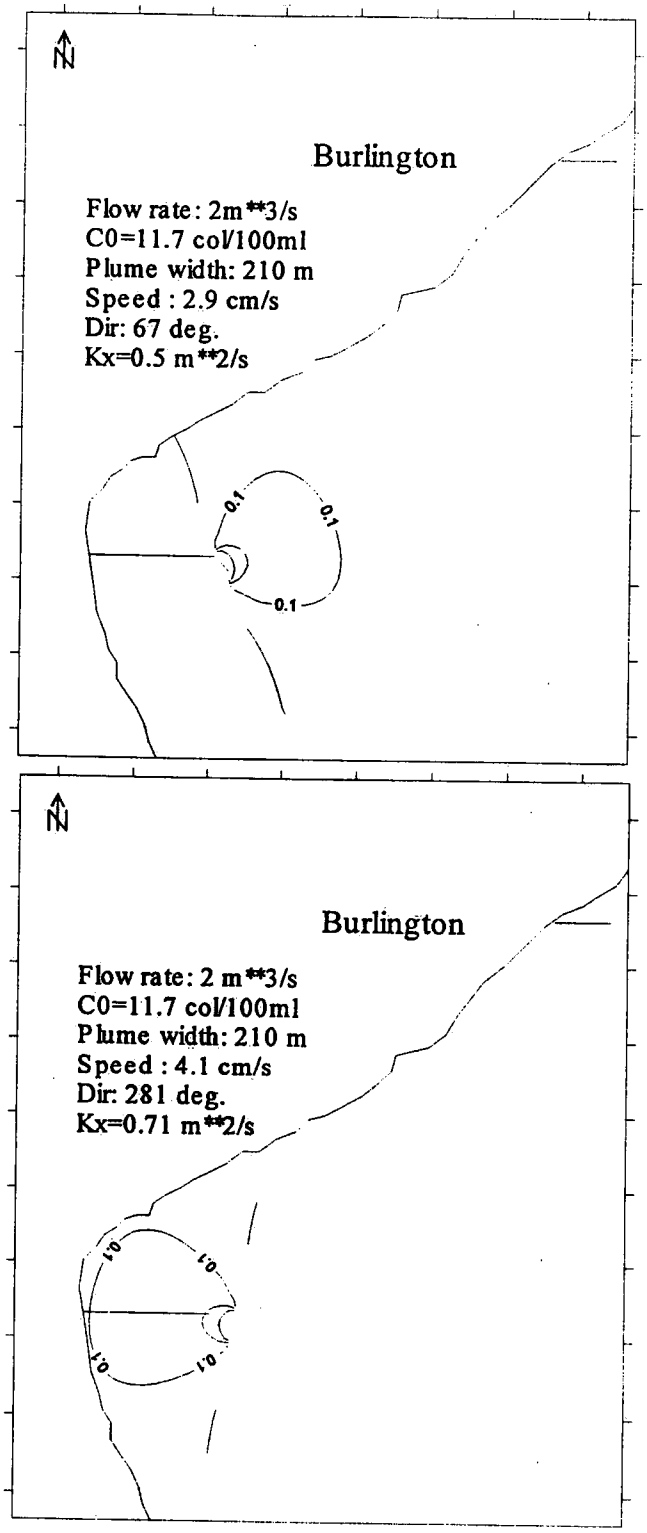

Figure 6.6a Contours of concentration field obtained from Gaussian plume model for summer and winter conditions.

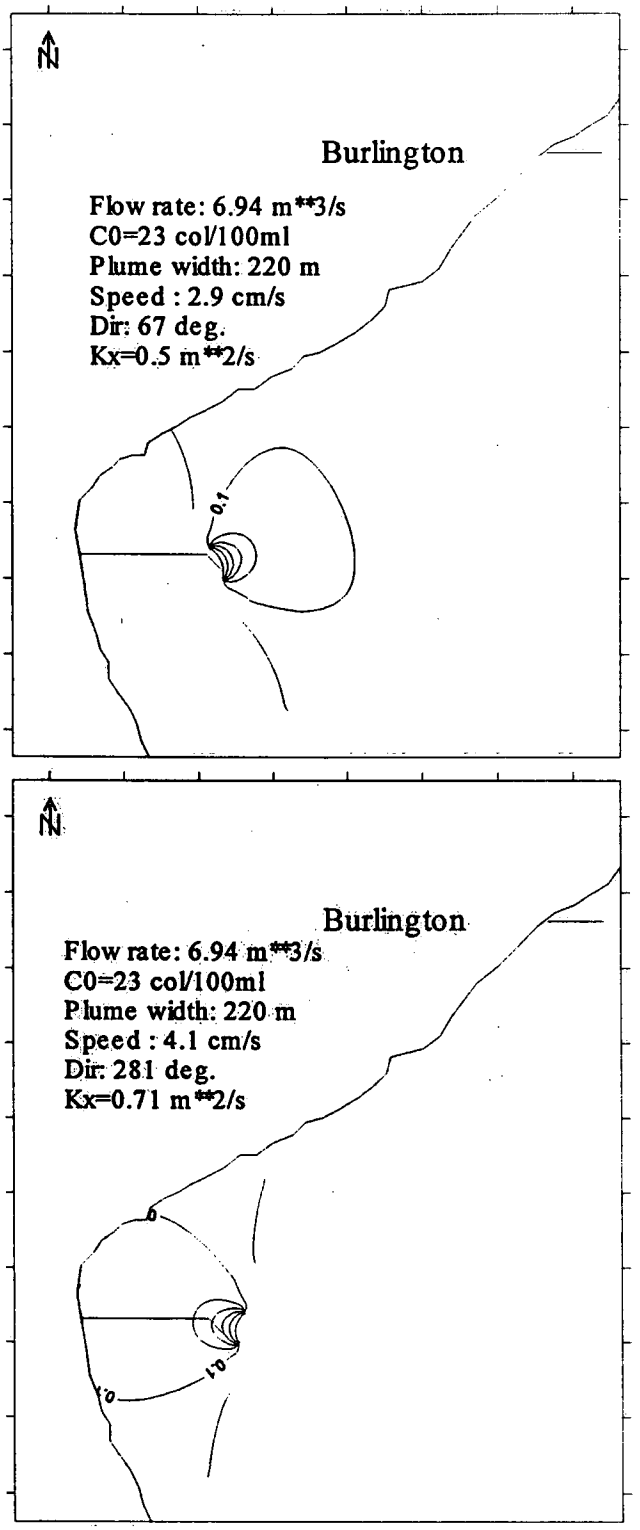

Figure 6.6b Same as in Figure 6.6a, but for expanded treatment capacity.

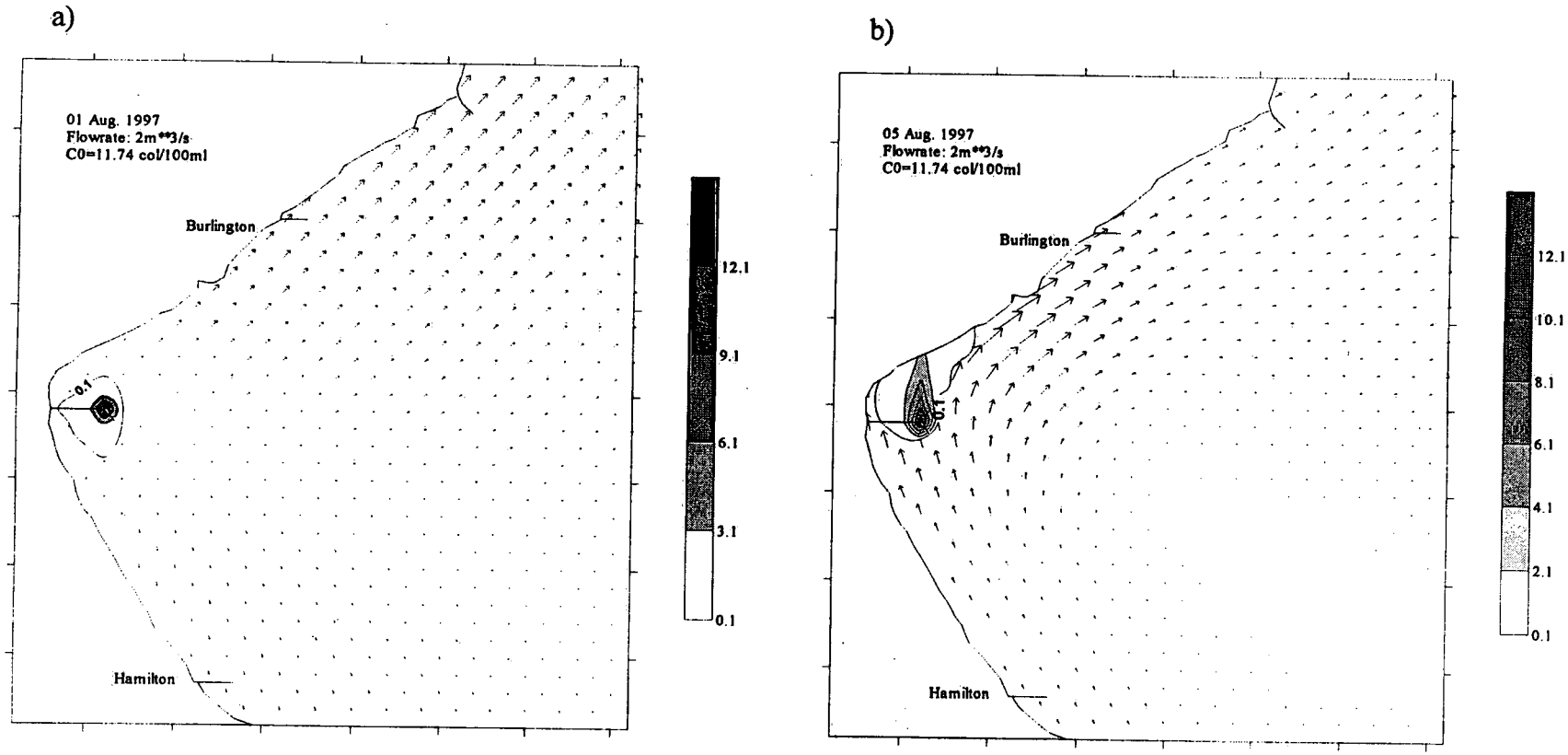

Figure 6.7 Contours of concentration field for a shore parallel current episode.

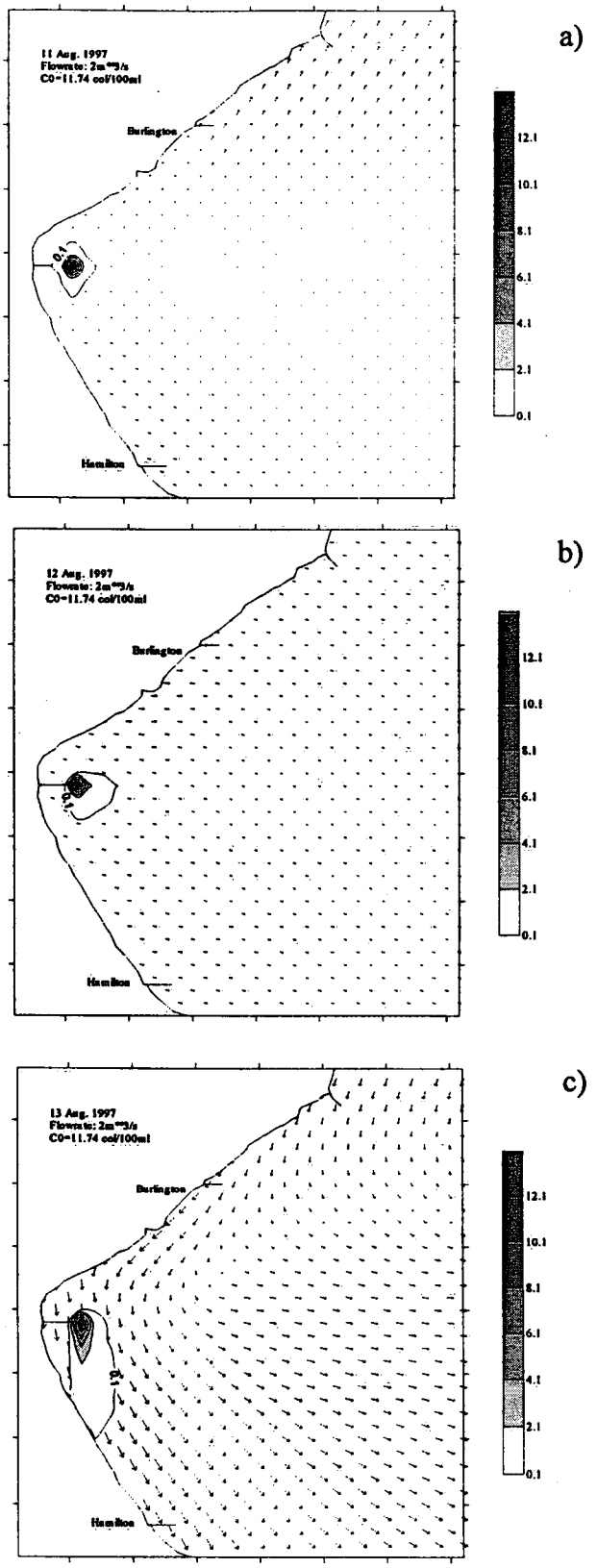

Figure 6.8 Contours of concentration field superimposed on the circulation from 11 to 13 August 1997.

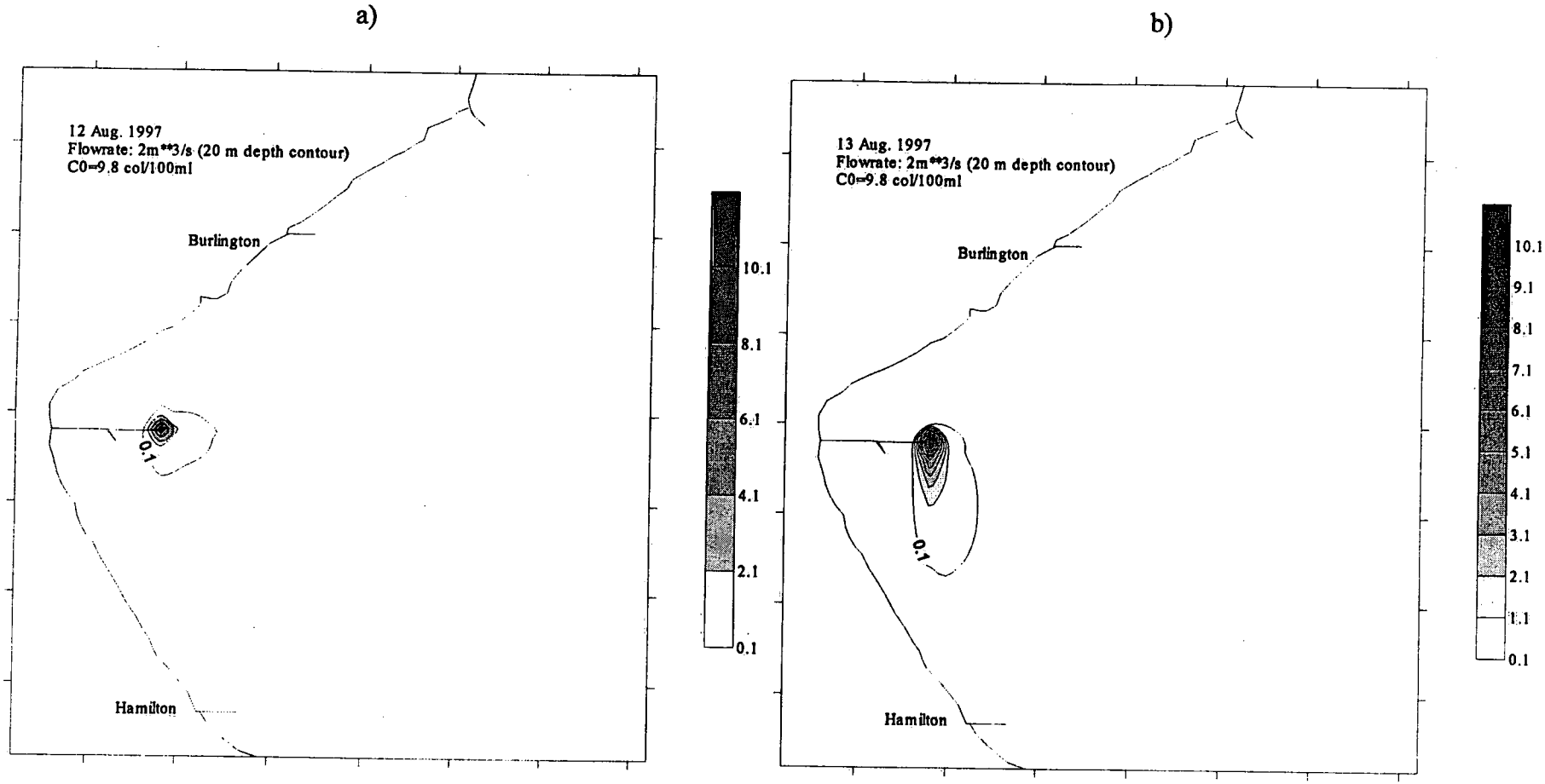

Figure 6.9 Contours of the concentration field by shifting the outfall to a distance of 2 km from the shoreline.

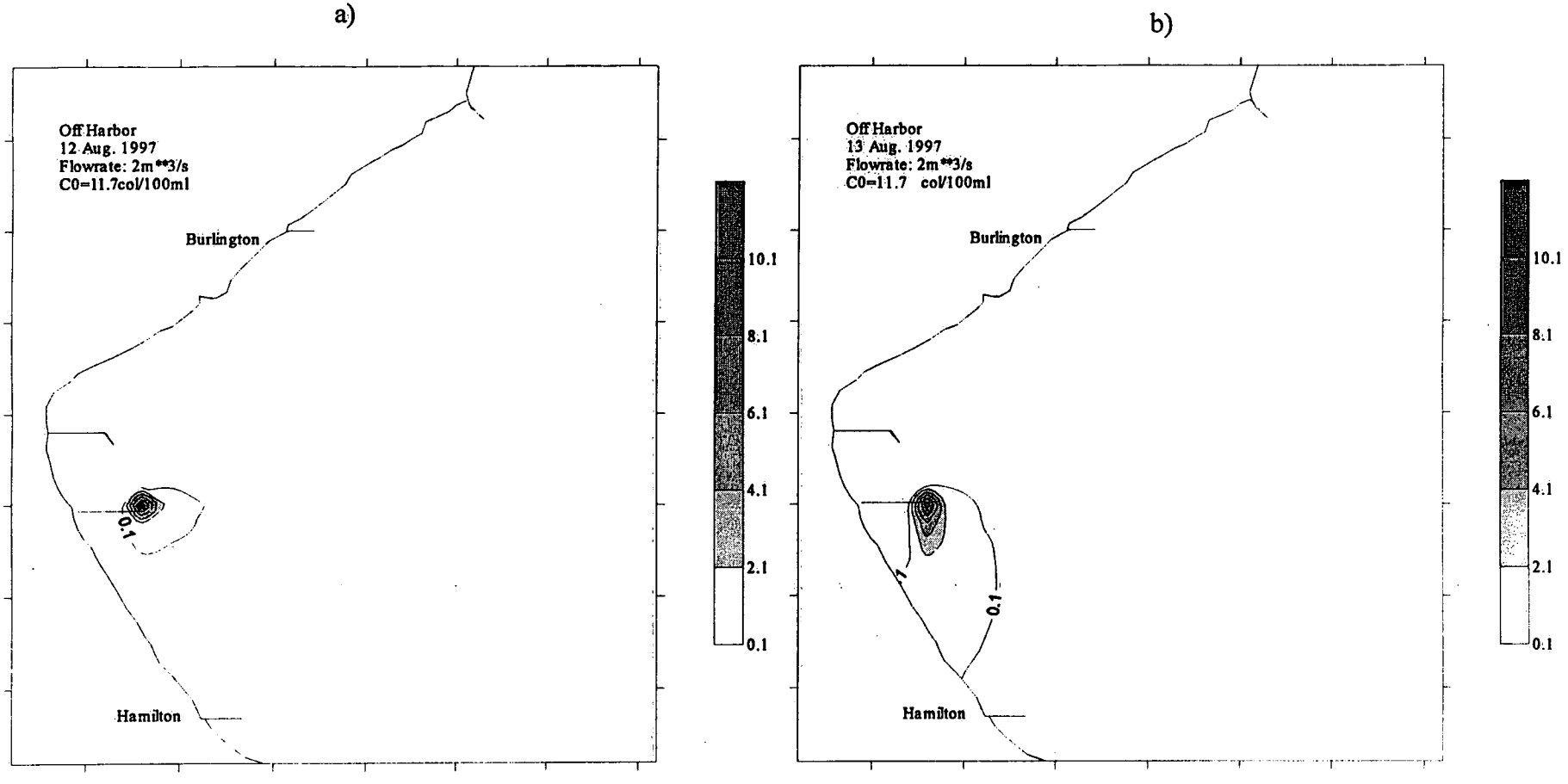

Figure 6.10 Contours of concentration distribution with outfall located off Hamilton Harbour with a discharge rate of $2m^3$/sec for a typical south-easterly current episode.

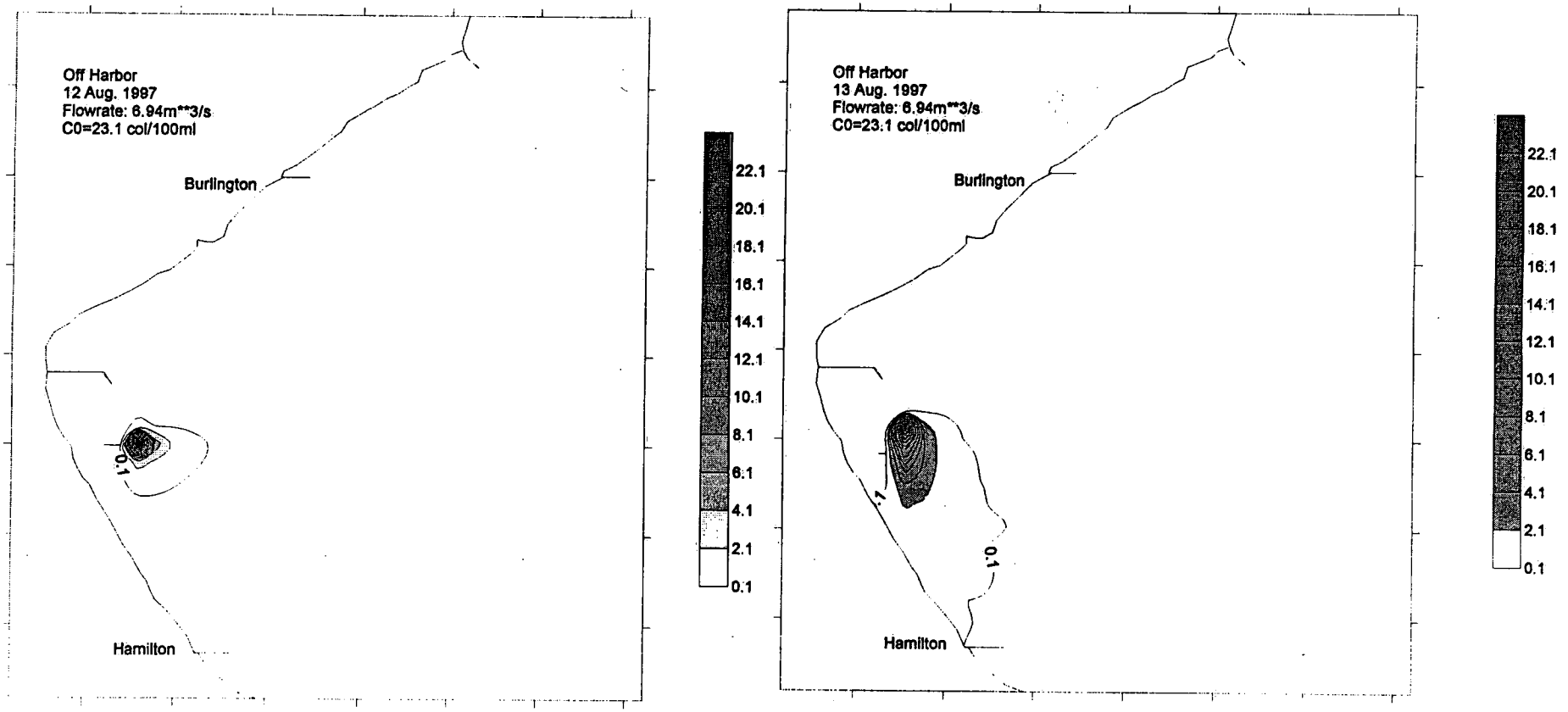

Figure 6.11 Same as in Figure 6.10 but for a discharge rate of 6.94 m^3/s.

PRINTED IN CANADA
IMPRIMÉ AU CANADA
ON RECYCLED PAPER
SUR DU PAPIER RECYCLÉ

National Water Research Institute
Environment Canada
Canada Centre for Inland Waters
P.O. Box 5050
867 Lakeshore Road
Burlington, Ontario
L7R 4A6 Canada

National Hydrology Research Centre
11 Innovation Boulevard
Saskatoon, Saskatchewan
S7N 3H5 Canada

NATIONAL WATER RESEARCH INSTITUTE
INSTITUT NATIONAL DE RECHERCHE SUR LES EAUX

Institut national de recherche sur les eaux
Environnement Canada
Centre canadien des eaux intérieures
Case postale 5050
867, chemin Lakeshore
Burlington, Ontario
L7R 4A6 Canada

Centre national de recherche en hydrologie
11, boul. Innovation
Saskatoon, Saskatchewan
S7N 3H5 Canada

Environment Canada Environnement Canada

Canada